

POLITECNICO DI MILANO

Department of Civil and Environmental Engineering

Ph.D. course in Environmental and Infrastructure Engineering

XXVI Cycle (2011-2013)



MERGING LOCAL DTMS:
HELI-DEM PROJECT, PROBLEMS AND SOLUTIONS

Tutor: Prof. Fernando SANSÓ
Supervisor: Dr. Ludovico Giorgio Aldo BIAGI
Coordinator: Prof. Alberto GUADAGNINI

Ph.D. Thesis by
Laura CARCANO
Id. 769435

Contents

Introduction	1
1 Earth representation through Digital Models	5
1.1 Brief history of the Earth surface representation	5
1.2 Field models	8
1.2.1 Digital Elevation models	11
1.3 Data acquisition process for producing a DEM	12
1.3.1 Data sampling process	12
1.3.1.1 Sampling strategies for data acquisition	14
1.3.1.2 Accuracy of sampled data source	15
1.3.2 Techniques for DEM source data acquisition	16
1.3.2.1 Cartographic digitalization	16
1.3.2.2 Ground survey and GPS	19
1.3.2.3 Photogrammetry	26
1.3.2.4 LiDAR	30
1.3.2.5 SAR	34
1.3.2.6 Comparison between DEM data from different sources	37
1.4 Quality of a DEM	38
1.5 Different methods of DEM representation: GRID vs. TIN	43
1.6 Different levels of grid DEM representations	45
1.6.1 Global low resolution Digital Surface Models	46
1.6.1.1 SRTM global DSM	47
1.6.1.2 ASTER global DSM	49
1.6.1.3 Global Multi-resolution Terrain Elevation DATA 2010 (GMTED2010)	51
1.7 DSMs filtering to obtain DTMs	53
2 The HELI-DEM project and the data preprocessing	57
2.1 The HELI-DEM project	57
2.2 Preprocessing of the data	60

2.2.1	Collection of the available elevation data	61
2.2.1.1	Regional DTMs	63
2.2.1.2	Medium and high resolution DTMs	66
2.2.1.3	Geoid models	67
2.2.2	Implementation of the GNSS transnational reference network	68
2.2.3	Transformation between different reference frames	70
2.3	Comparisons between DTMs	74
2.3.1	Cross-validation between similar DTMs	75
2.3.1.1	Lombardy DTM vs. Switzerland DTM	79
2.3.2	Cross-validation between low and high resolution DTMs	90
2.3.2.1	Lombardy Regional DTM vs. Ministry of Environment PST-A LiDAR DTM	91
2.4	External validation of the DTMs through GPS data	102
2.4.1	DTMs comparison with IGM95 benchmarks	102
2.4.2	PST-A LiDAR DTM comparison with RTK surveys	105
3	Analyses on different DTM interpolation methods	115
3.1	Regridding by polynomial interpolation: comparison between bilinear and bicubic surfaces	115
3.1.0.1	Comparison between bilinear and bicubic interpolations on Lombardy regional low resolution DTM	117
3.1.0.2	Comparison between bilinear and bicubic interpolations on Lidar high resolution DTM	124
3.2	Instability of the interpolation systems: problems and possible solutions	129
3.3	Different procedures to merge and interpolate DTMs on an output grid	135
3.3.1	Comparison between the two Direct methods in the interpolation of the input DTMs on the output grid	136
3.3.2	Comparison between SVD and LS_{RO} solutions to regularize unstable systems	141
4	The unified DTM: preprocessing and final computation	145
4.1	Characteristics and creation of the unified HELI-DEM DTM	145
4.1.1	Pre-elaboration of the input data	147
4.1.2	Elaboration of input data to create the unified DTM	147
4.1.3	Post-elaboration of the unified DTM: correction of the nodes belonging to lakes	151
4.2	Correction of HD-1 DTM with high resolution PST-A DTM	151

4.2.1	Adopted procedure	152
4.2.2	Application of the adopted procedure to HD-1 DTM	161
4.2.2.1	Validation of the corrected DTM with RTK measures	162
4.3	Creation of the HELI-DEM geoserver to publish the input and final elevation data	164
5	Inverse approach to interpolate the final HD DTM	169
5.1	Description and implementation of the Inverse method	169
5.2	Application of the method to the HELI-DEM case study	171
5.2.1	Validation of HD-1b and HD-2b DTM with RTK measures	182
	Conclusions and Outlooks	185
A	Reference systems and frames	189
A.1	ITRS and ITRF	189
A.2	ETRS89	191
A.3	ETRF89 - IGM95	192
A.4	ETRF2000-RDN and ETRF2000-IGM95	192
A.5	ROMA40 - Gauss Boaga	194
B	Grid interpolation methods	195
B.1	Exact interpolators of linear surfaces	196
B.1.1	Simple linear interpolation	196
B.1.2	Bilinear interpolation	197
B.1.3	Bicubic interpolation	198
B.1.3.1	Exact bicubic interpolation on a regular grid	199
B.2	Best interpolation of linear surfaces	200
B.2.1	Least Squares interpolation of a local surface	201
	List of figures	209
	List of tables	214
	Bibliography	215

Introduction

Digital Elevation Models (DEMs) provide a numerical description of the terrain surface and nowadays probably are the most important tools for modelling it. By definition, a DEM is a data set that is used to calculate, by interpolation, the elevation of a certain point of the ground (surface) which is described with a given accuracy. In general DEMs can be distinguished in Digital Surface Models (DSMs), which represent the actual surface and are mainly used to provide information also on objects that are built on it (buildings, woods, etc.) and Digital Terrain Models (DTMs) which represent the elevation of the bare soil without vegetation and buildings.

Official cartographic bases in Europe include Digital Terrain Models; in recent years, different countries and regions have produced their own DTMs. However, since unique and general rules are not completely shared, every institution has constructed DTMs in the deemed best and most appropriate manner. As a consequence, the different available DTMs have been acquired by different data sources and are characterized by different resolutions and accuracies; furthermore, they are georeferenced in different reference frames. In some cases it could happen that the elevation data are not homogeneous and consistent at the borders between countries or regions: in the worst cases also biases can be present along the border. This is a major problem when dealing for example with hydrogeological studies, and especially in alpine areas where hydrogeological risks may exist. For example, when an event like a landslide happens at the border between two countries or regions, making use of the available DTMs is not possible if a bias is present between the different elevation data that covers the landslide area. In such cases a unique and integrated DTM which covers the whole interest area could be useful to analyse the scenario. DEMs are mainly distinguished according to two characteristics: resolution and accuracy. Resolution is the spatial density of the elevation information contained in a DEM; accuracy is the degree of closeness of the elevation information to its actual true value.

In recent years, both in Italy and Switzerland, elevation data with different reference frames, technologies, accuracies and resolutions have been produced. The HELI-DEM (HELVetia-Italy Digital Elevation Model) project, funded by the

European Regional Development Fund (ERDF) within the Italy-Switzerland co-operation program, aims at developing a unique DTM for the alpine and subalpine area between Italy and Switzerland. For Italy the involved Regions are Lombardy and Piedmont, for Switzerland Ticino and Grisons cantons are involved; for all of them only the alpine part of the territory is considered.

The goal of the project is the creation of a Digital Terrain Model which covers the whole project area and which has to be correctly georeferenced and produced validating and integrating all the elevation information made available by the different project partners. The altimetric information should be continuous and consistent at the nominal level of the input DTMs; therefore the resolution of the final DTM should be at least equal to those of the original input DTMs and the vertical accuracy has to be in every area the best one obtainable from the input DTMs.

To create a unified DTM the available data have basically to be merged together on a common output grid. But this procedure, that apparently seems to be simple, implies a sequence of operations that are not so obvious. First of all the data have to be validated, both reciprocally and by external and more accurate data in order to verify their accuracy and the presence of possible global biases or local errors. After that, the data that seem suitable and correct have to be aligned to a common reference frame, which is that of the final grid. Finally the input DTMs have to be merged on the output grid, trying to use both the low resolution and high resolution data. This operation could be very complex, because the problems that may occur both in the mathematical method adopted and in its numerical implementation are due to the large amount of input data.

This thesis, carried out for the most part within the HELI-DEM project, will describe the deep analyses that have been performed to find the best procedures to be adopted and the final results of the project.

In **Chapter 1**, after a brief overview on the history of Digital Elevation Models, the processes for the acquisition of elevation data are described. Then the different techniques used to acquire elevation data are depicted and compared. The final part deals with the quality of a DEM, the standards for the classification of DEMs and the different levels of DEM representation today adopted, making a brief overview on the three global DEMs used today.

Chapter 2 presents the HELI-DEM project, the collected data and all the pre-processing operations that have to be done in order to use the available data for the creation of the unified DTM. The implementation and test of a GNSS transnational network useful to collect validation data and the implementation of a software that allows the transformation between different reference frames are described. The analyses and the obtained results of cross-validation and external validation of all the DTMs are outlined and commented.

Chapter 3 addresses the problem of regrid a DTM on a different grid. In particular attention is paid on the polynomial surfaces and in particular bilinear and bicubic models are compared on real data. Then ill-conditioning systems are treated and some solutions to this problem will be given and compared. At the end two different procedures for the merging and interpolation of different DTMs on an output grid are tested and compared on real data, in order to find the best procedure that will be then applied on HELI-DEM case study.

In **Chapter 4** the procedure for the production of the unified HELI-DEM DTM from the low/medium resolution available DTMs and the final product are presented. Also the procedure to correct the unified DTM with the high resolution data are described in detail. In particular a filtered approach is applied with a numerical implementation of the Fast Fourier Transform.

Chapter 5 depicts an alternative method, studied after the end of the project, to produce a unified elevation model from partly overlapping input DTMs, overcoming the limitations of the previous method. The method is tested on HELI-DEM data producing a different final product, which is then cross-checked with the input data and which can give better results.

Chapter 1

Earth representation through Digital Models

Digital Elevation Models are the most important tool to memorize elevation data and are very useful for many environmental and territorial applications. DEMs can be obtained by different elevation data sources as for example photogrammetry, digitalization of existing maps, SAR, LiDAR or GPS. Depending on the used source data and on the needed application, DEMs with different resolution and accuracies can be constructed.

In this chapter, after a brief overview on the history of Digital Elevation Models, the techniques to acquire elevation data and the data processes for producing a DEM are described. In the final part, the three global DEMs used today are presented.

1.1 Brief history of the Earth surface representation

Human beings have been using maps since ancient times. This can be related to the attitude of certain ancient communities to nomadism. This tendency to nomadism must have honed their ability to draw maps. In the beginning maps were drawn on stone, wood or rock. The Eskimos were probably the only ones who tried to draw maps showing also the terrain relieves: in fact they drew on the sand the relief of the coastline (Figure 1.1). In 1826 F.W. Beechey wrote that “First they marked the coastline, then they signed the mountains and the hills, then the islands, maintaining correctly the proportions. Then they marked the islands using pieces of stick planted vertically in the sand. In that way they gave a complete topographic map of the area”.

In ancient times, semi-symbolic and semi-pictorial descriptions were used to represent the actual three-dimensional terrain surface, but with a very low qual-



Figure 1.1: Eskimo stick carved to represent the coastline.

ity and accuracy. Today, modern maps with a well-designed symbol system and a solid mathematical foundation are scientific and abstraction features of the terrain surface (Li et al., 2005). A contoured topographic map is the most familiar way to represent the terrain surface (Figure 1.2). Beginning in the 16th century, lines connecting points of equal elevations were in fact used by Dutch and French engineers and cartographers; these lines were firstly used to portray forms of the underwater surface and later to show the dry land configuration of the Earth surface. As people gradually realized that elevation was important upon other aspects of the physical environment, they began to collect accurate data. Since the 18th century contoured topographic maps gradually became the most familiar way of representing the three dimensional surface. On a topographic map, the terrain features are projected orthogonally onto a two dimensional horizontal datum. The terrain details are in this way represented by lines and symbols: in particular the terrain heights can be represented by contour lines.

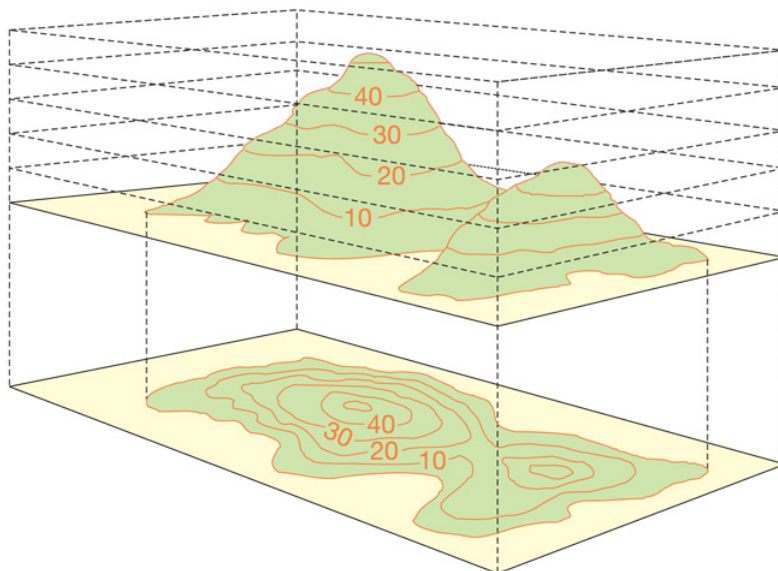


Figure 1.2: Example of the terrain representation through contour lines.

Another way to record the world is photography, which was born in the 19th century. With respect for example to maps, photographs are much more detailed and easier to understand. In particular photographs have been used since 1849 for the terrain surface representation, even if in a photo the height information is missing. With the birth of photogrammetry also elevation information have been extracted by aerial photographs. In fact photogrammetry can determine the geometric properties of objects as for example their height: 3-D surfaces can be reconstructed by using a pair of aerial photographs, taken from two slightly different points of view, representing the same area with a certain percentage of overlap.

Satellite images have been used to complement aerial photography since 1970s. Many satellite systems take overlapping images of the terrain so that these images can also be used to construct 3-D models of the Earth surface. With the birth of computers, since the middle of the 20th century, also space-borne cameras and electronic sensors of high metric accuracy have been spread, giving good data and new possibilities for land-form portrayal. With the widespread of computing technology, modern mathematics and computer graphics, digital representation of the terrain has been played an important role in surveying sciences. Digital terrain surfaces can be mathematically or geometrically represented; some common mathematical representations are Fourier series and polynomials. There are also a lot of methods for representing the terrain in digital form: regular or irregular grids are common graphic representations (Figure 1.3).

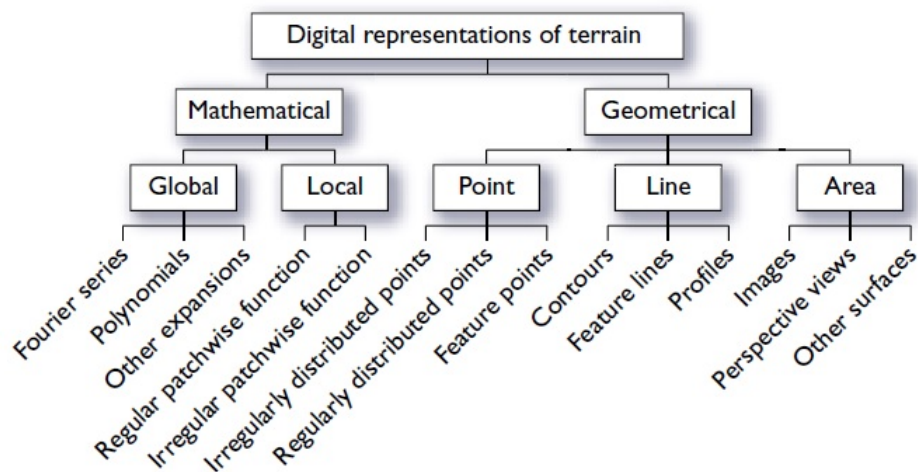


Figure 1.3: Digital representations of terrain.

1.2 Field models

A model is anything used as a representation of a real object, law, theory or event. A model is not the real world but merely a representation and a simplification of it; it is usually scaled down with respect to reality and converted to a form which can be more comprehensible. There are many types of models, as shown in Figure 1.4, and among these, the three main types are (Saaty and Alexander, 1981):

- conceptual,
- physical,
- mathematical.

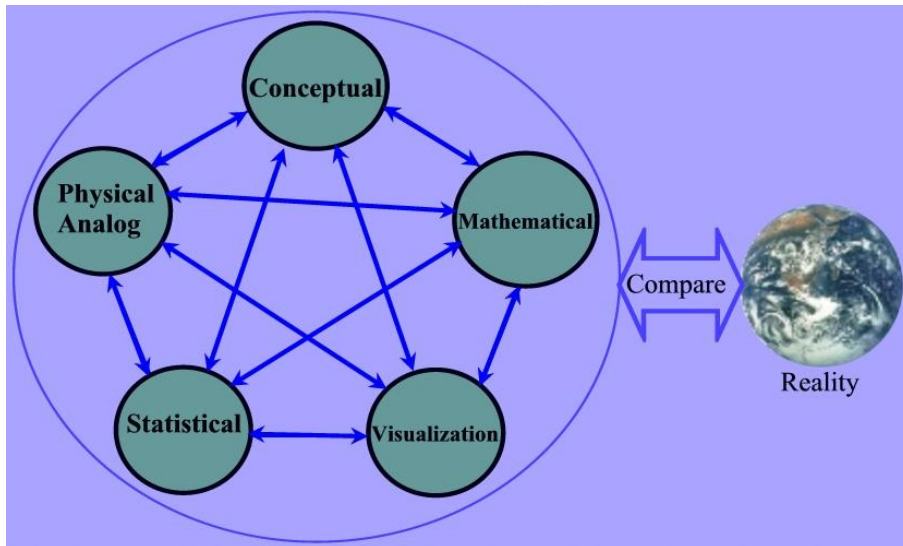


Figure 1.4: Different types of models.

The conceptual model is the model born in a person's mind about a situation or an object based on his experience. This type of model forms the primary stage of modelling and is followed by a mathematical or physical model. A physical model is usually an analogue model; an example of this kind of model is a terrain model made of plastic, or clay. Finally a mathematical model represents a situation, a phenomenon or an object in mathematical terms, through the use of mathematical concepts such as constants, variables, functions, equations, etc. Mathematical models can be divided into two types: quantitative models, based on a numerical system, and qualitative models, based on set theory, that cannot be reduced to numbers. Mathematical models can be classified into functional models, which

intend to solve mathematical problems, and stochastic models, which are useful to solve probabilistic problems. Six criteria allow to search for the best method, when a phenomenon has to be described by a mathematical model (Meyer, 1985):

- *accuracy*: the output of the model is correct or very nearly correct,
- *descriptive realism*: the model is based on correct assumptions,
- *precision*: the prediction of the model is composed by definite numbers, functions or geometric figures,
- *robustness*: the model is immune to errors in the input data,
- *generality*: the model can be applicable to a wide variety of situations,
- *fruitfulness*: the conclusions are useful, or inspiring to other good models.

Another criterion can be added to this list, which says that the smallest possible number of parameters should be used in the model; in fact not always the most complicated model is the best one to be used.

A field model is a representation of a characteristic or a phenomenon of the Earth, which is spatially referenced. In this sense a field model can be generalized as an ordered set of sampled data points that represents the spatial distribution of different kinds of information on the terrain. A mathematical expression of it could be:

$$K_i(P) = f_i(u_P, v_P), \quad i = 1, 2, 3, \dots, m, \quad P = 1, 2, 3, \dots, n \quad (1.1)$$

in which $K_i(P)$ is one attribute value of the K -th type of terrain feature at the location of point P ; u_P and v_P are the 2-D coordinates of the point P ; m ($m \geq 1$) is the total number of terrain information types and n is the total number of sampled points. In this way a field model presents the spatial distribution of one or more terrain information by 2-D locations plus a mathematical representation of the terrain information; this kind of model is a 2.5-D representation of the information in 3-D geographical space. To construct a field model of this type, a mathematical modelling process has to be carried out with some data collected from the terrain. Data should be collected with a proper density and distribution; the field is thus represented by the sample points. If attributes on a location different from the sample points are needed, then an interpolation is applied to extract information from the model of the surface.

The term “field” is associated not only with land, hydrographic features, soil or vegetation but also with the socio economic aspect of an area. Generally a model of a field could contain the following groups of information:

- landforms, such as elevation, slope and other geomorphological features that are used to depict the terrain relief,
- terrain features, such as hydrographic features (i.e rivers lakes, coast lines), transportation network (i.e roads, railways, paths), settlements, boundaries, etc.,
- natural resources and environments, such as soil, vegetation, geology, climate, etc.,
- socio-economic data, such as the population distribution in an area, industry and capital income, etc.

Many field models exist. To outline just an example of them, in geomatics field models that describe the subsidence of a terrain (the slow and progressive lowering of it) are very important. Figure 1.5 shows an example of subsidence map for Las Vegas area (Amelung et al., 1999) obtained through InSAR data.

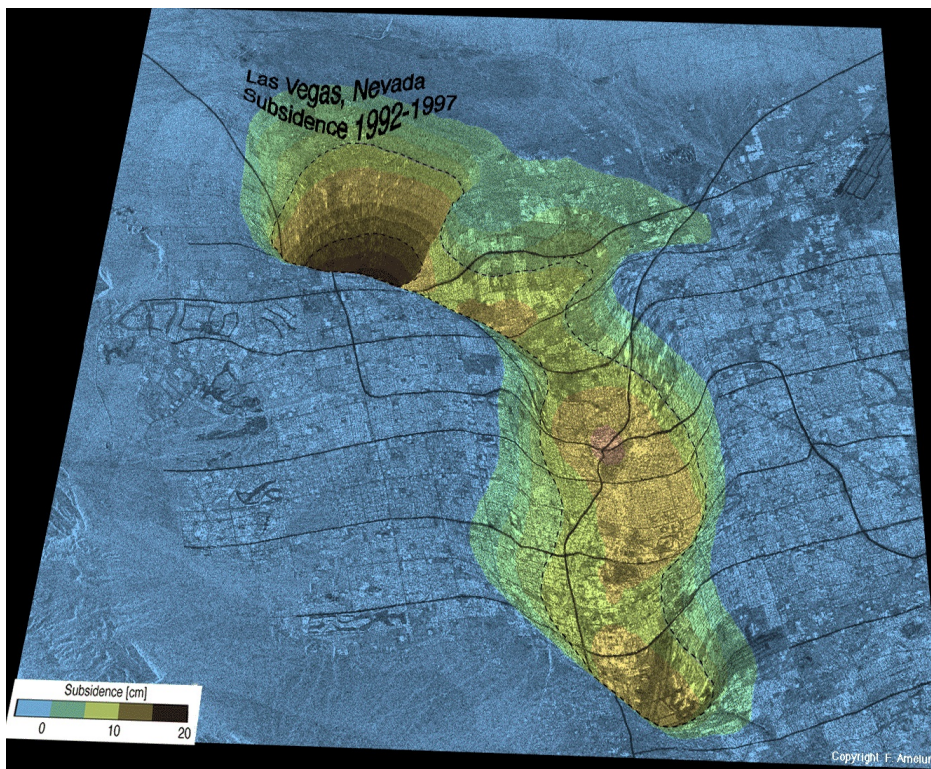


Figure 1.5: Example of subsidence model of Las Vegas area (Oksanen, 2006).

1.2.1 Digital Elevation models

A model that describes the surface of the Earth can be called Digital Elevation Model (DEM). Digital Elevation Models, which are nowadays probably the most important tools for representing the terrain surface, are a numerical representation of the terrain features in terms of elevation measurements obtained by sampling a topographic surface. In other words, they are a numerical representation of height details information that provide a continuous description of the surface. By definition, an elevation model is a data set that is used to calculate, by interpolation, the height (usually orthometric referred to the geoid taken as reference) of a certain point of the ground (or surface) which is described with a given accuracy. The traditional contours maps are an example of elevation models; they are a very effective representation of the terrain elevation because they provide both an accurate information along the contour lines and an overall morphology of the terrain: in fact smooth ground presents sparse lines and slight curvatures, while rough terrain is characterized by dense lines with large curvatures.

In general DEM indicates the 3-D representation of a surface; DEM, which refers to the generic family of the elevation models, can be distinguished in Digital Surface Models (DSMs), which represent the actual surface and are mainly used to provide information also on objects that are built on it (including buildings, woods, etc.) and Digital Terrain Models (DTMs) which represent the elevation of bare soil (Maune et al., 2001) without vegetation and buildings (example in Figure 1.6). DTMs may also include some man-made features, such as road embankments.

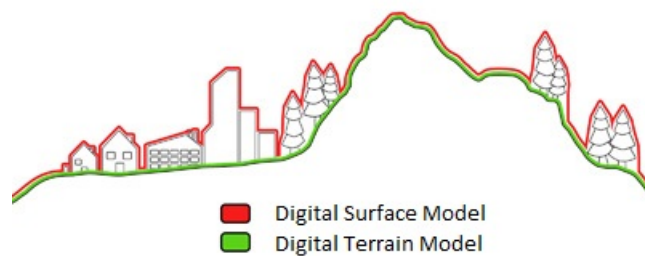


Figure 1.6: Difference between DSM and DTM.

DEMs often comprise much of the raw dataset, which may have been acquired through techniques such as photogrammetry, LiDAR, land surveying, etc. DSMs are topographic maps of the Earth surface with a geometrically corrected reference frame over which other data layers can be draped. DSMs, including the maximum heights everywhere (vegetation, roofs of buildings, bridges, roads and natural terrain features), are produced for example from the processing of stereoscopic im-

ages, because neither the operator nor the matching software can see the ground through roofs and leaves. If a DTM is requested from a DSM, it is necessary to do a correction process to rub out trees and buildings. While DTMs, providing the so called “bare-earth model”, are used for flood or drainage modelling, land-use and geological studies, DSMs are very useful for landscape modelling, city modelling and visualization applications.

1.3 Data acquisition process for producing a DEM

To produce a DEM the first step that has to be carried out is the acquisition of all the data that will be used to build the model itself. In this process, a set of data points is acquired from the terrain surface in two stages: sampling and measurement. During the sampling process, the locations in which the measure is done are chosen; during the measurement stage, the coordinates of these locations are measured. Density, distribution and accuracy are the three key concepts related to the DEM data source acquisition process.

1.3.1 Data sampling process

Sampling is the process of selecting points that have to be measured in a certain position and that are used to construct the DEM. This operation can be characterized by two parameters, distribution and density (Makarovic, 1973). An optimum sampling process is characterized by proper density and distribution, that are usually related to the location and pattern of the sampling. Measurement is the determination of the 2-D planimetric coordinates of a point and is concerned with accuracy. The sampling process can be done before or after the measurement: when it is done after the measurement a subset of measured data points are selected, usually with great density. The distribution of sampled data is usually specified by location and pattern. The location is defined in terms of the 2-D coordinates (Longitude and Latitude, or East and North). On the other side, concerning the sampling pattern, there is a variety of it that is available for selection and that can be classified in different ways. Figure 1.7 shows an example of this classification.

Data that are regular in 2-D dimensions are generally produced by means of regular grid or progressive sampling; the resulting pattern can be a rectangular, a square grid, or a hierarchical structure of these two. Square grids are the most commonly used. Also other special regular patterns can be used, as for example equilateral triangles and hexagons. However, these structures are not so used as profiled or regular grids.

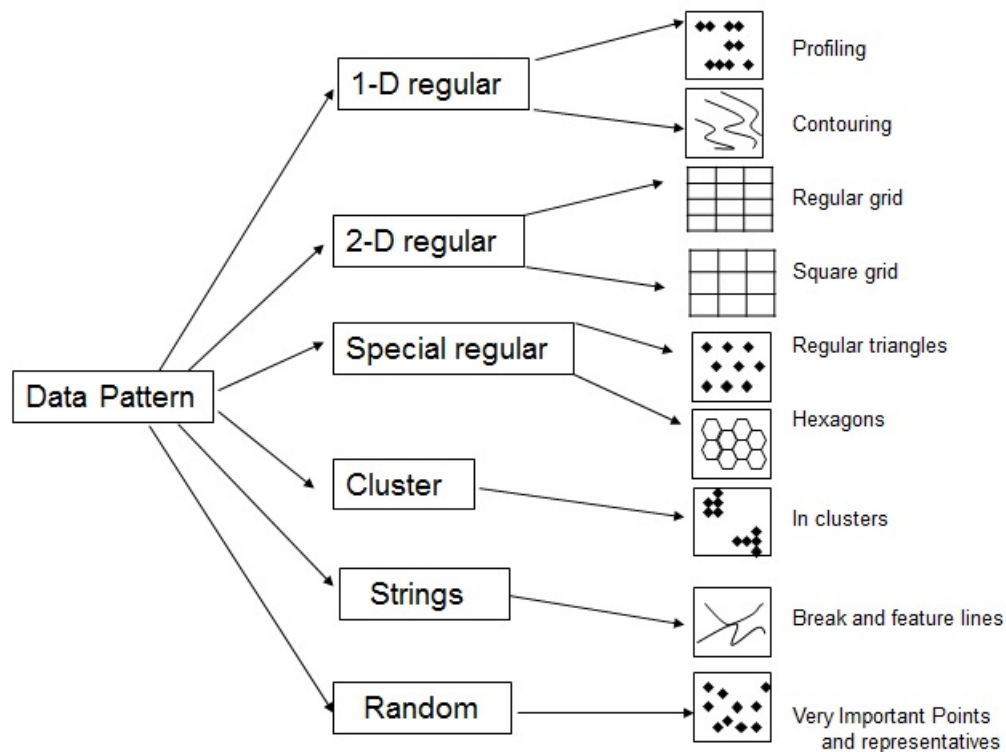


Figure 1.7: Pattern of sampled data points (Li et al., 2005).

Irregular patterns on the other hand include random, cluster and string data. When the measured points are located randomly, that means not in a specific form, the data pattern is called random; when the measured points are clustered, the data are clustered; this is very used in geology. As for string data, although they are not located in a regular pattern, they follow certain features, such as break lines, datasets that are sampled along rivers, ridges and other feature lines belong to this pattern.

Density is another attribute of sampled data and it can be specified by different modalities, such as the distance between two points, the number of points per unit area, and so on. Distance between two sampled points is expressed by sampling interval or distance: if the sampling interval varies with the position, an average value can be used. In space domain the sampling interval is specified by the distance, in frequency domain it is characterized by the number of points per unit area.

Points on a terrain surface can be viewed in various ways from the different viewpoints inherent in subject such as statistics, geometry, topography, science,

etc. Therefore, different sampling methods can be designed and evaluated according to each of the following viewpoints (Makarovic, 1973): statistic-based sampling, geometry-based sampling and feature-based sampling.

From the statistical point of view, a terrain surface can be considered as a population and the sampling can be carried out randomly or systematically. In random sampling, any sampled point is selected by a chance mechanism with known chance of selection; in systematic sampling, points are selected in a designed way, each with a chance of 100% to be selected. From the geometric point of view, a terrain surface can be described by a regular or irregular geometric pattern: a common used method corresponding to 1-D pattern is contouring, while a 2-D regular pattern could be sampled using a square or regular grid, a series of contiguous equilateral triangles, or other regularly-shaped geometric figures. Finally, with the feature-based point of view, a terrain surface is composed of a finite number of points, and the information content of these points may vary with their position. Therefore surface points can be classified into two types: feature-specific points and random points. Points belonging to the former group are more important because they don't contain only the coordinate information about themselves but also implicitly represent some information of their surroundings. For example peaks are the summits of mountains and hills, so they have a set of lower points around them and, by contrast, pits are the bottoms of valleys, so they have a set of higher points around them. Lines which connect certain types of feature-specific points are called "feature-specific lines" and they include course lines, ridge lines, break lines and so on. Course lines connect points that are defined by a local minimum in height, ridges lines connect points that have the local maximum in height, and finally break lines connect points that present a sudden slope change.

1.3.1.1 Sampling strategies for data acquisition

Various sampling strategies have been developed to optimize the process as for example selective sampling, sampling with one dimension fixed, sampling with two dimensions fixed, progressive sampling and finally composite sampling. Selective sampling mimics field surveying, because with this procedure all the very important points (VIPs, the most significant field points) are selected and measured. In addition some more points are selected in order to guarantee a certain density of the data. The advantage of this method is that only a limited number of sampling points, but the most significant, is needed to represent the terrain surface with high fidelity. Contouring and profiling are two commonly used techniques in sampling with one dimension fixed. Contouring means sampling the data along contours; this operation is similar to the traditional contour measurement on the stereo model, but in the DEM data sampling all points in the contour are recorded in digital form and the point recording could be selective along a contour line;

obviously the height value in the Z dimension is fixed when measuring a contour line. If X is the fixed dimension, the floating mark on the stereo model moves along the YZ plane and the result is a profile on the YZ plane: this process is called profiling (Makarovic, 1979). On the other hand sampling with two fixed dimensions regular grid and progressive sampling procedures: in the regular grid sampling points are obtained in the form of a regular grid, setting the fixed intervals in both X and Y directions to form the plane grid; then, all the points of the grid nodes are measured.

The progressive sampling can solve the problem of redundancy which is present in regular grid sampling: the sampling is carried out in a grid pattern whose intervals change progressively from coarse to fine over an area. The procedure is performed in this way: first a set of grid points is measured at a low density; then the collected elevation values of these data points are analysed by a computer. The computer then generates the locations of new points to be sampled in the next run. This procedure is repeated until some criteria are satisfied. Progressive sampling can solve part of the redundancy problem that is inherent in regular grid sampling, but still there are shortcomings:

- the sampled data points have a high degree of redundancy in the proximity of abrupt changes in the terrain surface,
- pertinent features may be lost in the first run which has its wide spacing,
- the tracking path is rather long, which decreases efficiency.

In the composite sampling a regular grid sampling is combined with a selective sampling, taking advantages of the efficiency in measurement of the former and the effective in surface representation of the latter. In this way abrupt changes, such as break lines or ridges, are sampled selectively and the values and feature sampling points are added to the regular grid-sampled data.

1.3.1.2 Accuracy of sampled data source

The sampling process depends on distribution and density of the sampled data. Measurement is connected with accuracy: the accuracy of sampled data depends on the methods used for measurement, including which method is used, which instruments are used and which technique (field survey, photogrammetry or map digitalization) is adopted. For example in general data acquired by field survey are more accurate with respect to those acquired by map digitalization. Obviously there are some exceptions: for example in case the instruments used for field surveying have low accuracy and the maps are at large scale and have been digitalized by a very accurate instrument, it can happens that the data digitized from maps are

more accurate than those acquired by field survey. The type of instrument implies potential accuracy limitation and very accurate results can be obtained only if the used instruments have a very high quality.

The measurement can be done in static or dynamic mode. Static mode means the measurement is carried out for a certain time period, maintaining the measurement instrument fixed in the same position for all the time (an example is the static GPS). In dynamic mode the measurement is carried out dynamically: for example in the field survey using kinematic GPS, the GPS receiver is in motion, also in photogrammetry the measurement is carried out when the float marks are still in motion. In dynamic mode data are acquired with lower accuracy with respect to the static mode.

1.3.2 Techniques for DEM source data acquisition

A DEM can be considered as a set of points on the terrain surface. Each points is described by its horizontal coordinates (X , Y) and height (Z). These points are usually used to generate topographical contour maps, surface modelling, volume computation and engineering design work. Various techniques are available to collect data used for creating DTMs (Acharya et al., 2000):

- cartographic digitalization: digital data are obtained from information gathered from existing maps,
- ground surveying: includes data coming from traditional (topographic) or spatial (GNSS) survey techniques,
- photogrammetry: includes the aerial and satellite photogrammetry,
- Airborne Laser Scanning (ALS) and LiDAR (Light Detection and Ranging): they use ultraviolet, visible and infra-red region of the electromagnetic spectrum,
- Interferometric Synthetic Aperture Radar (InSAR or IfSAR): it uses two or more Synthetic Aperture Radar (SAR) images to generate maps of surface deformation or digital elevation.

1.3.2.1 Cartographic digitalization

The digitalization of documents and graphs (maps, sketches, photographs, paintings, etc.) has been widely spread during the last years. A good indication of the great extent of documents digitalization can be extracted by examining the number of funded Research Programmes and the total amount of funds given by the

national and international organizations such as the National Science Foundation of US and the Frame Programmes of EU.

Generally there are two cartographic digitalization techniques: the vector-based line following and the raster-based scanning. In both cases digitalization can be done either manually or by automated devices, as schematized in Figure 1.8.

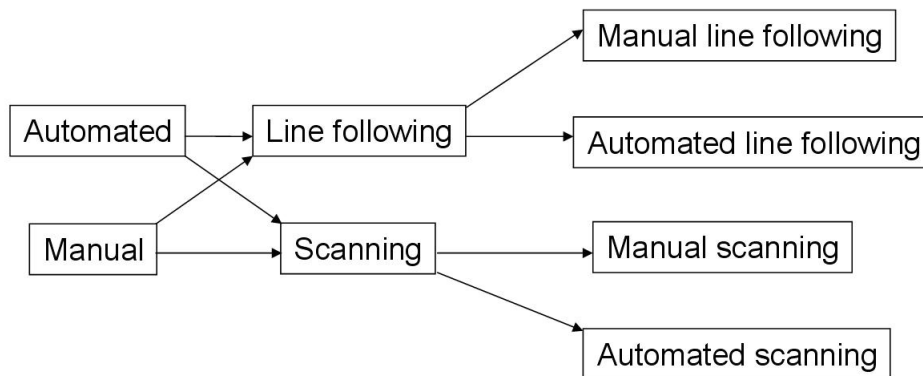


Figure 1.8: Schema of cartographic digitalization methods (Li et al., 2005).

The process of converting a paper map into vector format includes the following steps:

- digitalization of the map,
- removal of possible noise,
- detection, binaryzation and skeletonization of the contours,
- vectorization of the contours.

Manual line following is the most widely used method. Manual raster scanning means to superimpose a regular grid onto the map and then record whether contours pass through these grid cells. An example of map digitalization is shown in Figure 1.9.

In manual line-following digitalization, the map is carefully put onto the digitizer table and an operator traces the contour lines using a cursor with cross-hairs; coordinates are recorded in two ways, in stream mode or in point mode. In point mode digitalization, each time the operator presses a button, the x and y coordinates of the cursor position are recorded: in this case the operator has to decide which points are to be measured. Even if this is a tedious process, the advantage is that the operator controls the selection of points to reduce data volume. Stream

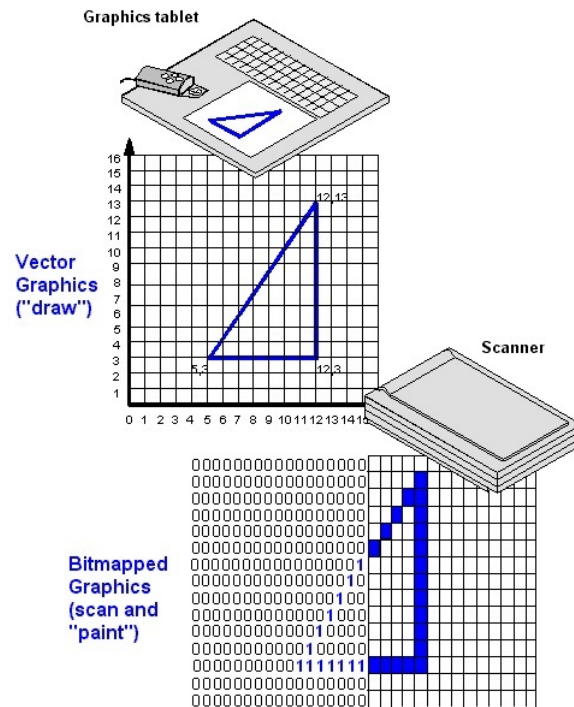


Figure 1.9: Example of map digitalization: the operator follows the borders of the triangle, and the image is automatically saved on the pc as a matrix of zeros and ones.

mode means that the tracing/measurement process is carried out dynamically and is thus less accurate; the points coordinates are recorded, while the cursor is moving along the contour lines. The disadvantage is that the operator does not need to execute the line following and so there may be a big data redundancy. Data points will be recorded at a certain intervals irrespective of whether the cursor is following the line well or is quite deviating from the line, which often happens at the turns of curves.

Also semi-automated devices for line following are available but they are very expensive. Semi-automated line-following devices have been developed to overcome the manual line-following digitalization problems; the process is semi-automated because an operator is still required to supervise the system and to execute some initial operations such as the initial positioning of the device on contours, guiding the device through areas of closely packed contours and cliffs, inserting contour elevation values, etc. In both cases, either the digitalization has been done manually or semi-automatically, data obtained by digitalization are in the digitizer coordinate system and must be transformed into a geodetic coordinate system, applying an affine transformation.

On the other hand, raster scanning makes fully automated digitalization possible. Each line scan is divided into resolution units and for each unit the scan provides different returns whether or not a contour line is present: in binary code, a 0 is recorded if nothing is present, a 1 is recorded if there is a line. Scanners for cartographic scanning have high resolution; the amount of data is very huge and there is redundancy. The vectorization, which can be manual or automated, is then required: in manual vectorization an operator carries out line-following digitalization on the scanned map visualized on a screen, automated vectorization is instead done with algorithms.

1.3.2.2 Ground survey and GPS

Land surveying by using Total Station is the conventional method that has been used for decades for high resolution elevation data collection, even if it requires intensive work by at least two operators, is very slow in term of survey speed and requires inter visibility between stations. A modern Total Station is an electronic device that combines the ability to measure a position horizontally and vertically at the same time. It is composed by two parts, a machine mounted on a static tripod and a prism (the target) on a metal support, which is moved around the site. The tripod is set up at a base station, usually a point that can be seen from as much as possible of the survey area. Several base stations may be needed to cover the survey area. The coordinates of the base station are inserted into the machine (they are calculated before the survey begins) as well as the direction to grid North and the heights of both the tripod and staff. The prism is then carried around the site and positioned vertically each time at a recording point. The machine mounted on the tripod sends out a light signal, which bounces back from the prism giving a time interval that is used to calculate the distance between the station and the target. The Total Station has a microprocessor which automatically collects these angle and distances measurements, calculates the trigonometrical equations and converts them into grid coordinates.

Global Positioning System (GPS) offers an alternative where relatively less operator work is needed for the survey, no inter visibility between stations is required and terrain information can be directly obtained. GPS, initially developed for military use, is used today for positioning purposes and measurement of the Earth surface: it is used in mobile phones, in car navigation, in search and rescue equipments, etc. GPS is commonly used also for surveying because it gives a position directly, without the need for measuring angles and distances between intermediate points. The equipment and calculations are quite complex, but for the user the process is generally very simple. The GPS system is composed by three parts (as shown in Figure 1.10): the space segment, the ground control system and the user segment.

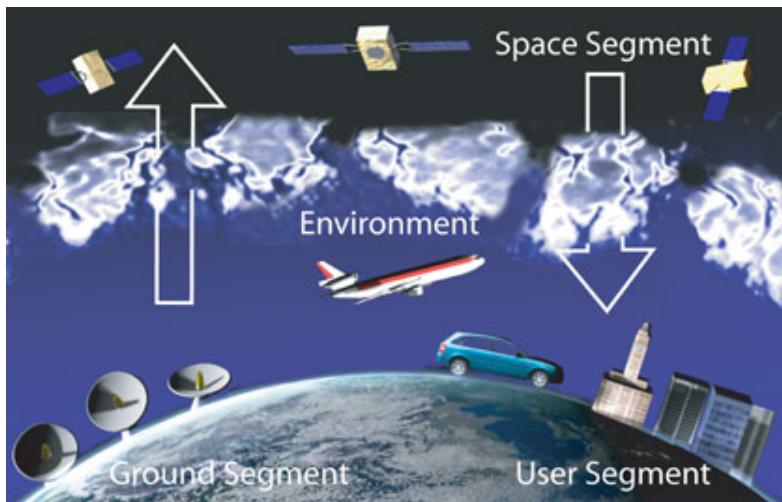


Figure 1.10: GPS system: space segment, ground control system and user segment.

Space segment refers to the GPS constellation of 32 satellites (nominally 24), that orbit at about 20'000 km above the Earth surface and continuously broadcast measurement signals and navigation messages to the GPS users (Biagi, 2009). Each satellite continuously transmits messages that include:

- the time the message was transmitted,
- broadcast orbital information (the ephemeris) of all the GPS satellites,
- the general system health.

These information are transmitted by two different electromagnetic waves, or carriers (L_1 and L_2), that are modulated with pseudo-random signals that, properly decoded, contain the above-mentioned messages.

The control segment consists of ground stations that manage the satellite constellation. It is composed by: one master control station located in Colorado, five monitor stations spread all over the world, and three ground antennas. The master control station collects the signal coming from the satellites tracked by the monitor stations; these information are used to compute and predict the satellite orbits, that are then sent to the satellites that will distribute them, and to monitor the status of the system.

The user segment consists of receivers used by the final users: they can be hand-held, mounted in cars, installed on aircrafts, ships, or put on a tripod, which is the case of field surveying. A GPS receiver consists of hardware and software for receiving, decoding, storing and processing the signal from the satellites. The GPS receiver computes its position by timing the signal sent by GPS satellites.

The basic principle of GPS-based measurement is in fact range detection. To determine an unknown position in 3-D space, three distances from three known points are needed. These distances, between satellite and the unknown receiver, can be obtained by measuring the time (τ) needed by the signal to travel from the satellite to the receiver; knowing the propagation velocity (c) of the signal through the path, the distance is easily computed as $D = c\tau$. To solve the receiver position, at least three satellites/distances must be available. Considering that the clock device mounted on the receiver is not exactly aligned to a common reference time scale, another distance is needed to estimate also the clock offset. That is why the GPS constellation was designed in order to guarantee at least four visible satellites from every place of the Earth.

GPS uses two type of measures: pseudorange and phase. The pseudorange measure is performed through the correlation of the binary signal transmitted by the satellite; it is very simple to use because it is almost a direct measure of the distance, but it has a precision only of 30 centimeters. The phase measure on the other hand is done measuring directly the electromagnetic wave (carrier), which has a precision of 1 millimeter. The problem is that due to the short wavelength (19 cm for L_1 and 24 cm for L_2), only the phase can be measured, it means only the fraction of the last wave arrived to the receiver. The distance is composed not only by this term, but also by the integer number of cycles of the wave, that cover the distance between the satellite and the receiver. This term, called Initial Ambiguity, represents the main problem of the processing of this type of observation. In fact a precision of the order with a magnitude of 1 mm can be obtained only in case the integer number of cycles is correctly estimated. For this purpose a lot of positioning methods that uses the phases exist, as for example the RTK relative positioning (Grejner Brzezinska et al., 2005).

GPS data are affected by a great number of different errors, related to different causes. Instrumental errors are those resulting from the functional modalities of satellites and receivers; they are due to the intrinsic precision that the devices are able to provide in the different measure modalities (pseudo-range or phase measures). Instrumental errors are:

- satellites clocks offset, which can be eliminated by the creation of opportune differences between observations,
- receiver clock offset, which can be eliminated by performing simultaneous observations from at least four satellites and another receiver,
- state of poor health of one satellite, eliminated by discarding the information of that satellite,
- noise of the receiver, which is not eliminable.

Other errors exist, related to the modality of use of the system and of execution of the observations. These errors can be quantified by their effect on the satellite-receiver distance and, since they are greater than the instrumental errors, have to be eliminated or minimized. Among these errors there are: model errors and observation errors.

Model errors (biases) are systematic errors present both in the pseudo-range and in the phase measures. They are the already explained ambiguity biases of the carrier waves, and those caused by the indetermination of the satellite orbit or by a perturbation of the signal during the propagation through the atmosphere (tropospheric and ionospheric errors). Tropospheric errors can reach 1-10 m, while ionospheric even 100 m.

Observation errors are accidental errors which occur during the acquisition of the signal by the receiver. Some of these errors cannot be eliminated, but they can be minimized by using proper techniques and procedures. They can be:

- Cycle slips: they are interruptions on the reception of the signal during a measurement session. They can be due to high signal noise or to a temporary obstruction of the line of sight receiver-satellite. During a session, until the carrier waves are received without interruption, a single unknown ambiguity is generated for each receiver-satellite couple. When an interruption of the signal occurs, at the time of the hang up of the signal, the fractional part of the phase measure is equal to the one that would be obtained if no discontinuity was present, but the number of cycles elapsed between the beginning and the end of the interruption is missing; this entire number of cycles represents the entity of the cycle slip.
- Multipath: it is a phenomenon that gets the signal/noise ratio worse and is due to the simultaneous reception of both the signal coming directly from the satellite and of other signals reflected from some surfaces surrounding the GPS antenna (woods, buildings, etc.). In order to remove this problem, the antenna has to be located in an open area, away from reflective surfaces, and/or equipped with special protections (radome). Multipath can affect the distance up to few centimeters.
- Variation of the antenna phase center: it is due to the fact that antennas cannot receive in an isotropic way signals both in azimuth and zenith directions; in fact the same signal received by two identical antennas, but differently orientated, generates different measures. This problem can be removed using antennas of the same type and orientated in the same direction, or by using proper models antenna-dependent that have been recently become available.

It is possible to carry out GNSS measurements in different modalities, to which different accuracies correspond. The most used are:

- **Absolute positioning or point positioning:** it is performed with a single receiver using the code and/or phase of the GNSS signal. The position of the point can be obtained in real time using a single epoch, as for example in case of cinematic or navigation, or occupying the same point for many epochs with a long measurement. In the first case the position accuracy is of the order of 10-15 meters, in the second case the accuracy can reach ten centimeters (with a static measurement that last for some hours), because bias or errors are reduced by redundant observations.
- **Differential positioning or DGPS:** it is operated with a single receiver using only the first frequency, but at the same time, also differential corrections transmitted by a second receiver with known position are acquired. The corrections give information useful to reduce biases and errors. The coordinates estimated in real time positioning have an accuracy of the order of 0.5 meters.
- **Relative static positioning:** it is performed using at least two receivers, one of which is located in a known position; the receivers have to be maintained in the same position for the entire measurement session (the duration can span from some minutes to some hours). In all points both the phase and the code of the GNSS signal are acquired (raw data) and then, through a post-processing elaboration the positions of the unknown receiver is estimated with respect to the reference, as a baseline. By differencing the observations, in fact, many errors and biases that the receivers have in common are reduced or eliminated. The measurement schema usually contemplate the realization of a network of baselines that connect known points and unknown points, whose coordinates have to be estimated. A GNSS permanent network service is often used as reference. This method is suitable for all measurements which require high accuracy and reliability, such as networks monitoring, photogrammetry and deformation monitoring. The accuracy of the baselines components depends on the baseline length and on the length of the session, and it can reach few millimeters.
- **Relative RTK positioning:** in this modality two receivers are used, the former is kept fixed on a points with known position (called “base” or “reference”), while the latter (called “rover”) is in motion and occupies points at unknown positions. The base receiver transmits to the rover the code and phase correction data estimated in real time and that contain information useful to reduce biases and errors, by which the position of the rover can be

instantly estimated in real time. The data transmission can be done through a modem GSM, internet, or radio. The coordinates accuracy has a magnitude of few centimeters. If the raw data acquired by the base and by the rover are kept, it is also possible to perform a control elaboration in post processing. The RTK technique is convenient in GNSS surveys where a lot of points have to be measured with a high accuracy; it can be used also in kinematic mode for the determination of the path of moving vehicles. An example of RTK measurement is shown on Figure 1.11.

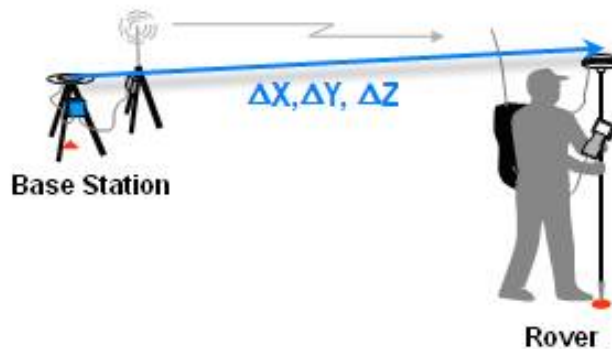


Figure 1.11: RTK GPS survey: the system is composed by two receivers, base and rover, and some GPS satellites.

One of the drawbacks of using GPS and in particular RTK GPS is that its performance depends on the level of the so called satellite visibility, which is a parameter that signs the area openness so that the GPS signal can be directly tracked by GPS receiver without being disturbed or being blocked by obstructions (building, trees, etc.). The quality of GPS data is proportional to this parameter: better the satellite visibility, better the GPS positioning can be done. Also the quality of the DEM obtained from GPS data is related to this parameter. In fact one of the important factors that should be considered in using DTM is the quality characterization of the DTM itself. Also the configuration of the satellites in view is important for the accuracy: in Figure 1.12 examples of a good and bad configurations are shown: satellites should occupy all the sky above the receiver as homogeneously as possible.

In relative positioning the accuracy depends on the length of the baselines, because the residual tropospheric noise is greater when the atmospheric conditions of the two receivers positions are very different, and so the longer is the base, the worse is the achievable accuracy of the measures. In medium atmospheric

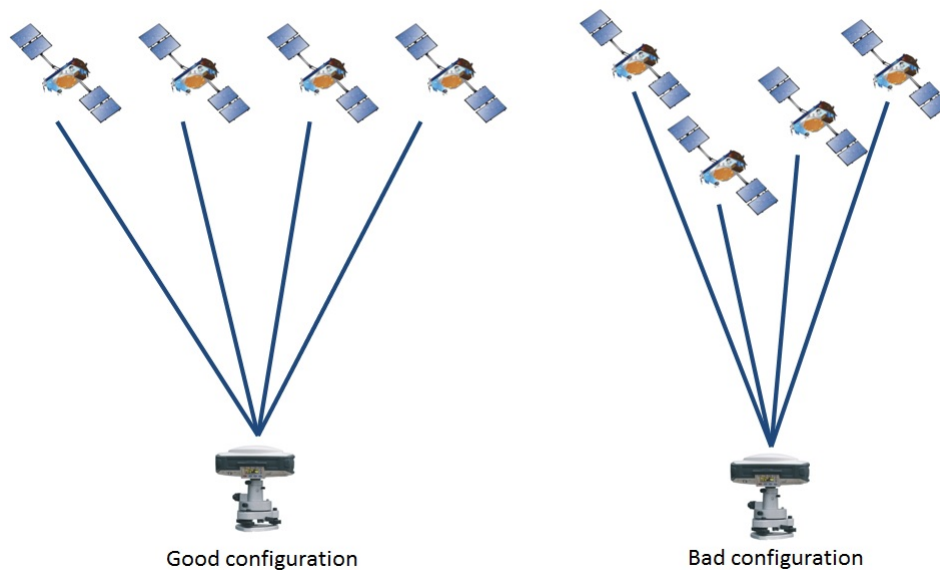


Figure 1.12: Absolute positioning: good (on the left) and bad (on the right) satellites configurations.

conditions, the achievable accuracies of RTK for example are 1 cm, 10 cm, 50 cm and 1 m with baselines 1 km, 10 km, 50 km and 100 km long.

In Table 1.1 (Biagi, 2009) the best accuracies achievable with the different GNSS positioning methods are summarized.

Survey type	Accuracy	Notes
Absolute kinematic in real time	from 10 m to 1 m	According to the receiver types and new signals availability
Absolute static in real time	10 cm	According to the research topic
Relative kinematic in real time or post processing	From 1 m to 2-5 cm	According to the receiver type and the distance between reference and rover
Static relative and post processing	Better than 1 cm	By very long surveys

Table 1.1: Achievable accuracies with the different GNSS positioning modalities.

1.3.2.3 Photogrammetry

Photogrammetry is the art, science and technology of obtaining reliable information about physical objects, and the environment, through the process of recording, measuring and interpreting images and patterns of electromagnetic radiant energy and other phenomena (ASPRS, 1980).

Although many photogrammetric theories date back more than a century, the use of digital photogrammetry in extracting information has developed for the last 40 years. The processing of films is usually made by analytical plotters, while digital data are processed by Digital Photogrammetric Systems (DPS). The processing algorithms are being continuously developed (Kraus, 2007). Intensive research for the automation of information extraction from digital images, based on image analysis methods, has been carried out for the last 40 years.

One standard method used in photogrammetry is to split the field based on the camera location during photography. On this basis there are aerial photogrammetry and close range photogrammetry. The main products are Digital Elevation Models (DTMs or DSMs), ortho-images, 2-D and 3-D reconstruction and classification of objects for mapping or thematic applications, visualizations maps, 3-D views, animations and simulations (Baltsavias, 1999).

In aerial photogrammetry the camera is mounted on an aircraft and is usually pointed vertically towards the ground and multiple overlapping photos of the ground are taken while the aircraft flies along its flight path. The collected photos are then processed in a stereo plotter; this instrument allows the operator to view at the same time two photos in a stereo view. To create a DEM in automated processing these photos are used. In close range photogrammetry, the camera is near the subject and is typically hand held on a tripod. The output of this kind of photogrammetry is a drawing or a 3-D model. Usually this kind of photogrammetry is used to model buildings, engineering structures, forensic and accident scenes, etc.

The fundamental principle of photogrammetry is to make use of a couple of stereo-pair images to reconstruct the original shape of the 3-D objects, that is, to form the stereo model and then to measure the 3-D coordinates of the objects on the stereo model (Whitmore and Thompson, 1966). A stereo-pair refers to two images of the same scene taken at two slight different places so that they have a certain degree of overlap. An example is shown in Figure 1.13. Actually, only in the overlapping area the 3-D model can be reconstructed. In aerial photography, generally there is a 60% overlap degree in the flight direction and 30% between the flight strips; where the ground is very mountainous the side lap must be up to 50%. The same consideration can be done for the overlap between two frames: in flat area the overlap percentage can be equal to 60%, but in mountainous area it should be increased up to 85%.

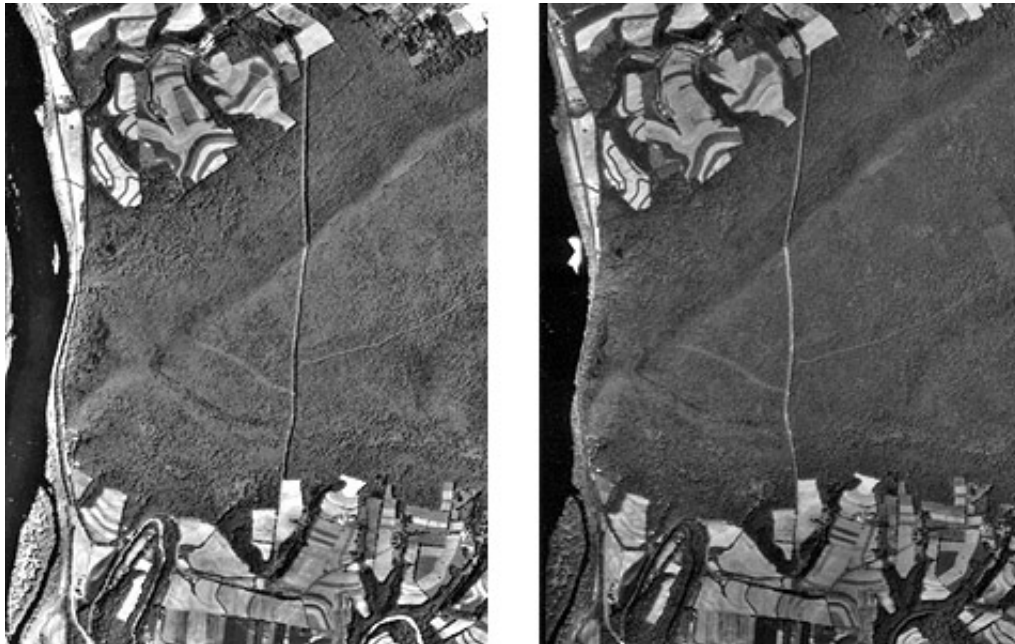
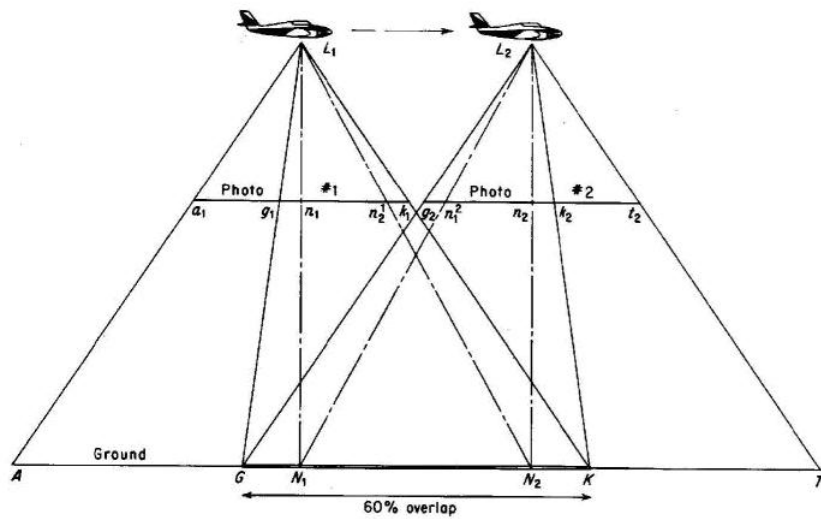


Figure 1.13: Example of stereopair: the images cover the same area with a certain overlap (Liu, 2010).

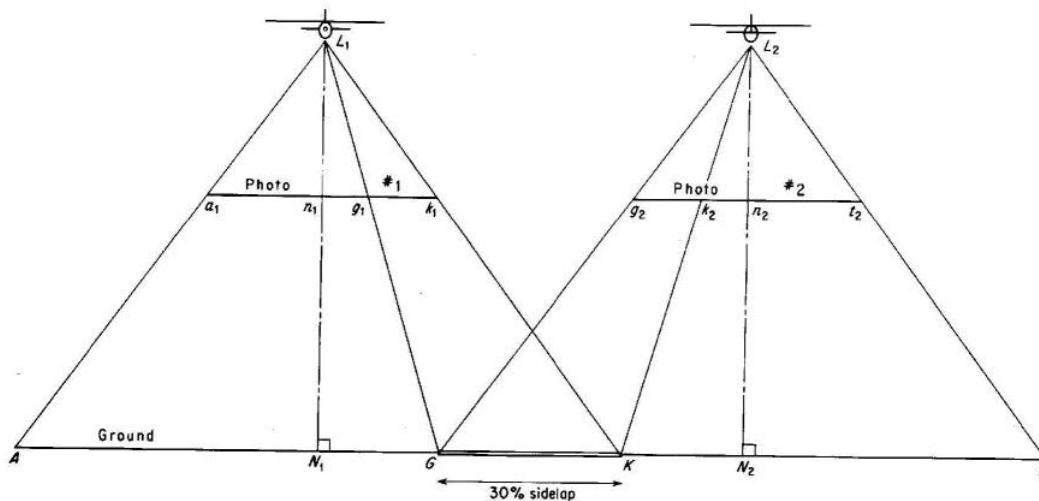
Each photograph is characterized by six orientation elements: three angular elements (one for each of the X , Y and Z axis) and three translations (ΔX , ΔY and ΔZ coordinates, usually in a geodetic coordinate systems). Any two images with overlap can be used to generate a stereo model. Space images can also be used to reconstruct stereo models; in this case the percentage of overlap is not so standardized.

Figure 1.14(a) reports how an overlap of photographic coverage is obtained while the airplane is moving along a flight line: from position L_1 , the area AK is photographed, while from position L_2 the area GT is photographed. As a consequence, the overlap area between the two images is the area GK, which represents an overlap degree of 60% with respect to the overall area. The nadir points N_1 and N_2 are included in the overlap area thus appear on both photographs. Figure 1.14(b) shows how a side lap in a photographic coverage is formed: at position L_1 the plane, flying towards the reader, photographs ground area AK. At position L_2 , the plane, flying away from the reader, photographs the area GT. The common area, that is the overlapping area between flight strips, is GK and it represents the 30% of the overall region.

Figure 1.15 shows an example of an overlap photography: the overall area is VWYZ, ground points N_1 and N_2 are the nadir points of the two photographs. The ground point P which is located in the midway between N_1 and N_2 , is the so



(a)



(b)

Figure 1.14: Photographic coverage: overlapping between photograms (a) and overlapping between flight strips (b).

called “stereoscopic perspective center”.

The degree of automatization and digitalization of the processing work is now quite high. All the automatic procedures measure blindly a spatially homogeneous field of generally highly redundant points, with the only exception of feature based matching, which in low texture areas can have few points. On the other hand manual photogrammetric measurements offer a high flexibility in the selec-

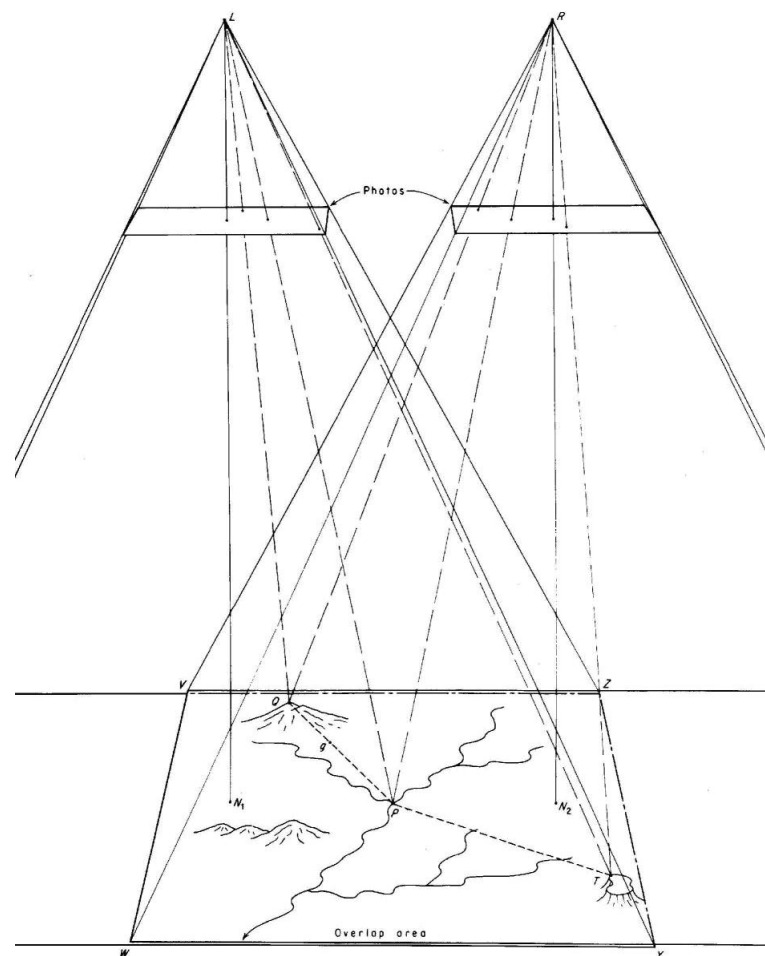


Figure 1.15: Example of overlap photography (Liu, 2010).

tion of measuring mode (raster, profiles, contours, etc.), a selective measurement (much less and almost non-redundant points) and an explicit modelling of characteristic geomorphological lines and points, that are crucial for obtaining a high accuracy DEM. Automatic methods, if the points are dense, measure the features only partially, at the cost of a high and redundant data volume. The automation of break-line detection is easy with images, because the grey level edges can be used as indicator of surface discontinuities. The high redundancy of automated methods can be useful to better model objects, filter errors, etc.; however, after these processes have been performed, an intelligent data reduction or compression is necessary, otherwise data amount explodes avoiding to be processed by most commercial packages (Baltsavias, 1999).

The quality assessment of photogrammetric products is well established and

the limits of photogrammetric methods are known. For example, when using film, specialized and expensive hardware, like image scanners or analytical plotters, is required. Today the research is focused on automation of feature extraction and further advancements in DTM generation and digital aerial triangulation are very slow but necessary, because the already implemented algorithms of commercial systems are partly insufficient.

1.3.2.4 LiDAR

Traditional methods such as field surveying and photogrammetry can yield high-accuracy terrain data, but they are time consuming and labour intensive. In some situations as for example in forested area with dense vegetation, it is impossible to use these methods for collecting elevation data, mainly because there is not directly visibility of the terrain from above. Airborne Light Detection and Ranging (LiDAR), called also Airborne Laser Scanning (ALS), is a good alternative for collecting high density and high accuracy three dimensional terrain point data.

Lasers as remote sensing instruments have been used for 30 years, for example in fields such as lunar laser ranging, satellite laser ranging, atmospheric monitoring and oceanographic studies. Researches and design on LiDAR for topographic data collection started from the '80s (Krabill et al., 1984). Commercial airborne LiDAR systems have been operational since the mid '90s, and they continue to represent an active research area. Over the last decade more reliable and accurate LiDAR systems have been developed and they have been used for the generation of DEMs.

LiDAR is an active remote sensing technique where a short laser pulse is sent out and the deflection angle as well as the round trip time of echoes are recorded (Lemmens, 2007). Multiplying this round trip time with the group velocity of the laser (approximately the speed of light) the estimation of the 3-D coordinates of the scanned targets is allowed.

LiDAR is composed by three components:

- the aircraft position, determined by kinematic dual frequencies GPS, typically at 1 second,
- the aircraft orientation or attitude, continually monitored by a sensitive Inertial Reference System (IRS), typically at 50 times per second,
- the terrain measurement device, that emits a number of discrete laser beams (typically 50000 to 25000 per second), measuring the time taken by the beam to reflect from the ground back to the aircraft.

The laser scanner consists of a pulse generator of laser and a receiver to get the signal of scattered and reflected pulses from targets (Pfeifer and Briese, 2007;

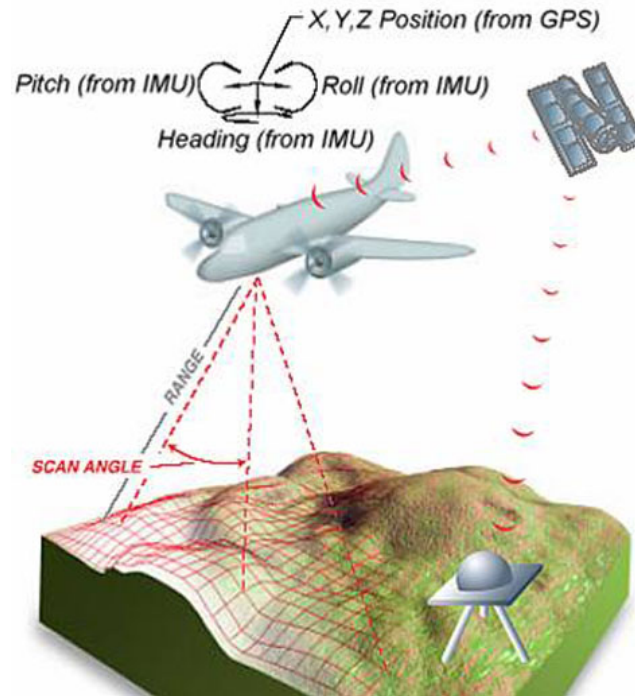


Figure 1.16: Components of LiDAR system: aircraft with an on-board IRS and a laser scanner, GPS satellites and GPS base station on the ground to know the position of the aircraft.

Wehr and Lohr, 1999). The laser pulses have a wavelength in the range of 0.8μ to $1.6 \mu\text{m}$, they are 4 to 5 ns in duration and have a peak energy of several millijoules. Laser pulses are emitted at a rate up to 250 kHz to the Earth surface. The distance between the LiDAR sensor and the object can be calculated by multiplying the speed of light by the time the signal takes to reach the target and return to the sensor.

As discussed in the previous section, in photogrammetry some perspective images are taken from different positions; if the interior geometry of the camera, the relative position and attitude of the images at their exposure times are known, the intersection of the images rays yields the spatial coordinates of the corresponding point. For each point, at least two observations are needed. Photogrammetry is a passive technique, thus dependent on sunlight in natural environment. Moreover, in aerial photogrammetry, where the camera is mounted on an airplane and it looks to the nadir direction, clear sky conditions are needed, too. In contrast to this, LiDAR is an active technique thus neither dependent on sunlight nor on clear sky. In addition, since all the three coordinates are observed at the same time, one single scan is sufficient to compute a three-dimensional point cloud of the whole

object if it is visible from one viewpoint.

LiDAR data have become a major source of digital terrain information, and are used today in many areas such as building extraction, 3-D urban modelling, hydrological modelling, glacier monitoring, soil classification, river bank or coastal management, etc. However, terrain modelling has been the primary focus of most LiDAR missions (Hodgson et al., 2005). Today LiDAR is one of the most used method for terrain data collection: in fact with LiDAR, data with high energy and high accuracy can be generated. Compared to photogrammetry, due to LiDAR capability of canopy penetration, DTMs generated from LiDAR data can overcome the limitations of photogrammetry in forested areas. Kraus and Pfeifer (Kraus and Pfeifer, 2002) demonstrated that the accuracy of LiDAR derived DTM in forested areas is similar to that of photogrammetry derived DTM in open areas. LiDAR is also useful in DTM generation in urban areas because LiDAR data are free of shadow.

Airborne LiDAR technology is still developing rapidly in both sensor and data processing with the focus aimed to increase laser frequency in order to collect more data points. High density data allow to represent the terrain in much detail, but this leads to a significant increase of data volume, imposing challenges also in the storage, processing and manipulation of the big amount of data. Because of the specific characteristics of LiDAR data, issues such as the choices of modelling methods, interpolation algorithms, grid size and data reduction are challenging study topics for the generation of a high quality DTM from LiDAR data.

Raw LiDAR data, that means the data as collected by the sensor, can contain return signals from each target the laser beam happens to strike, including human made objects (buildings, telephone poles, and power lines), vegetation or even birds, so actually the LiDAR allows to obtain also very accurate and high resolution DSM (Barber and Shortrudge, 2004). In order to obtain a DTM from LiDAR data, all the features (buildings, trees, etc.) have to be automatically detected and discarded from the previous DSM. At this purpose one of the most critical step is to separate the LiDAR points into ground (terrain) and non ground (non terrain) points: this process is called LiDAR filtering or extraction. Various filter methods exist, but none of them is 100% accurate and as a consequence a manual editing of the filtering results is still needed. Several filter algorithms have been developed for automatically extracting ground points from LiDAR point clouds. Tovari and Pfeifer give a classification of the filter algorithms (Tovari and Pfeifer, 2005):

- morphological or slope-based algorithms: these algorithms use height differences to recognize points belonging to objects. The classification is done using a threshold that determines the admissible height difference between two neighbour points such that one can be considered as bare ground. This approach can use also a fixed slope or gradient threshold instead of height

differences,

- progressive densification algorithms: these filters identify some points belonging to the ground and then, depending on those, classify more other points as ground. Usually the points used as seed are the ones with lower height. Additional ground points are determined by investigating their neighbours in the reference surface,
- surface based algorithms: these filters use a parametric surface that iteratively approaches to hypothetical bare soil. The surface is modified depending on the influence of the individual input points,
- clustering-segmentation algorithms: these filters are based on the idea that a cluster of points belongs to an object if its height values are greater than its neighbours. In these cases the classification is done in two steps, first a segmentation is performed and then the segments are divided in different classes depending on the differences in height between segments.

The filtering algorithms depend only on the geometric characteristics of LiDAR point data. In order to increase the accuracy and reliability of the filtering process, additional information such as intensity and derivatives from full waveform have to be used; for example the intensity of the laser beam response can be used in order to estimate and improve the position of the edge between areas with different reflectance properties.

With the new LiDAR sensors, range accuracy can reach 2-3 cm (Lemmens, 2007). The GPS receiver records the aircraft trajectory and the IRS unit measures the attitude of the aircraft (roll, pitch and yaw). The calculated range between the scanner and the target, and the position and orientation information collected from the GPS and IRS allow to determine the target location in 3-D space. The accuracy of the collected LiDAR points depends on the GPS and IRS accuracy. Airborne GPS is able to yield results 5 cm horizontally and 20 cm vertically accurate, while IRS can generate attitude with accuracy within a couple of centimeters. As a result LiDAR data can have accuracy equal to 15 cm Root Mean Square Error (RMSE) in height and 20 cm RMSE in planimetry.

Other important developments of airborne LiDAR systems include the integration of a high resolution digital camera with a LiDAR system. For each collected digital image, the position and orientation of the camera can be obtained by using the GPS or IRS data. Exterior orientation parameters for each frame of imagery are directly provided by these position and orientation data. No stereo overlapping images and ground control points are needed (Ackermann, 1999).

1.3.2.5 SAR

Synthetic Aperture RADARs (SARs) produce all weather, day and night, high resolution images of the Earth surface, which can be used for many applications:

- topographic maps,
- urban areas analysis,
- hydrological studies,
- landslides monitoring.

SAR is composed by a conventional RADAR mounted on a moving platform (airplane or satellite) (Ferretti et al., 1998). The RADAR antenna, pointed down to the direction of motion of the platform, allows to illuminate a portion of the terrain, by emitting short direction pulses at regular intervals during its movement along the predetermined path. The electromagnetic signal, sent by the antenna, is reflected by targets on the ground and by the soil itself.

The electromagnetic signals, characterized by frequencies between 500 MHz and 30 GHz, received at the different positions by the antenna, are then processed in order to obtain information about the targets. This process, which requires a lot of computational resources, is usually done a posteriori. The result is a reflectivity map containing information about the phase and amplitude of the registered signal: amplitude information are very useful because they contain indications about the soil coverage (Graham, 1974).

The main advantage of SAR with respect to usual optical systems is related to the capability of operating during night and also with cloud coverage, because the microwaves emitted by the RADAR have a wavelength greater than optical waves and they can penetrate clouds. In addition, compared to traditional RADAR systems, SAR allows to obtain images with a better spatial resolution. The movement of the platform with respect to objects fixed on the ground is used to synthesize via computer a antenna with much bigger dimensions than the physical antenna mounted on the aircraft. SAR observations collected on the different sensor positions are then combined in order to obtain a high resolution image: this process is called focusing. These are coherent images, it means that images contain information about intensity (related to targets reflectivity) and phase (related to the distance between the target and the RADAR).

By combining two or more SAR images of the same area, it is also possible to generate elevation maps and surface change maps with high precision and resolution. This technique is called SAR interferometry, also abbreviated InSAR or IfSAR. InSAR is an active technique with sensors that transmit pulses of electromagnetic energy and record the backscattered signal to derive the spatial position

of the survey target. InSAR sensors are usually installed on a fast moving aircraft which can also fly at high altitudes. Usually a two-side looking antenna (separated by a known baseline) are mounted on it. In this “single pass” configuration, the first antenna transmits radio waves and both antennas receive the backscattered signal. This configuration enables the system to scan the same target simultaneously from two different antenna positions. Advanced SAR data processing enables the system to generate a pair of high resolution images of the same scene. Each pixel preserves amplitude and phase of the backscattered signal. These information are exploited in the interferometry process where both images are differentiated. The resulting phase differences are then unwrapped and converted to heights and finally a DSM is generated. The same product can be obtained using a “repeat pass” configuration: in this case images are acquired from a single antenna at different times and then processed to obtain a DSM. However the simultaneous acquisition has significant advantages as the mitigation of temporal decorrelation that improves data quality.

SAR images can be affected by some geometric deformations. “Foreshortening” occurs when the radar beam reaches the base of a tall feature tilted towards the radar (for example a mountain) before it reaches the top. This effect can be seen in Figure 1.17(a). For this reason objects that are located in an area with slope parallel to the signal sent by the antenna are all represented in the same resolution cell. “Layover” occurs when the radar beam reaches the top of a tall feature before it reaches the base. The return signal from the top of the feature will be therefore received before the signal from the bottom. As a result, the top of the feature is displaced towards the radar from its true position on the ground, and lays over the base of the feature (Figure 1.17(b)). The last effect is “shadowing”: shadows on the image are present when the RADAR beam doesn’t illuminate a portion of the ground, as for example the terrain behind vertical objects or behind a mountainside (Figure 1.17(c)).

Sometimes InSAR elevation data are noisy and also some biases may exist, because of InSAR sampling cell contains individual (volume) scatters both on the ground and above. This happens principally in urban and forested areas where, for example, a building or a tree together with ground is present in a single sampling cell. On the other hand, the long wavelength of the InSAR system offers its biggest advantage as it can penetrate through clouds, haze and dust. This means that InSAR can operate virtually under all weather conditions. By using different wavelengths, the system penetration capabilities can be altered. For example, the X-band reflects the vegetation where P-band penetrates it to the ground.

Making a comparison between InSAR and LiDAR, the processing of InSAR data is more complex than LiDAR data. In fact the processing of InSAR data requires highly sophisticated software and, as in case of LiDAR, the process of trained data has to be done by an operator. Some system and processing errors are still

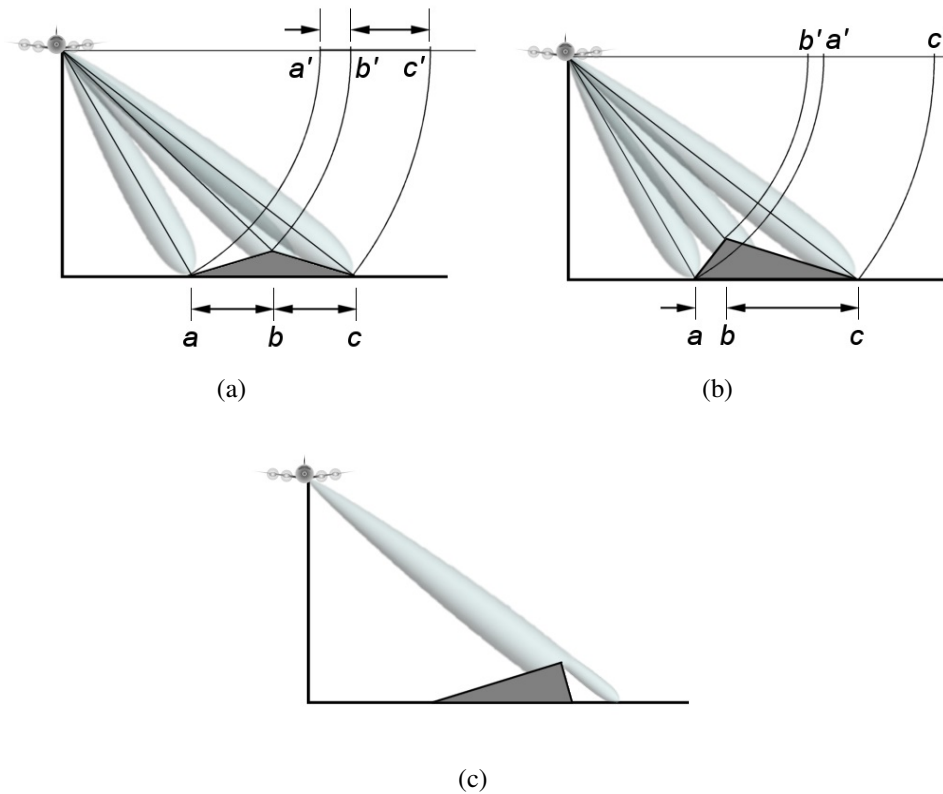


Figure 1.17: Geometric distortions. Figure (a) - Foreshortening effect: the RADAR measures distance in slant-range, the slope (from point a to point b) will appear compressed and the length of the slope will be represented incorrectly (a' to b') at the image plane. Figure (b) - Layover effect: the RADAR beam reaches the top of the feature (b) before it reaches the base (a); the top of the feature is displaced towards the radar from its true position on the ground (b' to a'). Figure (c) - Layover effect: the radar beam is not able to illuminate the portion of the terrain behind a vertical object or a mountainside.

problematic and are present in the data as noise. Although both systems are in principle capable of recording more data along a single range (LiDAR records more than one return, InSAR uses multiple frequency and polarization) in principle, they capture digital surface definition (as can be seen in Figure 1.18) and further processing is required to extract digital terrain definitions. Many algorithms have been developed to automate this process; however none of the available algorithms are fully reliable and an expensive and time consuming manual data filtering is still required. InSAR allows to generate maps of surface deformation, with a potential accuracy of few centimeters, or digital elevation also at the global scale (to produce global DEMs). This technique can potentially measure centimeter-scale changes in deformation over spans of days to years. An example

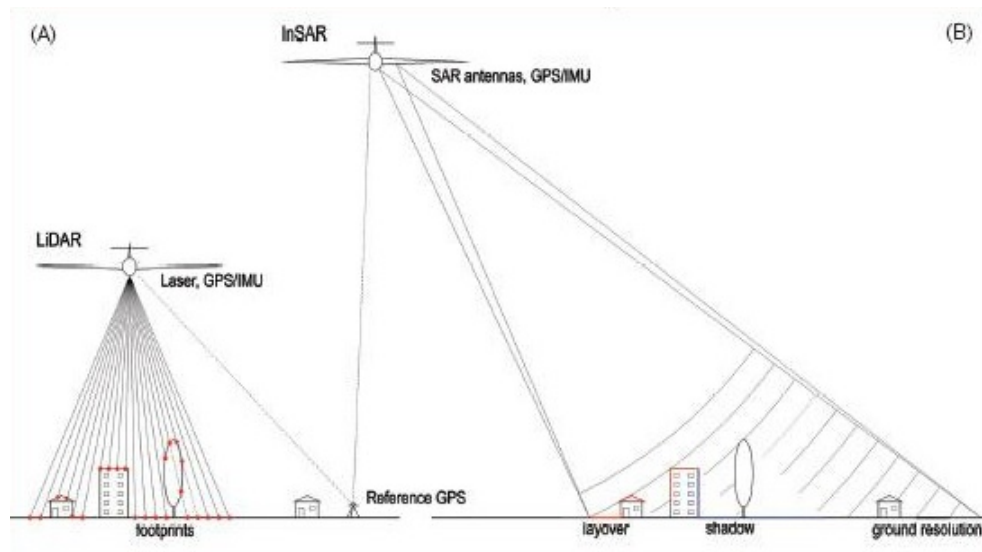


Figure 1.18: Comparison between LiDAR and InSAR.

of InSAR global scale product is the SRTM global DSM, described in detail in Section 1.6.1.1.

1.3.2.6 Comparison between DEM data from different sources

All the acquisition methods described in the previous sections have advantages and disadvantages. Therefore, when choosing a method, various aspects such as purpose, accuracy requirements or conditions of the equipment should be considered. A comparison between these methods in various aspects, such as efficiency, cost and accuracy is reported in Table 1.2 (Li et al., 2005).

In terms of measurement accuracy, a millimeter-level can be reached by ground survey, centimeter level by photogrammetry and meter level by digitalization from maps. The accuracy of photogrammetric data depends on the used images: in case of space photogrammetry using satellite images, the accuracy could be very low, depending on the resolution. For example, if SPOT images with 10 meters resolution are used, then the accuracy ranges between 5 and 10 m. InSAR allows to reach an accuracy of 1 cm, and it is a good technique for deformation measurement. With ground survey and photogrammetric techniques, terrain feature points can be obtained if desired, therefore high fidelity to the original surface can be preserved by the digital data. In terms of efficiency, ground survey is more labour intensive and so it is suitable when high accuracy is required but the area to be measured is small. On the other hand, for medium or large area, photogrammetry is preferable because most of the processes are today automated and data acquisition is more efficient. For cartographic digitalization human work is needed dur-

Acquisition method	Accuracy of data	Speed	Cost	Application domain
Traditional surveying	High (cm-m)	Very slow	Very high	Small areas
GPS survey	Relatively high (cm-m)	Slow	Relatively high	Small areas
Photogrammetry	Medium to high (cm-m)	Fast	Relatively low	Medium to large areas
InSAR	Low (m)	Very Fast	Low	Large areas
LiDAR	High (cm)	Fast	High	Medium to large areas
Map digitalization	Relatively low (m)	Slow	High	Any area size
Map scanning	Relatively low (m)	Fast	Low	Any area size
Space photogrammetry	Low to medium (m)	Very Fast	Low	Large areas

Table 1.2: Comparison of various DEM acquisition methods (Li et al., 2005).

ing the raster and vector conversion, even if the scanning process is automated. In countries where these are available, contour maps are the major source for digital terrain modelling and they have been used for producing national DTMs.

1.4 Quality of a DEM

A DEM is represented by a 2.5-D locations plus a mathematical representation of terrain information and it is commonly regarded as a 2.5-D representation of the terrain information in a 3-D geographical space. Therefore, the accuracy check and calibration approach is often in 2.5-D, that is if a translation in altitude between the two model is present, it is estimated and removed. On the other hand, a complete 3-D approach in validation and calibration is characterized by estimating and removing both the planimetric and altitude biases, applying a roto-translation.

Once a DEM has been created, the estimation of its quality is important. The common techniques for quality assessment were based on the statistical comparison of small reference areas of the DEM with respect to higher accuracy data, usually available in small reference areas, in order to find outliers (Thompson et al., 2001).

The quality of a DEM is related to the resolution. High resolution DEMs are more prone to errors. In addition, the higher the resolution is, the most difficult the evaluation of input data quality and the assessment of the resulting DEM are.

In a DEM a lot of errors can be present, that can limit its application. Thus, not only the system producers but also users are interested in the quality of a DEM. In order to be better used for various downstream studies, the quality of a DEM must be quantified using adequate methods and measures; these measures must be communicated to the users, in order to make the users conscious of the quality of the DEM. Unfortunately this is rarely done, and, if so, merely global measures are provided.

In the geomatic field, two different types of quality issues are usually discussed: interior and exterior quality. The interior quality is related to the level of similarity that exists between the produced data and the perfect ones that should have been produced (data produced without errors). The exterior quality corresponds to the level of concordance that exists between a product and the users need or expectations, in a given context. The concept of exterior quality implies a relative quality, in the sense that the same product may be of different quality to different users in different contexts.

The quality of a DEM consists of several components like accuracy, precision, reliability. The *accuracy* of a DEM is the degree of closeness of measurement of the attribute value (for instance, the height value) to its actual true value. The *precision*, instead, is the degree to which repeated measurements under unchanged conditions show the same results. In other words, as shown in Figure 1.19, accuracy indicates the proximity of measurement result to the true value while precision to the repeatability or reproducibility of the measurements. Finally *reliability* is the consistency of a set of measurements, often used to describe a test; it is inversely related to random error.

The exterior quality, i.e. the accuracy of the DEM, is computed through comparison with uncorrelated data that had not been used to construct the model, i.e. reference elevation data, which are usually data with a better quality (another DEM, or regularly/irregularly distributed 3-D points). The interior quality of the DEM is instead evaluated through precision, that is the standard deviation of the DEM estimated through error propagation of the input data. The interior quality should be checked in every single phase of the digital terrain modelling.

One of the DEM quality assessment goals is to fulfil the requirements of spatial data standards. The International Organization of Standardization (ISO) distinguishes five elements of data quality: completeness, logical consistency and three types of accuracy: positional, temporal and thematic. In terms of nature of data the accuracy can be distinguished also into absolute and relative. The position of the objects (for example the ridges or sink holes as part of the DEM) could be assigned to absolute accuracy, and the irregularity of the shapes to relative accuracy, that is morphologically relative to a general position. Accuracy may be measured in height, in horizontal position or along the normal surface.

Accuracy can be considered as the difference between the value of a variable

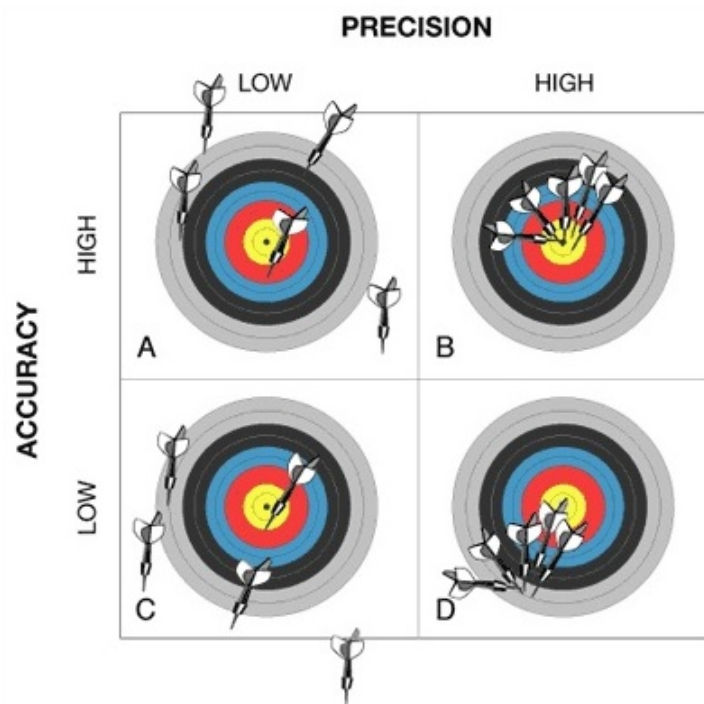


Figure 1.19: Schematic representation of accuracy and precision of a model.

as it appears in the dataset, and the value of the variable assumed in the data model (considered as reality). The accuracy of a DEM depends on a variety of factors (Karel et al., 2006):

- the source of the elevation data, which includes the techniques used for measuring the elevation, the locations and the density of samples,
- the methods used to construct the DEM from elevation data,
- the data model, which can be a grid, contour lines, or a triangulated irregular network,
- the topographic complexity of the landscape being represented,
- the algorithms used to calculate different terrain attributes.

The accuracy control is a complicated process, because to reach a high accuracy during the construction of the DEM, attention must be paid at each step, as errors arise in DEM data at every step during the acquisition and the processing. Some errors can be those in the source materials, the inaccuracy of the equipment

for data acquisition, human errors introduced in the acquisition process and errors introduced in coordinate transformation and other data processing, and many others.

Three types of errors exist: random errors, systematic errors and gross errors. *Random errors*, called also white noise, do not follow any deterministic rule and are statistical fluctuations in the measured data due to the precision limitations of the measurement device; for example the variability of measurements of a single quantity is due to random errors in observations. Random errors have a normal distribution and for this kind of errors a filtering process is usually applied to reduce their effect. On the other hand *Systematic errors* are reproducible inaccuracies due to a problem which persists throughout the entire experiment, they can be constant or counteracting and can appear as a function of space and time. These errors can be due for example to distortions in source materials (systematic distortion of a map as the source of the digitalization), to lack of adequate adjustment of the instrumentation before the use, or again to physical causes as for example photo distortion due to temperature changes. Alternatively, systematic errors may be the result of the human observer limitations, for example stereo acuity or carelessness such as failing to execute correct absolute orientation. *Gross errors* are mistakes. Compared to random and systematic errors, gross errors appear with a smaller probability during the measurement: for example a gross error is introduced into the measurement dataset if an operator records a wrong reading on the correct point or observes the wrong point through misidentification, or if the measuring instrument is not working properly when an automatic recorder is used. From a statistical point of view, gross errors are specific observations that should not be considered as belonging to the same sampling space as the other observations. As a consequence, measurements should be planned and observational procedures designed in such a way as to allow the detection of gross errors so that they can be rejected and removed from the set of observations.

DEMs generated by already existing cartography, photogrammetry, LiDAR and InSAR techniques have a lower precision compared for example to a model derived by the geodetic survey data. For this reason RTK GPS survey data can be considered as reference values to estimate the accuracy of a DEM. The differences between the DEM and the reference values are considered errors, which may be random or systematic. Systematic errors, or biases, are constant errors in the georeference of the DEM and they must be removed before the release of the DEM to users.

According to the ISO/TC standard 211¹, Digital Elevation Models are divided into eight classes or levels, based on planimetric resolution and tolerance. The

¹TS 19138 - Geographic Information - Data quality measures - N 2029 of the 5 June 2006 (211n2029)

planimetric resolution is the horizontal spacing between grid cells (in case of squared cells this corresponds to the Δx and Δy). The tolerance indexes are a priori calculated from the nominal scale of the numeric cartography to which the specific DEM corresponds (Belotti et al., 2013a). The tolerance is estimated after the calibration of the DEM. The calibration is performed estimating and removing the mean altimetric difference (systematic altimetric error) between the heights of the DEM and the elevations of the reference points; the calibration is done removing this bias. Once the altimetric and planimetric biases have been removed, the accuracy of the model depends on accidental (random or gross) errors and can be evaluated by means of the standard deviation, which coincides with the Root Mean Square Error (RMSE) or from other indexes deduced from the RMSE. These indexes are, as defined by the ISO/TC 211 standards, the linear tolerance in height (LE95) which corresponds to the probability of the 95% and the planimetric tolerance CE95 corresponding to the same probability.

Level	Type	Res	$LE95_H(a)$	$LE95_H(b)$	$LE95_H(c)$	$CE95_{NE}$
0	DTM, DSM	40-100	30	30	30	20
1	DTM, DSM	20	10	20	10	10
2	DTM, DSM	20	4	0.5	5	4
3	DTM, DSM	10	2	0.5	3	2
4	DTM, DSM	5	0.60	1.20	0.80	0.60
5	DTM, DSM	2	0.40	0.80	0.54	0.40
6	DDTM, DDSM	1	0.60	1.20	0.80	0.60
7	DDTM, DDSM	0.5	0.30	0.60	0.40	0.30
8	DTM, DSM	0.10-0.20	0.20	0.30	0.26	0.20

Table 1.3: Accuracy indexes of the different levels of DEMs according to the ISO/TC standard. Level: level of the DTM/DSM; Res: planimetric resolution; $LE95_H(a)$: elevation tolerance in open terrain; $LE95_H(b)$: elevation tolerance in case of existence of trees (canopy cover at least 70%), only for DTM; $LE95_H(c)$: elevation tolerance of the points belonging to buildings, only for DSM; $CE95_{NE}$: planimetric tolerance. Resolution and tolerances in meters. The terms DDTM and DDSM mean respectively Dense DTM/DSM.

From the practical point of view, for the LE95 index, it has to be verified that for the 95% of the reference points (points in which the elevation has been measured with a precision higher than the one expected for the digital model) the average difference between the heights of the DTM and the “real” values multiplied by 1.960² is lower than the theoretical reference index. Similarly, for the planimetric tolerance, the average deviation of the planimetric components of the elevation model with respect to the higher precision reference planimetric coordinates is checked; this value has to be multiplied by 1.7380 (to obtain the CE95 index) and

²1.960 is the probability value corresponding to 95% of a gaussian distribution.

the result should be lower than the theoretical reference index.

Table 1.3 contains the levels of DEMs and the accuracy indexes for the different levels according to the ISO/TC 211 standard. The terms DDTM and DDSM mean respectively Dense DTM/DSM and are usually adopted for models with spatial resolution lower than one meter. Concerning DTMs, the three fundamental parameters to describe the model are the planimetric resolution, the $LE95_H(a)$ index, which corresponds to the vertical accuracy and the $CE95_{NE}$, which corresponds to the horizontal accuracy.

1.5 Different methods of DEM representation: GRID vs. TIN

As already explained in the previous sections, elevation data are numerically stored in DEMs that can be realized by sampling elevations for a certain number of significant points and by storing the sample of 3-D dimensional coordinates. Different data models can be adopted to store the data, such as contour lines, grids (or elevation matrices) and Triangulated Irregular Network (TIN). Grid DEMs are georeferenced regular matrices of (x_i, y_i) nodes, whose elevations H_i are stored; the horizontal coordinates of the nodes can be either in a cartographic projection (x : East, y : North) or geographic ($x : \lambda, y : \phi$). Typically, the horizontal spacings between nodes (the grid resolution Δx and Δy) are equal in both the horizontal directions. This is a de-facto standard because many GIS softwares can manage only grid with squared space cells. When geographic coordinates are used, an equal resolution in latitude and longitude implies that the cells are not metrically squared.

The storage size of a grid is inversely proportional to the resolution squared: if rough terrain alternates to flat terrain, the high resolution needed to accurately describe the former causes a useless redundancy in the latter (Fang and Piegl, 1993). There are other data models that overcome this disadvantage, as for example TIN. A TIN is a vector based representation of the physical land surface, made up of irregularly distributed nodes and lines with three dimensional coordinates (x, y , and z) that are arranged in a network of non-overlapping triangles. Figure 1.20 shows the two DEM representation methods, grid and TIN: a grid model is created from points distributed following a chessboard pattern, a TIN model is created from randomly distributed points.

The main difference between TIN and GRID is the fact that in the first case the elevation model is represented in terms of regular cells, in the second the terrain is represented by means of triangles which have different shapes and dimensions depending on the morphology of the terrain; in TIN the terrain model is implicitly

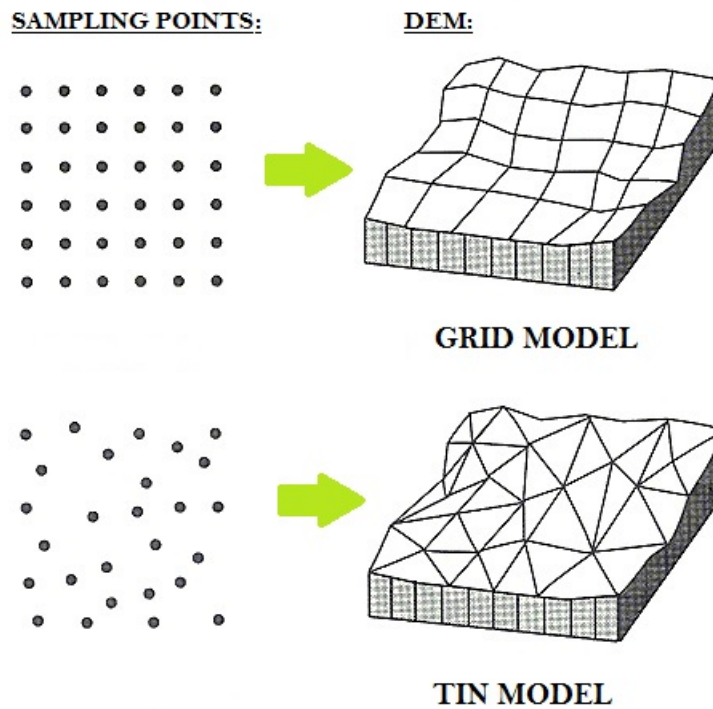
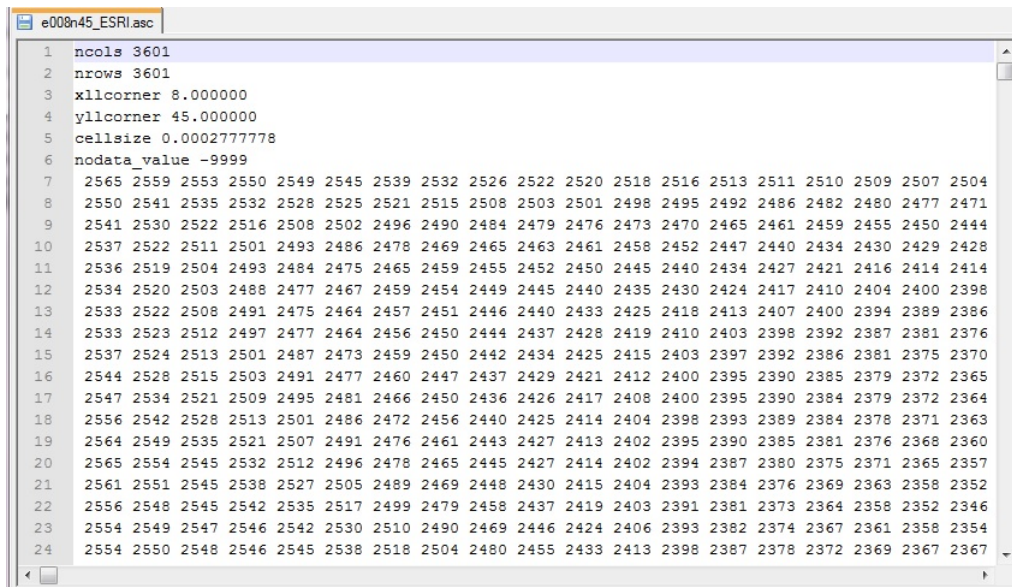


Figure 1.20: Different DEM representation methods: GRID and TIN.

defined by the faces of the Delaunay triangles that connect the points. The use of grid has the advantage of simple data storage, because only the origin of the grid (for example the planimetric coordinates of the lower left cell), the step of the grid in both X and Y directions, and a matrix containing all the elevation values, one for each cell, have to be saved. In addition, grid representation is compatible with satellite data and making cross validation between DEMs in case of grid representation is simpler than TIN. On the other hand the advantage of using TIN method is the rapidity of computation, the adaptation to the terrain morphology and the fact that it needs fewer points to achieve the same accuracy.

Since grid is a very simple conceptual model and can be easily accessed, visualized and spatially analysed by map algebra, it is the most popular DEM representation method. The main way of storing a DEM grid is an ASCII file composed by two parts:

- the header containing the number of rows and columns of the matrix, the horizontal coordinates of the lower left node/corner of the grid, the horizontal spacing between cells (only one parameter if the cells are squared, two parameters if the Δx and Δy are different), and finally the value associated to pixels that don't have an available elevation value,



```

e008n45_ESRI.asc
1  ncols 3601
2  nrows 3601
3  xllcorner 8.000000
4  yllcorner 45.000000
5  cellsize 0.0002777778
6  nodata_value -9999
7  2565 2559 2553 2550 2549 2545 2539 2532 2526 2522 2520 2518 2516 2513 2511 2510 2509 2507 2504
8  2550 2541 2535 2532 2528 2525 2521 2515 2508 2503 2501 2498 2495 2492 2486 2482 2480 2477 2471
9  2541 2530 2522 2516 2508 2502 2496 2490 2484 2479 2476 2473 2470 2465 2461 2459 2455 2450 2444
10 2537 2522 2511 2501 2493 2486 2478 2469 2465 2463 2461 2458 2452 2447 2440 2434 2430 2429 2428
11 2536 2519 2504 2493 2484 2475 2465 2459 2455 2452 2450 2445 2440 2434 2427 2421 2416 2414 2414
12 2534 2520 2503 2488 2477 2467 2459 2454 2449 2445 2440 2435 2430 2424 2417 2410 2404 2400 2398
13 2533 2522 2508 2491 2475 2464 2457 2451 2446 2440 2433 2425 2418 2413 2407 2400 2394 2389 2386
14 2533 2523 2512 2497 2477 2464 2456 2450 2444 2437 2428 2419 2410 2403 2398 2392 2387 2381 2376
15 2537 2524 2513 2501 2487 2473 2459 2450 2442 2434 2425 2415 2403 2397 2392 2386 2381 2375 2370
16 2544 2528 2515 2503 2491 2477 2460 2447 2437 2429 2421 2412 2400 2395 2390 2385 2379 2372 2365
17 2547 2534 2521 2509 2495 2481 2466 2450 2436 2426 2417 2408 2400 2395 2390 2384 2379 2372 2364
18 2556 2542 2528 2513 2501 2486 2472 2456 2440 2425 2414 2404 2398 2393 2389 2384 2378 2371 2363
19 2564 2549 2535 2521 2507 2491 2476 2461 2443 2427 2413 2402 2395 2390 2385 2381 2376 2368 2360
20 2565 2554 2545 2532 2512 2496 2478 2465 2445 2427 2414 2402 2394 2387 2380 2375 2371 2365 2357
21 2561 2551 2545 2538 2527 2505 2489 2469 2448 2430 2415 2404 2393 2384 2376 2369 2363 2358 2352
22 2556 2548 2545 2542 2535 2517 2499 2479 2458 2437 2419 2403 2391 2381 2373 2364 2358 2352 2346
23 2554 2549 2547 2546 2542 2530 2510 2490 2469 2446 2424 2406 2393 2382 2374 2367 2361 2358 2354
24 2554 2550 2548 2546 2545 2538 2518 2504 2480 2455 2433 2413 2398 2387 2378 2372 2369 2367 2367

```

Figure 1.21: Example of a grid DEM stored in an ASCII-file - *ncols*, *nrows*: number of columns and rows of the matrix; *xllcorner*, *yllcorner*: planimetric coordinated of the lower left cell of the grid; *cellsize*: dimension of the grid spacing between cells; *nodata_value*: value associated to no data pixels.

- the matrix containing the elevations of all the cells composing the grid.

An example of a ASCII grid DEM file of a portion of the national Switzerland DEM is reported in Figure 1.21.

In this thesis, attention will be paid only to grid DEM representation method.

1.6 Different levels of grid DEM representations

In previous sections the different ways of representing a Digital Elevation Model have been described. Grid is the most commonly used method for representing a DEM. Depending on the specific need, as for example the size of the area that the user has to describe and the level of accuracy that he wants to obtain, different kinds of grid DEMs can be adopted. If a big portion of the Earth surface has to be studied, like an entire region or an entire country, but with low details, a global DEM can be used; on the contrary local DEM can be adopted when there is the need to study a small portion of the surface but with high details. For example if in geology a landslide has to be studied, obviously a global DEM is not the best product, but a local DEM with high resolution and accuracy has to be chosen. Between global and local DEM, regional or national DEMs exist.

In general grid DEMs can be divided into three main categories:

- global DEMs: they cover the whole Earth surface and are usually characterized by low resolution and accuracy,
- national/regional DEMs: they cover an entire nation or region and are characterized by low/medium resolution and accuracy,
- local DEMs: they cover small portions of the Earth surface (a river bank, a landslide area, etc.) and are characterized by high accuracy and resolution.

Clearly, it is very difficult or nearly impossible to satisfy together both the requirements of large coverage and high accuracy, because the methods that allow to reach best accuracies, as for example LiDAR or GPS, are the most expensive methods. Thus, for each need the best type of DEM in terms of labour, time, money, coverage, has to be used. Each kind of DEM can be obtained by different techniques for data acquisition. Usually a global DEM can be obtained by SAR data (or InSAR) and in some cases by photogrammetry; a national/regional DEM can be obtained by photogrammetry, SAR or LiDAR data. A local DTM is usually obtained by LiDAR data or by digitalization of existing maps. GPS data are mainly used as support for the other methods and as the main method to gather data for the quality validation, as they provide a high accuracy but sparse punctual data and constructing a DTM with GPS data would be very time spending.

1.6.1 Global low resolution Digital Surface Models

Global Digital Surface Models, as the name suggests, cover the whole Earth globe. The global coverage makes them very useful in many applications and where no local models exist: however, the low resolution and accuracy make them useless if precise data are needed. In Table 1.4 the three main global DSMs available today and their characteristics are summarized.

Model	Resolution (m)	Accuracy (m)
ASTER	30	7-14 vertical 7-14 horizontal
SRTM	90	16 vertical 20 horizontal
GMTED	250	26-30 vertical
	500	29-32 vertical
	1000	25-42 vertical

Table 1.4: Global DSMs: resolutions and accuracies.

In the following sections a brief description of the three global DSMs is done.

1.6.1.1 SRTM global DSM

Shuttle RADAR Topography Mission (SRTM) was a joint project of the National Aeronautics and Space Administration (NASA), the German Aerospace Center (DLR) and the Italian Space Agency (ASI). SRTM satellite was launched by NASA in 2000. The goal of the mission³ was to survey the Earth surface and to generate an homogeneous elevation dataset of all land between 60° North and 56° South latitude (about 80% of the whole land surface) with a grid spacing of at least 3 arcseconds (Rabus et al., 2003). The derived cartographic products are two DEMs at resolution levels of 1 arcsecond (approximately 30 by 30 m) and 3 arcseconds (approximately 90 x 90 m); at the present the 1 arcsecond product is available only for the USA area, while the 3 arcseconds one is available in every area with an accuracy in elevation of about 16 meters and in planimetry of about 20 meters.

The dataset was acquired by the same sensor in a single mission and was produced with a single technique, the Synthetic Aperture RADAR Interferometry (InSAR). The mission⁴ took place in 2000 between February 11th and 22nd and all the data were acquired in eleven days since the RADAR scanning system worked independently of darkness or cloud coverage.

Two antenna pairs operating in C-band (5.6 cm; C-RADAR) and X-bands (C-RADAR) were simultaneously illuminated and recording RADAR signals. The operational goal of C-RADAR was to generate data along discrete swaths 50 km wide; X-RADAR was included as an experimental demonstration, since the X-band RADAR had a slightly higher resolution and a better signal to noise ratio than the C-band but had not been yet used before. Two single-pass interferometers were built and operated in parallel, the US C-band system and a German/Italian X-band system X-SAR (details reported in Table 1.5).

Wavelength (cm)	3.1
Range pixel spacing (m)	13.3
Azimuth pixel spacing (m)	4.33
Range bandwidth (MHz)	11.25
Effective baseline length (m)	59.9
Baseline angle (°)	54.55
Orbit height (km)	233

Table 1.5: SRTM X-SAR characteristics.

The main antenna of the system was located inside the cargo bay of the Space

³<http://www2.jpl.nasa.gov/srtm/>

⁴<http://www2.jpl.nasa.gov/srtm/mission.htm>

Shuttle Endeavour and it transmitted and received microwave pulses. The secondary antenna was fixed at the tip of a 60 meters long lightweight mast and acted as a receiver; the mast materialized the interferometric baseline. With this configuration, in which two antennas received and reflected RADAR pulses at the same time, single-pass interferometry was allowed. The SRTM space segment is shown in Figure 1.22.

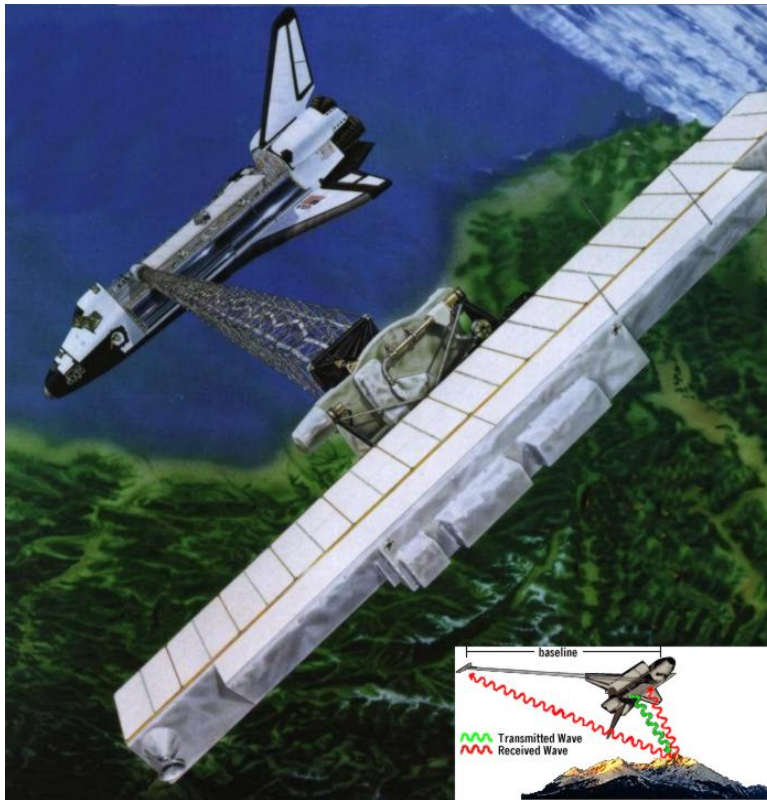


Figure 1.22: SRTM configuration: the main antenna sends the signal, both main and outboard antenna receive the backscattered signal.

The C-band interferometer employed active antennas with electronic steering. To meet the global gap-less mapping, the design goal was a swath width of 225 km; the X-SAR swath width is in the order of 45 km so the quality of the X-bands interferograms and DEMs is expected to be better than of those from C-band. The RADAR instruments were completed with the instruments of Attitude and Orbit Determination Avionics (AODA) to measure the geometric baseline between the antennas. The absolute position of the baseline in space was measured by a GPS receiver with an accuracy of 1 m (Rabus et al., 2003).

Even if the data coverage is theoretically global, some regions are without data, because of some problems during the data collection, such as a lack of con-

trast in the RADAR image, presence of water or excessive atmospheric interference. These data holes are present along rivers, in lakes and in steep regions, for example on hillsides with a similar aspect due to shadowing. There are a total of 3'436'585 voids, and in extreme cases as for example in Nepal region, they constitute the 9.6% of the total country area (32'688 voids totalling an area of 13'740 Km²). This non-random distribution of holes impeded the potential use of the SRTM data, for example for research studies as in the application of hydrogeological models which require continuous flow surfaces. In order to solve this problem, some "filling-in" algorithms have been implemented.

The C-RADAR data were processed over a period of nine months by NASA and NGA (National Geospatial-Intelligence Agency). At the end of this work NASA released the version 1 data products:

- DSM at 1 x 1 arcsecond (SRTM-1),
- DSM at 3 x 3 arcseconds (SRTM-3), produced by averaging nine 1 arcseconds pixels,
- DSM at lower resolution 30 x 30 arcseconds (SRTM-30), produced from USGS GTOPO30 by averaging 30 x 30 pixels and replacing GTOPO30 data with SRTM data where possible.

NGA also produced a version of the SRTM with further improvements: spikes and wells in the data were detected and voided out if they exceeded 100 m compared to surrounding elevations; small voids were filled by interpolation, large voids were left in the data. Water bodies were depicted: the ocean elevation was set to 0 m, lakes of 600 m or more in length were flattened and set to a constant height. The version 2 data products incorporate the NGA finished data.

The processing of X-RADAR data originated an interferometric DSM with ellipsoidal heights and an additional height error map (HEM).

1.6.1.2 ASTER global DSM

The Advanced Spaceborne Thermal Emission and Reflection Radiometer (ASTER) is a multispectral imaging system built in Japan for the Ministry of Economy Trade and Industry (METI), that operates on the United States National Aeronautics and Space Administration (NASA) Terra platform. A joint US/Japan Science Team was responsible for instrument design, calibration, and validation. ASTER was launched the 19th December 1999 on the Terra platform as part of the National Aeronautics and Space Administration (NASA) Earth Observing System (EOS) and it collected data between 82° North and 82° South latitude (NASA, 2009).

In Table 1.6 the main differences between ASTER and SRTM at 3 arcseconds are listed.

	ASTER	SRTM 3 arcseconds
Data source	ASTER	Space Shuttle RADAR
Generation and distribution	METI/NASA	NASA(USGS)
Release year	2009	2003
Data acquisition period	2000-ongoing	11 days (in 2000)
Posting interval	30 m	90 m
DEM accuracy (stdev)	7-14 m	16 m
DEM coverage	82° North - 82° South	60° North - 56° South
Area of missing data	Areas with no ASTER data due to constant cloud cover	Steep areas (due to RADAR characteristics)

Table 1.6: ASTER vs. SRTM.

ASTER combines the along stereo image data recorder in the along-track direction and digital photogrammetry. Using three telescopes and sensor systems, it acquires images in 14 spectral bands: three visible and near-infrared (VNIR) bands with a spatial resolution of 15 meters, six short wave infrared (SWIR) bands with a spatial resolution of 30 meters, and five thermal infrared (TIR) bands with a spatial resolution of 90 m.

The VNIR subsystem consists of two independent telescopes: one nadir looking with a three-spectral band detector, and the other backward looking with a single-band detector; it produces the highest data rate of the three ASTER imaging subsystems. As can be seen from Figure 1.23 it is used for study land use pattern, vegetation, soil, volcano monitoring, surface temperature, glaciers, clouds structure and temperature. VNIR Band3 is acquired using a backward-looking telescope, thus providing along-track stereo coverage from which high quality DEMs can be generated.

The SWIR subsystem works through a single nadir-pointing telescope and a pointing mirror that accomplishes cross-track pointing. SWIR is useful for studies on land use, vegetation, soil, surface temperature and for volcano monitoring.

Unlike the other instrument subsystems, TIR subsystem has a “whiskbroom” scanning mirror which functions both for scanning and cross-track pointing. In the scanning mode, the mirror oscillates at about 7 Hz and, during the oscillation, data are collected in one direction. Because of the instrument high data rate,

restrictions have been imposed so that the average data rate is manageable by the spacecraft data management system. This subsystem allows to study evapo-transpiration, soil, volcanoes, surface and ocean temperature, glaciers and clouds.

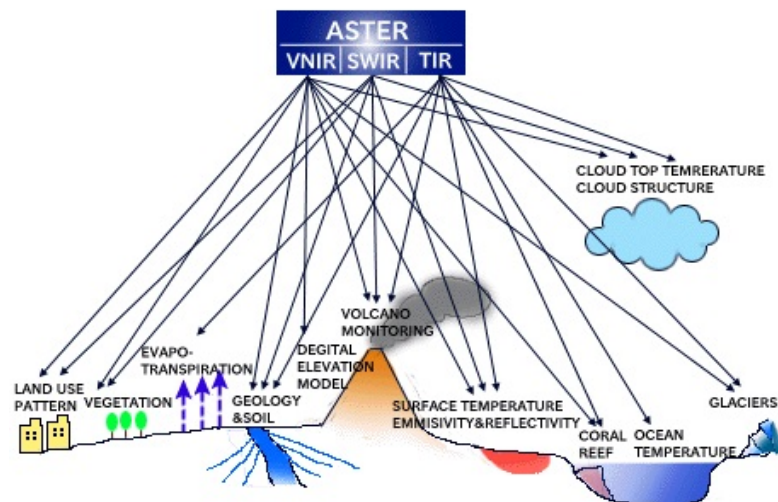


Figure 1.23: ASTER subsystems and their applications.

ASTER provides Standard Data Products throughout the life of the mission; the algorithms to compute these products were studied and implemented by the ASTER Science Team. Different products are available: ASTER GDEM is the most used. ASTER GDEM is in GeoTIFF format with geographic lat/long coordinates, georeferenced in WGS84. It has a planimetric resolution of 1 arcsecond (~ 30 m) and an accuracy in elevation ranging between 10 and 25 m. The ASTER DEM has been produced with an automated processing of the entire ASTER archive containing 1.5-million scenes, including: stereo correlation to produce 1'264'118 individual scene-based ASTER DEMs, cloud masking to remove cloudy pixels, removing of the residual bad values and outliers, averaging of selected data to create final pixel values, and then correction of residual anomalies before partitioning the data into tiles with dimension equal to 1 degree in both directions.

1.6.1.3 Global Multi-resolution Terrain Elevation DATA 2010 (GMTED2010)

The Global Multi-resolution Terrain Elevation Data 2010 (GMTED2010) is an enhanced replacement of Global 30 Arc-Second Elevation (GTOPO30), Global Land One-Km Base Elevation (GLOBE) model and other comparable 30 arc-second resolution global models as for example the SRTM DSM and was created using the best available data among these elevation models. The new model has been generated by United States Geological Surveys (USGS) and NGA at three

separate resolutions of 30 arc-seconds (about 1 km), 15 arc-seconds (about 500 m) and 7.5 arc-seconds (about 250 meters) (NASA, 2011). It provides global coverage of all land areas from lat 84°N to 90°S (Figure 1.24) for several products, but some areas, like Greenland and Antarctica, do not have available data at the 15 and 7.5 arc-seconds resolutions.

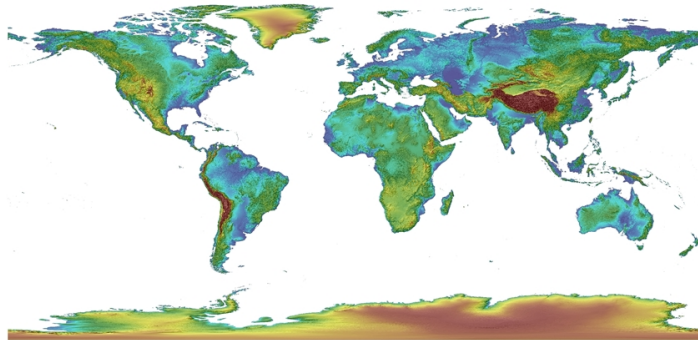


Figure 1.24: GMTED2010 global DSM.

GMTED2010 is based on data derived from eleven raster-based elevation sources. The primary source dataset is NGA SRTM Digital Terrain Elevation Data (DTED) 1 arc-second data. For the geographic areas outside the SRTM coverage area and to fill in remaining holes in the SRTM data, the following sources were used:

- non-SRTM DTED,
- Canadian Digital Elevation Data (CDED), at two resolutions,
- Satellite Pour l'Observation de la Terre (SPOT5) Reference 3-D,
- National Elevation Dataset (NED) for the continental United States and Alaska,
- GEODATA 9 second Digital Elevation Model (DEM) for Australia,
- Antarctica satellite RADAR and altimeter DEM,
- Greenland satellite RADAR altimeter DEM.

Every input dataset was ingested on a tile-by-tile ($1^\circ \times 1^\circ$) basis and transformed to the geographic WGS84 system and then regridded using a bilinear resampling. The new elevation product has been produced using the following aggregation methods: minimum elevation, maximum elevation, mean elevation, median elevation, standard deviation of elevation, systematic subsample and breakline emphasis. According to these methods, seven raster elevation products have been produced at each resolution. The statistical-based approach products were generated

using the Aggregate functions resamples within ArcGIS. The standard deviation product was generated using a combination of two ArcGIS functions: a Blockst function was first applied to part the input raster grid into blocks, to find the standard deviation for the specified posts defined by the neighbourhood blocks, and to send the computed standard deviation to the post locations in the corresponding blocks on the output raster grid. In addition, a “systematic subsampling” of the full resolution source data was used to produce a reduced resolution version at each of the output grid spacing. Finally, the last approach, called “breakline emphasis” was used to produce reduced resolution products that maintain stream and ridge characteristics as delineated in the full resolution source data; this method preserves the critical topographic features within the landscape by maintaining any minimum elevation or maximum elevation value on a breakline that passes within the specified analysis window.

The final elevation products are the seven maps generated at each of the three resolutions, for a total of 21 different maps. All products are in a geographic coordinate system referenced to the WGS84 horizontal datum, with the horizontal coordinates expressed in decimal degrees. The vertical units for the elevations are integer meters, referenced to the EGM96 geoid as vertical datum.

The different products can be used in a variety of applications. For example, the maximum elevation product is useful for the airport runway surface heights or to determine the height of vertical obstructions. The minimum elevation product is useful for determining stream channel areas and the water surface. The standard deviation product provides a measure of the texture, or local variation in elevation, of the landscape surface. The breakline emphasis product is used for many hydrologic applications that involve watershed extraction and surface streaming routing.

1.7 DSMs filtering to obtain DTMs

From the different techniques used for collecting elevation data, a DSM can be usually extracted. In particular DSMs origin mostly from laser scanning, radar interferometry, stereo processing of optical aerial or satellite images (Kraub et al., 2011). DTMs can be generated from direct terrain measurements (e.g. from GPS data) or extracted from DSMs. If the aim is to construct directly a DTM, use an airborne laser sensor can be advantageous, specially in forested or build-up areas. The sensor is able to measure the reflected part of a laser at different points. In fact a certain amount of the emitted laser beam is reflected by the three canopy, while other parts penetrate the canopy through holes in the foliage and reach the ground. Therefore the last reflected laser pulse, i.e. the part of the signal which is received at last, refers to the ground surface and it is used to extract information about

the ground. But if the foliage is very dense, the laser beam can be completely reflected by the foliage and no information about the ground is available. The same can happen in urban areas with a high density of buildings. A further filtering is therefore needed for extracting terrain information.

From LiDAR data or every kind of DSM, the corresponding DTM can be derived, by the detection and removal of all the surface objects (buildings, trees, etc.). The main problem is therefore mainly the detection of non-ground objects. Various techniques of DSMs or LiDAR data filtering have been studied and proposed from different authors in order to generate DTMs.

Kilian et al. (Kilian et al., 1996) presented some first methods to generate a DTM from LiDAR data recorded in forested areas. The method is based on a morphological opening operation. First a window is opened on the dataset and inside the window the lowest point is founded. Each point inside a band width above the lowest point is defined as an approximated ground point; using those points a weighted surface interpolation is applied to compute the DTM. The size of the window is a critical parameter for which there is no unique optimal value. Therefore, the conclusion of that work was that the use of multiple openings with different sizes is the best approach.

Axelsson (Axelsson, 1999) described a method for DTM generation based on the progressive densification of a Triangulated Irregular Network. The basic idea of this approach is to connect a surface from below the point cloud; in every iteration the surface is free to fluctuate within certain values and at every iteration some points from the point cloud are added to the TIN. The iterations proceed until no further ground control points can be added.

Vosselmann (Vosselman, 2000) proposed a method for DSM filtering based on slope. The points are divided in ground or non-ground points, studying the points that are around them. In fact a point is classified as ground point if in its surrounding no other point exist such that the height differences between these points is higher than an allowed maximum difference.

Kraus and Pfeifer (Kraus and Pfeifer, 2002) studied a different approach for DTM generation in wooded areas: the method is based on linear prediction. First the ground surface is approximated; the distances of the ground surface from the measured points are used to define weights which are exploited to compute the DTM based on linear prediction model. A height threshold is defined in order to classify the points as ground or non-ground points: a point is classified as a non-terrain point if the residual height is above the threshold and as a ground point if the residual height is below the threshold. All the non-ground points are then eliminated from the digital model.

Wack and Zimmer (Wack and Wimmer, 2002) described a hierarchical grid-based approach for the generation of DTMs. Starting from a coarse grid they defined the raster height by selecting the lowest heights from the 99% of all points

within the raster. In order to detect and remove the points that are not considered to be ground points, a Laplacian Gaussian operator in combination with a weight function is used.

Zhang et al. (Zhang et al., 2003) developed a new method to remove the non-ground points from a DSM. The algorithm uses the classical morphological opening and gradually increases the size of the window. The resulting elevation differences are used to classify ground and non-ground points by applying a threshold which depends on the window size.

Chapter 2

The HELI-DEM project and the data preprocessing

Most of the work done for this thesis regards a research project funded by the European Community: the project is named HELI-DEM. This chapter is devoted to a brief description of HELI-DEM and to a detailed description of the preprocessing of the data used to achieve its aim, which is the production of a Digital Terrain Model that covers the whole alpine area between Lombardy, Piedmont and Switzerland.

2.1 The HELI-DEM project

In the joint management of geographic information by different institutions, for example in the cross border between two states or regions, the problem of data management in a federated and widespread way exists. Almost all official national cartographic bases in Europe include Digital Terrain Models (DTMs) (Biagi et al., 2011). For this reason, in recent years, different countries and regions have produced their own DTMs. However, since unique and general rules do not exist, every institution has constructed DTMs in the deemed best and most appropriate manner. As a consequence, the different available DTMs have been acquired by different data sources and are characterized by different resolutions and accuracies; furthermore, they are georeferenced in different reference frames. In some cases it could happen that the elevation data are not homogeneous and consistent at the borders between countries or regions: in the worst cases also elevation biases can be present along the border. This is a major problem when dealing for example with hydrogeological studies, and especially in alpine areas where hydrogeological risks may exist (Li and Lihao, 2004; Wise, 2000; Shaw, 2005). For example, indeed this analyses strictly require the consistent knowledge of slopes

and aspects, that can be significantly corrupted by the merging of not consistent height datasets. When an event like a landslide happens at the border between two countries or regions, making use of the available DTMs is not possible if a bias is present between the elevation data that covers the landslide area. In such cases a unique and integrated DTM which covers the whole interest area could be useful to analyse the scenario. This requires that:

- the coordinates of the points inside the cross-border area have to be consistent and correctly georeferenced in a unique reference frame,
- a digital terrain with a unique resolution and accuracy has to be created, so that it is consistent between the two parts and does not present discontinuities.

A transnational DTM is therefore necessary and can be obtained by merging national/regional DTMs (usually at low resolution) and local high resolution DTMs where they exist.

In recent years, both in Italy and Switzerland, elevation data with different reference frames, technologies, accuracies and resolutions have been produced. The HELI-DEM (HELvetia-Italy Digital Elevation Model) project, funded by the European Regional Development Fund (ERDF) within the Italy-Switzerland cooperation program, aims at developing a unique DTM for the alpine and subalpine area between Italy and Switzerland. For Italy the Regions involved are Lombardy and Piedmont, for Switzerland two cantons are involved, Ticino and Grisons; for all of them only the alpine parts of the territory are considered. Figure 2.1 shows the area of interest of HELI-DEM.

The project, with a duration of 36 months, started in September 2010 and ended in September 2013. The institutions involved in the project were: Fondazione Politecnico di Milano, Politecnico di Milano, Politecnico di Torino, Regione Lombardia, Regione Piemonte and SUPSI (Scuola Universitaria della Svizzera Italiana). Two other institutions, SwissTopo and the IGMI (Istituto Geografico Militare Italiano) were also involved as external partners.

The goal of the project is the creation of a Digital Terrain Model which covers the whole project area and which has to be correctly georeferenced and produced validating and integrating all the elevation information made available by the different partners. This poses the problem of creating a system that would allow to handle these data in a federate and diffuse form. To which concerns the elevation data, this requires that the planimetric coordinates of the input data along a cross-border zone are consistent reciprocally and correctly georeferenced into a unique reference frame. In addition, the altimetric information should be continuous and consistent at the nominal level of the DTMs; therefore the resolution of the final

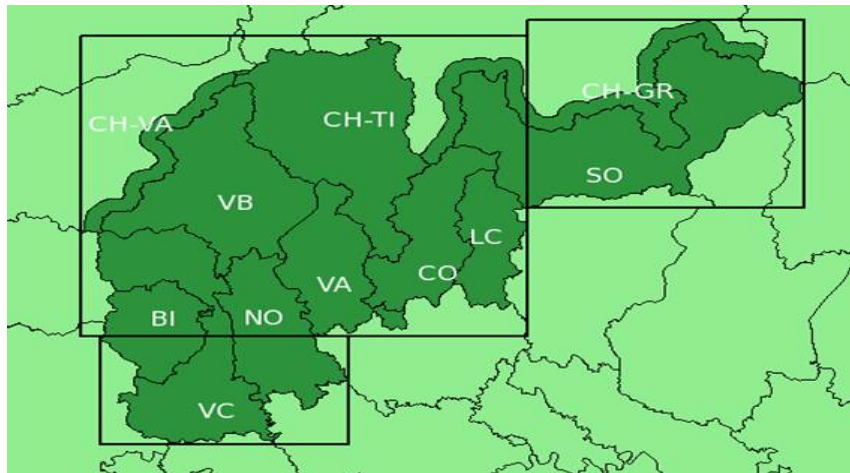


Figure 2.1: Area of interest of HELI-DEM project: Lombardy and Piedmont Italian Regions and Ticino and Grisons Switzerland Cantons are involved.

DTM should be at least equal to those of the original input DTMs and the vertical accuracy has to be in every area the best one obtainable from the input DTMs. To fulfill these tasks the following steps have to be done:

- collection and analysis of all the elevation data available for the project (DTMs, GPS data, geoid data, etc.), to create the HELI-DEM database,
- cross-check of the existing geoids and recomputation of a unified geoid that covers the area of the project,
- creation of a cross-border GNSS permanent network in order to support static and RTK GNSS surveys aimed to collect punctual high accuracy data, for the validation and georeferencing of the data along the border line,
- cross-check of the DTMs, including cross-validation between similar resolution DTMs and external validation of the DTMs, by the comparison with higher accuracy elevation data as for example GNSS data and levelling data; this operation is very important because it allows to choose the best data in terms of resolution and vertical accuracy. At this purpose new algorithms are studied and softwares for the cross-validation are implemented,
- integration of all the available and already validated DTMs to create the final unified DTM, using the low resolution and high resolution data,
- study and implementation of algorithms firstly to integrate the low resolution DTMs into a unified output DTM, then to correct the unified low resolution DTM with the higher resolution data,

- dissemination of the results, through their publication on a geoportal, which reads the output data from a geoservice, publishes them through an interface and allows to do some basic operations on them.

2.2 Preprocessing of the data

The preprocessing of the data includes all the operations that have to be done in order to make them usable for the project. First of all the data available for the project are collected: the regional DTMs of Lombardy and Piedmont, the national Swiss DTM, some high resolution DTMs as a LiDAR DTM covering the hydrographic basins of Lombardy and Piedmont, and some other elevation data as for example previously surveyed GNSS markers. In addition also the geoid data are collected. Then the different DTMs have to be cross-checked: for the overlapping DTMs with similar planimetric resolutions a cross-validation is done; then the low resolution DTMs have to be externally validated using the higher resolution data available. Since the DTMs are georeferenced in different reference frames, in order to perform the cross-check between two DTMs, it is necessary to unify their reference frame. In addition, for the external validation of the high resolution DTMs, some higher accuracy data have to be used, as for example GNSS data surveyed in RTK modality. A user who is performing the measures beyond the border should connect to an Italian GNSS network when he is inside in the Italian territory, and to a Swiss network when he is inside the Swiss territory. Problem could pose when the RTK measures are performed along the border between Italy and Switzerland: the user can connect to both the networks and could get different positioning since the GNSS services implement different position modalities and reference frames. A cross-border GNSS network expressly created can solve this problem; the main advantages of using a common network during the cross-border measures are:

1. from the computational points of view the uniformity of the reference frames of the measured points coordinates and of the products delivered for the real-time,
2. from the operational point of view the higher simplicity, because the user can connect to one single network.

The HELI-DEM network was not strictly necessary to perform the measures required by the project, but it has been effectively created in order to test the use of this type of network and its feasibility.

In the following sections the different steps for the preprocessing of the HELI-DEM data are in details described.

2.2.1 Collection of the available elevation data

The collection of the elevation data mainly involves the search and selection of local DTMs, that are the medium/low resolution DTMs (at least 50 meters planimetric resolution), developed by Local Authorities (Regions or national geodetic Authorities), that have a regional or national extension and some high resolution DTMs.

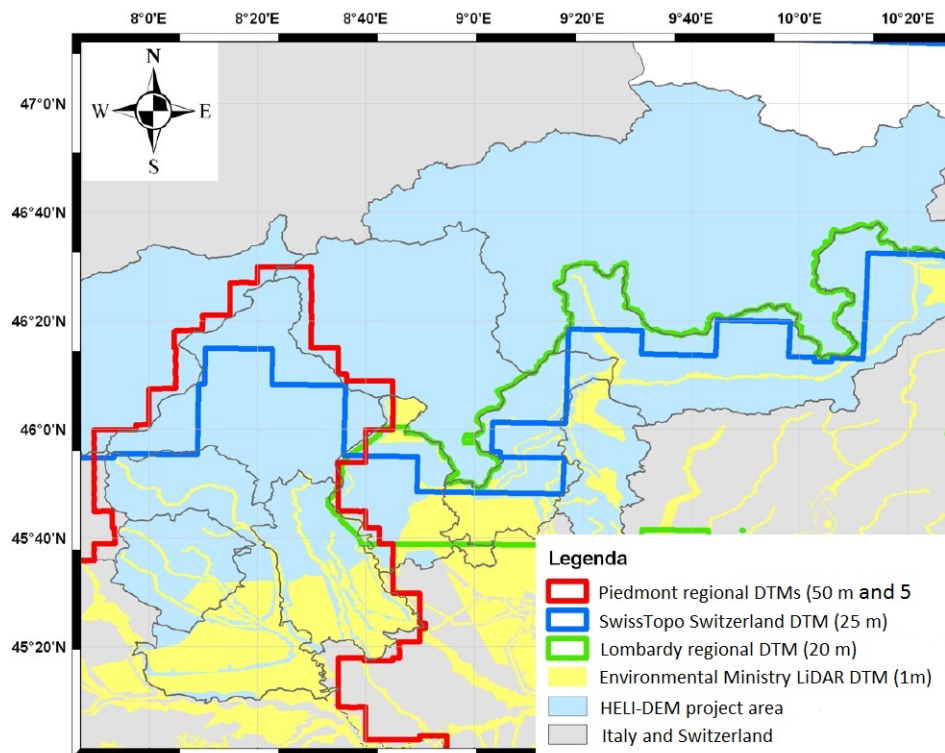


Figure 2.2: Coverage of the local DTMs collected for the HELI-DEM project (the values expressed in meters are the planimetric resolutions).

The data collected for the project can be divided in two categories: DTMs derived from cartography and DTMs acquired by LiDAR techniques. The DTMs belonging to the former group are characterized by low vertical accuracies (usually some meters or tens of meters) and low resolutions (some tens of meters), but they cover large areas of the territory, such as a whole region or in some cases an entire country, as for example the Swiss DTM released by SwissTopo which covers the whole Switzerland area. The latter group comprehends DTMs with higher vertical accuracies, in some cases better than one meter, and spatial resolutions of the order of one meter; these DTMs cover small portions of the territory, generally river beds, lake areas or small mountain zones (Belotti et al., 2013b). According to this

classification the collected DTMs can be classified in two main categories:

1. Regional low resolution DTMs. They are the three DTMs officially released by the Regional Authorities of Lombardy, Piedmont and Switzerland; according to the ISO/TC classification (Table 1.3) they are DTMs of Level 1 to 3 and they have resolutions between 10 and 50 meters.
2. Local medium and high resolution DTMs. They are two DTMs realized through LiDAR techniques: the former, produced by the Piedmont Region, covers the whole Piedmont area, the latter, named PST-A DTM, is realized by the Italian Ministry of Environment under the Piano Straordinario di Telerilevamento Ambientale (Extraordinary Plan of Environmental Remote Sensing) and covers the stripes corresponding to the valleys of the main river basins of Lombardy and Piedmont.

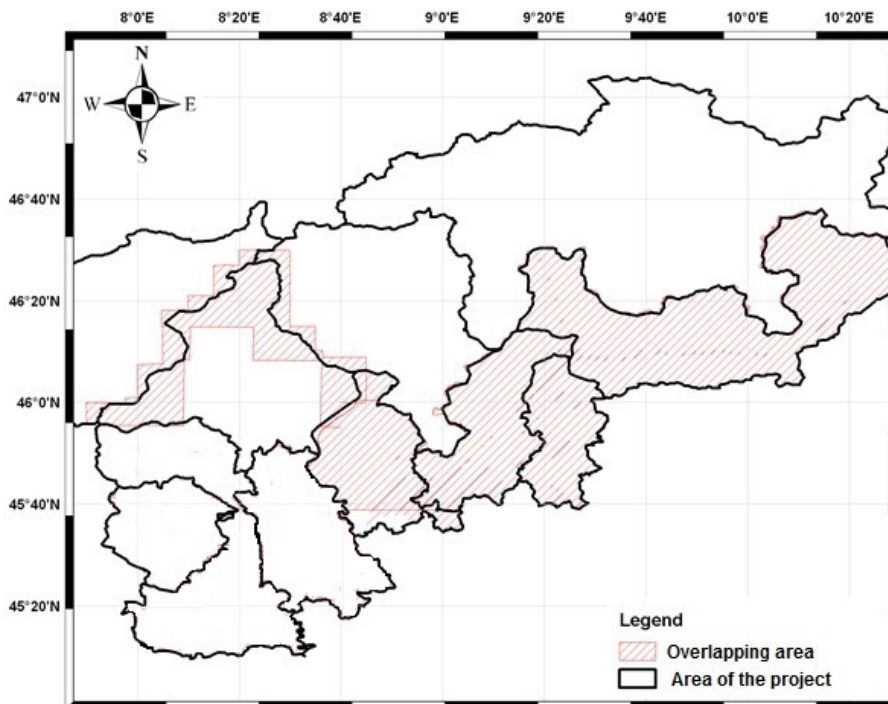


Figure 2.3: Overlapping areas of the DTMs collected for the HELI-DEM project.

Figure 2.2 reports the overall picture of the coverage of the local DTMs collected for the project. The overlapping areas between the collected DTMs has been defined. A graphical representation of the areas where two or more DTMs exist is shown in Figure 2.3: the 24% of the whole project territory has an overlap of at

least two regional/national DTMs. The 15% of the Lombardy Region is covered also by an high resolution DTM, Piedmont is covered for the 100% by an high resolution DTM.

All the collected DTMs are stored in ASCII grids (usually ESRI ASCII) with an assigned cellsize; they are in cartographic coordinates ($\Delta E, \Delta N$) in case of Piedmont and Lombardy regional DTMs and in geographic coordinates ($\Delta \phi, \Delta \lambda$) in case of Swiss and PST-A DTMs.

In the following sections the DTMs collected during the project and their characteristics are described.

In addition ASTER and GMTED global DSM, freely available from the official websites, have been collected for the project area. But the accuracy analysis performed on these data demonstrated that the elevation information contained in them would not have improved the quality of the HELI-DEM product obtained using only the local DTMs. So the global DSMs have been however collected but they have not been used to create the final unified DTM. Their characteristics are reported in the Section 1.6.1. The collected DTMs are briefly described in the following.

2.2.1.1 Regional DTMs

LOMBARDY REGION DTM (LEVEL 1, TABLE 2.1)

About the generation of the DTM. The vectorial base of the altimetric model has been done through vectorization and merging of the raster files of the sections 1:10'000 of the official regional cartography, by a densification of the contour lines and analyses of the elevation points. A TIN model containing the elevation data has been produced and then converted to a grid model with a grid spacing equal to 20 meters. Reference contour lines (50 m, 100 m) have been completed where they presented interruptions with the help of elevation points. Auxiliary curves (10 m, 20 m, 40 m, 60 m, 90 m) have been added only inside areas with low altimetric gradient, while ordinary curves (30 m, 80 m) have been traced continuously on the whole territory. Points belonging to buildings have been excluded from the original set of elevation points. To obtain the TIN structure from contour lines an algorithm implemented on GIS MGE (Intergraph) has been used. The conversion from TIN to grid has been performed through bilinear interpolation algorithms.

PIEDMONT REGION DTM (LEVEL 1, TABLE 2.2)

About the generation of the DTM. The DTM has been acquired by photogrammetry in two different ways. For the middle-north territory some altimetry ele-

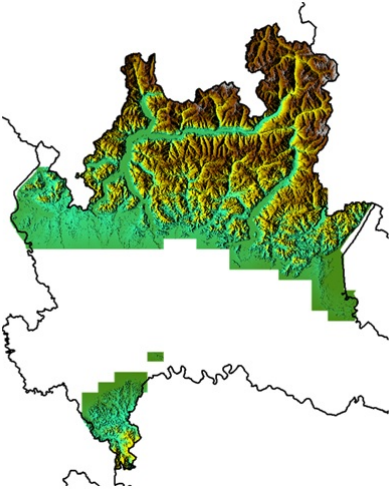
	Resolution: 20 meters
	Extension: Lombardy - mountainous area
	Year of production: 2002
	Reference frame: Roma40
	Coordinate system: Gauss Boaga West zone, orthometric heights
	Accuracy: 5-10 m (in height), 2 m (planimetry)
	Format of memorization: ASCII grid (ESRI)
	Organization of the files: Sections 1:10'000 Lombardy Region

Table 2.1: Lombardy Region DTM.

ments, that are necessary during the creation of the regional official cartography, have been acquired through photo-restitution, as for example contour lines with equidistance of 10 meters, elevation points and breaklines; then elevation points have been interpolated on a grid with spatial resolution of 50 meters. On South Piedmont, on the contrary, the interpolation has been done from the scanner profiles derived from stereoscopic models of frames with an interval equal to 60 meters.

SWISSTOPO DTM, DHM25 (LEVEL 2, TABLE 2.3)

About the generation of the DTM. The digital model provided by SwissTopo has been derived from DHM25. The DHM25 model¹ has been obtained from contour lines of maps 1:250'000 and on the border with other nations from maps 1:50'000. The precision depends on the one of the cartography map. Cross-check of the model with reference and control points revealed a standard deviation of 1.5 m in the Jura mountains, 2 m in Prealps zone and Ticino and 3-8 m in Alps.

¹<http://www.swisstopo.admin.ch/internet/swisstopo/it/home/products/height/dhm25.html>

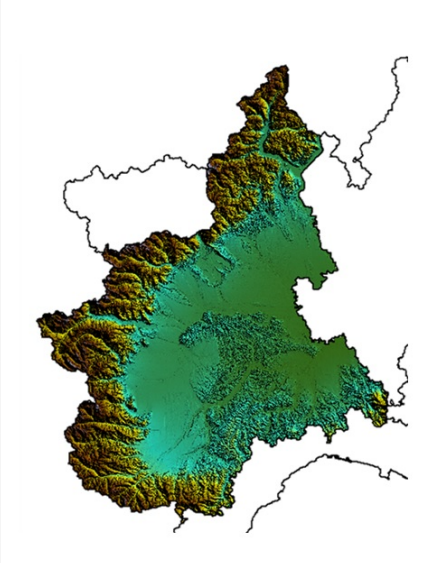
	Resolution: 50 meters
	Extension: Piedmont region
	Year of production: '90s (reorganized in 2003)
	Reference frame: WGS84 - IGM95 (ETRF89)
	Coordinate system: UTM zone 32 North, orthometric heights
	Accuracy: 2.5 m (in height), 4 m (planimetry)
	Format of memorization: ASCII grid (ESRI)
	Organization of the files: Sections, Sheets, entire Region

Table 2.2: Piedmont Region DTM.

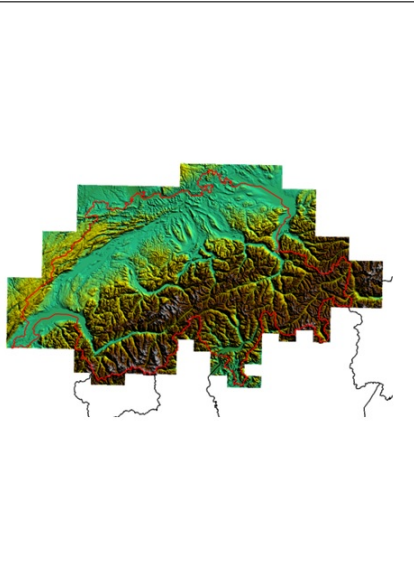
	Resolution: 1" sexagesimal (≈ 25 meters)
	Extension: Switzerland
	Year of production: 2001
	Reference frame: ETRS89
	Coordinate system: geographic, orthometric heights LN02
	Accuracy: 1.5 - 3 m (in height)
	Format of memorization: ASCII grid
	Organization of the files: Grids with constant dimension (3601x3601 points)

Table 2.3: Switzerland SwissTop DTM.

2.2.1.2 Medium and high resolution DTMs

PIEDMONT REGION DTM 5M (LEVEL 4, TABLE 2.4)

About the generation of the DTM. The DTM has been acquired through photogrammetry with LiDAR instrumentation. An automatic classification and a manual purification have been performed on the collected data.

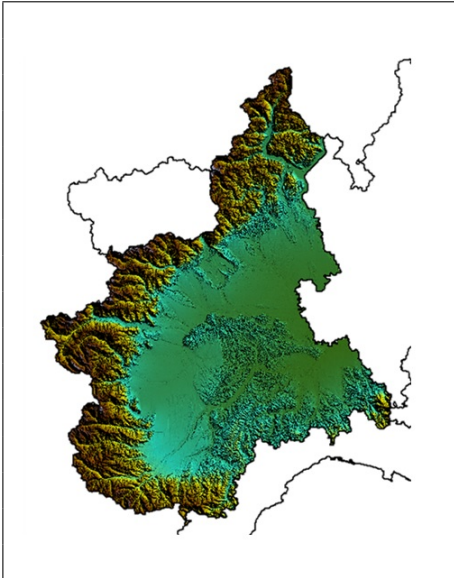
	Resolution: 5 meters
	Extension: Piedmont Region
	Year of production: 2012
	Reference frame: WGS84 - IGM95 (ETR89)
	Coordinate system: UTM zone 32 North, orthometric heights
	Accuracy: 0.3 m (in planimetry and height)
	Format of memorization: ASCII grid (ESRI)
	Organization of the files: Sections, Sheets, entire Region

Table 2.4: High resolution (5 m) Piedmont Region DTM.

MINISTRY OF ENVIRONMENT PST-A LiDAR DTM (LEVEL 4, TABLE 2.5)

About the generation of the DTM. The DTM was created as product of the Extraordinary Project of Environmental Remote Sensing; its goal is the generation and the sharing to the Public Administrations of the territorial information. The project provided the acquisition, by the Ministry of Environment, of data produced by Remote Sensing with LiDAR techniques (from aerial platform) and interferometry technique (from satellite platform) and the following cataloging of these data inside the Bank of the National Cartographic Geoportal (PCN). The final product of this project was the creation of a database for supporting decision-making processes in all areas interested by hydrogeological risk.

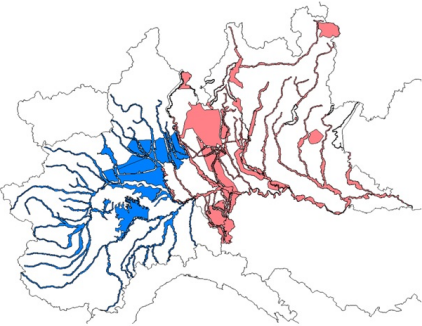
	Resolution: 0.0001 sexagesimal degrees (\simeq 1 meters)
	Extension: Piedmont and Lombardy main hydrographic basins
	Year of production: still under development and testing
	Reference frame: WGS84 - IGM95 (ETR89)
	Coordinate system: geographic, orthometric heights
	Accuracy: about 1 m (in height)
	Format of memorization: ASCII grid (ESRI)
	Organization of the files: Grids with constant dimensions (1'000 x 1'000 points)

Table 2.5: High resolution (1 m) Ministry of Environment PST-A LiDAR DTM.

2.2.1.3 Geoid models

As for the Digital Terrain Models, also for the geoid the main available models for the study area have been collected in the full accurate version. They are: the Italian geoid *Italgeo2005*, the Swiss geoid *CHGeo2004* and the two global models, *EGM2008* and *GOCEPWR2*.

These models, all recently realized, have different reference frames and resolutions. The data collected for the project are stored in ESRI grid format and cover the same area (45°N - 47°N in latitude and 7°E - 11°E in longitude).

Italgeo2005 is the official geoid model of Italy, it covers the national territory and some small neighbouring areas. It is consistent with the altimetric national model of IGMI, with the zero reference height on the Genoa marigraph. The vertical accuracy of the model is about 10 cm and the resolution is 3' (\simeq 5 km).

CHGeo2004 is the official Swiss DTM, with a precision of the order of 2-3 cm and a resolution of 30'' (less than 1 km). Outside Switzerland direct measures were not available, but the model has been regularized using local models of the neighbouring countries.

EGM2008 is a global model of the Earth gravitational field, with a resolution of 5' (\simeq 10 km) and a vertical accuracy of the order of 5-7 cm inside the HELI-DEM area.

GOCEPWR2 is a global geoid model derived by satellite observations; even if the spatial resolution is low ($\simeq 80$ km), the observations have been acquired by the same instrument all over the world and for this reason this model does not contain biases. Its vertical accuracy is of about 4 cm.

Geoid models have been used to convert ellipsoidal to orthometric heights (and vice-versa), when required, during the project. The two local models (Italgeo2005 and CHGeo2004) have been cross-validated and the results of the comparison is that they present some inconsistencies and discontinuities at the border between Italy and Switzerland, that are mainly due to the different height datum used in the estimation of the local geoids. Therefore a unique “unbiased” geoid model that covers the whole HELI-DEM area has to be created with an accuracy of few centimeters. Firstly the biases of the two local geoids have to be estimated by a least squares adjustment and after that the unbiased geoids have to be combined by means of a collocation procedure. The detail of this work are not described inside this thesis, because they have not been part of this thesis work, but they are described in detail in another previous work (Biagi et al., 2013c).

2.2.2 Implementation of the GNSS transnational reference network

To experiment a GNSS real time positioning system in a transalpine area and to validate the DTMs collected and produced during the project, a GNSS transnational network of permanent stations has been set up. First step has been the analysis of the status of already operating permanent stations (Biagi and Sansó, 2006; Cina et al., 2004; De Agostino and Manzino, 2011) able to provide data for real time positioning: most of all the permanent stations located inside the HELI-DEM area and some other stations of the neighbourhood areas (in order to enhance the geometric configuration) have been selected. The stations belong to the already existing GNSS permanent networks: GPSLombardia² for Lombardy, GNSSPiemonte³ and GeoTop for Piedmont and AGNES⁴ for Switzerland. Agreements with the managing institutions have been taken in order to obtain data in real time from the selected stations.

Figure 2.4 shows the permanent stations belonging to these networks. The network presents a high variability in height, going from a station with an elevation of 300 meters (Novara - NOVR) to a station higher than 3500 m (Jungfrau Joch - JUJO). This variability can have a significant impact on the modelling of atmospheric errors (tropospheric delays of the signal) of the network. Table 2.6

²<http://www.gpslombardia.it/>

³<http://gnss.regione.piemonte.it/frmIndex.aspx>

⁴<http://www.swisstopo.admin.ch/internet/swisstopo/en/home/topics/survey/permnet/agnes.html>

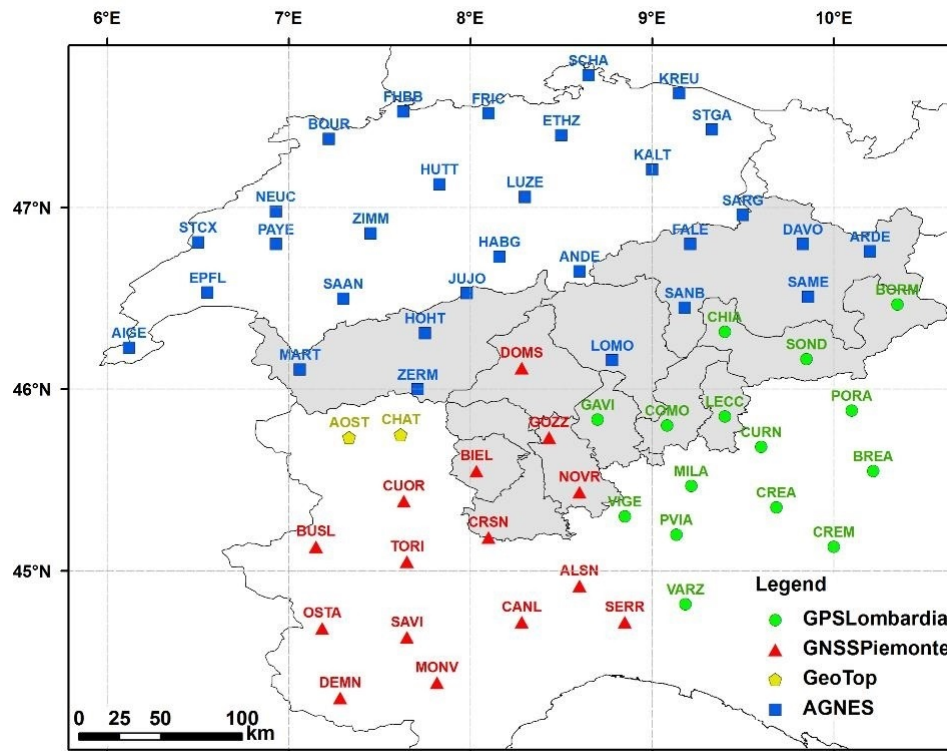


Figure 2.4: GNSS permanent stations inside the HELI-DEM project area (area in grey) (Biagi et al., 2013c).

contains the list of the HELI-DEM stations with their relative original network. Before doing tests in real time, the three networks have been adjusted with the BERNESE 5.0 software (BSW5.0) in the IGS08 reference frame. The network adjustment has been done according to the *EPN Processing Instruction for Local Analysis Centres* guidelines. 14 sections with a duration of 24 hours, correspondent to the GPS days from 269 to 282 (from the 26th September to the 9th October 2011), have been processed. The permanent stations of the HELI-DEM network have been adjusted by constraining the barycentre of five permanent stations belonging to the IGS network, BZRG, GENO, IENG, PADO, ZIMM, highlighted in Figure 2.5, to their official coordinates. The network has been adjusted in IGS08, with 2011.8 as reference epoch. The software that manages the network to provide a real time data and corrections is Spider 4.2. Once the positioning service has been activated, three operations have been done:

- Italian and Swiss surveys to verify the quality of the RTK positioning at different heights,
- measurement surveys useful to validate the existent DTMs and the final

DTM,

- measurement surveys to support some levelling campaigns, that have been done to re-survey some lines of the old levelling networks of Lombardy, Piedmont and Switzerland.

Station		Network	Managing Authority	Elevation (m)
Bormio	BORM	GPS Lombardia	GPS Lombardia	1263.4
Chiavenna	CHIA	GPS Lombardia	GPS Lombardia	391.6
Como	COMO	GPS Lombardia	GPS Lombardia	292.3
Gavirate	GAVI	GPS Lombardia	GPS Lombardia	343.7
Lecco	LECC	GPS Lombardia	GPS Lombardia	311.1
Sondrio	SOND	GPS Lombardia	GPS Lombardia	529.2
Vercelli	VERL	-	Politecnico di Torino	183.9
Biella	BIEL	GNSS Piemonte	GNSS Piemonte	480.5
Domodossola	DOMS	GNSS Piemonte	GNSS Piemonte	365.6
Gozzano	GOZZ	GNSS Piemonte	GNSS Piemonte	416.6
Novara	NOVR	GNSS Piemonte	GNSS Piemonte	218.6
Andermatt	ANDE	AGNES	SWISS-TOPO	2384.3
Jungfrau	JUJO	AGNES	SWISS-TOPO	3634.6
Locarno Monti	LOMO	AGNES	SWISS-TOPO	438.0
Samedan	SAME	AGNES	SWISS-TOPO	1759.2
San Bernardino	SANB	AGNES	SWISS-TOPO	1702.2
Zermatt	ZERM	AGNES	SWISS-TOPO	1931.2

Table 2.6: Permanent network stations inserted inside the HELI-DEM transnational network.

To verify the correctness of the operation and the quality of the permanent HELI-DEM network for the real time positioning, some GNSS measures have been done, choosing some portion of the territory with high elevation variability. In Piedmont for example the Val Sesia Valley has been chosen because it presents high morphological variability. The results of these surveys allow to confirm that the network works well, also at high elevations (Biagi et al., 2013c).

2.2.3 Transformation between different reference frames

As said in Section 2.2.1, the input elevation data collected within the project are georeferenced in different reference frames and coordinates. Some DTMs are in ETRF89: the Switzerland DTM and the PST-A LiDAR DTM produced by the Ministry of Environment in geographic coordinates, the two Piedmont Region

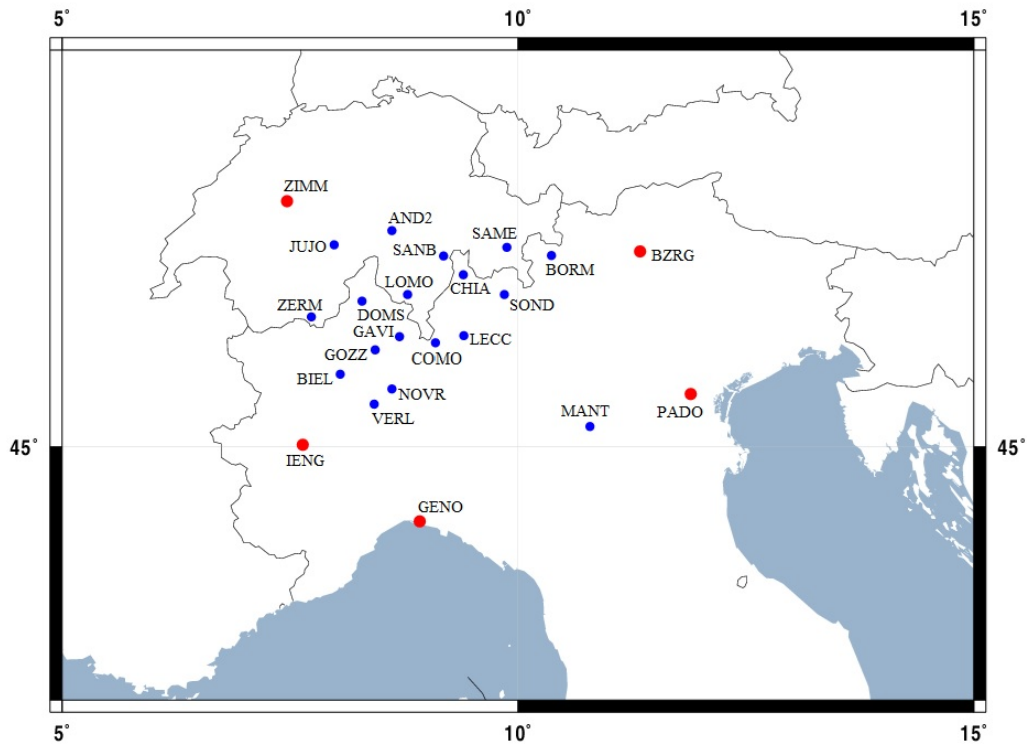


Figure 2.5: HELI-DEM network: in red the reference frame constraining stations, in blue the HELI-DEM stations.

DTMs with a planimetric resolution respectively of 50 and 5 m in cartographic coordinates. The Lombardy DTM is instead in the old Italian Roma40 reference frame, Gauss Boaga projection. In order to merge the collected DTMs into a unique archive, all the data have to be expressed in a common reference frame. In Appendix A the reference frames mentioned here are briefly described.

The choice of the final reference frame has been done uniquely, because the HELI-DEM project has a transnational extension and is founded by the European Community. According to the EUREF (IAG Reference Frame Sub-Commission for Europe) guidelines, the reference frame of the final unified DTM has been chosen to be the ETRF2000. Note that the transformation between ETRF89 and ETRF2000 could in principle be avoided because the differences between different realizations of ETRFyy have a magnitude of few centimeters and are very small with respect to the grid spacing of the original DTMs and of the final unified DTM. On the contrary, the transformation is not negligible in case of Roma40, because the differences between Roma40 and ETRFyy have a magnitude of hundred meters and are very variable on the national territory, as can be seen in Figure 2.6.

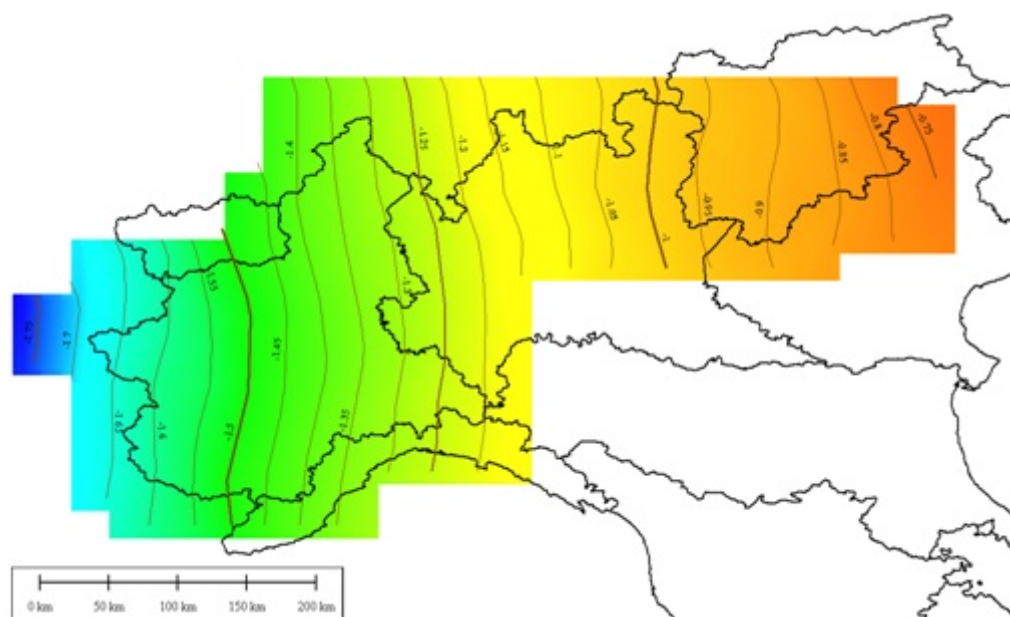


Figure 2.6: Corrections in longitude between the Roma40 and ETRF89 (sexagesimal seconds) reference frames on the HELI-DEM area of interest.

To transform all the data to ETRF2000 a software for performing DTMs transformation between different reference frames and coordinates has been implemented. The program, called *GK2CNV*, allows the transformation among the different above described reference frames (ETRF2000, ETRF89 and Roma40) and coordinate systems. The program can receive in input a list of 3-D coordinates, a single DTM (in the most used ASCII formats) or a list of DTMs. The output is always a list of 3-D coordinates, independently of the type of input data. Even in case of a gridded input in fact the center of each cell in the original reference frame is converted in a tern of coordinates in the final reference frame: the transformation of a grid from a reference frame to another produces a set of scattered points already regularly distributed but not no longer located on the nodes of an oriented grid. It follows that in case a grid is transformed from its original reference frame to another, it is necessary to regrid the output.

GK2CNV software is developed in FORTRAN language under the GNU (General Public License⁵). The transformation among reference frames is performed according to Euref guidelines and their Italian adaptation written by IGMI (Altamimi and Boucher, 2001; Donatelli et al., 2002) and already implemented in the VERTO software. In case of transformation from Roma40 to ETRFyy, the transformations are based on latitude, longitude and height shift values, gridded for the

⁵<http://www.gnu.org/licenses/gpl-2.0.html>

```

#####
## GK2CNU - GK2 Converter                                     ##
##                                                                 v. 2.0 ##
##                                                                 ##
##      <C> 2011 Politecnico di TORINO - DITAG                ##
##                                                                 ##
## Programma di conversione tra sistemi di riferimento      ##
## e/o sistemi di coordinate secondo la procedura          ##
## UERTO di I.G.M.I.                                       ##
##                                                                 ##
## Sviluppato nel progetto:                                   ##
## Interreg IT-CH 2007-2013 <ID: 13881216>                 ##
## HELIDEM - Helvetia-Italy Digital Elevation Model       ##
##                                                                 ##
## Distribuito con licenza GNU General Public License     ##
## v. 3.00 e successive. Digitare "10" per ulteriori      ##
## dettagli sulla licenza.                                  ##
##                                                                 ##
#####
Questo programma consente di effettuare trasformazioni
tra diversi sistemi di riferimento e di coordinate.

-----
CONVERSIONE TRA SISTEMI DI RIFERIMENTO
-----
<1> Conversione di un singolo DEM
<2> Conversione di una lista di DEM
<3> Conversione di una lista di coordinate

-----
CONVERSIONE TRA SISTEMI DI COORDINATE
-----
<4> Conversione di un singolo DEM
<5> Conversione di una lista di DEM
<6> Conversione di una lista di coordinate

```

Figure 2.7: Initial screen of the GK2CNV software (Biagi et al., 2013b).

entire national territory with a spatial resolution of 5' in latitude and of 7'30" in longitude (Figure 2.8). A total of seven sets of grids, georeferenced in the Roma40 reference frame (differences with respect to ETRF89) and in the ETRF89 reference frame (differences with respect to ETRF2000) are distributed by IGMI. The vertices (more than 800) used for the calculation of the national transformation parameters between the different frames belong to the National geodetic network IGM95.

In the most common case, in which the point to be transformed does not coincide with a grid node, the shift value is obtained interpolating the four nodes closest to the point through a bilinear interpolation algorithm .

During HELI-DEM, the GK2CNV program has been used for all the procedures in which transformations between reference frames or coordinates were necessary.

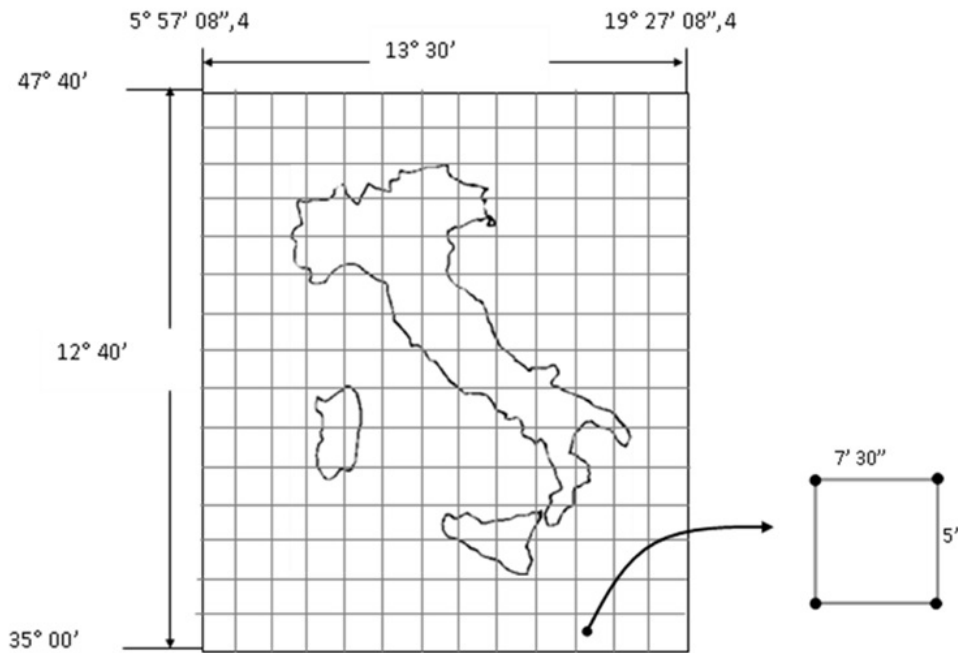


Figure 2.8: Structure of the VERTO grids.

2.3 Comparisons between DTMs

To check the accuracy of the available DTMs and to decide which DTMs can be used for the creation of the final unified DTM, some cross-validations between the different elevation products have been performed. To cross validate the DTMs, two different analyses have been carried out. The first is the cross-validation between cross-border DTMs with similar planimetric resolution and height accuracies, where they overlap, i.e. at the border between their domain. The second comparison, which can be considered as an external validation, has been performed between low and high resolution DTMs in the areas where the latter ones exist. Within the project, several comparisons have been carried out by the different research units. All them are described in detail in the project reports. In the following only the analyses performed by the author of the thesis will be discussed.

Since these DTMs are not all in the same reference frame, before doing the cross-validations some datasets have been transformed to a common reference frame. To do that, the program GK2CNV which allows to transform a list of points or a grid from one input reference/coordinate frame to another one has been used (details of the program are in 2.2.3).

It has to be taken into account that the aim of this work of comparisons be-

tween different DTMs is only an assessment of the accuracies of the available DTMs; the correction of the DTMs has been not part of this thesis work and also of the HELI-DEM project. Another specification has to be done before dealing with the results of the comparisons and validations: the σ of the differences and of the Least Squares, when appears in the tables of the statistics, are not representative of the input data. In fact the correlations of the input data have not been considered and for this reasons the analyses have to be considered as consistency evaluations and not significance analyses.

2.3.1 Cross-validation between similar DTMs

The cross-validation between similar DTMs has been performed on the low or medium resolution regional and national DTMs, that are the regional Lombardy DTM with a planimetric resolution of 20 m, the regional Piedmont DTM with a planimetric resolution of 50 m and the national Switzerland DTM with a planimetric resolution of about 30 m. Their characteristics are reported in section 2.2.1. With these low-resolution DTMs three cross-validations have been carried out, considering each time a different couple of DTMs:

1. Lombardy DTM and Switzerland DTM,
2. Lombardy DTM and Piedmont DTM,
3. Piedmont DTM and Switzerland DTM.

The cross-validations have been executed implementing proper procedures in MATLAB environment. Details of the comparison between the Lombardy and the Switzerland DTMs are described below. Analogous procedures have been adopted for the other comparisons, that have been done by Politecnico di Torino (Biagi et al., 2013a) and are not described in this thesis.

A preprocessing of the Lombardy data has been necessary before performing the comparisons. In fact, studying the slope and aspect of the DTM, it has been highlighted that it presents some problem in the data. The first problem affects only one grid (grid A3) of the DTM. The East-Northern part of this grid, which covers the northern area of Lago Maggiore, near Luino (Figure 2.9), does not follow the exact profile of the Lombardy regional border.

The anomalous morphology of these data is visible in the left image of Figure 2.10, which shows the slopes of the original Lombardy A3 grid. In the East-Northern side of the grid, the slopes have all the same values and the data seems to be located on a uniformly inclined plane. Since these erroneous data are outside the Lombardy boundary and this area is covered also by the Swiss DTM, this

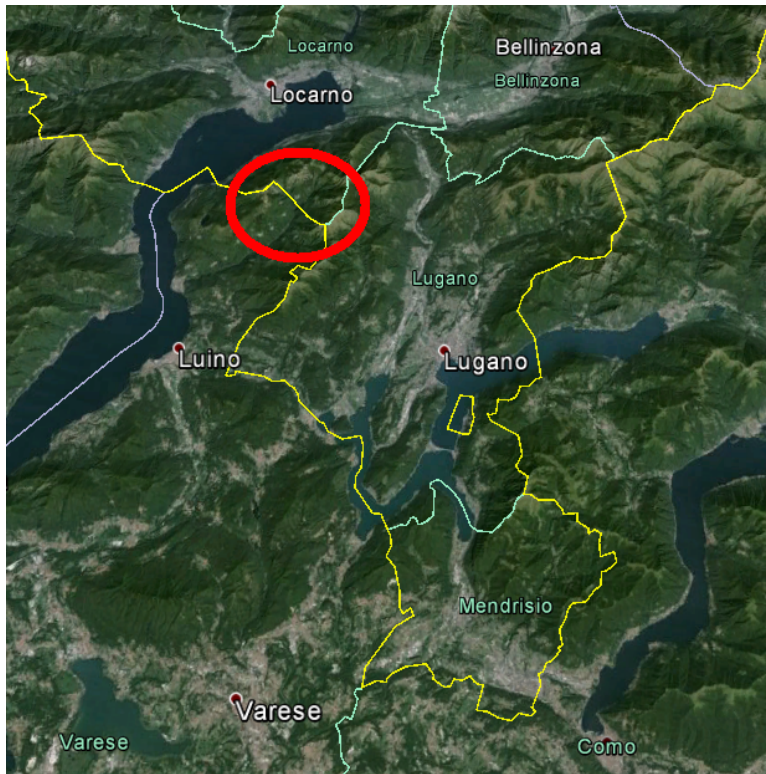


Figure 2.9: Area of the Lombardy DTM which presents some incorrect data.

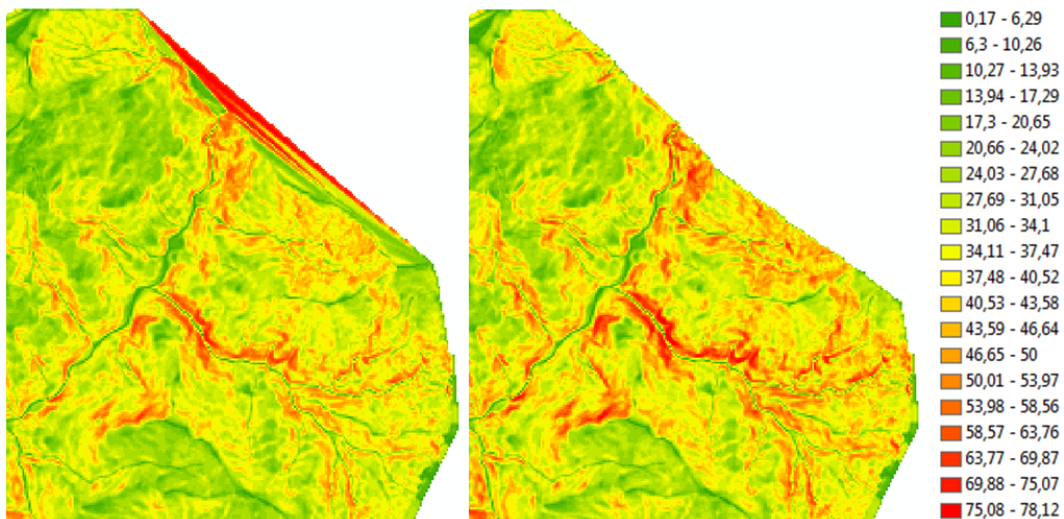


Figure 2.10: Slope of Lombardy DTM grid A3 which presents incorrect data: on the left the original data, on the right the corrected data. Values of slopes in degrees.

piece of DTM is not strictly necessary. For this reason these incorrect data have been deleted from the Lombardy grid.

The second problem has been found in the part of Lombardy DTM which protrudes in Piedmont. In fact, even if the border between Lombardy and Piedmont splits Maggiore Lake and Ticino River in two parts (Figure 2.11), both Lombardy and Piedmont DTMs cover also a portion of Maggiore Lake and Ticino River that is located in the other region.

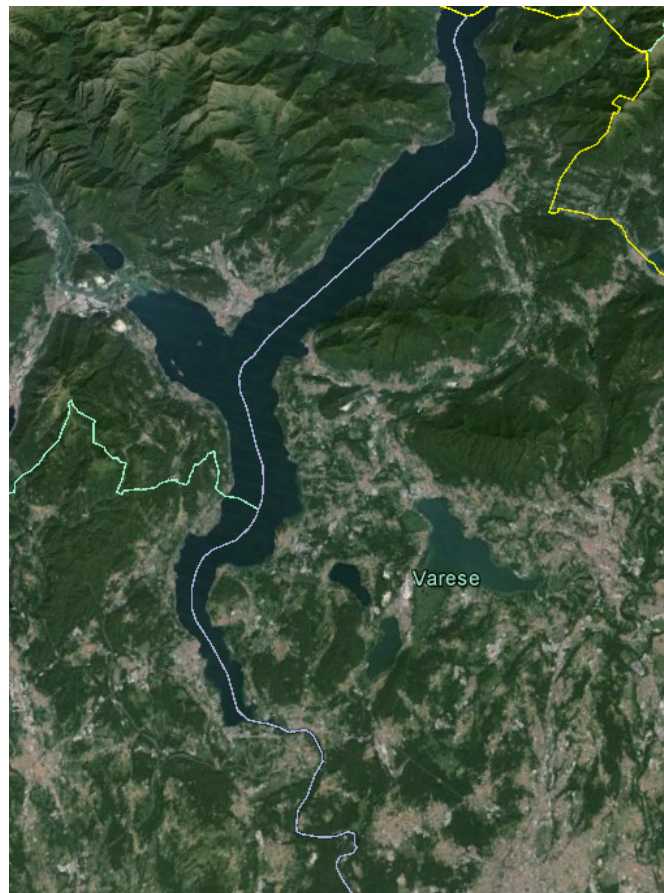


Figure 2.11: Border of Lombardy and Piedmont through Maggiore Lake and Ticino River (violet line).

Figure 2.12 shows a portion of the two DTMs: inside the red circle the area of Maggiore Lake and Ticino River is highlighted. The part of Piedmont DTM in Lombardy area is correct, while the part of Lombardy DTM in Piedmont area is not correct, because Lombardy DTM prolongs the lake (conventionally at an elevation of 193 m) for at least 12 km² of the Ticino valley immediately below the Ticino River river-head. In the figure the color scale has been saturated from 150

to 250 m so that the elevation values of this area are more visible: it is visually clear the error in the Lombardy DTM.

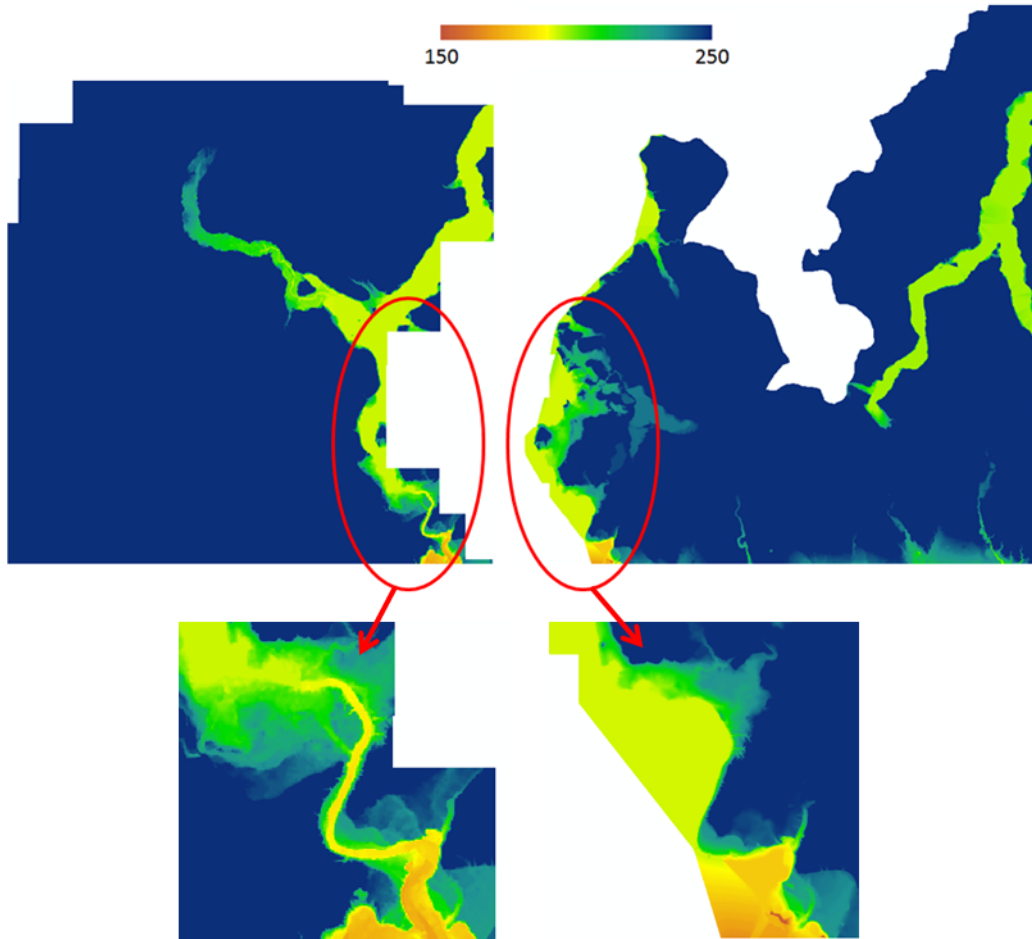


Figure 2.12: Portion of Piedmont (on the left) and Lombardy (on the right) regional DTMs covering Maggiore Lake and Ticino River: in red the same border area between the two DTMs is highlighted. The colour scale is reduced from 150 to 250 m so that the problem in the Lombardy DTM is more visible.

As for the Luino case, also these erroneous data have been removed from the Lombardy DTM, before performing every following analysis.

2.3.1.1 Lombardy DTM vs. Switzerland DTM

The Lombardy and Switzerland DTMs have different planimetric resolutions and vertical accuracies and are georeferenced in two different reference frames. Their main characteristics are reported in Table 2.7. The two DTMs have different but similar resolutions and accuracies; for this reason to perform their cross-validation, no one of them can be considered as truth. Therefore the two DTMs have been compared on some points that do not coincide with the nodes of one of them (Biagi et al., 2012), but that are located in random positions in the overlapping area. The overlapping area, shown in Figure 2.13, is entirely included in the Italian territory: Lombardy DTM is in fact cut in order to cover only Lombardy, while the Swiss DTM occupies part of the Lombardy area near the border between the two countries.

	LOMBARDY DTM	SWITZERLAND DTM
Planimetric resolution	20 m	$2.8 \cdot 10^{-4}$ deg ($\simeq 30$ m)
Elevation accuracy	5-10 m	1.5-3 m
Reference frame	Roma40 - Gauss Boaga	ETRF89 - geographic coordinates

Table 2.7: Main characteristics of Lombardy and Switzerland regional DTMs.

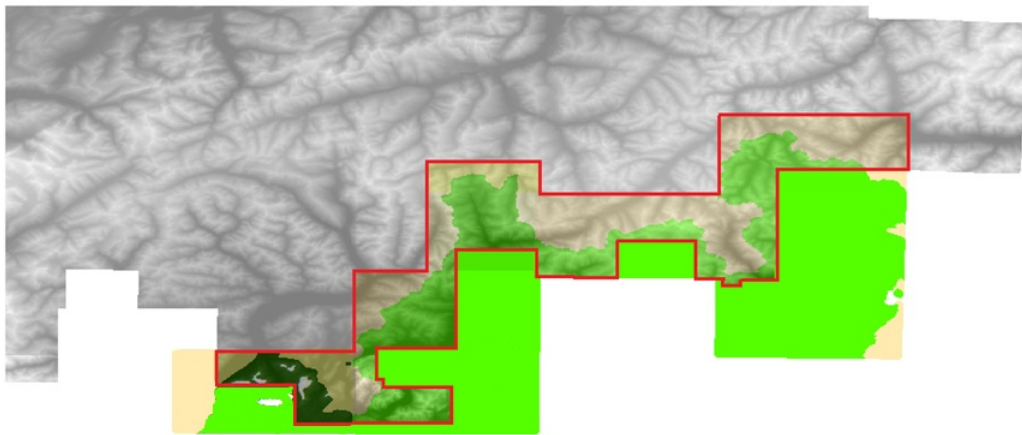


Figure 2.13: Overlapping area between Lombardy and Switzerland DTMs. In gray scale the Switzerland DTM, in colors the Lombardy DTM, in red the border of their overlapping area.

The set of points (set of their 2-D coordinates) on which the two DTMs have been interpolated was extracted from a uniform random variable, so that they are located inside the limits of the overlapping area. The number of extracted points

has been chosen so that the inter-distance between two nearest points in both x and y directions is of about 100 meters. A denser mesh would imply much longer computation times.

Since the two DTMs are georeferenced in two different reference frames, firstly the points have been extracted randomly in the ETRF89 reference frame in geographic coordinates. The Switzerland DTM has been interpolated directly on the 2-D extracted coordinates, while to interpolate the Lombardy DTM, the coordinates of the points have been previously converted using the GK2CNV program from ETRF89 (ϕ, λ) to Roma40 (East, North).

For each point two elevations have been obtained, through exact bicubic interpolation from the nodes of the Switzerland DTM (h_S) and then from those of the Lombardy DTM (h_L). To perform the exact bicubic interpolation in one point with known planimetric coordinates, the 16 nearest nodes around it are searched. Because the nodes are on a regular grid, it is possible to use an exact bicubic interpolation, described in detail in Section B.1.3.1. Then for each point the elevation difference, $\Delta h = h_S - h_L$, has been calculated. NO-DATA value was assigned to a difference in two cases:

1. the extracted point is outside the area of one of the two DTMs,
2. one of the interpolated elevations (or both) results equal to NO-DATA, that happens if at least one elevation of the 16 nearest points is equal to NO-DATA.

Several statistical analyses have been done on the elevation differences:

- computation of some statistical values, maximum, minimum, mean, standard deviation, only for the points with a useful value,
- division in classes and estimation of the percentage of points that belong to each class,
- adaptation test to a Gaussian to verify if the sample is normally distributed,
- analysis of linear correlation of the differences with some orographic parameters, in order to verify if the elevation differences depend on the original points elevation or slope,
- covariance analysis in order to verify the spatial correlation between points.

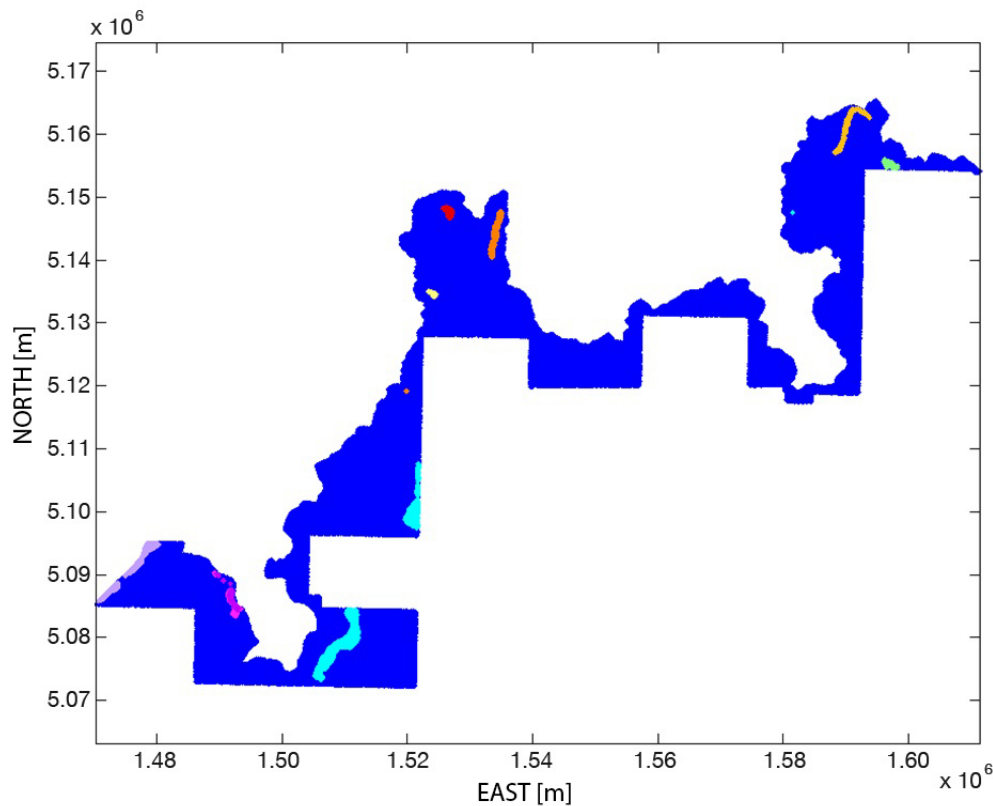


Figure 2.14: Overlapping area between Lombardy and Swiss DTMs and density of the randomly extracted points. In colours the areas belonging to lakes (no comparisons on them) are highlighted.

Results

Figure 2.14 shows the distribution of the points with valid differences. The points belonging to lake areas, highlighted in figure, have been deleted from the set of differences before computing the statistics: in fact these areas are memorized with different reference values in the two DTMs. This is not due to measurement errors in one of the two DTMs, but probably different values have been assigned to the free water surface of the lakes in the two DTMs. For example points belonging to Como Lake have a value of 197 m in the Lombardy DTM and 199 m in the Switzerland DTM, while to Truzzo Lake a value equal to 2050 m is assigned in the first DTM and 2080 m in the second, with a constant difference of 30 m for all the points belonging to this lake. In order to exclude from the dataset points belonging to lakes, the histogram of the differences has been studied. For each lake, a pick with a constant value exists in the histogram; each pick has been identified and removed, deleting all points with differences equal to that value.

Number of valid points	256'737
Mean	-0.1 m
Std	18.9 m
Maximum	352 m
Minimum	-256 m

Table 2.8: Statistics of the elevation differences between Switzerland and Lombardy DTMs.

In Table 2.8 the statistics of the useful differences of the interpolated elevations of the global overlapping area between Lombardy and Switzerland are reported. The differences are distributed with a mean value almost equal to zero. Considering that the nominal standard deviation of the Swiss DTM is equal to 5 meters and those of the Lombardy DTM is equal to 10-15 m, their difference should have a standard deviation of $\sigma = \sqrt{\sigma_1^2 + \sigma_2^2} \approx 13.4m$. The standard deviation obtained from the comparison is greater, but it is at least comparable. To this regard it should be taken into account that this comparison is relative to an area with alpine and pre-alpine orography, that is morphologically complex. On the other hand, some significant anomalies, which are differences that reach 300 meters, are present.

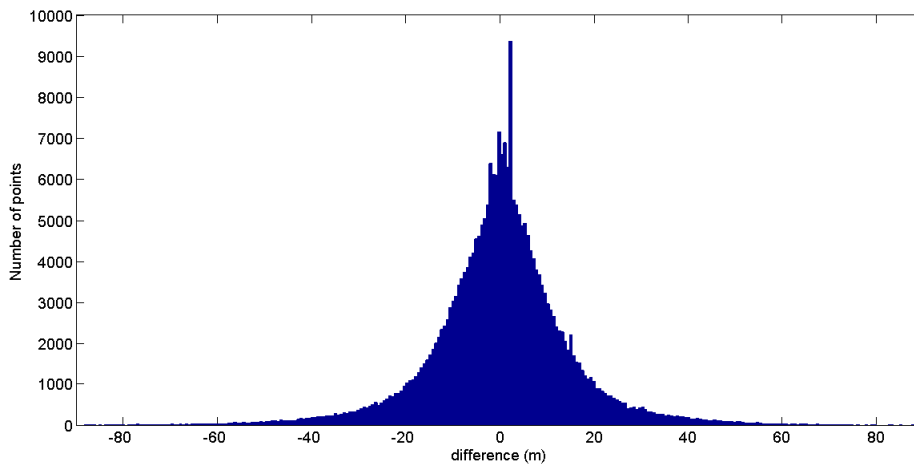


Figure 2.15: Histogram of the elevation differences between Lombardy and Swiss DTMs.

From the histogram of the differences (Figure 2.15) and the subdivision of the points in different classes depending on the difference values (Table 2.9) it can be seen that most of the points, about the 85%, have differences lower than 20 meters

Differences (m)	Percentage with respect to the total number of points
$\Delta H < -100$	0.2%
$-100 \leq \Delta H < -40$	2.0%
$-40 \leq \Delta H < -20$	5.6%
$-20 \leq \Delta H < -10$	11%
$-10 \leq \Delta H < 0$	29%
$\Delta H = 0$	0.0%
$0 < \Delta H < 10$	32%
$10 \leq \Delta H < 20$	12%
$20 \leq \Delta H < 40$	5.7%
$40 \leq \Delta H < 100$	1.8%
$\Delta H \geq 100$	0.1%

Table 2.9: Classes and percentage of elevation differences between Lombardy and Swiss DTMs.

and so acceptable with respect to the nominal accuracies of the two DTMs; only the 4% of the differences is higher than 40 meters and the 0.3% exceeds 100 m.

A normality test has been done to verify if the distribution of the differences fits a Gaussian distribution with mean and standard deviation equal to those of the data (-0.1 m and 18.9 m respectively), computed inside the interval $-3\sigma \div +3\sigma$, where σ is the standard deviation of the differences. The result of the test is shown in Figure 2.16.

As can be seen, there is no good adaptation between the measured height differences distribution and the Gaussian distribution; in particular the empirical values are more concentrated around the mean and they tend to differ from the theoretical distribution, in particular in the neighbourhood of $\pm\sigma$. This is confirmed also by the classical chi square adapting test, that is not satisfied.

To obtain some information about the spatial distribution of the differences, following the same classification shown in Table 2.9, that is the subdivision of the interpolated points in eleven different classes depending on the differences between the two DTMs, a map of the differences has been created: a different colour has been assigned to each class.

From a simple visual inspection the differences seem to present an anomalous spatial distribution: the highest values (dark red and dark blue) are concentrated in some specific areas, that correspond only in some cases to the most mountainous zones. The anomalous distribution is evident if the modulus of the differences is plotted and, over this, the grids subdivision of the Lombardy DTM is overlapped (Figure 2.17). Grids B2 and C2 contains the highest differences; even

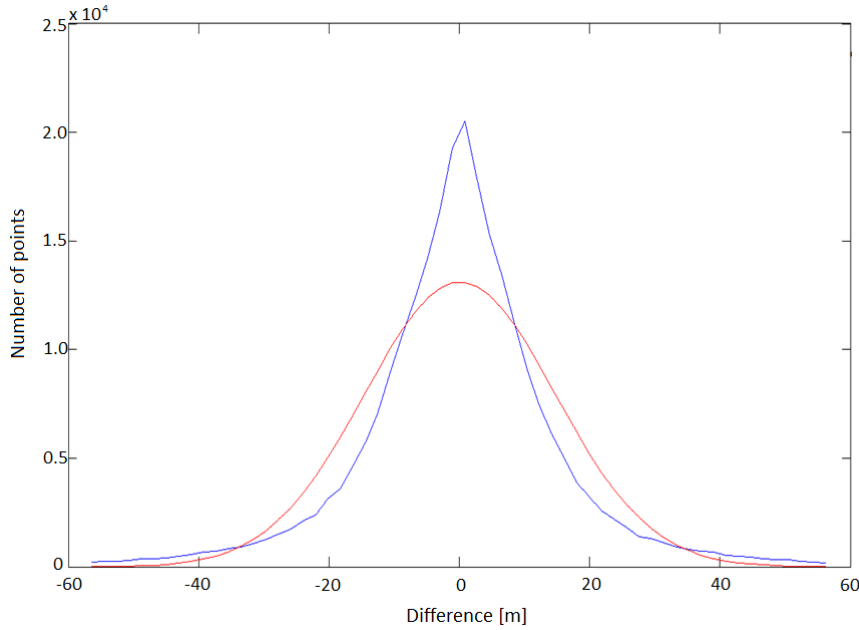


Figure 2.16: Normal test of the differences between Lombardy and Swiss DTMs (theoretic distribution in red, real distribution in blue).

if both grids cover mountainous areas, it seems strange that they present worse differences with respect for example to grid B1, which is closer to the Alpine watershed and presents smaller difference values.

The empirical covariance of the differences has to be studied in order to verify if a spatial correlation between the planimetric positions of the points exists. In fact the degree of similarity between pairs of surface points can be described by a correlation function (Li et al., 2005), described as follows:

$$R(d) = \frac{Cov(d)}{Cov(0)} \quad (2.1)$$

where $Cov(d)$ is the covariance of all the points with horizontal distance d , and $Cov(0)$ is the covariance in the origin. The mathematical function of $Cov(d)$ is:

$$Cov(d) = \frac{\sum_{i=1}^{N_d} (Z_i - M)(Z_{i+d} - M)}{N_d - 1} \quad (2.2)$$

where Z_i is the elevation of the point i , Z_{i+d} is the elevation of a point with an horizontal difference of d from point i , M is the average height value of all the points; the sum is computed on the N_d couples of points with reciprocal distance equal to d . In general the values of $Cov(d)$ decreases at the increase of d .

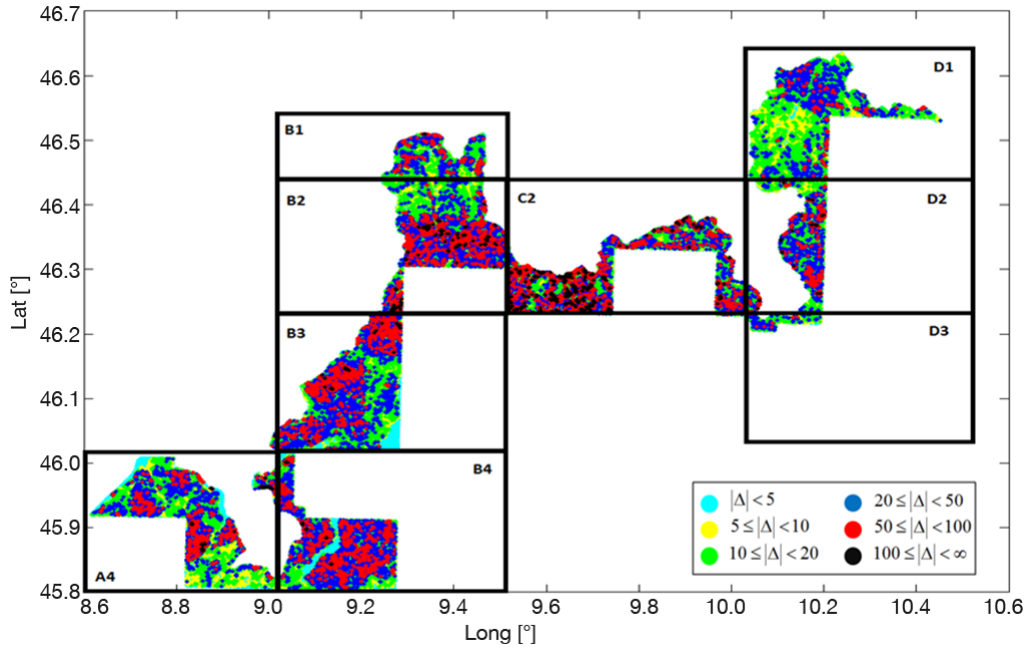


Figure 2.17: Absolute values of the elevation differences between Lombardy and Swiss DTMs, divided in 6 classes. The borders of the Lombardy DTMs grids are overlapped.

The analysis of covariance of the differences between Italy and Swiss DTMs have been performed on some areas with an extension of few kilometers. Here only one example is shown (Figure 2.18): the covariance function is relative to 3000 points that are located inside an area of 5 km² inside grid C2 of the Lombardy territory. The maximum distance between points is of about 1 km. Covariance values of the differences between Lombardy and Swiss DTMs have been plotted against the distance between pairs of data points. From the graph it can be seen that a certain spatial correlation exists between the elevation differences. The empirical covariance halves at an interdistance between points of about 90 m. The empirical covariance function follows an exponential trend. In the figure the exponential model function

$$Cov(d) = a \cdot e^{b \cdot x} + c \quad (2.3)$$

in which values of 360.5, -45040 and 10 have been associated to the three coefficients a , b and c , has been plotted on the same graph of the empirical covariance. The exponential model seems to well fit the empirical values. Other tests reproduce similar results.

Other analyses have been done in order to verify if a certain correlation exists between the differences and the territory orography. Therefore the linear correlation

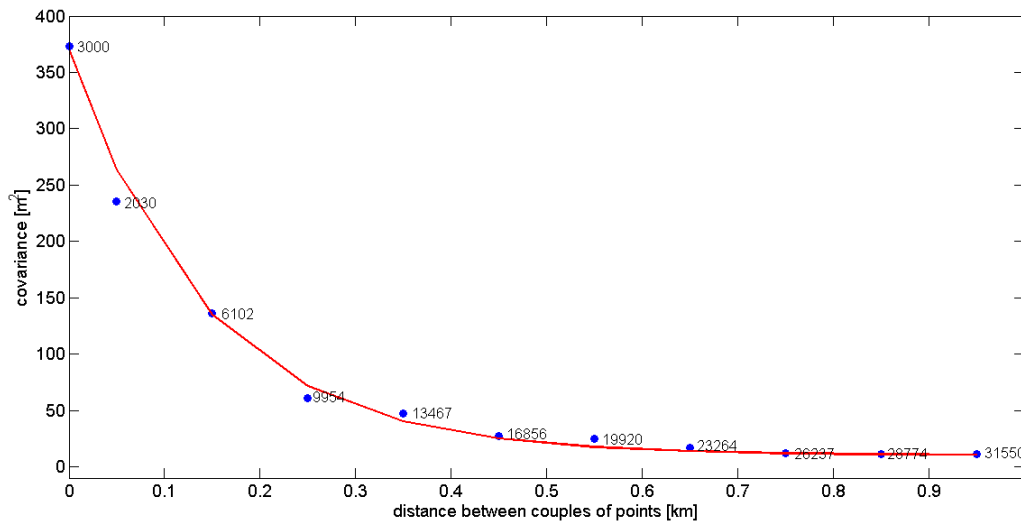


Figure 2.18: Empirical covariance function (blue points) of the differences between Lombardy and Swiss DTMs and exponential model (red line).

coefficient between differences and elevations has been computed: this coefficient resulted not significative and so no dependency of the differences from terrain elevations exists. Since the terrain slope is more representative of the orographic complexity of the terrain, for every extracted point the slope has been computed with the usual algorithms (Li et al., 2005).

As for the elevations, also in this case the correlation between the absolute values of the differences and the slopes has been estimated. Again, the correlation between differences and slopes is not significative. An example of this analysis is shown in Figure 2.19, where the differences between Lombardy and Swiss DTMs of points belonging to Lombardy grid C2 have been plotted respectively against terrain elevations (Figure 2.19(a)) and terrain slopes (Figure 2.19(b)).

In conclusion the worst differences follow regular cuts that have nothing in common with orography, but that seem to have some relation with the shapes of some digitalization panels: this situation is particularly visible in grids B3 and B2 (Figure 2.17). For example in this grid it seems that two different operators have done the digitalization or the photogrammetric restitution in a not consistent way: in fact only a part of the grid has high differences, while the others are low, but with a net division.

To better study this phenomenon some additional analyses on smaller areas have been executed, considering each time a single grid of the Lombardy DTM and the Swiss grid that is superimposed to it. The two grids are thus compared on the points that are located inside the overlapping area between the two grids, among all the dataset of points extracted from the whole overlapping area. As

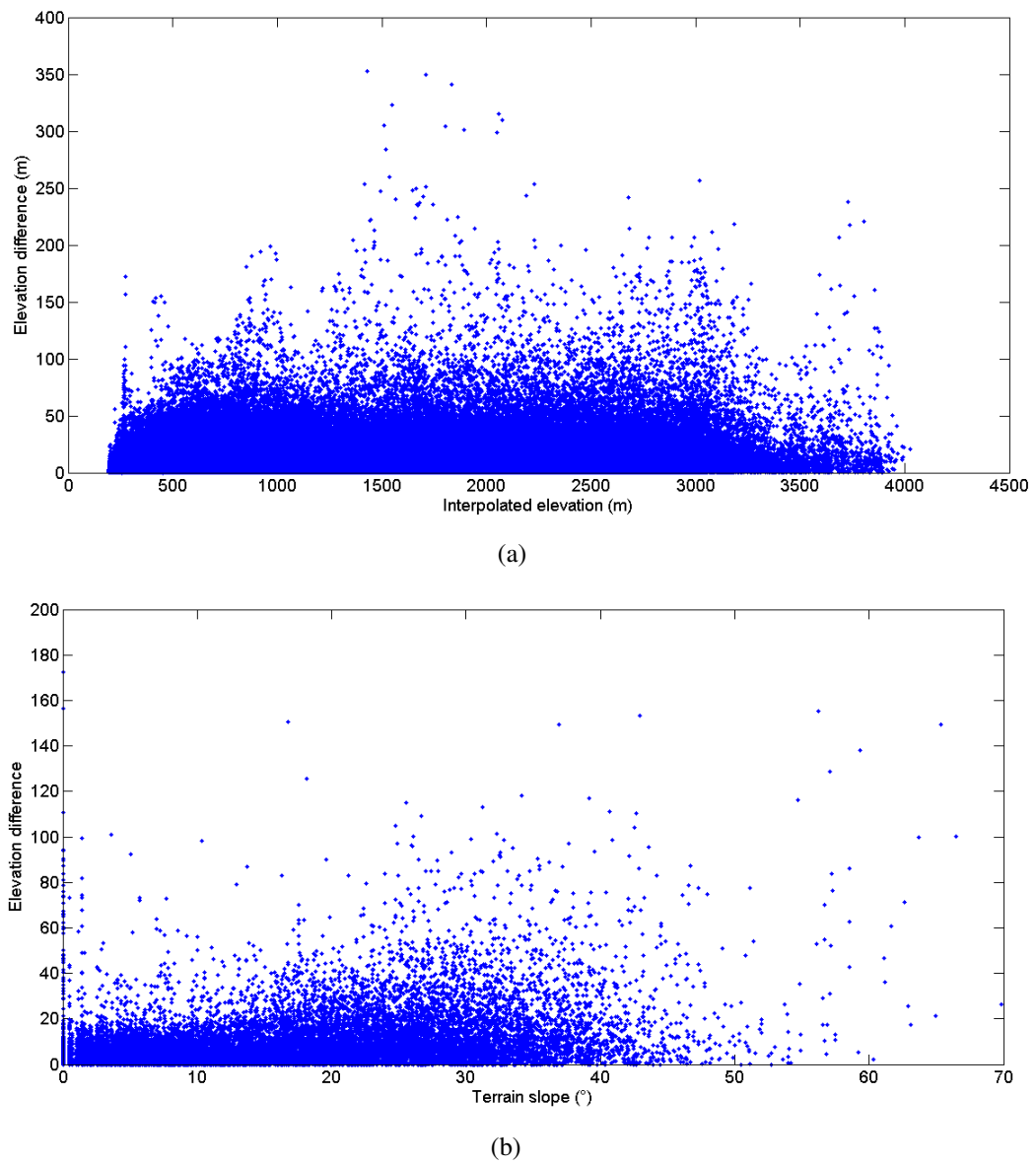


Figure 2.19: Correlation between differences (Lombardy-Switzerland) in elevation and original elevations (a) and slopes (b).

examples the worst and the best areas are presented here.

Grid C2: Area included in grid C2 presents the worst differences between Lombardy and Swiss DTMs. The number of useful points that fall inside this grid is 32'698 and the statistics of the differences are summarized in Table 2.10.

Number of useful points	32'698
Bias	-4 m
Std	29 m
Maximum	352 m
Minimum	-256 m

Table 2.10: Statistics of the elevation differences between grid C2 of Lombardy DTM and grid e009n46 of Switzerland DTM.

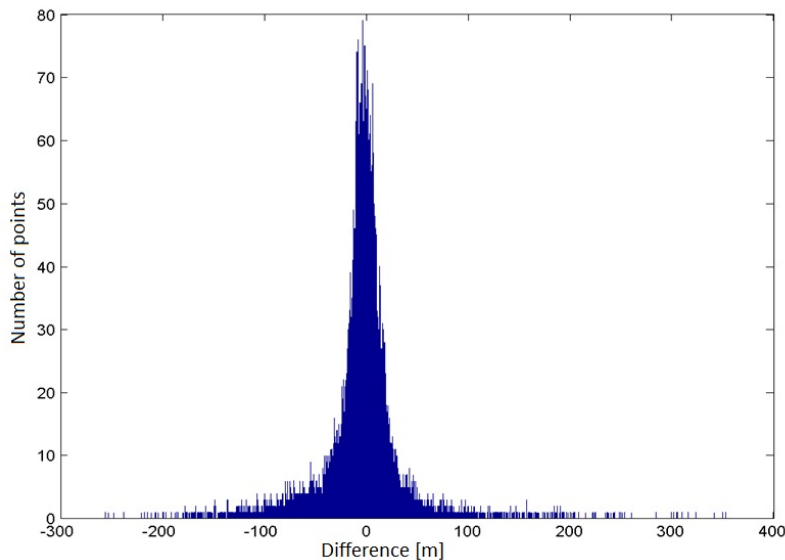


Figure 2.20: Histogram of the elevation differences between grid C2 of Lombardy DTM and grid e009n46 of Switzerland DTM.

In this area the statistics of the differences are actually worse with respect to those of the whole overlapping area between the two DTMs. In fact, the mean equal to 4 meters and the standard deviation equal to 29 m are far higher with respect to the global ones (mean of 0.1 and std of 18 m). Figure 2.20 shows the histogram of the differences: the values are less concentrated around the mean and the 13.4% of the points presents a difference greater than 40 meters. Also in this case the results of the normality test and of the analyses of the correlations between differences and elevations/slopes indicates that the differences sample does not follow a Gaussian distribution and does not depend from original elevations or slopes.

Grid D1: Area included in grid D1 presents the best difference values among all the Lombardy grids. In fact, as can be seen from Table 2.11, the statistics are in this case better than those of the whole overlapping area.

Number of useful points	36'801
Mean	0.3 m
Std	11 m
Maximum	79 m
Minimum	-84 m

Table 2.11: Statistics of the elevation differences between grid D1 of Lombardy DTM and grid e010n46 of Switzerland DTM.

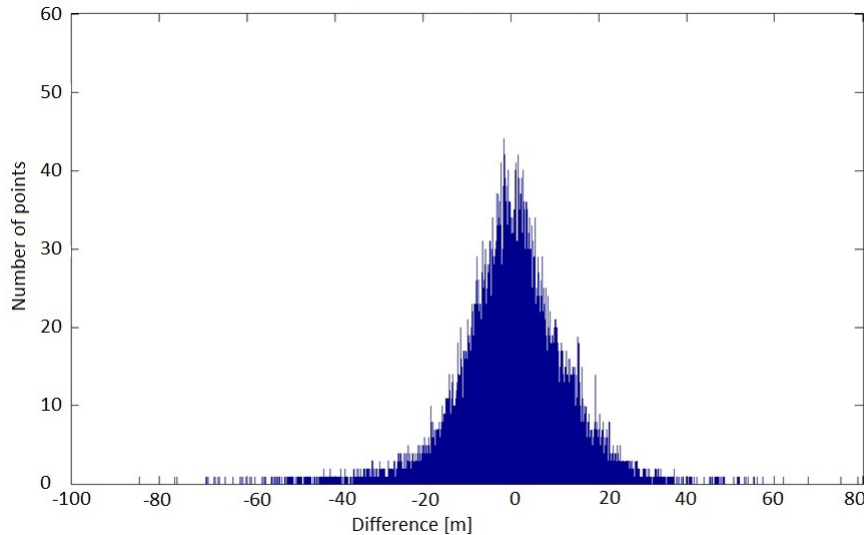


Figure 2.21: Histogram of the elevation differences between grid D1 of Lombardy DTM and grid e010n46 of Switzerland DTM.

Figure 2.21 shows the histogram of the differences. Also in this case the normality test and the estimation of correlation between differences and elevations and slopes show that also for this area the sample does not follow a Gaussian distribution and no correlation exists between the differences and the terrain orography.

Also in this case the normality test and the estimation of correlation between differences and elevations and slopes have been performed: the results are that also for this area the sample does not follow a Gaussian distribution and no correlation exists between the differences and the terrain orography.

To have a general idea, the statistics of the elevation differences in all the grids are summarized in Table 2.12.

Grids couple	Mean (m)	Std (m)	Max (m)	Min (m)
A4 - e008n45	-0.1	16	173	-168
B1 - e009n46	-0.4	14	93	-177
B2 - e009n46	3.0	20	195	-206
B3 - e009n46	-1.0	17	131	-128
B4 - e009n46	-0.1	20	129	-212
C2 - e009n46	-4.0	29	352	-256
D1 - e010n46	0.3	11	79	-84
D2 - e010n46	2.0	16	113	-207
D3 - e010n46	-5.0	12	84	-64

Table 2.12: Statistics of the elevation differences between all the grids couples of Lombardy and Switzerland DTMs.

2.3.2 Cross-validation between low and high resolution DTMs

The cross-validation between low and high resolution DTMs is performed comparing the regional DTMs with the high resolution DTMs available for the HELI-DEM project area. In particular in Lombardy the high resolution PST-A DTM is present and covers only the hydrographic basins; in Piedmont two high resolution DTMs are available, again PST-A DTM which covers the river basins, and the regional DTM which covers the whole region with a planimetric resolution of 5 meters. For a detailed description of these DTMs see section 2.2.1. For Switzerland only one DTM is available, the national low resolution DTM, and so in this case no cross-validation between low/high resolution DTMs is possible. Three cross-validations have been performed:

1. Lombardy regional DTM and PST-A LiDAR Ministry of Environment DTM,
2. Piedmont regional DTM and PST-A LiDAR Ministry of Environment DTM,
3. Piedmont regional DTM and 5 meters Piedmont DTM.

Among these comparisons, the author of this thesis has worked on the first one. For this reason the comparison between the Lombardy regional DTM and the PST-A DTM is in detail described below. Analogous procedures have been adopted by Politecnico di Torino for the other comparisons (related to Piedmont), that are not described here.

2.3.2.1 Lombardy Regional DTM vs. Ministry of Environment PST-A LiDAR DTM

The low resolution Lombardy regional DTM (LR DTM) and the high resolution PST-A LiDAR DTM of Ministry of Environment (HR DTM) are georeferenced in different planimetric reference frames and have different resolutions and vertical accuracies. Their main characteristics are reported in Table 2.13.

	Lombardy Region DTM	PST-A LiDAR DTM
Planimetric resolution	20 m	1 m
Elevation accuracy	5-10 m	10-50 cm
Reference frame	Roma40 - Gauss Boaga	ETRF89 - geographic coordinates

Table 2.13: Main characteristics of Lombardy regional DTM and PST-A LiDAR DTM.

In Figure 2.22 the area covered by the two DTMs is represented: only the part of the two DTMs that falls within the HELI-DEM project area has been considered. It should be noted that the Lombardy DTM covers the Lombardy project area for a total of 12'068 km², while the PST-A LiDAR DTM covers only one sixth of this territory for a total of 2'342 km². The very partial overlap between the two DTMs does not allow in any way, even if desired, a complete correction of the low resolution DTM through the high resolution data.

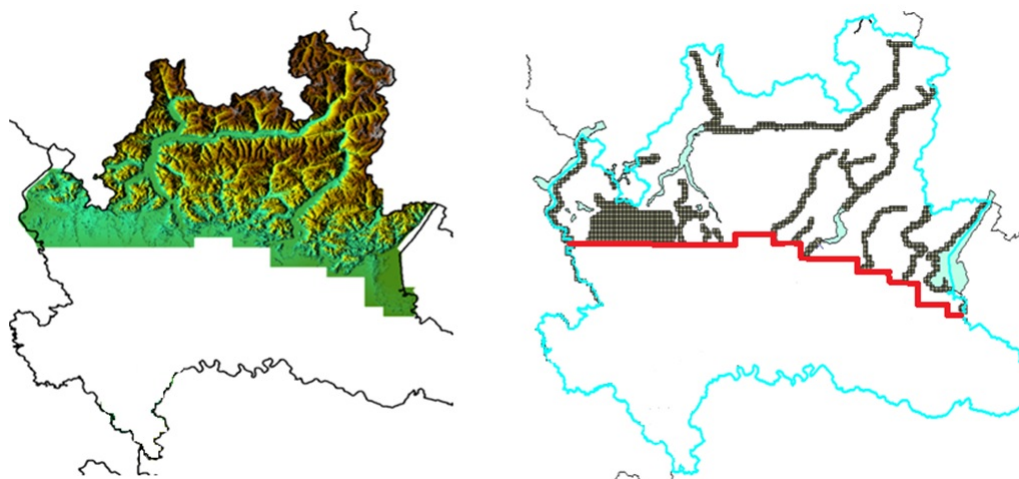


Figure 2.22: Area covered by the regional Lombardy DTM (on the left) and the Lombardy part of the PST-A DTM (on the right).

The PST-A DTM is characterized by higher resolution and accuracy; therefore in the comparison it has been considered as truth. The two DTMs have different

reference frames and coordinates systems; therefore, before performing the cross-validation, the Lombardy regional DTM has been transformed using the program GK2CNV from its original reference frame to ETRF89, geographic coordinates (reference frame and coordinate system of the PST-A DTM). The result is a list of 3-D coordinates, that clearly are almost regularly spaced but no more on a regular grid.

The PST-A LiDAR DTM covers only a portion of the Lombardy territory, therefore the comparison has been done only in the portion of the Lombardy territory where also the LiDAR model exists. To perform the comparison, for each point (3-D coordinates) of the Lombardy regional DTM, it has to be verified whether the point is present also inside the PST-A DTM or not. In the positive case, a square window of $(20 \times 20) \text{ m}^2$ is considered around the position of the point, and all the nodes of the PST-A DTM that fall inside this window are searched. Then, they are averaged and their mean (H_{HR}) is compared to the low resolution height (H_{LR}). For each point a difference is in this way computed as $\Delta H = H_{LR} - H_{HR}$. The dimension of the window has been chosen equal to 20 m, because the points of the transformed LR DTM are spaced approximately 20 meters, and the area of influence of each point is about $(20 \times 20) \text{ m}^2$: inside an area of that dimension about 400 HR DTM nodes (with a inter-distance of 1 meters) are present.

Results

In Table 2.14 the global statistics of the differences, without the NO-DATA values, are summarized.

Number of useful points	4'048'660
Mean, $\mu(\Delta H)$	0.5 m
Std, $\sigma(\Delta H)$	6.6 m
Maximum, $max(\Delta H)$	204 m
Minimum, $min(\Delta H)$	-138 m

Table 2.14: Statistics of the elevation differences between Lombardy DTM and PST-A LiDAR DTM.

Considering the nominal accuracies of the Lombardy DTM, the statistics of the differences are distributed as expected, with a mean lower than one meter and a standard deviation smaller than ten meters. To verify the existence of global biases, the differences have been clustered in eight classes, according to their absolute values: the results are reported in Table 2.15. The 79% of the points has a difference lower than 5 meters and only the 7% of the differences is greater than

10 meters. According to Figure 2.23 the highest values seem to be concentrated in mountainous areas, as for example the area in the North part of Valtellina Valley and in the are North of Lago D’Iseo.

Differences (m)	Percentage with respect to the total number of points
$0 \leq \Delta H < 5$	79%
$5 \leq \Delta H < 10$	14%
$10 \leq \Delta H < 20$	6.0%
$20 \leq \Delta H < 50$	1.2%
$50 \leq \Delta H < 100$	0.2%
$ \Delta H \geq 100$	0.01%

Table 2.15: Classes and percentage of the absolute values of elevation differences between Lombardy and PST-A DTMs.

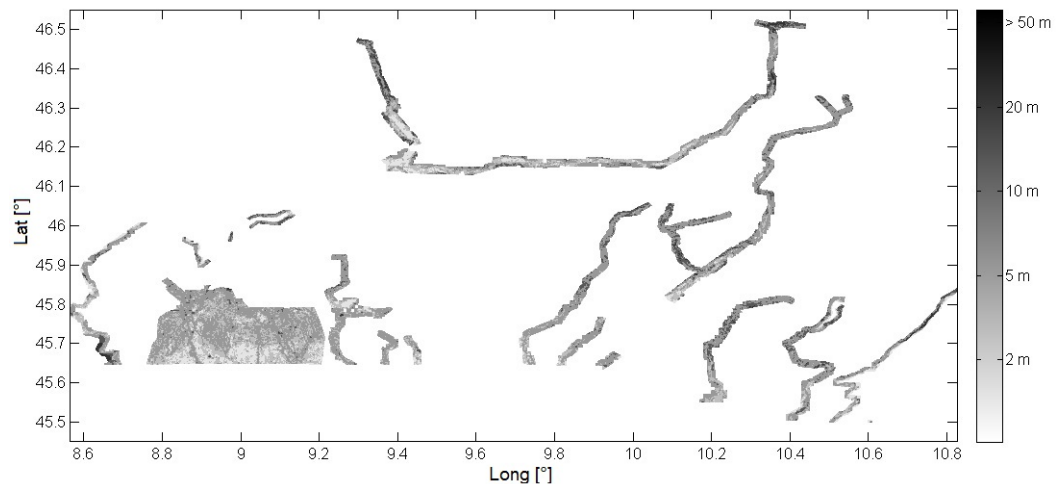


Figure 2.23: Absolute values of the differences between Lombardy and PST-A LiDAR DTMs.

Some detailed analyses on the differences have been done. A first analysis has been performed according to the subdivision of the Lombardy DTM in grids, selecting each time all the points that fall inside the area covered by one of the grids of the LR DTM, that are shown in Figure 2.24 .

In Table 2.16 the statistics of the differences are reported grid by grid. Grids A4, A5, B1, D1, E4 and E5 present the worst statistics (high mean and standard deviation). A comparisons between these results and those obtained by the comparison of Lombardy and Swiss low resolution DTMs (Table 2.12) has to be

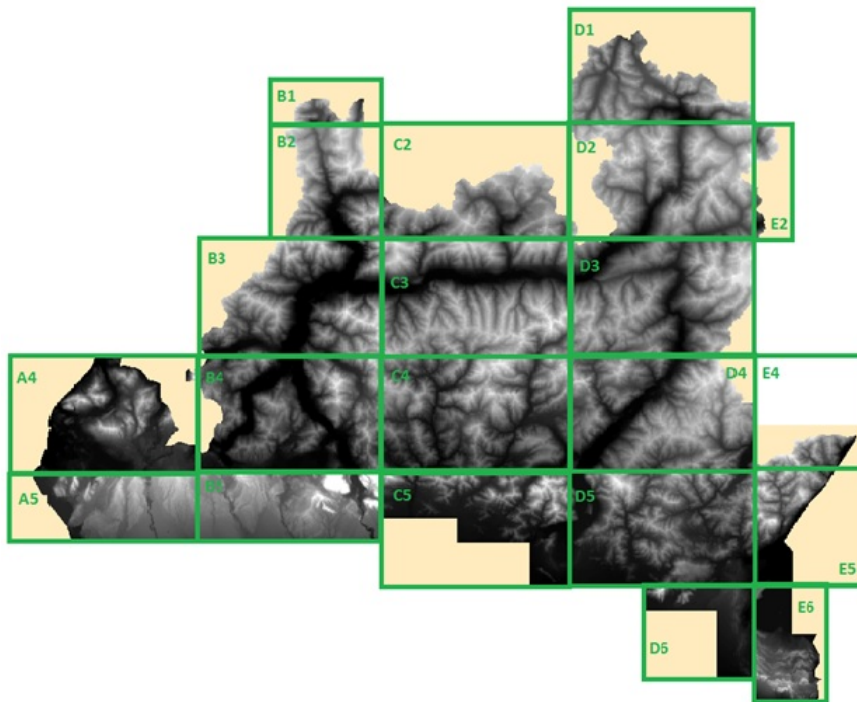


Figure 2.24: Subdivision of the Lombardy DTM in grids.

done. Grids B2, B4 and C2 had high values in the previous case; here B2 and B4 grids present good statistics, while for grid C2 unfortunately no comparison can be done because no overlap exists between PST-A and Lombardy DTMs. Grids D5, E5 and E6 have in this case high difference values, but no comparison can be done because these statistics were not considered in the previous analysis; a detailed analysis demonstrated that the highest values of these grids are due to isolated outliers. Finally grid D1 presents here a high maximum value, while in the previous case statistics were acceptable: this grid covers Valtellina area that will be analysed in detail in the following paragraphs.

In some grids, a strange phenomenon is visible. One example is given in Figure 2.25, where the differences in grid B1, plotted over Google Earth 3-D map, are shown. The area covered by grid B1 is located in the Northern part of Lombardy, near the border with Switzerland: in particular this area covers part of the Valley of San Giacomo. The differences seem not to be randomly distributed but they seem to follow a strange sistematism: the positive differences are concentrated on one side of the valley, the negative differences on the other side.

To better analyse this phenomenon, the investigation has been extended considering the entire Valley of San Giacomo. Table 2.17 reports the statistics of

Grid	Mean [m]	Std [m]	Min [m]	Max [m]
A4	0.5	8.7	-100	60
A5	-0.6	7.8	-96	48
B1	-1	7	-74	73
B2	0.5	5.2	-88	125
B3	0.1	4.4	-69	73
B4	0.9	3.8	-39	55
B5	0.7	3.1	-48	104
C2	No overlap			
C4	0.3	4.8	-83	98
C5	0.9	3.4	-38	59
D1	2.8	9.5	-61	192
D2	0.4	6.5	-98	43
D3	0.8	4.3	-80	59
D4	0.9	7.5	-75	92
D5	0.6	4.8	-89	154
D6	0.2	7	-26	44
E2	1.8	3.1	-7	13
E4	-0.9	8.7	-48	122
E5	0.9	8.7	-115	210
E6	0.5	6.6	-21	204

Table 2.16: Statistics of the elevation differences between Lombardy and PST-A LiDAR DTMs, grouped by grids.

the differences for this valley and Figure 2.26 shows the histogram of the differences. The differences have been subdivided in twelve classes (Table 2.18). From an overall analysis, the statistics of the differences are satisfactory. In fact mean and standard deviation, equal respectively to -0.5 and 6 meters, are not significant with respect to the LR DTM accuracy; moreover, the most part of the values (the 93%) are between ± 10 m as in the general statistics.

Number of useful points	10'817
Mean, $\mu(\Delta H)$	-0.5 m
Std, $\sigma(\Delta H)$	6 m
Maximum, $max(\Delta H)$	81 m
Minimum, $min(\Delta H)$	-77 m

Table 2.17: Statistics of the elevation differences between Lombardy and PST-A DTMs on the Valley of San Giacomo.

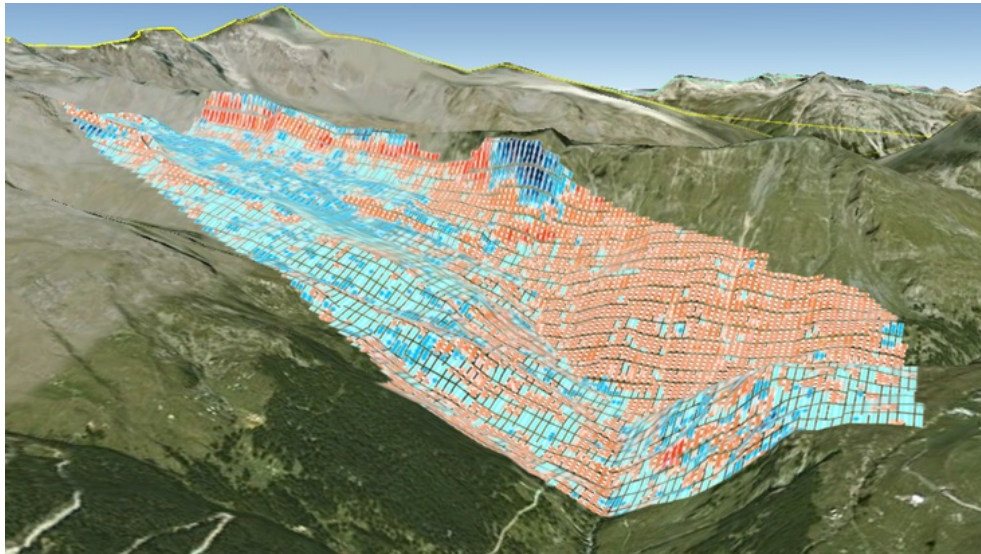


Figure 2.25: Differences of elevations between Lombardy DTM B1 grid and PST-A DTM, plotted in 3-D on Google Earth (in red positive differences, in blue negative differences).

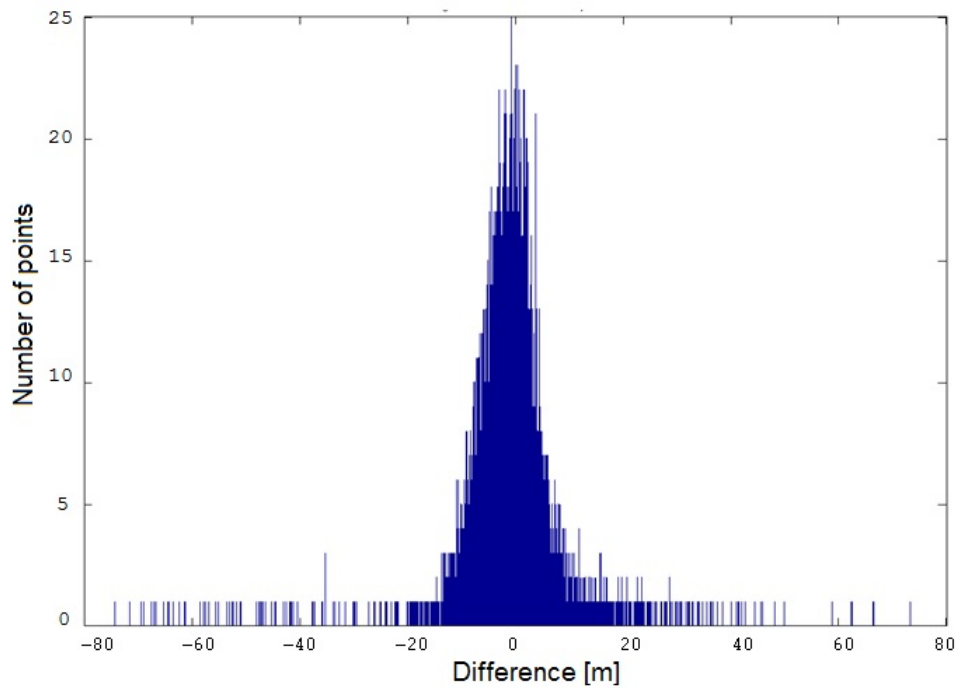


Figure 2.26: Histogram of the differences between Lombardy and PST-A DTMs on the Valley of San Giacomo.

Differences (m)	Percentage with respect to the total number of points
$\Delta H < -100$	0.0%
$-100 \leq \Delta H < -50$	0.3%
$-50 \leq \Delta H < -20$	0.5%
$-20 \leq \Delta H < -10$	3.1%
$-10 \leq \Delta H < -5$	15.7%
$-5 \leq \Delta H < 0$	39.9%
$0 < \Delta H < 5$	31.2%
$5 \leq \Delta H < 10$	5.9%
$10 \leq \Delta H < 20$	2.2%
$20 \leq \Delta H < 50$	0.9%
$50 \leq \Delta H < 100$	0.1%
$\Delta H \geq 100$	0.0%

Table 2.18: Classes and percentage of elevation differences between Lombardy and PST-A DTMs on the Valley of San Giacomo.

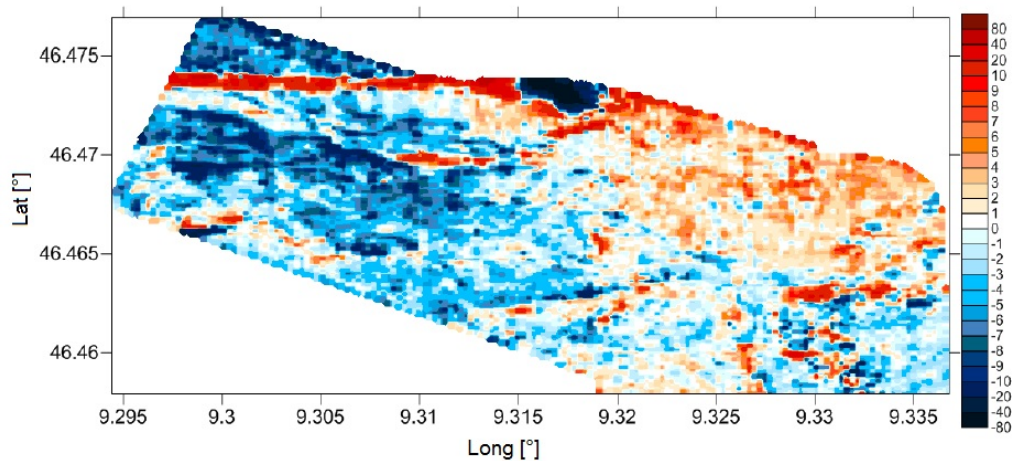


Figure 2.27: Differences of elevations between Lombardy and PST-A DTMs on the Valley of San Giacomo.

However, as has been detected in case of grid B1, also considering the whole San Giacomo Valley, a local bias seems to be present, as can be seen in Figure 2.27. Firstly a strange artefact is visible: in the upper left part of the image, a group of points with very high positive differences distributed along a horizontal path is present. From a check of the elevation data of the two DTMs, it has been highlighted that this problem is due to a local bias in the Lombardy regional DTM. In addition in this valley in the West slope (the lower part of the figure) a negative

bias between Lombardy and PST-A DTMs appears; in the other slope an opposite bias is present. Such a behavior could be justified by a translation of the two DTMs with respect to the valley axis. Moreover this phenomenon interests not only the San Giacomo Valley but other valleys of Lombardy. Therefore a procedure to estimate biases between DTMs has to be implemented to verify the existence of translations; the procedure is explained in the following paragraph.

Estimation of the translation between Lombardy and PST-A DTMs

To verify the existence of a translation or a bias of the regional DTM with respect to the local PST-A LiDAR DTM, which has been considered as truth, an algorithm in MATLAB environment has been implemented. The estimate of the translation is performed by Least Squares (Koch, 2007).

The height of a point P can be described by:

$$\begin{aligned} h(P) &= f_1(\underline{x}_P) + \nu_1 \\ h(P) &= f_2(\underline{x}_P) + \nu_2 \end{aligned} \quad (2.4)$$

where f_1 and f_2 are respectively the P height functions of DTM1, which is the one that has to be verified (in this case the Lombardy LR DTM) and DTM2, considered as truth (in this case the PST-A LiDAR high resolution DTM). ν_1 and ν_2 are the observation noises of the two functions. $\underline{x}_P = [x_P \ y_P]^T$ are the planimetric coordinates of point P.

In absence of translation and biases, the value of the two DTMs in P coincide and clearly the following equation is verified:

$$f_1(\underline{x}_P) = f_2(\underline{x}_P) \quad (2.5)$$

Let's then suppose that a translation $\underline{t} = [t_x \ t_y]^T$ and a bias h exist in DTM1. The functional model becomes the following:

$$f_1(\underline{x}_P) = f_2(\underline{x}_P + \underline{t}) + h + \nu \quad (2.6)$$

This model can be linearised by the following equation (Biagi et al., 2012):

$$\delta f(\underline{x}_P) = f_1(\underline{x}_P) - f_2(\underline{x}_P) = \nabla f_2(\underline{x}_P)\underline{t} + h + \nu \quad (2.7)$$

where $\nabla f_2(\underline{x}_P)$ is the gradients vector of DTM1, computed by the usual numerical approximation. The gradients are used to fill the design matrix of the linearised Least Squares system. $\delta f(P_i), i = 1, 2, \dots, M$ are all the observed differences. The grid containing the gradients and the grid containing the differences between high and low resolution DTMs have the same cellsize, because the differences are

those computed between the low resolution DTM and the high resolution DTM subsampled on the low resolution grid.

Therefore the following system can be built:

$$\begin{bmatrix} \delta f(P_1) \\ \delta f(P_2) \\ \dots \\ \delta f(P_n) \end{bmatrix} = \underline{y}_0 = \begin{bmatrix} \nabla_x f_1(P_1) & \nabla_y f_1(P_1) & 1 \\ \nabla_x f_1(P_2) & \nabla_y f_1(P_2) & 1 \\ \dots & \dots & \dots \\ \nabla_x f_1(P_n) & \nabla_y f_1(P_n) & 1 \end{bmatrix} \begin{bmatrix} t_x \\ t_y \\ h \end{bmatrix} + \begin{bmatrix} \nu_1 \\ \nu_2 \\ \dots \\ \nu_n \end{bmatrix} = \mathbf{A}\underline{\zeta} + \underline{\nu} \quad (2.8)$$

In the equation $\mathbf{Q} = \mathbf{I}$. Solving the linearised Least Squares system the three unknown parameters can be estimated ($\hat{\underline{\zeta}} = (\mathbf{A}^T \mathbf{A})^{-1} \mathbf{A}^T \underline{y}_0$):

- \hat{t}_x, \hat{t}_y , that are the translations respectively in x and y directions,
- \hat{h} , that is the elevation bias.

From the usual Least Squares equations (see section B.2.1) the sigma a posteriori can also be estimated.

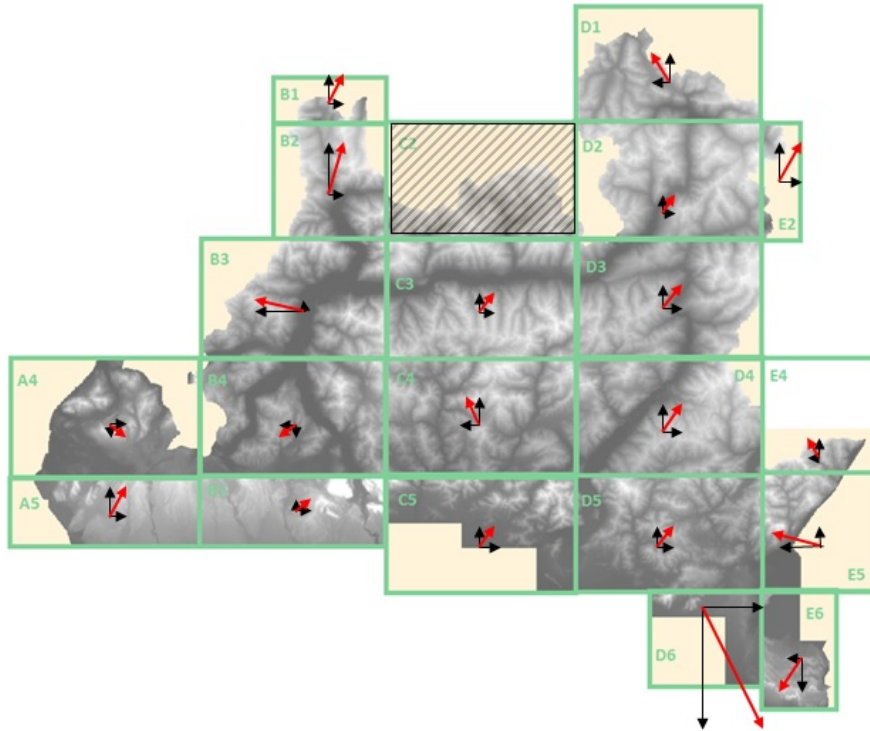


Figure 2.28: Planimetric translations (represented by the red narrows) between the Lombardy LR and the PST-A LiDAR high resolution DTMs, evaluated by grids partition.



Figure 2.29: Landslide of Val Pola (Valtellina area, in Sondrio province), came off the 28th July 1987.

The translations and height bias have been estimated by clustering in different ways the differences: firstly considering the official cartographic partition in grids and then considering the natural orographic partition in valleys. In the first case the estimated translations for the individual grids are always smaller than $\pm 1.5m$, and their global mean is 0.3 meters. In Figure 2.28 the translation vectors are shown; each arrow represents the translation of the Lombardy DTM grid with respect to the PST-A DTM. The statistics, subdivided by grids, are summarized in Table 2.19. No systematic translations or biases seem significant at the global regional scale or in the individual sheets: the only anomalous case is given by grid D6. For which concerns the second study, or better the analysis of the differences by single valleys, no significant translation or biases exist also in this case, with estimates always smaller than 4 and 2 meters respectively. These results are in all cases acceptable if compared to the nominal accuracy of the LR DTM. Also in the Valley of San Giacomo no significant translation or bias seem present. In Valtellina area (Adda River Valley) some anomalies seem to exist, with a maximum difference of 200 m: for that reason the comparison has been performed in this valley non only considering the entire valley but also dividing it in strips.

From this analysis and from a deep study of the history of that valley, the differences that reach 200 m are located in Val Pola, where the 28th July 1987 a landslide (an image of it is shown in Figure 2.29) came off from the Zandila Mountain and 40 million cubic meters of material fall down, overwhelming and completely

destroying the villages of Sant'Antonio Morignone and Aquilone (in the province of Sondrio). In the landslide area the two Lombardy and PST-A DTMs are in disagreement because the first one has been created respectively before and after the natural disaster. However, local biases seem to be present, if considering both the results of the translations and biases analysis and the differences between the Lombardy DTM and the LiDAR DTM. For that reason, a deeper check, that is described in the following section, has been carried out through external validation of the two DTMs using geodetic/GPS data.

Grid	Number useful nodes	t_x [m]	t_y [m]	h [m]	$\hat{\sigma}_0$ [m]
A4	331'411	1.1	-0.3	0.5	4.3
A5	721'275	1.2	4.1	-0.7	7.7
B1	10'790	1.7	3.3	-1.5	6.7
B2	126'346	0.7	4.1	0.3	5.0
B3	164'647	-11-1	1.2	-0.2	3.5
B4	160'130	-1.1	-1.4	0.9	3.8
B5	777'608	0.8	0.3	0.7	3.1
C2	No overlap				
C3	244'752	0.3	1.5	0.1	3.3
C4	103'128	-1.7	1.9	0.3	4.7
C5	167'141	1.3	2.5	0.8	3.3
D1	60'566	-2.3	6.4	2.3	8.7
D2	200'537	0.6	2.7	0.3	6.5
D3	231'121	0.6	1.2	0.8	4.2
D4	290'753	-0.9	3.0	0.8	5.1
D5	303'989	0.6	1.4	0.6	4.8
D6	37'472	12.4	-33.1	0.5	6.8
E2	422	3.5	6.3	-0.6	2.8
E4	17'811	-0.2	1.5	0.8	8.6
E5	87'614	-10.5	1.9	-1	7.7
E6	10'872	-1.0	-4.9	-0.2	2.1

Table 2.19: Translations and biases between the Lombardy DTM and the PST-A LiDAR DTM (t_x, t_y are the estimated planimetric translations, h is the estimated bias, $\hat{\sigma}_0$ is the a-posteriori sigma).

2.4 External validation of the DTMs through GPS data

From the comparison between the two DTMs available for Lombardy, the LR Lombardy regional DTM and the Ministry of Environment PST-A LiDAR DTM, some local biases seem to exist. In order to check if these biases are really present, the two DTMs have been externally validated, using GPS data. Two different approaches have been used:

- at first, both DTMs have been compared in the points corresponding to the monographs of the zero order IGM95 Italian geodetic network benchmarks,
- then, the PST-A DTM has been compared with respect to ad hoc surveyed RTK GNSS measures for a particular case study.

In the following sections, the two analyses and the obtained results are described in detail.

2.4.1 DTMs comparison with IGM95 benchmarks

The Lombardy regional DTM and the PST-A DTM have been compared with the GPS data of the zero order geodetic network IGM95 (details in section A.3). The GPS results of the IGM95 geodetic benchmarks are catalogued inside the so called “IGM95 monographs”, that facilitate the localization and describe their characteristics.

The monographs, one for each benchmark, contain the following information:

- the name of the benchmark,
- the geographic and cartographic coordinates in ROMA40 reference frame,
- the geographic and cartographic coordinates in ETRF2000 reference frame,
- the orthometric and geodetic heights,
- some photos and schema useful to recognize instantly the point and its location.

An example of monograph of a geodetic point located in Cassano (Lombardy) is shown in Figure 2.30.

The monographs can be partially downloaded from the official website of IGMI, where on a map (Figure 2.31) the geodetic benchmarks are represented with different symbols depending on their type. From the map it is possible to

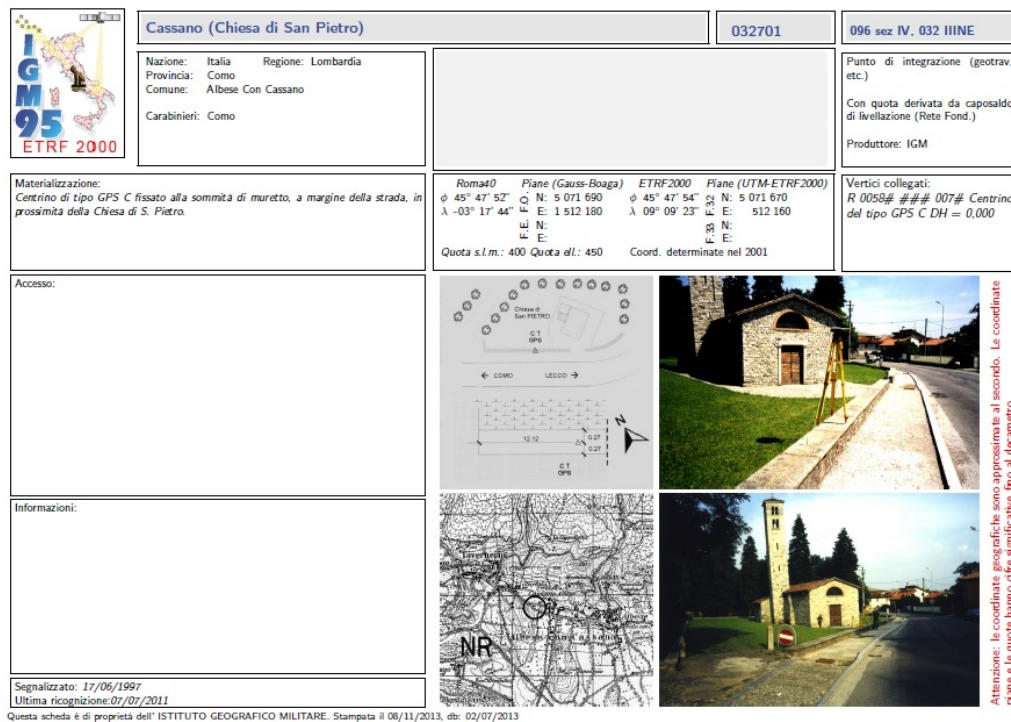


Figure 2.30: Example of IGM95 free monography of a geodetic point.

select a point and to download its monograph. The coordinates free downloadable from the website have an accuracy of about one arcsecond for geographic coordinates and of the order of the decameter for cartographic coordinates. The freely available data can be used to identify the benchmark and reach rapidly it. The accurate ETRF2000 and the Roma40 coordinates can be bought from IGMI.

To perform the comparison between the two DTMs and the IGM95 points, firstly the IGM95 benchmarks located in the HELI-DEM study area have been selected. The accurate monographs were not available by the partners for all the identified benchmarks but were only partial and related to benchmarks re-surveyed in the last years. For this reason only recently re-surveyed IGM95 benchmarks have been used for the check, in order to guarantee their cm accuracy. In total 64 IGM95 points are available inside the area covered by the LR DTM and 45 of them are located also inside the area of the HR DTM (Figure 2.32).

The comparison has been executed interpolating the orthometric elevation of the considered DTM on each of the selected IGM95 points. Clearly, in case of the Lombardy DTM, the ROMA40 cartographic planimetric coordinates have been considered to perform the comparison; in case of PST-A LiDAR DTM, the coordinates have been previously transformed to ETRF89, using the tools available

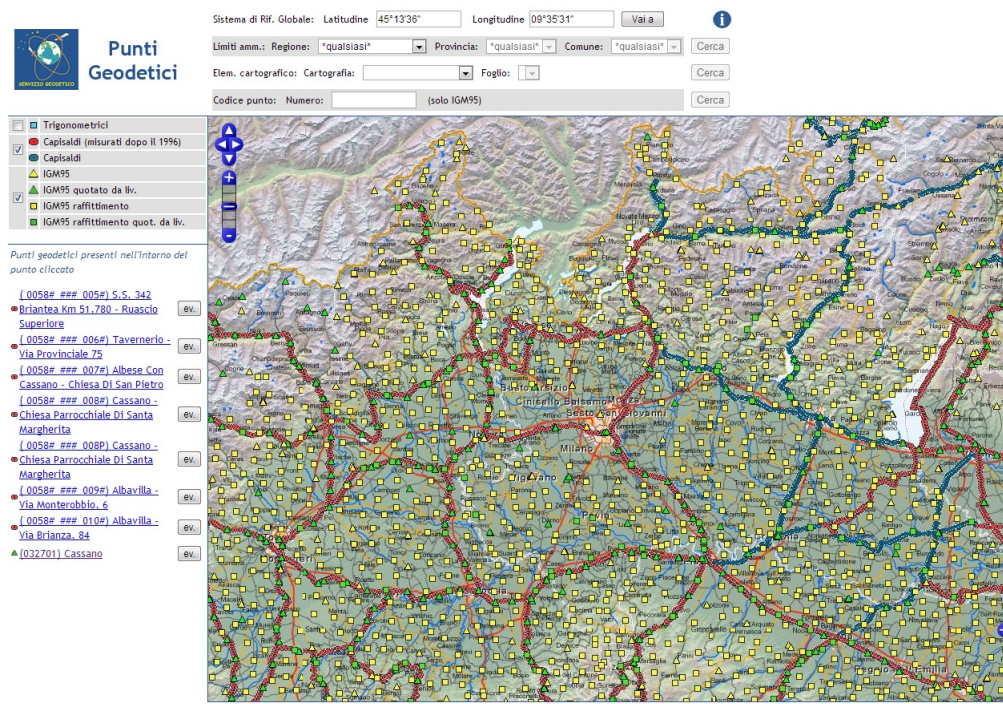


Figure 2.31: IGMI website with the map where the IGM95 monographies can be downloaded.

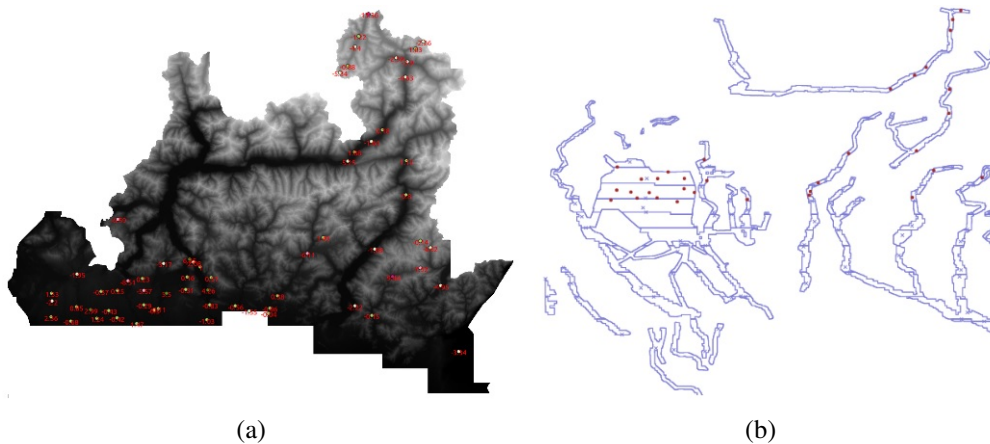


Figure 2.32: IGM95 points that fall inside the area of the Lombardy LR DTM (a) and inside the area of the PST-A DTM (b).

on the GPSLombardia website. In this way for each point the difference between the estimated DTM elevation and the elevation of the IGM95 point has been computed. In Table 2.20 the statistics of the differences for the two DTMs are reported.

	LR DTM - IGM95	HR DTM - IGM95 (all points)	HR DTM - IGM95 (only selected points)
N° of points	64	45	28
Mean (m)	-1.38	0.45	0.06
Std (m)	3.45	0.84	0.13
Min (m)	-13.36	-0.16	-0.16
Max (m)	6.35	4.63	0.32

Table 2.20: Statistics of the differences between the two DTMs (Lombardy and LiDAR) and the IGM95 points.

In the comparison between the LR Lombardy DTM and the IGM95 points, the mean difference is about 1 meter and the standard deviation is 3 meters: these results are consistent with the nominal accuracy of the DTM. On the other hand the comparison with the high resolution PST-A LiDAR DTM requires more detailed analyses. On the whole set of points, the mean difference is about 45 cm, with a standard deviation of 84 cm and a maximum value of 4.63 meters. These values are unacceptable if compared to the nominal accuracy of the PST-A DTM (less than 50 cm in elevation). Making a deep analysis of the results, just 17 points among the total of 45 present differences greater than 30 cm. Checking the characteristics of these benchmarks on the relative monographs, all of them are not located on the ground but are monumented on artefacts that clearly are not in the DTM, like for example walls or road embankments. Therefore these points have been excluded from the whole set before computing the statistics of the differences. And so on this regard, despite the small number of check points, these results are completely satisfactory: in fact after the removal of the point on artefacts, the mean is about 6 cm, with a standard deviation of 13 cm and a maximum values of 32 cm.

2.4.2 PST-A LiDAR DTM comparison with RTK surveys

Even if in the comparison between the LR Lombardy DTM and the Ministry of Environment PST-A LiDAR DTM the results are acceptable and also the comparisons of the two DTMs with the IGM95 benchmarks (Table 2.20) are very satisfactory, in some areas differences between the two DTMs greater than 10 meters are present: probably the high differences are due to some incorrect data in the Lombardy DTM. In order to verify this statement and the general correctness of the PST-A DTM, in areas where big differences exist between the LR Lombardy DTM and the PST-A DTM, the latter has to be validated with some more accurate data. However, no IGM95 monographs are available in these areas; therefore, ad

hoc GNSS surveys have been planned in order to collect useful GNSS data also there. RTK (Real Time Kinematic) survey seems adequate, because it provides accuracies typically better than one decimeter.

To collect GNSS RTK data twelve zones have been chosen among areas with differences between LR and HR DTMs greater than 10 m. Attention has been paid to Valtellina valley because in this area, during the HELI-DEM project, IGMI (Geographic Military Italian Institute) has performed some levelling measures, to re-survey some already existing levelling lines. In Lombardy the surveyed lines cover a total of more or less 200 km along the Adda River valley (Figure 2.33). The twelve areas, shown in Figure 2.34 and located along Adda River valley, have been selected for their accessibility and their good satellite visibility (in order to limit potential obstructions). Trough Google Maps it has been possible to select the areas via computer without physically reconnoiter on the places before the surveying campaigns.

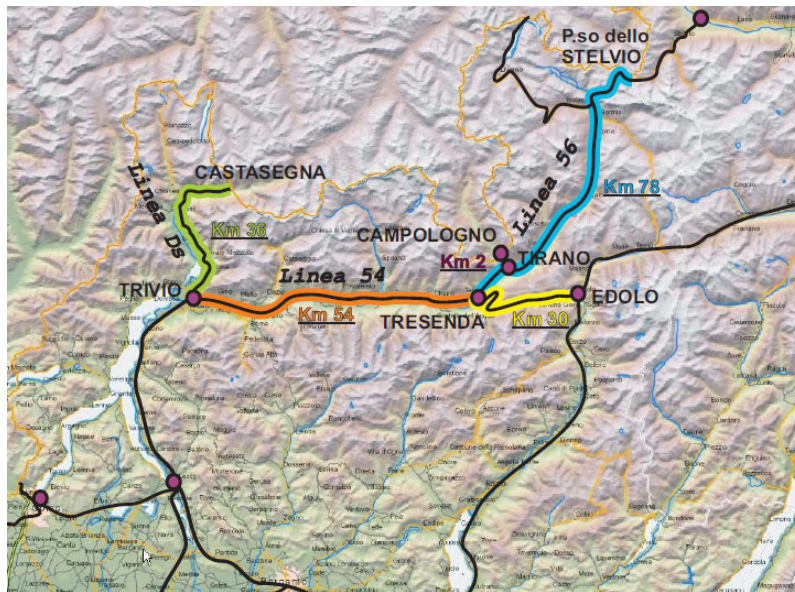


Figure 2.33: Levelling lines resurveyed by IGMI.

The characteristics (geographic position, length of the RTK survey path and medium height) of the areas are summarized in Table 2.21. Areas VT01-VT02 and VT03 are localized in the West side of the Valley, between Colico and Sorico cities, while areas from VT05 to VT12 are in the East side between Sondrio and Bormio. VT01 to VT06 are below 500 m of elevation, VT07 and VT10 are from 500 m to 1000 m, VT11 and VT12 are above 1000 m.

RTK measures have been realized with Leica RX 1200 receivers. Rover receivers communicated with the HELI-DEM permanent network by UMTS con-



Figure 2.34: Selected areas in Valtellina Valley for the external validation of PST-A DTM with GNSS RTK surveys. In the map are indicated: the twelve areas selected for the RTK surveys (VT01-VT12), the Permanent Stations of the HELI-DEM GNSS network (HELI-DEM PS) and the IGM95 benchmarks.

Id	L (m)	h (m)	ϕ	λ
VT01	420	213	46°08'27.19"	9°22'40.41"
VT02	508	243	46°08'45.36"	9°23'04.54"
VT03	1029	201	46°09'02.57"	9°24'29.45"
VT04	697	204	46°09'02.74"	9°24'30.21"
VT05	379	328	46°09'34.39"	9°57'31.41"
VT06	1083	357	46°09'32.60"	10°01'33.33"
VT07	908	520	46°14'18.85"	10°13'25.74"
VT08	2488	542	46°15'24.32"	10°14'49.69"
VT09	1161	795	46°18'51.51"	10°18'21.74"
VT10	1175	910	46°19'53.33"	10°19'57.67"
VT11	1609	1155	46°26'02.20"	10°21'27.60"
VT12	472	1277	46°29'11.20"	10°21'10.03"

Table 2.21: Positions of the RTK survey areas: L: length of the path, H , ϕ , λ : approximate ITRF2008 position of the area.

nections. Contrary to the usual surveying practice, the measures have been performed not monumenting benchmarks, but just surveying height profiles on given paths; in this way elevation profiles have been collected not by scattered points but by trajectories. Measures have been performed along roads, embankments or

easily accessible paths. Along flat sections, stop&go measures with a duration of 5 seconds (5 epochs, one epoch per second) have been carried out approximately every 20 meters. In slope sections, stop&go measures have been taken more frequently, spaced about 10 meters, always with a duration of 5 seconds. Every path has been surveyed twice to have a double check of the results. In addition the surveys campaigns have been repeated two times, the former in June/July 2012, the latter in October 2012. Survey conditions were not always optimal, due to the presence of some unavoidable vegetation and obstructions. Therefore, in some places, ambiguity resolving has not been possible. In any case, for each study area, at least 50 points have been surveyed in each campaign; in total 1300 RTK points have been collected. Considering the alpine nature of the case study, the number of collected points is successful. Colico zone (areas VT01, VT02 and VT03) provides the only one exception. Indeed, in October campaign, few points have been collected due to significant problems in GNSS data acquisition in the whole zone. Probably, this was probably caused by electromagnetic disturbance emitted by some repeaters present in the zone (Telespazio Radio Antenna).

RTK method has been chosen due to its advantages in terms of costs, times and reliability. To give an example of costs of the performed campaigns, it has to be considered that:

- the first identification of each area from maps prepared during the planning never involves significant times; travelling times from an area to the next were always less than 30 minutes,
- the survey of each area has required 35 minutes in average for the double surveys (forward and backward paths) with an average of 70 surveyed points.

Therefore the method presents low cost compared to a significant numerosity of points.

Data collected during surveys, stored in memory cards, have been downloaded and analyzed using Leica Geo Office software. The software allows to visualize, import, manage and process GNSS data and RTK results. Then, the RTK results have been converted to text files for further analyses with other GIS and statistic softwares. The external validation of the PST-A DTM has been done by its comparison with the RTK collected data. Since the RTK results are in ITRF2008 while PST-A DTM is in ETRF89, before the comparison, RTK results have been converted to ETRF89 by the standard transformations. In order to compare the estimated elevation to the RTK height, the latter has to be transformed from geodetic to orthometric by applying the undulation of the official Italian geoid Italgeo08 (Barzaghi et al., 1987). After the conversion, PST-A DTM and

RTK points have been compared in the following way. Each RTK results consists of the 3-D coordinates of a point measured on the ground. A simple routine has been implemented in MATLAB: its inputs are the DTM grids and a list of the RTK estimated coordinates. For each RTK point, the sixteen nearest nodes of the DTM are searched; the elevation assumed by the DTM in the RTK point is estimated by exact bicubic interpolation from the sixteen nodes. The elevation difference between the elevation obtained by DTM interpolation and the RTK orthometric height is computed. Clearly, in this way, horizontal RTK errors are neglected, but for the purpose of this comparison they can be considered as not significant.

The statistics of the differences of the two survey campaigns (June/July and October 2012) are reported in Tables 2.22 and 2.23.

Id	N° points	O	%O	Mean (cm)	Std (cm)	Max (cm)
VT01	48	1	2	14	9	31
VT02	60	1	2	12	13	32
VT03	40	0	0	18	8	38
VT04	22	1	4	19	6	40
VT05	50	0	0	4	4	17
VT06	72	0	0	-5	3	14
VT07	60	7	12	5	13	45
VT08	64	0	0	11	8	28
VT09	55	0	0	4	6	25
VT10	48	5	10	-3	10	36
VT11	7	4	6	7	8	35
VT12	39	0	0	13	6	27

Table 2.22: Statistics of the elevation differences between interpolated PST-A DTM and GNSS-RTK (first survey campaign on June/July 2012). Id, number of surveyed points (N° points), number of outliers (O) - differences greater than 50 cm, percentage of outliers (%O), mean, standard deviation, maximum.

The results are in general satisfactory. As example the differences obtained for area VT09, located in Tiolo (Sondrio province), with a path 1 km long, is shown in Figure 2.35.

In this case all the differences are lower than 45 cm in both the survey campaigns; only one outlier exists in the South-West part of the area in the data collected during the second campaign. In total, 10 results present differences greater than 1 m; in any cases all the 43 results that have differences greater than 50 cm have been considered as outliers and have been removed from the datasets. At first, visual inspections of RTK/DTM profiles evidence that most of outliers are clearly caused by RTK survey problems and do not represent DTM blunders. As

Id	N° points	O	%O	Mean (cm)	Std (cm)	Max (cm)
VT01	35	1	3	2	12	23
VT02	7	0	0	7	17	31
VT03	18	1	5	2	15	19
VT04	36	3	8	2	12	19
VT05	68	0	0	3	8	37
VT06	50	2	4	-1	5	7
VT07	93	0	0	5	12	37
VT08	90	3	3	13	6	27
VT09	70	1	1	6	10	42
VT10	77	10	13	5	17	39
VT11	101	2	2	2	9	30
VT12	61	1	2	7	7	19

Table 2.23: Statistics of the elevation differences between interpolated PST-A DTM and GNSS-RTK (second survey campaign on October 2012). Id, number of surveyed points (N° points), number of outliers (O) - differences greater than 50 cm, percentage of outliers (%O), mean, standard deviation, maximum.



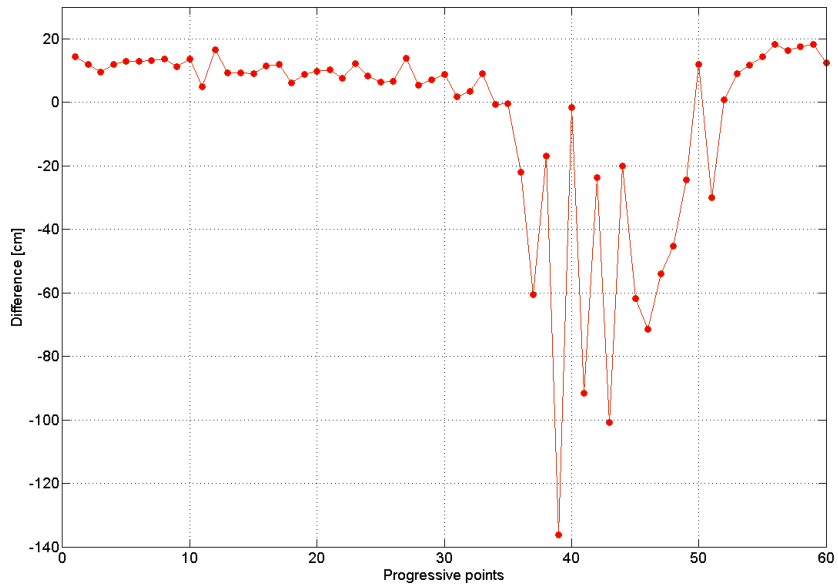
Figure 2.35: GNSS RTK points and absolute height differences with respect to PST-A LiDAR DTM - area VT09.

expected, these points are located under vegetation or in obstructed sites. Part of them regards sparse points, the others affect close points in small and particularly obstructed areas and are repeated in both the campaigns. In any case, results are

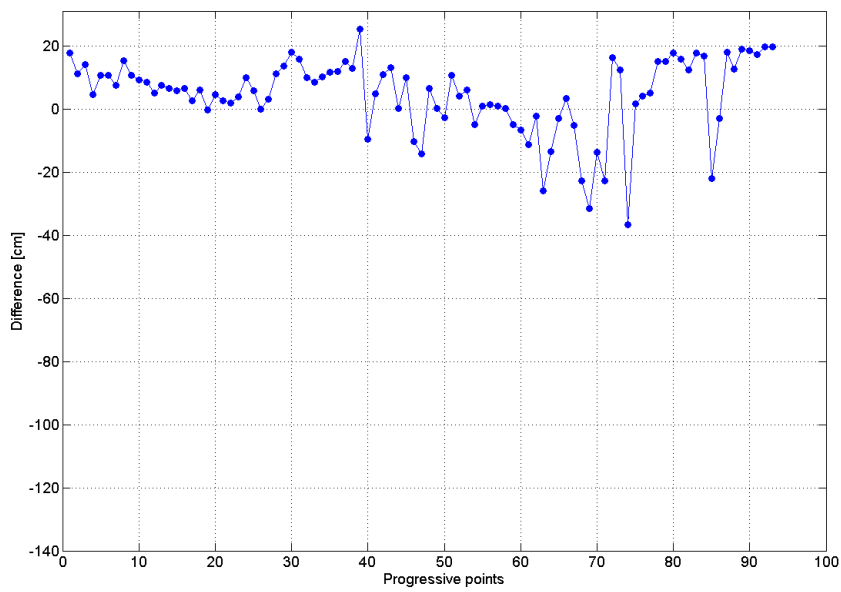
generally satisfactory for almost all the areas, because outliers percentages are acceptable.

Two exceptions exist, areas VT07 and VT10. Area VT07 is localized near Lovero (in Sondrio province); the path is 900 meters long and with a height difference from the beginning to the end equal to 45 meters. In Figure 2.36 the progressive differences between the PST-A DTM and RTK GNSS points of both the survey campaigns are shown. During the first campaign 7 outliers are present (represented in red and brown in Figure 2.37), while the other difference values are between 0 and 30 cm. This problem is not repeated during the second survey campaign. For this reason the problem is probably due to a prolonged wrong ambiguity resolution during the first campaign that happened in an area that, from a GNSS point of view, should be defined good.

Area VT10 (Figure 2.38) is located near Sondalo (in Sondrio province): measures have been executed along a paved road 600 meters long that climbs orthogonally a steep slope of the valley, with a total height difference of 44 m. The elevations of the RTK points on the side of the road towards the valley are systematically higher than those on the PST-A DTM; this survey contains also most of the outliers, with elevation differences greater than 1 meter. This bias is probably due not to a wrong ambiguity resolution as in the previous case, but to some problems in the PST-A LiDAR DTM; probably the very high differences are due to some errors in the horizontal georeferencing of the DTM or in the filtering used to produce the DTM from points clouds acquired by LiDAR.



(a)



(b)

Figure 2.36: Progressive differences (cm) between PST-A DTM and RTK points in area VT07: first campaign (a) and second campaign (b).



Figure 2.37: GNSS RTK points and absolute height differences with respect to PST-A DTM - area VT07.

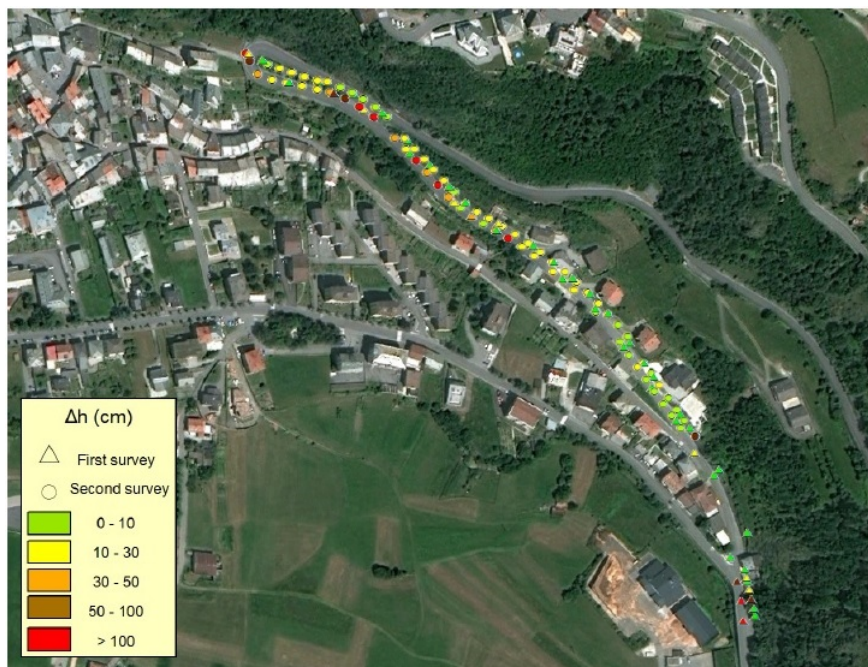


Figure 2.38: GNSS RTK points and absolute height differences with respect to PST-A LiDAR DTM - area VT10.

Chapter 3

Analyses on different DTM interpolation methods

The problem of DTM interpolation is of interest when unifying different partly overlapping DTMs on a common grid. This is the particular case of the HELI-DEM project. In order to decide which interpolation procedure will be adopted, several analyses have been carried out. First of all the comparison between bilinear and bicubic polynomial surfaces to re-grid DTMs is presented.

When interpolating an input DTM on an output grid, the input nodes used to estimate the elevation of an output node can be geometrically distributed in a way that might cause numerical instability of the interpolation system. In these cases a simple interpolation could not produce good results; some approaches useful to stabilize the system exist and have been studied and implemented.

Finally, various methods to merge different overlapping DTMs on a common grid have been analysed and compared. All the implemented procedures and the obtained results are described in this chapter and are necessary to justify the choices taken to create the output HELI-DEM DTM.

3.1 Regridding by polynomial interpolation: comparison between bilinear and bicubic surfaces

The regridding of a DTM on a new grid implies an interpolation. To do that different interpolators can be adopted. A first classification divides the interpolators between exact and approximate. In the following they will be called interpolators and approximators respectively. An interpolator creates a model that passes through all the available data, or observations, and allows the complete reconstruction of the entire sample; on the other hand an approximator applies statistical methods, like Least Squares, to estimate a smoother function that fits the obser-

vations. Interpolators have the disadvantage that the observation errors, if some one exist, are not filtered and thus are propagated into the model. Approximators are instead not affected by this problem, because errors can be filtered; but their disadvantage is that also actual details can be lost in the smoothing. Details are not reported here because in this context it would be dispersive with respect to the discussion on their application to our data; more details are instead contained in Appendix B.

In general, to predict a DTM in a point $P = (x_P, y_P)$, interpolators are used. Indeed, stored elevations have been usually already filtered for the errors. Typically, in GIS softwares the most commonly applied interpolators are splines or polynomial surfaces. At the beginning of the HELI-DEM project, attention has been focused on the polynomial surfaces and in particular on the already well known bilinear and bicubic ones. In literature some comparisons between bilinear and bicubic polynomial interpolators already exist. For example Rees (Rees, 2000) demonstrates that simple bilinear or bicubic interpolation is an adequate approach when DTMs have to be interpolated to higher resolutions, saying also that “for real data, bicubic interpolation is significantly more accurate than bilinear interpolation for resolution-doubling”. Also Kidner (Kidner, 2003), always referring to interpolation of a DEM in positions different from the original nodes of the model, says that any algorithm which uses more than the closest four grid vertices is always more accurate than a simple bilinear interpolation; in particular the work states that “interpolation accuracy will significantly increase, over the bilinear interpolation, if the search neighbourhood is extended from the nearest four vertices to the nearest sixteen vertices”.

Analyses have been carried out to confirm if the bicubic polynomial surface gives better results with respect to the bilinear approach also on our case study. To compare the two different polynomial surfaces interpolators, the following procedure has been implemented:

- interpolation of the original grid on the midpoint of the original nodes,
- re-interpolation from the new points back on the original grid nodes,
- computation of the differences between the estimated and the original elevations for all the DTM grid nodes.

In both cases an interpolation has been performed. In case of bilinear surface, the four neighbourhood nodes are used to estimate the elevation of each node, in case of bicubic surface the number of neighbourhood nodes is sixteen. Figure 3.1 shows the schema of the procedure of interpolation in case of bilinear surface.

Details of bilinear and bicubic interpolations and the relevant equations are reported in Appendix B.

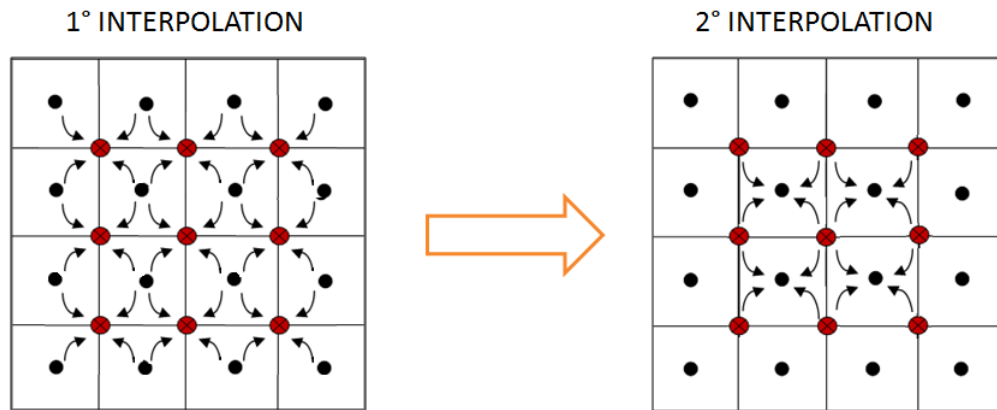


Figure 3.1: Schema of the procedure of bilinear interpolation on the intersections between grid nodes (1° interpolation) and back-interpolation on the original nodes (2° interpolation).

These analyses have been performed on different DTMs, characterized by different resolutions. In particular here the results of the application of the bilinear and bicubic interpolators on the Lombardy low resolution regional DTM (for details see 2.1) and on the high resolution LiDAR DTM of Ministry of Environment (details reported in Table 2.5) are compared. Both the DTMs are composed by several grids, and, since Lombardy has a territory morphologically heterogeneous, the grids cover different types of terrain (lowland, hill or mountain). To better analyse the behaviour of the two different polynomial surfaces in the different types, the interpolation has been performed selecting for each DTM one or two grids belonging to different terrains.

3.1.0.1 Comparison between bilinear and bicubic interpolations on Lombardy regional low resolution DTM

Six grids of the Lombardy regional DTM have been taken into account to perform the analysis: two grids covering plain terrain (grids A5 and E6), two covering hilly terrain (grids C5 and D5) and two covering mountainous terrain (grids B3 and C2). The statistics of the original elevations and the extensions of the six grids are summarized in Table 3.1. The morphology of the grids is shown in Figures 3.2, 3.3, 3.4 and the location of the considered grids is shown in Figure 2.24.

The statistics of the differences between re-interpolated and original elevations have been computed for the six grids after the removal of all the cells with no data value. The statistics (summarized in Table 3.2) are not reported for each grid, but they have been grouped by type of terrain.

As can be seen from the table, statistics are in general satisfactory, with stan-

	LOWLAND	
	GRID A5	GRID E6
mean (m)	289	91
std (m)	56	24
max (m)	472	203
min (m)	145	56
Covered area (km ²)	[40 x 15]	[16 x 25]
	HILL	
	GRID C5	GRID D5
mean (m)	435	565
std (m)	251	328
max (m)	1400	1954
min (m)	153	65
Covered area (km ²)	[40 x 25]	[40 x 25]
	MOUNTAIN	
	GRID B3	GRID C2
mean (m)	1002	2304
std (m)	598	563
max (m)	2637	4025
min (m)	195	708
Covered area (km ²)	[40 x 25]	[40 x 25]

Table 3.1: Statistics of the elevations of six grids of the Lombardy regional DTM.

dard deviations always better than the nominal accuracy of the Lombardy regional DTM. The statistics of the differences obtained by bicubic interpolation are better than those obtained by bilinear interpolation. In particular the standard deviations obtained in the bicubic case are almost half of those produced by bilinear method.

In addition, also slope and aspect have been studied. Slope and aspect are calculated for each point of the grid, by comparing the point elevation with that of its neighbours. The slope is the maximum inclination in a cell. The aspect is the angle between the North and the direction of the slope; it is measured clockwise from North direction. As for elevations, also for slopes and aspects the analysis has been performed evaluating for each grid node the difference between the original slope/aspect value and the one obtained after the two-times interpolation. This procedure has been done both with bilinear and bicubic interpolation.

In Tables 3.3 and 3.4 the statistics obtained respectively for slope and aspect are reported. Also in this case the statistics of the differences are better in case of bicubic approach. The statistics of the aspect of lowland terrain are worse than those of mountainous terrain; this can be easily justified thinking about the two

		LOWLAND	HILL	MOUNTAIN
Differences between re-interpolated and original elevations				
BILINEAR	bias (m)	~0	~0	~0
	std (m)	0.4	1.5	2.5
	max (m)	12.5	34.9	54.3
	min (m)	-11.5	-33.4	-55.8
	Number of useful data	1'871'340	3'986'923	3'080'219
BICUBIC	bias (m)	~0	~0	~0
	std (m)	0.2	0.8	1.4
	max (m)	8.8	21.4	38.4
	min (m)	-7.7	-24.1	-34.9
	Number of useful data	1'852'977	3'960'833	3'053'164

Table 3.2: Statistics of differences in elevation between the original values and those obtained after two-times exact bilinear/bicubic interpolation on the six selected grids of the Lombardy regional DTM, grouped by terrain typologies.

types of terrain. In case of mountain, slope and aspect are easily recognizable even if the differences in elevations between the forward and backward interpolation are high: if a cell of the grid has for example a slope of 10 degrees in North direction, it is difficult that after the interpolation even if the new elevation is very different from the original one, the cell assumes the opposite direction of aspect. On the other hand in flat terrains, if the difference in elevation is very low, it can happen that if the DTM is almost flat, and has a very low slope (less than 0.5 degrees) and a certain aspect value, after the interpolation, the slope can vary a little and the aspect can assume the opposite direction (difference equal to 180 degrees).

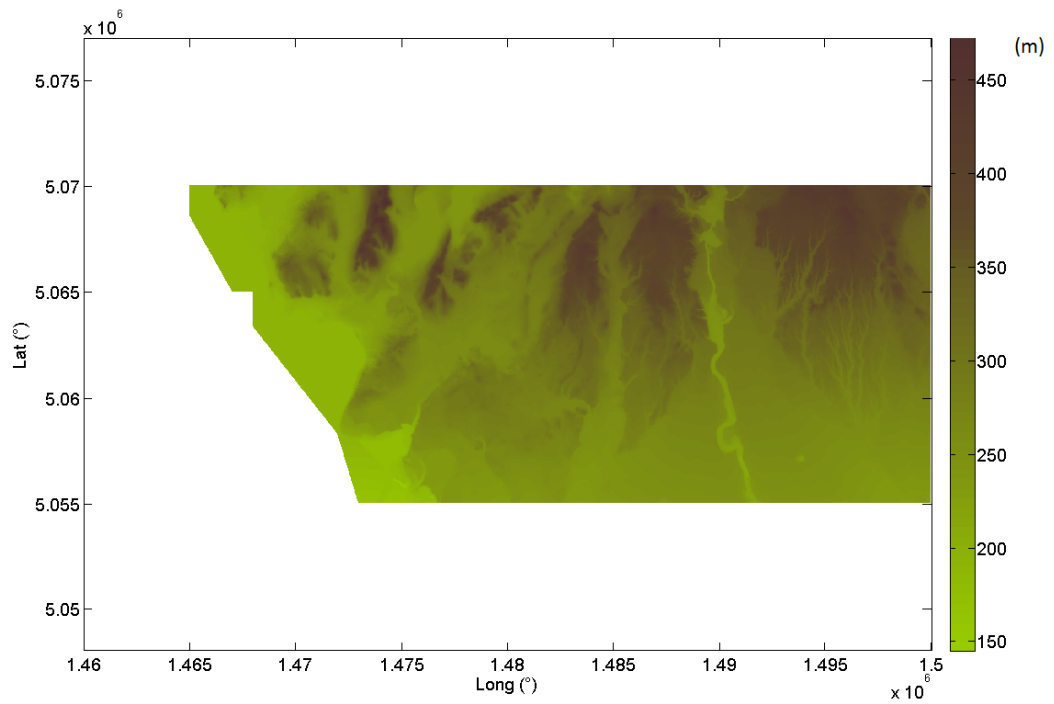
From the analyses, in case of the Lombardy low resolution DTM, the use of bicubic interpolation seems for every type of terrain better with respect to bilinear.

		LOWLAND	HILL	MOUNTAIN
Differences between re-interpolated and original slopes				
BILINEAR	bias (deg)	0.2	0.7	0.4
	std (deg)	1.3	2.1	4.5
	max (deg)	30.0	42.4	70.3
	min (deg)	-20.4	-33.1	-72.2
	Number of useful data	1'871'340	3'986'923	3'080'219
BICUBIC	bias (deg)	~0	0.2	~0
	std (deg)	0.7	1.2	2.6
	max (deg)	18.5	23.1	58.3
	min (deg)	-15.3	-25.6	-65.0
	Number of useful data	1'852'977	3'960'833	3'053'164

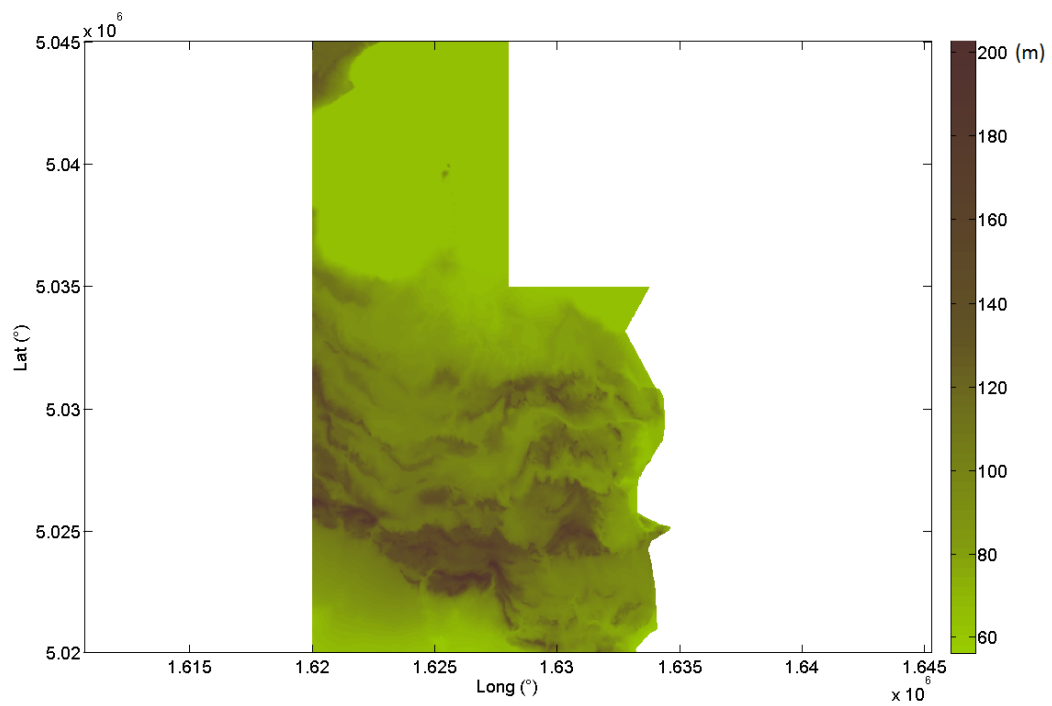
Table 3.3: Statistics of differences in slope between the original values and those obtained after two-times exact bilinear/bicubic interpolation on the six selected grids of the Lombardy regional DTM, grouped by terrain typologies.

		LOWLAND	HILL	MOUNTAIN
Differences between re-interpolated and original aspect				
BILINEAR	bias (deg)	~0	~0	~0
	std (deg)	11.3	9.7	13.6
	max (deg)	180.0	180.0	180.0
	min (deg)	-180.0	-179.9	-180.0
	Number of useful data	1'871'340	3'986'923	3'080'219
BICUBIC	bias (deg)	~0	~0	~0
	std (deg)	9.6	6.6	8.9
	max (deg)	180.0	179.9	180.0
	min (deg)	-180.0	-179.9	-180.0
	Number of useful data	1'852'977	3'960'833	3'053'164

Table 3.4: Statistics of differences in aspect between the original values and those obtained after two-times exact bilinear/bicubic interpolation on the six selected grids of the Lombardy regional DTM, grouped by terrain typologies.



(a)



(b)

Figure 3.2: Grids A5 (a) and E6 (b) of the Lombardy low resolution regional DTM, covering lowland terrain.

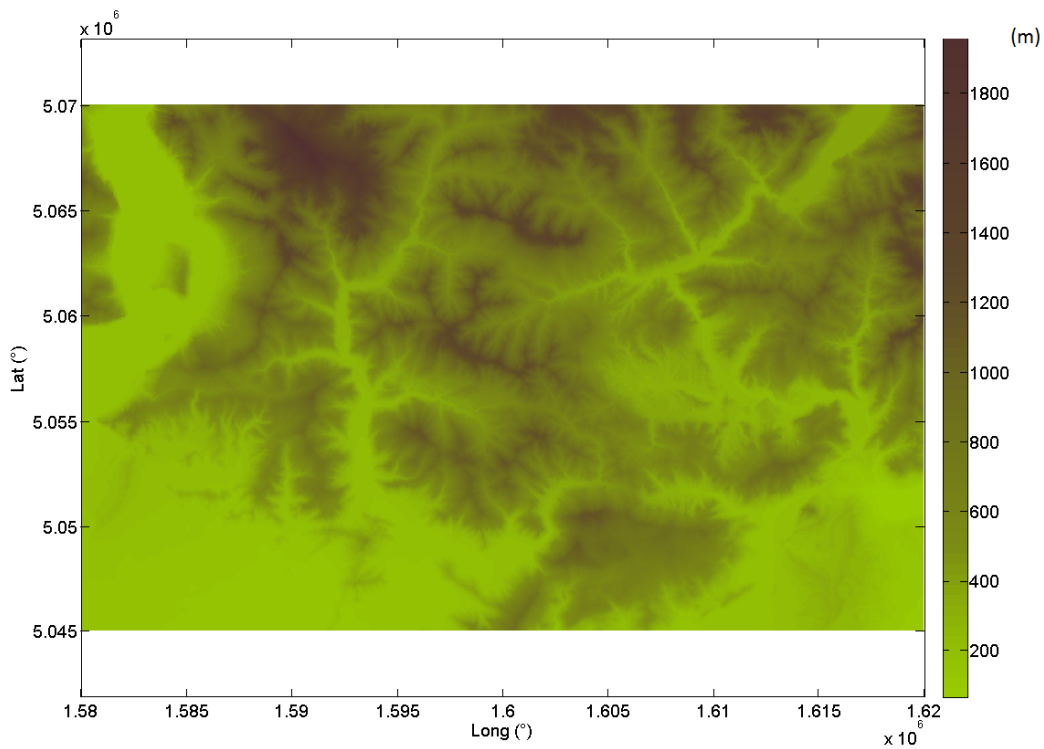
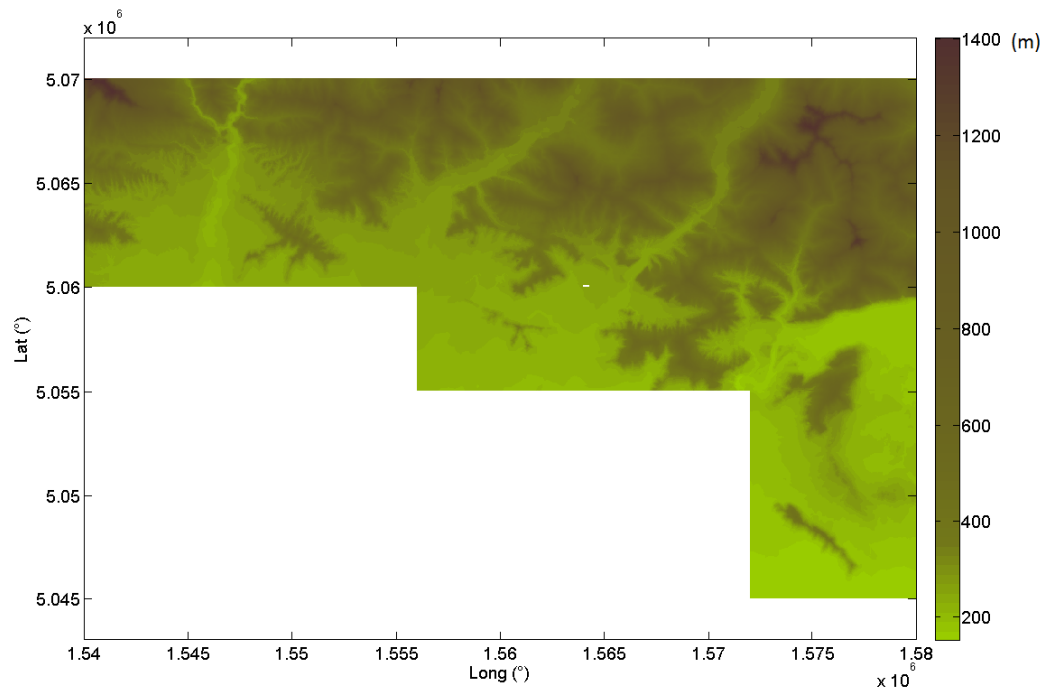
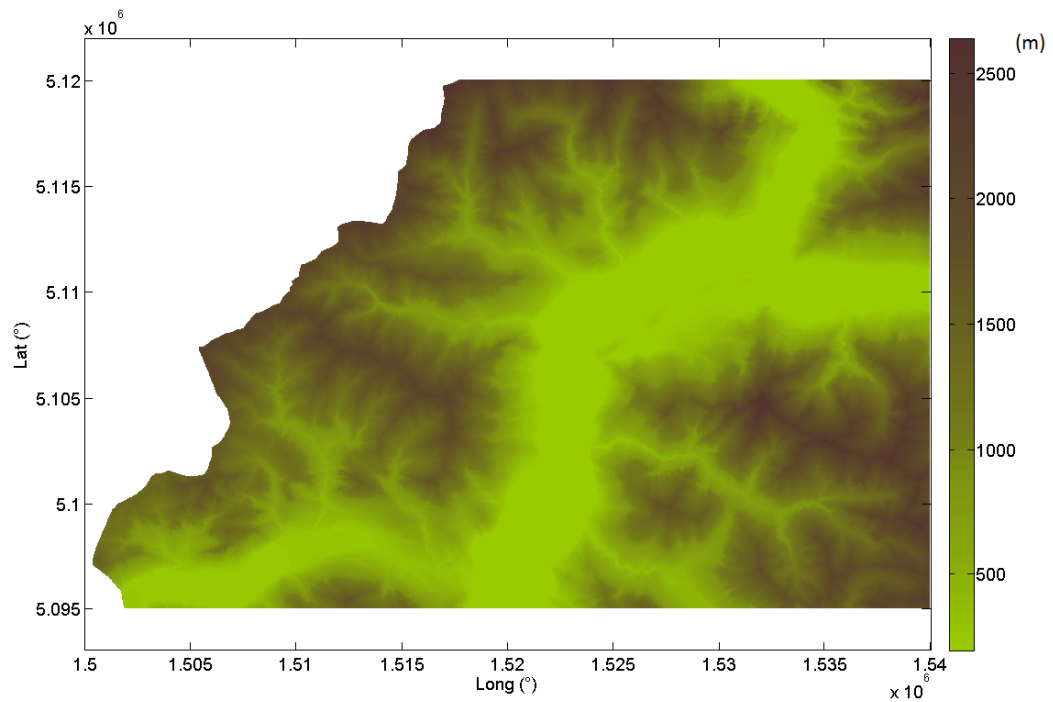
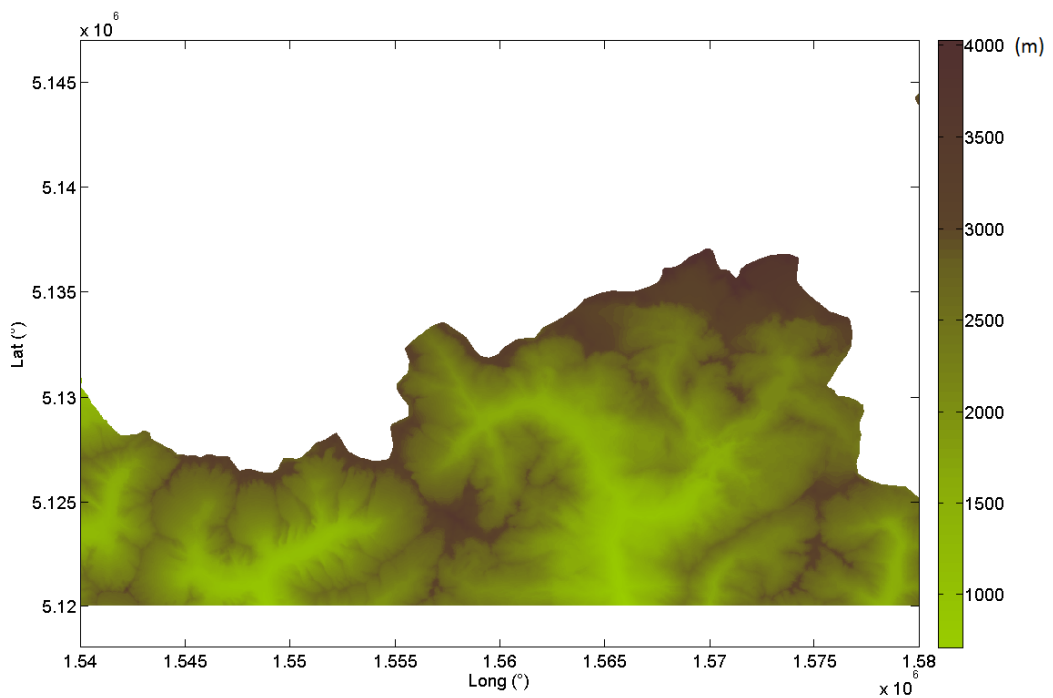


Figure 3.3: Grids C5 (a) and D5 (b) of the Lombardy low resolution regional DTM, covering hilly terrain.



(a)



(b)

Figure 3.4: Grids B3 (a) and C2 (b) of the Lombardy low resolution regional DTM, covering mountainous terrain.

3.1.0.2 Comparison between bilinear and bicubic interpolations on Lidar high resolution DTM

The comparison between bilinear and bicubic interpolations has been performed also with six grids of the LiDAR high resolution DTM. Even in this case the grids have been chosen such that they cover different terrain typologies: two grids belong to plain terrain (grids D46051034 and D46160966), two to hilly terrain (D46081032 and D45810986) and two to mountainous terrain (D46031023 and D46501037). In Table 3.5 the statistics of the original elevations and the extensions of the selected grids are summarized.

	LOWLAND	
	GRID D46051034	GRID D46160966
mean (m)	411	264
std (m)	25	1
max (m)	489	269
min (m)	379	260
Covered area (km ²)	[1 x 1]	[1 x 1]
	HILL	
	GRID D46081032	GRID D45810986
mean (m)	555	486
std (m)	88	51
max (m)	823	636
min (m)	443	391
Covered area (km ²)	[1 x 1]	[1 x 1]
	MOUNTAIN	
	GRID D46031023	GRID D46501037
mean (m)	1863	1951
std (m)	59	146
max (m)	1998	2276
min (m)	1730	1627
Covered area (km ²)	[1 x 1]	[1 x 1]

Table 3.5: Statistics of the elevations of six grids of LiDAR PST-A high resolution DTM.

In Table 3.6 the statistics of the differences between the twice interpolated elevations and the original ones, grouped by terrain typologies, are reported after the removal of all the no data values.

Statistics are good in all the three cases, if compared to the nominal accuracy of the LiDAR DTM. In general, as for the case of Lombardy regional DTM, statistics obtained with the use of a bicubic model are better than those obtained

		LOWLAND	HILL	MOUNTAIN
Differences between re-interpolated and original elevations				
BILINEAR	bias (m)	~0	~0	~0
	std (m)	0.09	0.18	0.10
	max (m)	1.97	6.25	1.47
	min (m)	-1.83	-6.37	-1.47
	Number of useful data	4'705'954	7'973'846	6'160'438
BICUBIC	bias (m)	~0	~0	~0
	std (m)	0.06	0.13	0.07
	max (m)	1.44	5.93	1.32
	min (m)	-1.36	-5.81	-1.18
	Number of useful data	4'660'680	7'921'666	6'106'328

Table 3.6: Statistics of differences in elevation between the original values and those obtained after two-times exact bilinear/bicubic interpolation on the six selected grids of the PST-A DTM, grouped by terrain typologies.

by bilinear. Also in this case the comparison between bilinear and bicubic interpolators has been also performed considering slope and aspect of the original and final DTM. In Tables 3.7 and 3.8 the statistics obtained respectively for slope and aspect are reported. The statistics of the differences provided by bicubic approach are better than those of the bilinear case.

Hill presents anomalies both in the elevation and aspect differences. In particular the maximum and minimum values both in bilinear and bicubic cases are higher than those of the other terrain types; also in case of aspect the differences of the hill terrain present greater values if compared to the others. For this reason a deeper analysis has been performed on the two grids covering hilly terrain. One example is given by grid D46081032: the elevations and aspects of the original grid are shown in Figure 3.5. The morphology of the terrain is identifiable and some artefacts as riverbanks and roads are visible.

In this case the differences in elevation, slope and aspect follow a non random distribution: the highest differences are in fact located along recognizable paths (riverbanks, roads, etc.). This can be seen in Figure 3.6 where the differences in elevation and aspect are reported: differences equal to zero have been coloured in yellow to better have a visual inspection of their distribution.

In conclusion it can be stated that higher order polynomials follow the shape of the terrain better than bilinear, especially where morphology is rough. Since the terrain covering the area of interest of the HELI-DEM project is for the major part hilly or mountainous, it was decided to use the bicubic approach to interpolate the

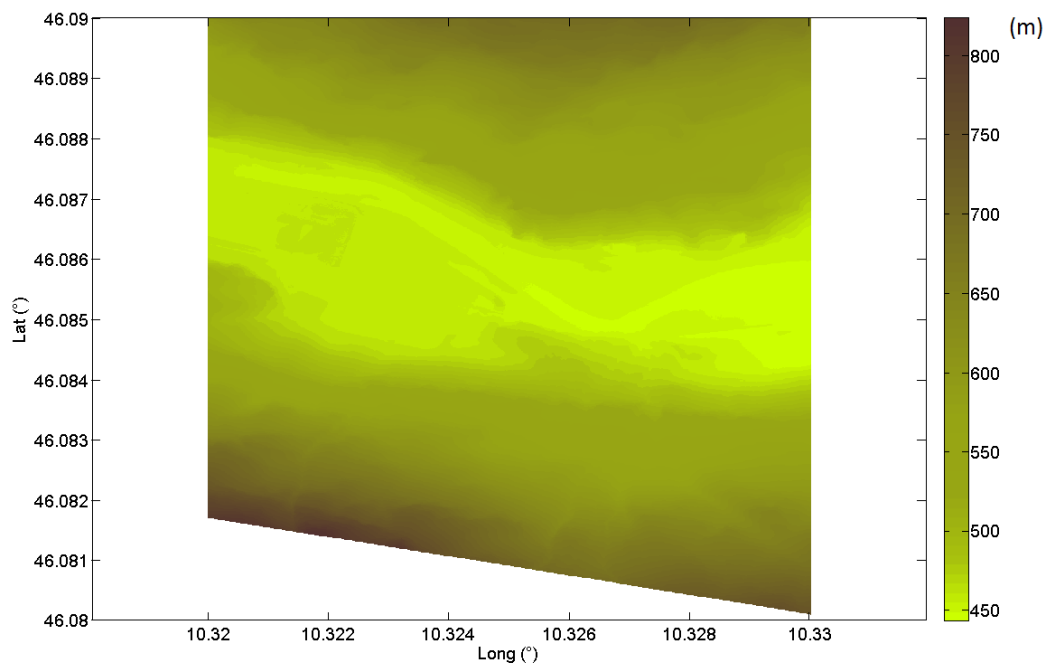
		LOWLAND	HILL	MOUNTAIN
Differences between re-interpolated and original slopes				
BILINEAR	bias (deg)	0.3	~0	0.2
	std (deg)	2.9	3.2	2.9
	max (deg)	37.3	34.3	15.2
	min (deg)	-43.0	-58.9	-27.2
	Number of useful data	4'705'954	7'973'846	6'160'438
BICUBIC	bias (deg)	0.1	~0	~0
	std (deg)	1.8	2.1	1.8
	max (deg)	25.0	27.9	15.6
	min (deg)	-34.7	-56.4	-19.1
	Number of useful data	4'660'680	7'921'666	6'106'328

Table 3.7: Statistics of differences in slope between the original values and those obtained after two-times exact bilinear/bicubic interpolation on the six selected grids of the PST-A DTM, grouped by terrain typologies.

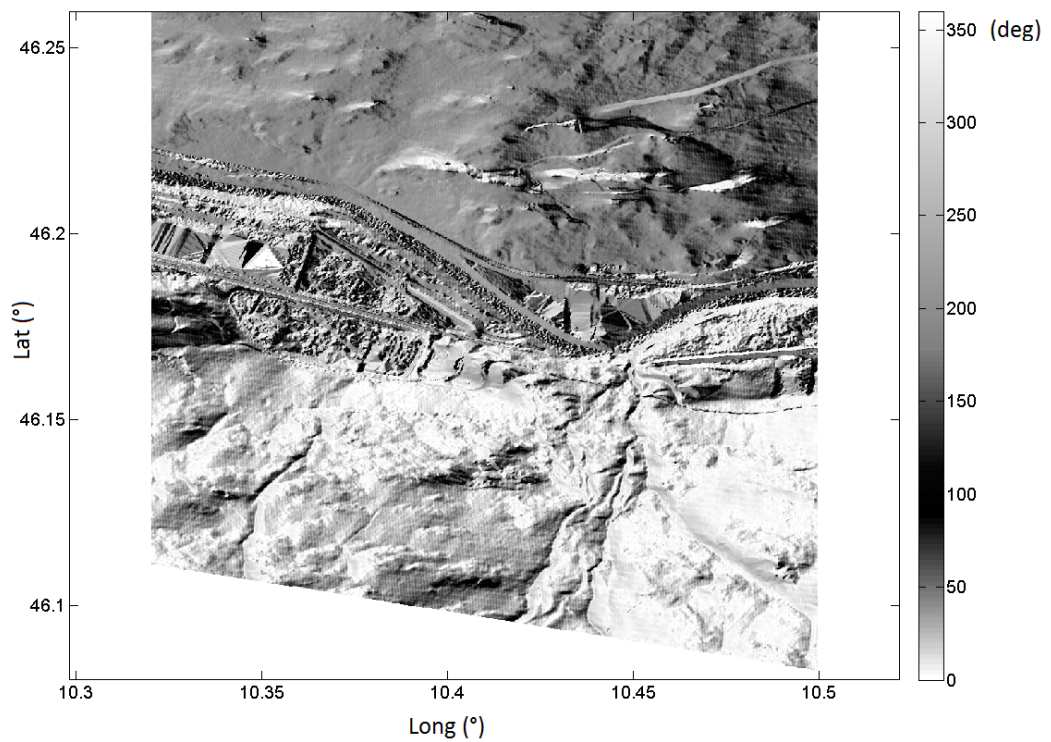
		LOWLAND	HILL	MOUNTAIN
Differences between re-interpolated and original aspect				
BILINEAR	bias (deg)	0.4	-0.2	0.2
	std (deg)	25.4	18.5	8.3
	max (deg)	180.0	180.0	180.0
	min (deg)	-180.0	-180.0	-178.4
	Number of useful data	4'705'954	7'973'846	6'160'438
BICUBIC	bias (deg)	0.1	~0	~0
	std (deg)	19.9	14.5	5.7
	max (deg)	180.0	179.9	177.6
	min (deg)	-179.9	-180.0	-179.4
	Number of useful data	4'660'680	7'921'666	6'106'328

Table 3.8: Statistics of differences in aspect between the original values and those obtained after two-times exact bilinear/bicubic interpolation on the six selected grids of the PST-A DTM, grouped by terrain typologies.

input DTMs on the output grid. The main disadvantage of the bicubic approach is that it might be more affected by ill-conditioning problems: this issue is analysed in detail in the following section.

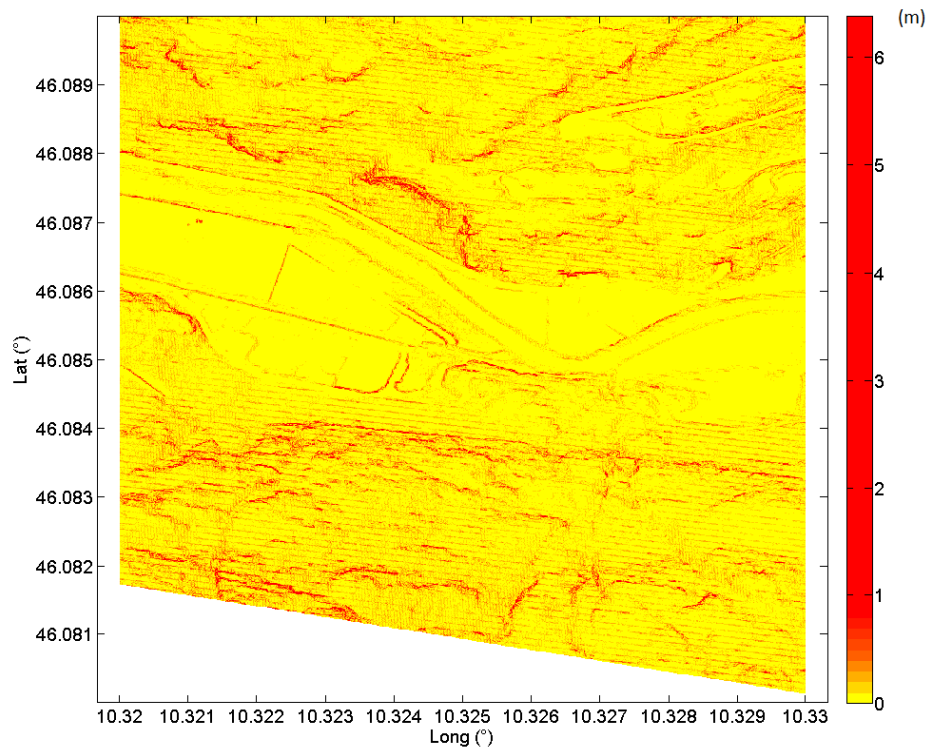


(a)

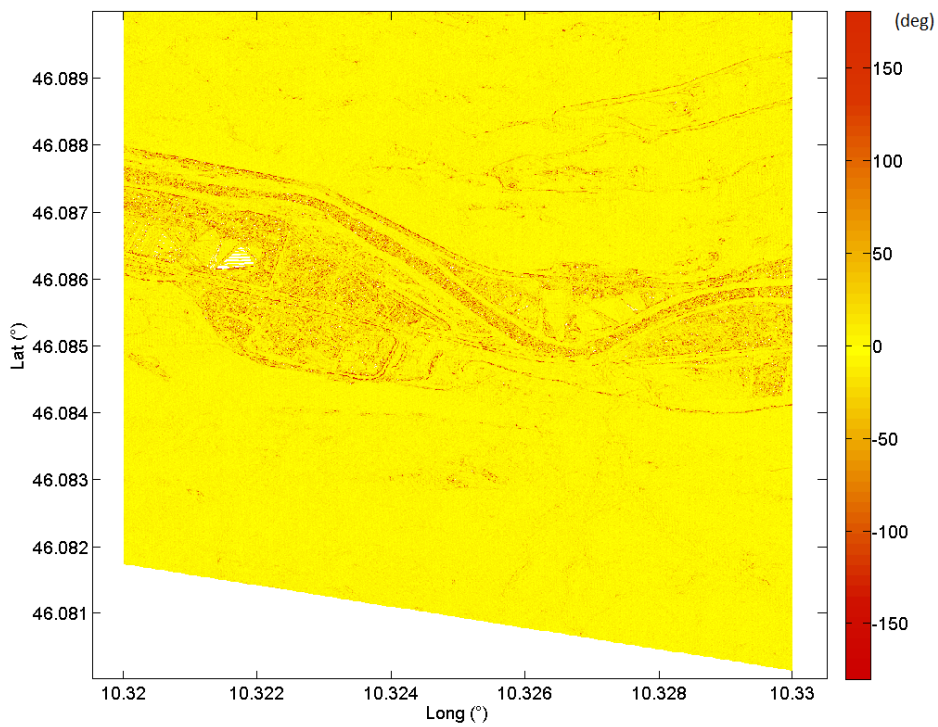


(b)

Figure 3.5: Elevations (a) and aspect (b) of the D46081032 PST-A grid (values in degrees clockwise from North direction).



(a)



(b)

Figure 3.6: Differences between the double-interpolated and original elevations (a) - only differences different from 0 are represented - and aspects (b) of the D46081032 PST-A grid.

3.2 Instability of the interpolation systems: problems and possible solutions

Bicubic approach provides the best results on the HELI-DEM data, and so it will be used in each DTM regriding. In particular an interpolator will be preferred in order to keep the original information contained inside the input elevation data as unchanged as possible. The use of an exact bicubic interpolator implies that to estimate the elevation of a certain output node, the sixteen nearest input points have to be searched, and from them, the system is constructed. The matrices \mathbf{A} (in case of interpolation) and \mathbf{N} (in case of LS solution) can be therefore computed and the elevation of the interpolated node (Equations B.17 and B.18).

The good conditioning of a system depends on the relative position of the input points. Particular spatial distributions around the predicted node produce a system that can be ill conditioned and unstable and, as a consequence, the elevation estimated from the original points can result erroneous. In Figure 3.7 an example of bad configuration on real data is shown: the sixteen nearest points are not homogeneously distributed and they present a void area on the right.

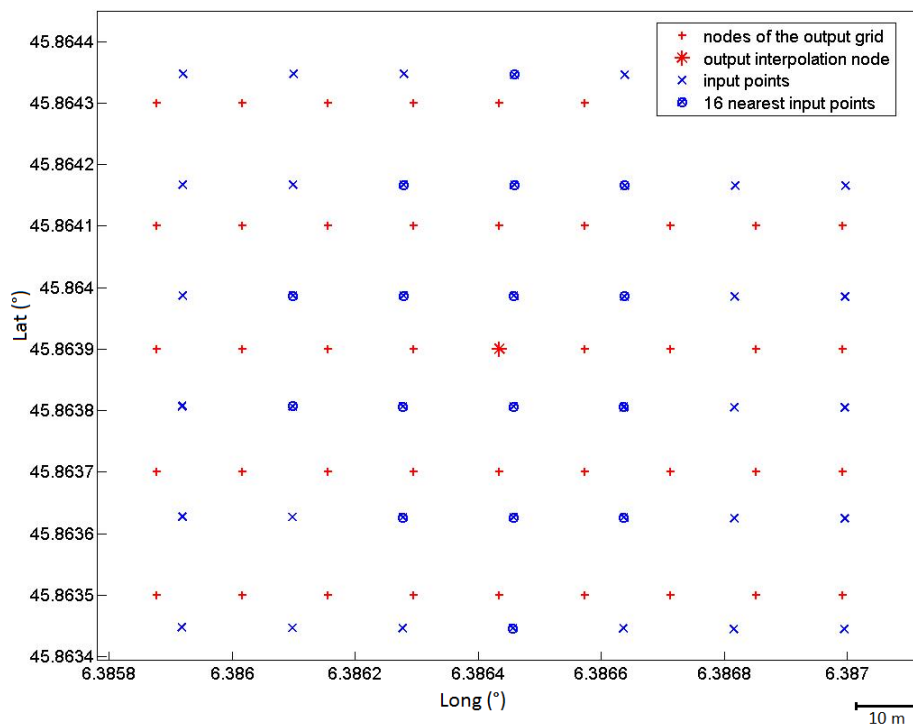


Figure 3.7: Example of bad configuration of an exact bicubic system on real data.

If the observations used to construct the system are well distributed, \mathbf{A} matrix

in case of exact system and \mathbf{N} matrix in case of Least Squares system (for details on equations see Section B.1.3) are easily invertible; on the contrary if observations are badly distributed, some problems can occur in the inversion of the \mathbf{A}/\mathbf{N} matrix, also if the coordinates are normalized as explained in Appendix B.2.1.

The problem of ill-conditioning has been faced in order to implement efficient methods to stabilize the system. The parameter that defines the well or bad conditioning is the condition number¹ of the design \mathbf{A} matrix constructed from the sixteen observations (in case of exact system) and of the \mathbf{N} matrix (in case of Least Squares system). In fact the condition number of a matrix is an important parameter to verify if the matrix is stable or not. If the condition number tends to infinite the matrix is called singular and is not invertible; in case the condition number is high but not infinite, the matrix is theoretically invertible, but in practise the estimates are not stable. When the matrix is singular (condition number infinite) or ill-conditioned (high condition number) some approaches can be used to stabilize and solve the system:

1. increment of the number of observations (Least Squares with a redundant number of observations, LS_{RO}),
2. Tychonoff Regularization,
3. Singular Value Decomposition (SVD),
4. Finite Elements regularizations.

Clearly, by introducing redundant observations a Least Squares system has to be solved instead of an interpolation. The methods are presented belows.

1. Least Squares with a redundant number of observations. This method is based on the addition of redundant observations to the iso-determined system. If the system is originally unstable, it can be stabilized adding some new observations. If the new points are located in positions that previously were empty or with too few data, after their addition, the new configuration of the global set of points will be better and the system will become more stable. Clearly the addition of new observations leads from the original iso-determined system ($\underline{\xi} = \mathbf{A}^{-1}\underline{z}$) to the solution of a Least Squares system ($\underline{\xi} = \mathbf{N}^{-1}\mathbf{A}^T\mathbf{Q}^{-1}\underline{z}$).

In this case, an iterative approach is implemented: if the original system is still ill conditioned, a new observation (the nearest that has not been yet included) is added at each step to the observations vector. At each step \mathbf{N} is recomputed and

¹The condition number of a matrix is the ratio between the highest and the minimum eigenvalues.

its condition number is compared with a certain threshold. When the resulting system is well conditioned, that is when the new condition number is lower than the threshold, the interpolation is finally performed. The final system is redundant (the number of observations is greater than the number of parameters) and is solved by Least Squares (equations in Section B.2.1).

To study the other three methods, let now suppose that a system ($\mathbf{K}\underline{\xi} = \underline{\eta}$) has to be solved with \mathbf{K} squared and not rank deficient: in our case the system can be either the isodetermined problem ($\mathbf{K} = \mathbf{A}$, $\underline{\eta} = \underline{z}$) or the redundant LS system ($\mathbf{K} = \mathbf{A}^T \mathbf{Q}^{-1} \mathbf{A}$, $\underline{\eta} = \mathbf{A}^T \mathbf{Q}^{-1} \underline{z}$).

Let now suppose that \mathbf{K} is not rank deficient but presents some ill conditioning. The three following approaches can be implemented to improve the solution of the problem.

2. Tyochonoff Regularization. Given a system $\underline{\xi} = \mathbf{K}^{-1} \underline{\eta}$ to be solved, where $\underline{\xi}$ are the unknown parameters, in some cases the usual solution:

$$\underline{\hat{\xi}} = \begin{bmatrix} \hat{a}_{00} \\ \hat{a}_{10} \\ \dots \\ \hat{a}_{33} \end{bmatrix} = \mathbf{K}^{-1} \underline{\eta} \quad (3.1)$$

doesn't produce a good result, because the matrix \mathbf{K} is ill conditioned. In this case a further condition can be added to guarantee the regularity of the estimated model:

$$\underline{\hat{\xi}} = \begin{bmatrix} \hat{a}_{00} \\ \hat{a}_{10} \\ \dots \\ \hat{a}_{33} \end{bmatrix} = (\mathbf{K} + \alpha \mathbf{I})^{-1} \underline{\eta} \quad (3.2)$$

where α is the regularization parameter and can be chosen of different types; one possibility, that has been applied in this work is $\alpha = 10^{-6} \bar{\lambda}$, where $\bar{\lambda} = \frac{1}{n} \sum_{i=1}^n \lambda_i$, (λ_i are the eigenvalues of the \mathbf{K} matrix). This choice is consistent with many references on the solution of ill conditioned problems (Takos, 1999).

3. Singular Value Decomposition. The SVD method is based on the theorem of linear algebra for which the \mathbf{K} matrix can be expressed as the product of a column-orthogonal matrix \mathbf{U} , a diagonal matrix \mathbf{S} whose elements are the singular values of the original matrix and the transpose of an orthogonal \mathbf{V} matrix.

$$\mathbf{K} = \mathbf{U}\mathbf{S}\mathbf{V}^T = \mathbf{U} \begin{bmatrix} s_{11} & 0 & \dots & 0 \\ 0 & s_{22} & \dots & 0 \\ \dots & \dots & \dots & \dots \\ 0 & \dots & \dots & s_{nn} \end{bmatrix} \mathbf{V}^T \quad (3.3)$$

Since the \mathbf{K} matrix is squared, then \mathbf{U} , \mathbf{V} and \mathbf{S} are squared matrices of the same size. In addition $\mathbf{U}^T\mathbf{U} = \mathbf{U}\mathbf{U}^T = \mathbf{I}$. The same holds for \mathbf{V} . If \mathbf{K} is of full rank, the coefficients are real positive valued and can be ordered $s_{11} > s_{22} > \dots > s_{nn}$. The inverse of \mathbf{K} can be then computed as:

$$\mathbf{K}^{-1} = \mathbf{V}\mathbf{S}^{-1}\mathbf{U}^T = \mathbf{V} \begin{bmatrix} \frac{1}{s_{11}} & 0 & \dots & 0 \\ 0 & \frac{1}{s_{22}} & \dots & 0 \\ \dots & \dots & \dots & \dots \\ 0 & \dots & \dots & \frac{1}{s_{nn}} \end{bmatrix} \mathbf{U}^T \quad (3.4)$$

If \mathbf{K} is almost singular some terms s_i are almost zero and their inverse is almost infinite. Therefore the inverse of the \mathbf{K} matrix cannot be computed. To let the matrix \mathbf{K} be invertible, the elements $\frac{1}{s_{ii}}$ that are greater than a certain threshold are set to zero. In this way \mathbf{S} is calculated putting in the diagonal $\frac{1}{s_{ii}}$ if s_{ii} is greater than the threshold, or zero if s_{ii} is smaller than the threshold.

In practice, with the SVD method, the number of estimated parameters is reduced, or better the parameters that cannot be estimated are set to zero and only the parameters that are estimable are actually estimated.

4. Finite Elements. This method is halfway between a deterministic and a stochastic method. It is based on the addition of a pseudo-observation to the original observations (the elevations of the points) used to construct the system. The pseudo-observation is the elevation of the interpolation point estimated using an interpolation function simpler than the bicubic; in particular it can be obtained by linear interpolation on the triangle that contains the point.

Given the set of input points, the TIN (triangulated Irregular Network) of them is constructed and the triangle that contains the interpolation point is searched (Figure 3.8). The triangle that includes the interpolation point P (Figure 3.9(a)) can be found by applying the following search rules (Li et al., 2005). If P is inside the triangle, then (Figure 3.9(a))

- P must be on the left of the vector connecting the vertices 1 and 2 of the triangle,
- P must be on the left of the vector connecting the vertices 2 and 3 of the triangle,

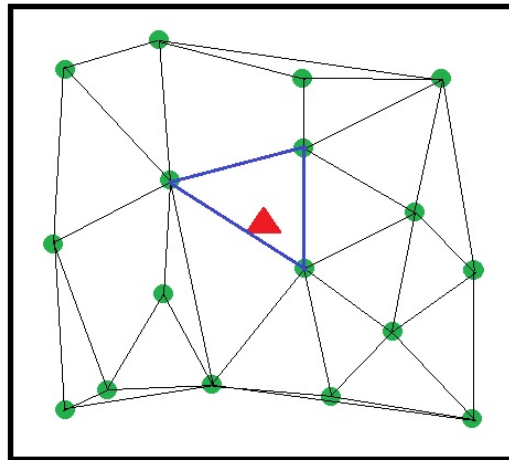


Figure 3.8: Example of TIN constructed with the Least Squares system observations (the green dots are the original observations, the red triangle is the interpolation point, the blue triangle is the one that contains the interpolation point).

- P must be on the left of the vector connecting the vertices 3 and 1 of the triangle.

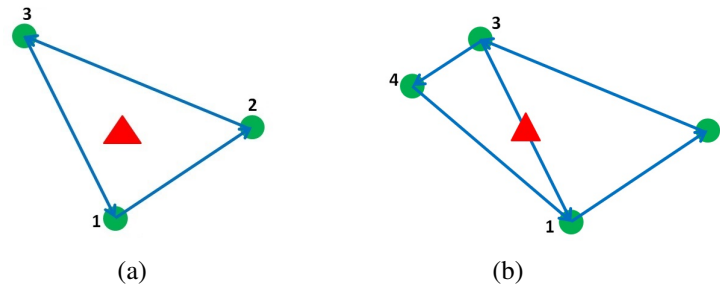


Figure 3.9: Triangle of the TIN used to construct the pseudo-observation in the Finite Element method: the point can be within one single triangle (a) or can be within in the line between two triangles (b).

To check the relative position of P with respect to each one of the above sides v_{ij} , the determinant of the matrix

$$\begin{bmatrix} x_i & y_i & 1 \\ x_j & y_j & 1 \\ x_P & y_P & 1 \end{bmatrix}$$

has to be calculated. In the formula (X_P, Y_P) are the coordinates of the interpolation point. If the determinant is positive the three points are in anticlockwise order

(the point is on the left side), if the determinant is null the three points are on a straight line, if the determinant is negative the three points are in clockwise order (the point is on the right side).

If the three determinants have mixed or all negative signs, P is not inside the triangle and the search must continue. Two results are possible:

1. if the determinants of the three matrices are all positive, the point is on the left of all the three vectors and therefore the point is inside one triangle,
2. if two determinants are positive and the third one is null, the point lies on one line joining two triangle vertexes and therefore the point is between two adjacent triangles.

With respect to the two cases, the elevation of the interpolation point that will be used as pseudo-observation for the Least Squares system is computed in two different ways.

In the first case the elevation of the interpolation point is computed by Least Squares using the three elevations of the vertexes of the triangle that contains the point as observations and the elevation is computed using the 3-D plane formed by the triangle. The observation equation is:

$$z(x, y) = a_{00} + a_{10}x + a_{01}y \quad (3.5)$$

Three equations are obtained from the three vertexes of the triangle:

$$\begin{cases} z_1 = a_{00} + a_{10}x_1 + a_{01}y_1 \\ z_2 = a_{00} + a_{10}x_2 + a_{01}y_2 \\ z_3 = a_{00} + a_{10}x_3 + a_{01}y_3 \end{cases} \quad (3.6)$$

The elevation of the interpolation point that is then used as pseudo-observation is therefore estimated through the resolution of the system (section B.1.1). Note that if a local coordinates system is defined imposing the interpolated point as the origin, the system becomes:

$$\tilde{z}_{P,pseudo-obs} = a_{00} \quad (3.7)$$

In the second case it is not necessary to interpolate the elevation using the three vertexes of the triangle, but simply it is sufficient to compute the elevation using the equation of a straight line connecting two points in a 3-D space:

$$\frac{x_P - x_1}{x_2 - x_1} = \frac{y_P - y_1}{y_2 - y_1} = \frac{z_P - z_1}{z_2 - z_1} \quad (3.8)$$

The elevation of the point P is estimated by the formula:

$$\tilde{z}_{P,pseudoobs} = \frac{x_P - x_1}{x_2 - x_1}(z_2 - z_1) + z_1 \quad (3.9)$$

In both cases the estimated elevation of point P is then added as pseudo-observation to the original Least Squares system

$$\underline{Z}_{new} = \begin{bmatrix} z_1 \\ z_2 \\ \dots \\ z_n \\ \hat{z}_{P,pseudoobs} \end{bmatrix} = \begin{bmatrix} 1 & x_1 & y_1 & \dots & x_1^3 y_1^3 \\ 1 & x_2 & y_2 & \dots & x_2^3 y_2^3 \\ \dots & \dots & \dots & \dots & \dots \\ 1 & x_n & y_n & \dots & x_n^3 y_n^3 \\ 1 & 0 & 0 & \dots & 0 \end{bmatrix} \begin{bmatrix} a_{00} \\ a_{10} \\ \dots \\ a_{33} \end{bmatrix} \quad (3.10)$$

All the four methods have been implemented. Several tests have been performed, that demonstrated the substantial equivalence of them. deeper details are not reported in this thesis. Since Thyconoff is already a well known method and Finite Element is a method that has to be still studied and optimized, attention has been paid on the other two methods: the reduction of parameters with the SVD approach and the addition of number of observations with the LS_{RO} solution. In Chapter 4 the two methods are in detail analysed and compared using real data.

3.3 Different procedures to merge and interpolate DTMs on an output grid

Different procedures can be adopted to produce a unified output DTM from different original elevation data. In general, three independent operations are necessary regardless of the order:

- alignment of the available DTMs to a common reference frame,
- interpolation of the DTMs on the output grid,
- merging of the interpolated elevations between two or more DTMs, where they overlap.

The order in which the operations are performed depends on the type of adopted procedure. Three different procedures have been studied and implemented. The first two methods are both considered as Direct methods and will be called respectively DirectAndAverage and DirectOnMerged. They are similar because their first operation is the alignment of the input DTMs to the final output reference

frame. The two procedures differ then in the order by which the operations of merging and interpolation are performed. In the former the input DTMs, previously transformed from their original reference frames to the output reference frame, are independently interpolated on the output grid and then merging is executed computing, inside the overlapping areas where two or more DTMs are present, the average of the elevations obtained from the individual interpolations. In the latter the DTMs, after their reference frames alignment, are all unified into a unique dataset that is then interpolated on the output grid. Both solutions, possible and valid, have been implemented and compared.

The third and last studied procedure (called Inverse method) acts in an opposite way with respect to the Direct methods: in this case for each input DTM the nodes of the output grid are back-transformed from the output reference frame to the input reference frame. Each input DTM, still gridded, is interpolated on the back-transformed output points. The interpolated heights are then assigned to the output nodes. Finally, as for DirectAndAverage method, the individual estimated elevations are averaged in the overlapping areas.

In order to find the best procedure to perform the merging of the available data for the HELI-DEM project, some preliminary analyses have been performed on real data. Within HELI-DEM and for its final purposes the two merging Direct procedures have been studied and compared. The results of this comparisons are discussed in the following paragraphs. At the conclusion of the project, for completeness, also the Inverse method has been tested and compared to the others. This work is in detail described in Chapter 5.

3.3.1 Comparison between the two Direct methods in the interpolation of the input DTMs on the output grid

The output unified DTM has to be obtained from the unification of the three available low resolution elevation models: the two Lombardy and Piedmont regional DTMs with a planimetric resolution of 20 and 5 meters and the Swiss national DTM with a planimetric resolution of 1 second (about 30 meters). All of them have to be converted from their original reference frames to the reference frame of the output grid, ETRF2000. It has to be considered that, when a grid is transformed from its original reference frame to another, the resulting dataset is no more regularly gridded but the output points (terns of coordinates) are distributed following a spatially regular geometric pattern. In Figure 3.10 an example is provided: on the same graph the nodes of a small portion of the final HELI-DEM grid and the nodes of the Lombardy regional DTM after their transformation from their original reference frame (Roma40) to ETRF2000 are plotted.

The test has been performed on a small study area located near Como Lake

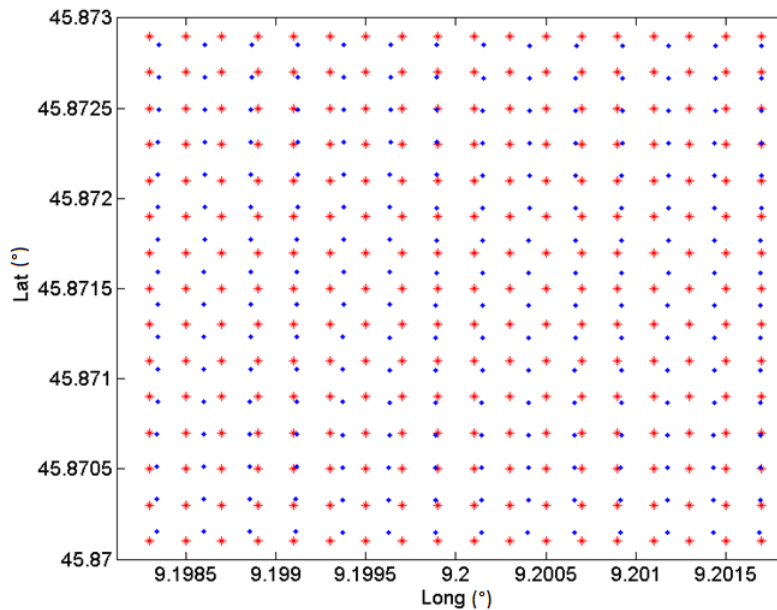


Figure 3.10: Lombardy DTM data transformed from their original reference frame (Roma40) to those of the output HELI-DEM grid (ETRF2000): in red the output grid nodes, in blue the input transformed elevation data.

and called Triangolo Lariano (Figure 3.11) with an extension of about 56 km²: the area covers a portion of the output HELI-DEM grid with 200'000 (400 x 500) nodes. The statistics of the original elevations inside this area are summarized in Table 3.9.

Statistics (m) of elevations	
Mean	660
Std	345
Maximum	1679
Minimum	197

Table 3.9: Statistics of the input data of the case study area (Triangolo Lariano, near Como and Lecco).

This area has been chosen because it is covered by two of the three low resolution models, the Lombardy and the Swiss DTMs. Their original differences are shown in Figure 3.12: they have mean equal to 2.1 m and standard deviation equal to 20 m. 21 differences are greater than 100 m and the maximum value is 123 m. The differences are spatially correlated and rather smooth (Biagi and Carcano, 2013): in any case discontinuities and breaklines exist.



Figure 3.11: Area used as case study (Triangolo Lariano in lombardy, between Como and Lecco). Coordinates of the central point of the area: $\lambda = 9.22^\circ\text{East}$, $\phi = 45.86^\circ\text{North}$.

The two DTMs have been interpolated and merged on the output grid following the two different `DirectAndAverage` and `DirectOnMerged` approaches. In both cases the interpolation of the input data is performed through a bicubic exact surface that, for each node of the output grid, passes through the sixteen nearest observations.

To analyse the efficiency of the two methods and compare them, first of all the conditioning of the exact system is analysed. In this case the comparison is made between the condition number of the \mathbf{A} matrix of the exact bicubic system in case of individual interpolation of the Lombardy DTM (first part of `DirectAndAverage` method) and the condition number of the \mathbf{A} matrix of the system obtained by the interpolation of the merged dataset of Lombardy and Swiss DTMs (`DirectOnMerged` method). The condition numbers are shown in Figure 3.13. The colour scale of the two images has been levelled to have a better visual comparison. The individual interpolation of the Lombardy DTM presents condition numbers smaller than the unified interpolation: in fact in the left image the condition number never exceeds 10^7 and the 99.5% of the nodes has a value lower than $10^{2.5}$. In case of preliminary merging of the two DTMs the condition number reaches the

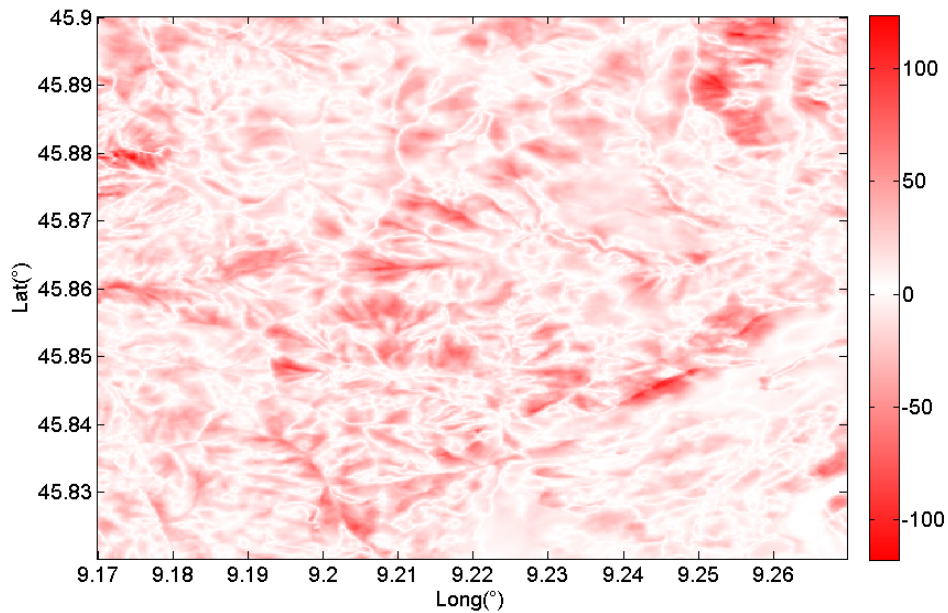


Figure 3.12: Elevation differences of Lombardy and Swiss DTMs inside the case study area of Triangolo Lariano (values in m).

value of 10^{10} in some nodes and is greater than $10^{2.5}$, 10^5 , 10^7 and 10^9 respectively in the 99.5%, 83.25%, 24.75% and 0.62% of the nodes.

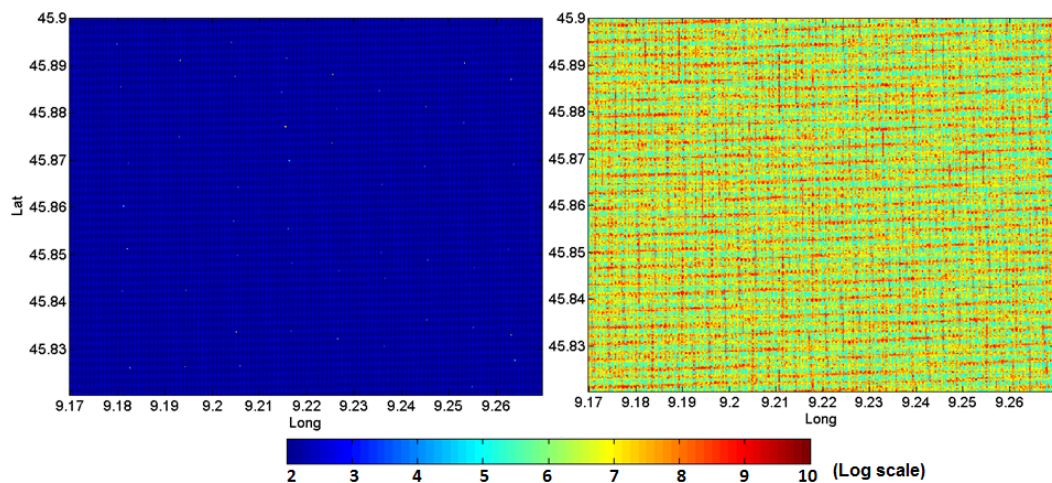


Figure 3.13: Condition number of the A matrix of the system obtained through bicubic interpolation of the Lombardy DTM (first part of DirectAndAverage method on the left) and of the dataset obtained by the merging of the Lombardy and Swiss DTMs (DirectOnMerged method, on the right) - Triangolo Lariano case study.

Also the final DTMs resultant from the application of the two methods have been compared. Figure 3.14(a) shows them: on the left the result of the average of the elevations obtained by individual interpolation of the two DTMs on the final grid, on the right the DTM resultant from the interpolation of the merged dataset. The first result does not present artifacts and its roughness is consistent with those of the individual interpolations. In the second case the interpolated grid contains significant outliers and present artificial roughness due to the local inconsistencies between the two input datasets. The problem is clearly due to the spatial pattern of the unified Lombardy and SwissTopo datasets and also to the bias existent between the two DTMs: in fact the interpolation surface has to follow points that are located on two different surfaces. Therefore this method strictly requires a regularization approach to stabilize the system. Also the aspect of the final interpolated grids helps to better understand the good or bad efficiency of the two methods. Figure 3.14(b) shows the aspect of the final resultant DTM for the two cases of DirectAndAverage method and DirectOnMerged method: the second method clearly produces sparse outliers moreover, even where no outliers are present, a visual inspection highlights that the aspect obtained with the first approach is better than the one obtained with the second.

Since the first approach is performed computing for each node the average of the two results obtained by individual exact bicubic interpolation of the Lombardy and Swiss DTMs, in practice it is like if the elevation was obtained by a total of 32 points (16 belonging to Lombardy DTM and 16 belonging to Swiss DTM). Theoretically the comparison between the two methods should be therefore performed not considering in both cases the result of the exact interpolation, but considering for DirectAndAverage method the result of the average of the exact interpolations (and so the 32 points) and for DirectOnMerged method the interpolation obtained through 32 points instead of the 16 used in the previous comparison. Also this comparison has been then performed. The results are not reported here because the results are not so better with respect to the previous case and DirectOnMerged method continues to produce some problems.

At the end of this analysis it can be concluded that between the two Direct interpolation and merging methods, DirectAndAverage method seems to produce better results than DirectOnMerged method. Therefore it has been decided to use the first method to interpolate and merge the three low resolution DTMs on the output HELI-DEM grid. In any case, also with this method, it can happens that the bicubic interpolation produces an unstable system and can bring to an erroneous estimation of the elevation of the considered interpolation node. In fact, even if with the first method this problem seems to happen in a very small number of cases, in those cases the system has to be regularized applying one of the procedures described in section 3.2. This problem will be analysed in the

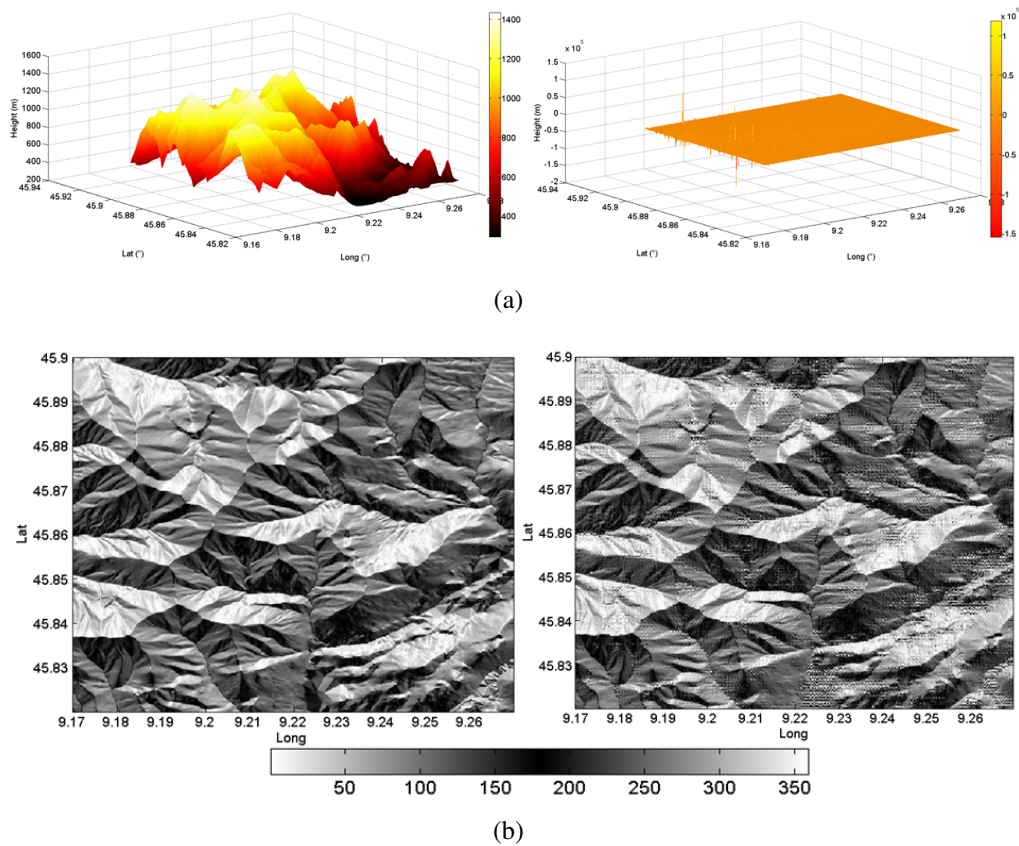


Figure 3.14: DTM (a) and aspect (b) obtained by the application of DirectAndAverage (figures on the left) and DirectOnMerged (on the right) methods on the merging of Lombardy and Swiss DTMs on the Triangolo Lariano case study area.

following paragraphs.

3.3.2 Comparison between SVD and LS_{RO} solutions to regularize unstable systems

Ill conditioning problems are only caused by the reciprocal position of input points with respect to the interpolated node. In all the cases in which the exact bicubic interpolation does not produce a satisfactory result, a procedure that regularizes the system and stabilize it has to be adopted. The stability of the system can be evaluated checking the condition number of the \mathbf{A} matrix. The threshold by which a system is considered stable or not is set to $10^{2.5}$. In fact it has been studied that this value is a conservative threshold.

Two methods have been compared on the case study. The first is the SVD

approach, in which the number of parameters is reduced to the maximum number of estimable ones; the second approach is called LS_{RO} and consists on the addition of a certain number of observations besides the original sixteen. For details on the two methods see section 3.2. The area of Triangolo Lariano has been used also in this case as study area. The two DTMs of Lombardy and Switzerland have been interpolated independently on the output grid and for both DTMs the two regularization methods have been used to regularize all the ill-conditioned nodes. In this case only 915 nodes (the 0.46%) present a condition number that overcomes the threshold and require a system regularization. In Table 3.10 the number of parameters removed with the use of the SVD solution and the number of observations used in case of LS_{RO} solution are summarized.

	LS_{RO}	SVD
1 added point / removed parameter	199	896
2 added points / removed parameters	607	16
3 added points removed parameters	109	3

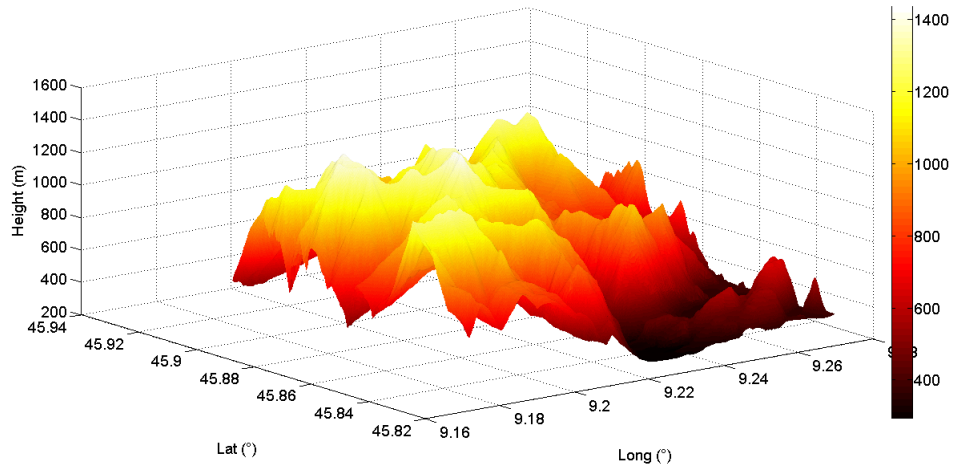
Table 3.10: Number of nodes (with respect to the 915 that require a regularization) for which 1,2,3 points are added to the initial 16 observations in case of LS_{RO} solution or 1,2,3 parameters are removed from the 16 original parameters in case of SVD solution (Triangolo Lariano case study).

With LS_{RO} solution, one, two or three redundant observations are added, while in SVD solution one, two and three eigenvectors are annihilated. In case of SVD for the majority of the 915 nodes (97.92%) only one parameter has to be removed to reach the stability of the system; in the other case for the 78.25% of the 915 nodes not only one point has to be added to the sixteen initial ones, but at least two points are necessary. This is in some way expected, because annihilation is selective on the less significant eigenvectors, while redundant observations are added simply on a distance criterion. In both cases, after the regularization of the 915 nodes, all the interpolated elevations of the output grid are well estimated and the resultant DTM is smooth and does not present outliers or irregularities anymore.

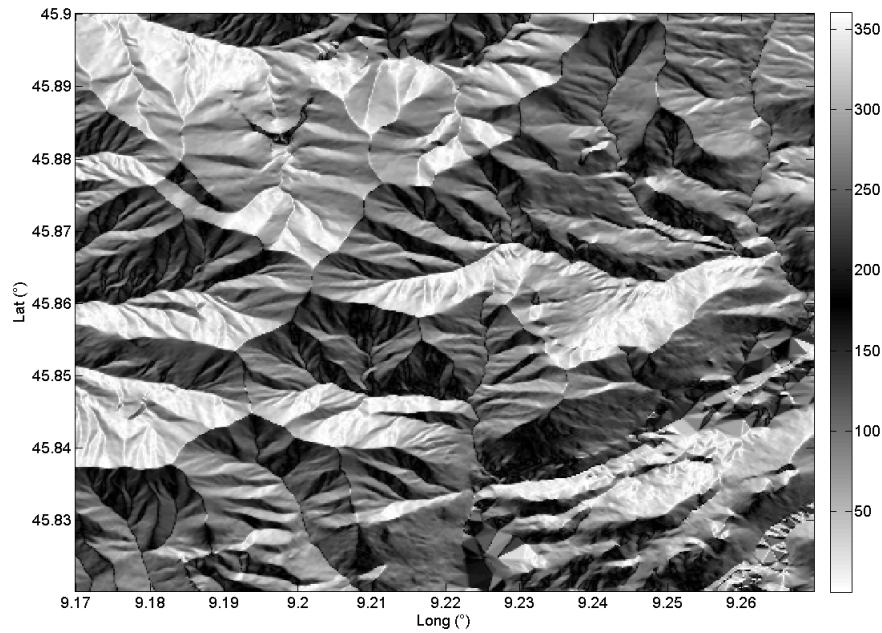
As example, Figure 3.15 displays the interpolated DTM regularized through LS_{RO} solution and its aspect. LS_{RO} and SVD have been compared by computing for each node their differences: the statistics are summarized in Table 3.11.

The statistics suggest that the two regularization solutions lead to the same result. Both methods can be therefore used to stabilize the system in all the cases of ill-conditioning.

Some additional analyses have been performed in order to test the two regularization methods. The statistics, contained in Table 3.12, are referred to the Triangolo Lariano case study. The Lombardy DTM is interpolated on the output



(a)



(b)

Figure 3.15: DTM (a) and aspect (b) resultant from the interpolation of the Lombardy DTM (with LS_{RO} regularization) on the Triangolo Lariano case study area.

grid nodes and then back interpolated on the original nodes. In the table the terms *ExBic*, *LR_{RO}* and *SVD* refer to the differences obtained between the original and

Statistics (m) of elevation differences	
Bias	0.05
Std	0.5
Maximum	4.8
Minimum	-2.5

Table 3.11: Statistics (m) of the differences between the elevations obtained through Lombardy DTM interpolation on the output grid with SVD and with LS_{RO} regularization (Triangolo Lariano case study).

the back interpolated elevations through the use of respectively an exact bicubic system, the LR_{RO} solution in case of ill conditioning system and the SVD solution. The comparison between $ExBic$ and LS_{RO} confirms the usefulness of the introduction of a regularization approach when the interpolation is ill conditioned instead of the simple use of the sixteen observations. The two rows containing $ExBic - LS_{RO}$ results in the regularized nodes proves that the regularization has the expected effect on nodes where conditioning is really needed. LS_{RO} and SVD provide consistent results and only 10 regularized interpolations deviate more than 5 m from the corresponding interpolations. The same test has been applied to the SwissTopo input data. In this case, the maximum condition number is smaller than $10^{2.5}$: indeed, SwissTopo elevations are already gridded in ETRF and, in this case, never present a critical spatial configuration for bicubic interpolation. The statistics of exact bicubic interpolation are similar to those provided by the regularized interpolation on Lombardy dataset.

	Mean	Std	Max	Min
ExBic	0.3	6.4	92.6	-1031.0
LS_{RO}	0.3	5.3	39.3	-56.8
ExBic - LS_{RO} ($10^{2.5} \leq CN < 10^5$)	0.0	0.5	6.3	-3.7
ExBic - LS_{RO} ($10^5 \leq CN$)	148.9	581.3	2714	-127.0
LS_{RO} - SVD	0.1	0.5	4.3	-2.5
ExBic (SwissTopo)	0.3	5.0	37.2	-25.2

Table 3.12: First five rows: Lombardy tests. $ExBic$: differences in the input points between original and back interpolated elevations using Exact Bicubic interpolation. LS_{RO} : same differences using LS_{RO} solution in case of ill-conditioning. $ExBic - LS_{RO}$ ($10^{2.5} \leq CN < 10^5$): differences between Exact Bicubic and LS_{RO} interpolations in the (858) regularized nodes with $10^{2.5} \leq CN < 10^5$. $ExBic - LS_{RO}$ ($10^5 \leq CN$): differences between Exact Bicubic and LS_{RO} interpolations in the (20) regularized nodes with $10^5 \leq CN$. LS_{RO} - SVD: differences between LS_{RO} and SVD interpolations in all the regularized nodes. SwissTopo tests: only $ExBic$ is reported. CN: Condition Number.

Chapter 4

The unified DTM: preprocessing and final computation

The main final product of HELI-DEM is a unified DTM obtained through the merging of the available data. In particular the output grid, with a spatial resolution of $2 \cdot 10^{-4}$ sexagesimal degrees both in longitude and latitude and georeferenced in ETRF2000, can be obtained unifying into a unique output grid the low resolution (regional and national) DTMs. In order to find the best procedure to create the final model a preprocessing has been performed on the original data. Once the low resolution final DTM has been produced, some analyses have to be done to decide how the high resolution available data can be used to enhance it.

In this chapter the final adopted procedure and the obtained results are in detail described. Finally a geoserver ad-hoc created to store the input data and the output products is then described.

4.1 Characteristics and creation of the unified HELI-DEM DTM

The final product of HELI-DEM is a unified DTM which will cover the whole project area (Figure 2.1). The model should be obtained through the merging of the available low/medium resolution DTMs. For the Switzerland area a unique DTM (DTMCH25) is available, in the ETRF89 reference frame, geographic coordinates (λ, ϕ) , with a grid spacing of 1" equal in longitude and latitude (about 30 meters). Lombardy is covered by the regional DTM, originally gridded in Roma40, in Gauss-Boaga coordinates (East, North) with a grid spacing of 20 meters. In Piedmont two DTMs with regional extension are available. One has a spatial resolution of 5 meters and is georeferenced in ETRF89, UTM coordinates; since for this area it is the DTM with the highest accuracy, it is reasonable to use

only that for the Piedmont contribution.

The output DTM, which will be called in the following HD-1 DTM, will be obtained by harmonization, filtering and interpolation of the Lombardy, Piedmont and Swiss DTMs. As previously already said, the model will be georeferenced in ETRF2000 and will be expressed in geographic coordinates. HD-1 will cover the whole area of interest of the project and will have a resolution comparable with those of the input DTMs. The area of interest is included inside a geographic rectangle whose limits are 7.80° East and 10.70° East in longitude and 45.10° North and 46.70° North in latitude. The HD-1 model will be computed on a grid with a spacing of $2 \cdot 10^{-4}$ sexagesimal degrees both in longitude and latitude: this has the disadvantage that the cells are not metrically square, because at the latitudes of the HELI-DEM area $\Delta\phi = 2 \cdot 10^{-4}$ corresponds to 22 m and $\Delta\lambda = 2 \cdot 10^{-4}$ corresponds to 15 m. However, the use of geographic coordinates avoids the problem of the management of different cartographic zones, which does not concern the actual extension of the project area, but that could pose some problems in case of a future extension of the area of interest of the DTM. The choice of a grid spacing equal in longitude and latitude is a standard that allows the use of the data also with GIS programs that not accept grids with different grid spacing values in the two directions. The resolution is on one hand comparable with the resolutions of the Lombardy and Swiss DTMs, while on the other hand it is a subsampling of the Piedmont DTM, but it is however acceptable. The output matrix will be composed by 8'000 rows and 14'500 columns for a total of 116 millions nodes. The computation of HD-1 DTM is described in the following paragraphs.

From the analysis described in Section 3.3.1 DirectAndAverage method seems to be the best for the HELI-DEM case. In accordance to the adopted procedure, the first operation is the transformation of the three DTMs from their original reference frame to ETRF2000. After the transformation each DTM is a list of three-dimensional points that have to be interpolated on the output grid. No data values have to be deleted from the datasets. After this operation the number of useful data are 29'287'577, 607'997'593 and 19'400'361 respectively for Lombardy, Piedmont and Switzerland. The total number of useful data is about 650 millions.

The elaboration of the data can be synthetically schematized as the sequence of three main operations:

1. pre-elaboration, to prepare the input data,
2. elaboration, or interpolation of the DTMs to create HD-1,
3. post-elaboration, or correction of possible anomalies and outliers.

4.1.1 Pre-elaboration of the input data

After the reference frame transformation, the 650 millions of data belonging to the three datasets of Lombardy, Piedmont and Switzerland, although almost regularly disposed, are no more gridded and have to be memorized as sparse points. A validation is necessary before using them to create the HD-1 DTM.

The first validation has been performed to verify if some duplicate points, or better points with coincident planimetric coordinates, exist in the datasets. If this occurs, the duplicate points have to be removed. In particular this operation is necessary for Piedmont data, because the 464 grids (files) in which the DTM is originally memorized, present overlaps: unfortunately sometimes nodes with the same planimetric coordinates have different elevation values. These nodes represent inconsistent observations and can cause problems during the interpolation of HD-1 DTM. This set of duplicate points is composed in most cases by a couple of points, but in some cases the coincident points can be also three or four. The implemented approach is to find for each group of N coincident points the maximum and minimum elevation values and to compute their difference; if the difference is greater than 5 meters, the N points are rejected and deleted from the dataset, otherwise the group is substituted by a single point which has the same horizontal coordinates of the N points, while the stored elevation is the mean of their elevations.

The analysis of multiple points has revealed the presence of:

- 8'762'749 couples of coincident points, of which 14'725 have been deleted because their difference exceed 5 m, while the others have been averaged,
- 65'980 terns, including 47 to be eliminated,
- 11'145 quaterns of points, among which 36 have been deleted.

The statistics of the coincident points, included those with differences higher than 5 meters, are reported in Table 4.1. About 103'000 and 15'000 groups present elevation differences that exceed 1 and 5 meters respectively. Thus the anomalous differences with respect to the nominal vertical accuracy of the Piedmont DTM ($\simeq 1$ m) represent the 0.12% of the number of coincident points groups and the 0.015% of the total number of points belonging to the Piedmont dataset.

In Lombardy and Swiss DTMs no overlapping points are present.

4.1.2 Elaboration of input data to create the unified DTM

The three DTMs, converted to the output reference frame, have been independently interpolated on the output final grid. To perform the interpolation and es-

Number of coincident points groups	8'839'874
Mean	0.05 m
Std	0.39 m
Maximum	34.61 m
Minimum	0.00 m

Table 4.1: Statistics of the differences between the maximum and minimum elevations of the groups of coincident points belonging to Piedmont LiDAR DTM with planimetric resolution 5 m.

to estimate the elevations of the nodes of the final grid, the choice has been fallen on the use of a bicubic method, because from the analyses reported in 3.1 a bicubic approach resulted better than a bilinear. Since the number of parameters to be estimated is sixteen, a bicubic interpolation requires a minimum of sixteen observations. As discussed in Section 3.2 the problems of ill conditioning that can occur when the observations are badly distributed around the interpolation node can be in most cases solved increasing the number of observations. The bicubic interpolation is therefore performed using a minimum of 32 observations. Using 32 observations a Least Squares solution is adopted (formulas in Section B.2.1). The 32 nearest points are searched inside a window opened around the interpolation node with a dimension of about 4000 m^2 ($200 \times 200 \text{ m}$): this value allows to have about 100 points for Lombardy and Switzerland and 1600 points for Piedmont.

To verify if the system constructed by the 32 observations is stable, the N matrix of the system is computed and its condition number is evaluated and compared to a threshold equal to 10^5 (that corresponds to the threshold of $10^{2.5}$ adopted for A in case of exact bicubic). Following the LS_{RO} approach described in Section 3.3.2, if the condition number is smaller than the threshold, the elevation is estimated; on the contrary, if the condition number exceeds the threshold, the number of observations is incremented: at each step other 32 nearest points are added to the system and the condition number of the N matrix is again computed. The process ends when one of the two following conditions is verified:

1. the condition number of the N matrix is acceptable,
2. the condition number of the N matrix is still too high, but all the points located inside the window have been added to the system.

In case condition 1 is verified, the elevation of the node is therefore estimated. If condition 2 is verified, the elevation of the node can not be estimated with a good condition of the system, and so a different approach is used. The number of observation is reset to 32 (the 32 nearest points) and a bilinear surface is adopted: this

is like a drastic reduction of parameters by applying the SVD approach discussed in 3.2.

Following this procedure the three datasets have been independently interpolated on the output grid. The statistics of the three interpolated DTMs are summarized in Table 4.2.

		Mean	Std	Max	Min
LOMB.	Number of points	32.0	0.3	96	32
	Condition number	9211	4226	10^5	2300
	Sigma (m)	0.1	0.1	27.7	0.0
PIEDM.	Number of points	32.1	3.2	1392	32
	Condition number	9245	4369	10^5	2313
	Sigma (m)	0.6	0.6	91.2	0.0
SWITZ.	Number of points	32.0	0.2	64	32
	Condition number	7927	3840	10^5	2593
	Sigma (m)	0.6	0.6	23.5	0.0

Table 4.2: Statistics of the results of the individual interpolation of the three low/medium resolution input DTMs on the output HD-1 grid, before the average results operation (total of 22°822'816, 33°746'321, 35°699'169 useful nodes respectively for Lombardy, Piedmont and Switzerland datasets). Number of points: number of points really used to interpolate the elevation of each node. Condition number: condition number of the final system. Sigma: final standard deviation of the interpolated heights by Least squares system.

At the borders of the regions an erosion has been performed. In fact, when interpolating an input DTM on the output nodes located along the DTM border, the interpolation of the node is anyway possible because the observations used to estimate the elevation of the node are searched inside a square window of 4000 m². Therefore it can happens that the interpolation is performed also for the nodes that lie near the border of the input DTM but outside it. In these cases the observations are concentrated only in one side of the window and since their distribution is not homogeneous, the system can result ill-conditioned; with the regularization solutions it can happens that the interpolation is however performed but producing a non optimal solution. The erosion has been performed deleting, for each interpolated DTM, a buffer five cells large.

At this point a unique final unified DTM has to be obtained. To do that the three interpolated and eroded DTMs have been averaged. Therefore each node of the output unified HD-1 grid assumes a value equal to:

- the average of three elevations if all the three interpolated DTMs have useful

values in this node,

- the average of two elevations if only two of the three interpolated DTMs have useful values in this node,
- the value of the elevation assumed by one of the three DTMs, if only this DTM exists in this node,
- no data value if none of the three DTMs exists in this node.

Figure 4.1 shows HD-1 DTM.

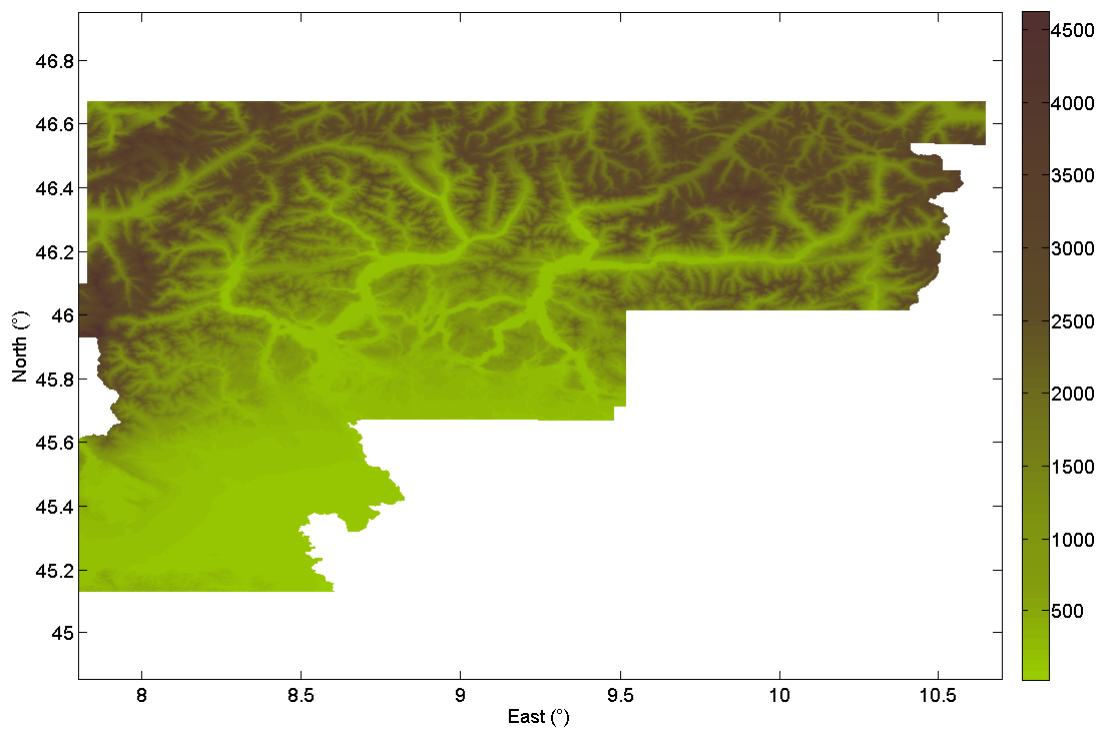


Figure 4.1: Unified HELI-DEM DTM (HD-1) obtained through the merging of Lombardy, Piedmont and Swiss low/medium resolution DTMs.

In total about 72 millions nodes are actually interpolated, the other nodes of the rectangular output grid (8000 x 14500 nodes) are outside the project area and assume no data value.

4.1.3 Post-elaboration of the unified DTM: correction of the nodes belonging to lakes

Points belonging to lakes require a dedicated post elaboration. In some DTMs they are memorized with a constant reference value, while in others the value is variable in space (of the magnitude of few centimeters). In addition the conventional elevation attributed to lakes can be different in the different DTMs. During the creation of HD-1 a reference constant value is set for nodes belonging to the surface of each lake: after the interpolation of the coastlines, this constant value is computed as the minimum elevation among all the coastline points.

The interpolation of points that are near a lake countour have proved to be less reliable, because points belonging to lakes introduce false elevations in the interpolation dataset and therefore in the interpolation estimate itself. For this reason for the major lakes (Como Lake, Maggiore Lake, Lugano Lake, Iseo Lake, Orta Lake) some corrective measures have to be applied. For each lake, a buffer with a width of 100 meters, which extends from the border of the lake to the inland, has been created; then points belonging to this area have been interpolated using only the input points that fall inside the buffer.

4.2 Correction of HD-1 DTM with high resolution PST-A DTM

In the previous section the creation of the unified low resolution HD-1 DTM from the three low resolutions Lombardy, Piedmont and Swiss DTMs, has been in detail described.

In addition to the low resolution elevation data used to create HD-1, also a high resolution LiDAR DTM is available. This DTM has a resolution of 10^{-5} degrees and a vertical accuracy better than 0.5 meters; it covers the stripes corresponding to the valleys of the main river basins of Lombardy and Piedmont (Figure 4.2). It is named PST-A.

Cross-validations and external validations on the available DTMs highlighted the following results: the Lombardy and Piedmont models have almost everywhere accuracies comparable with the nominal ones but some anomalous areas exist, where their differences in elevation are significantly different from those in the PST-A DTM; in these situations, deeper analyses though GNSS surveys confirmed the correctness of the LiDAR data. Clearly, HD-1 is affected by the same anomalies of the input models that have been used to create it. However, HD-1 can be improved using the elevation information contained inside the PST-A DTM, at least where this last is available.

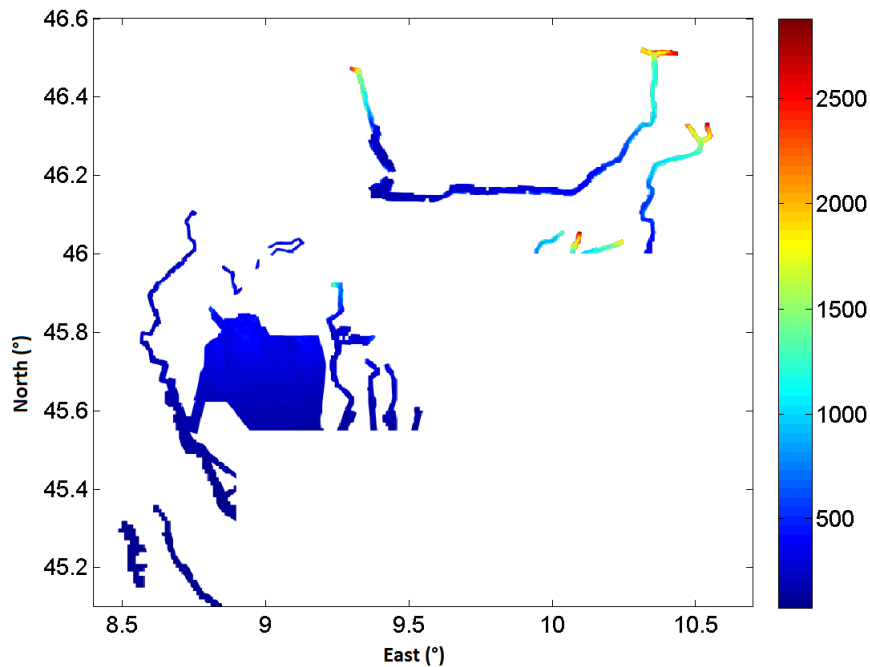


Figure 4.2: PST-A LiDAR DTM: only the portion which is overlapped to HD-1 is shown.

One possible approach can be the correction of HD-1 DTM by the simple substitution of HD-1 values with those of PST-A. This approach is too simple and can introduce problems at the borders of areas covered by PST-A: in fact, when some global biases in elevation or some high punctual differences exist, the simple substitution can introduce discontinuities. An example is shown in Figure 4.3, where a bias of 8 m, with differences at the border up to 4 m, is present. In many spatial analysis operations, the introduction of such artificial biases may be more harmful than smooth errors or biases.

4.2.1 Adopted procedure

In general, the problem is the correction of a low resolution DTM (model that has to be corrected) with a local model with higher resolution and accuracy, avoiding the introduction of jumps at the border between zones in which the correction data are present or not. The problem can be solved simply properly filtering the corrections before their application. The filtering must be studied in order to produce a reasonably smooth model, which at the same time preserves as much as possible the accuracy of the correction. The proposed procedure has been previously calibrated and tested on simulated data and then applied to HELI-DEM data. It is

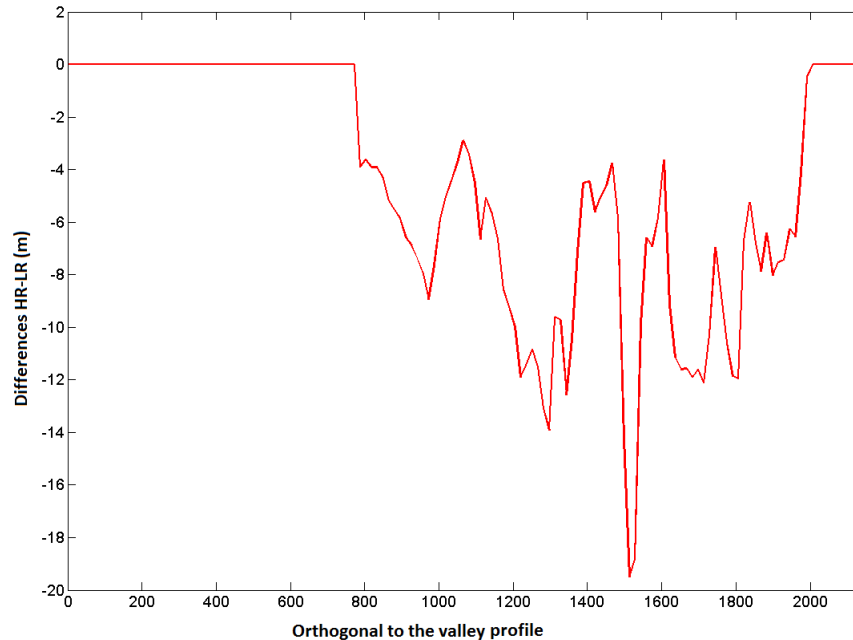


Figure 4.3: Example of discontinuity between PST-A and HD-1 DTMs: Oglio River valley.

however a general methodology that can be shown schematically in the following way:

1. computation of the corrections (differences between high resolution and low resolution DTMs),
2. appropriate filtering of the corrections,
3. application of the filtered corrections to the model that has to be corrected.

Computation of the corrections

Corrections have to be computed on the nodes of the low resolution model; to this purpose the high resolution DTM has to be subsampled on the low resolution nodes, for example by the use of the next nearest node or some properly average operations. The nodes where the high resolution model does not exist assume no data value. Then the matrix containing the differences between high resolution and low resolution elevations has to be computed: differently from what is generally applied in the algebra of matrices, the differences corresponding to no data

value in the first DTM, are set to null. In the following the model of the differences is called “corrections model”.

Filtering of the corrections by low pass filter

A low pass filter allows to smooth the discontinuities where corrections pass from null value to a value different from zero. In fact when a low pass filter is applied to a function, it produces a signal smoother than the original one; this effect is realized by the removal of the highest frequencies that compose the signal. In this particular case discontinuities can be considered as high frequency signals which have to be removed or at least smoothed. The application of a low pass filter can be described as the convolution of a signal with an appropriate mask which, in a bi-dimensional and discrete case, can be seen as a matrix of coefficients, in which i and j represent the distance in the two directions from the filter origin, it means the center of the mask; the sum of all the coefficients must be equal to one and the coefficients are null outside the window in which the filter is defined.

Moving average is the simplest low pass filter, in which the coefficients inside the window have all a constant value. In this case the coefficients go from null value (outside the window) to a constant value inside the window without continuity (Figure 4.4). Once applied, the moving average assigns to the central element the average of the surroundings elements.

$$\frac{1}{9} \begin{bmatrix} 1 & 1 & 1 \\ 1 & 1 & 1 \\ 1 & 1 & 1 \end{bmatrix}$$

Figure 4.4: Example of moving average 3x3 low pass filter matrix.

Others filters, as for example the Butterworth Filter, present a smoother behaviour. The Butterworth Filter is described by the following equation (Biagi and Dermanis, 2002b):

$$f(i, j) = \frac{1}{1 + \left[\frac{i^2 + j^2}{D_0^2} \right]^n} = \frac{1}{1 + \left[\frac{d}{D_0} \right]^{2n}} = f(d) \quad (4.1)$$

where n is the order of the filter and describes the attenuation factor.

The function assumes maximum value in the origin, where $f_{\max} = f(0, 0) = 1$ and is halved at a distance $d = D_0$. The Butterworth Filter is an isotropic filter, that is a filter in which the value $f(i, j) = f(d)$ depends only by the distance

$d = \sqrt{i^2 + j^2}$ from the origin. In Figure 4.5 the matrix of a low pass Butterworth filter with dimension 5x5 is shown.

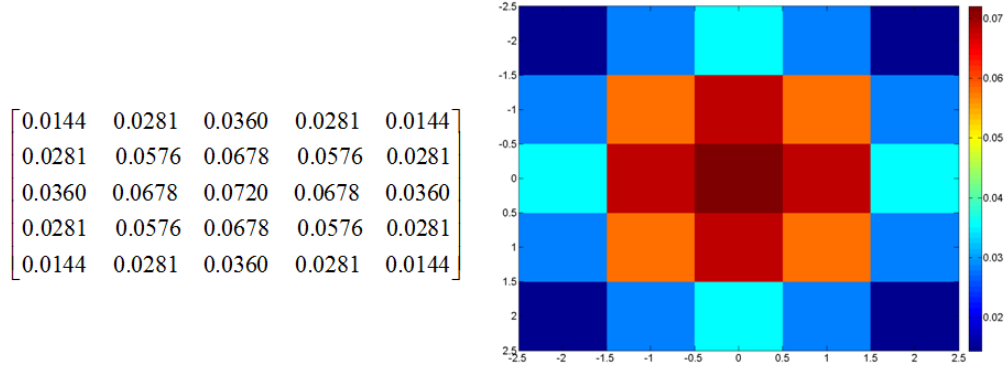


Figure 4.5: Example of low pass Butterworth filter ($D_0 = 2, n = 2$).

The frequencies domain and the Fourier Transform. As said in the previous paragraph, the application of a filter to a signal can be seen as the convolution of the signal with a mask of appropriate coefficients. It is useful to introduce the Fourier Transform and the frequencies domain.

The Fourier Transform of a generic function $f(x)$ is:

$$F(u, v) = \int_{-\infty}^{+\infty} \int_{-\infty}^{+\infty} f(x, y) e^{-i2\pi(ux+vy)} dx dy \quad (4.2)$$

where the linear frequency $u = 1/T$ is used (T is the corresponding period). In case of a $N \times M$ matrix containing values as the matrix that describes a DTM, where data are arranged into a discrete and regular grid (composed by N rows and M columns), it is more useful to give a definition of the Fourier Transform in two dimensions. In this case the Fourier Transform is called DFT (Discrete Fourier Transform) and is expressed as:

$$F_{uv} = \frac{1}{NM} \sum_{n=1}^N \sum_{m=1}^M f_{nm} e^{-i2\pi\left(\frac{un}{N} + \frac{vm}{M}\right)} \quad (4.3)$$

where $u = 1, 2, \dots, N, v = 1, 2, \dots, M$; its inverse (IDFT - Inverse Discrete Fourier Transform) is given by:

$$f_{nm} = \sum_{u=1}^N \sum_{v=1}^M F_{uv} e^{i2\pi\left(\frac{un}{N} + \frac{vm}{M}\right)} \quad (4.4)$$

Matrices F_{uv} and f_{nm} are in exact relation one to the other: if the DFT is used to compute F_{uv} , so the application of the IDFT will reproduce exactly the input f_{nm} . The coefficients for the development of the discrete Fourier Transform F_{uv} are complex numbers $F_{uv} = F_{uv}^R + iF_{uv}^I$, where F_{uv}^R represents the real part and F_{uv}^I is the imaginary part; these numbers can be represented also in polar form:

$$F_{uv} = F_{uv}^R + iF_{uv}^I = |F_{uv}| (\cos \Phi_{uv} + i \sin \Phi_{uv}) = |F_{uv}| e^{i\Phi_{uv}} \quad (4.5)$$

where $|F_{uv}| = \sqrt{(F_{uv}^R)^2 + (F_{uv}^I)^2}$ is the *amplitude* or *spectrum* and $\Phi_{uv} = \arctan \frac{F_{uv}^I}{F_{uv}^R}$ is the *phase*. The DFT of a matrix produces two matrices with the same dimension, F_{uv}^R and F_{uv}^I or $|F_{uv}|$ and Φ_{uv} . The coefficients F_{uv}^R and F_{uv}^I are not independent: in fact, from the following relations:

$$\cos \left[2\pi \left(\frac{un}{N} + \frac{vm}{M} \right) \right] = \cos \left[2\pi \left(\frac{(N-u)n}{N} + \frac{(M-v)m}{M} \right) \right] \quad (4.6)$$

$$\sin \left[2\pi \left(\frac{un}{N} + \frac{vm}{M} \right) \right] = -\sin \left[2\pi \left(\frac{(N-u)n}{N} + \frac{(M-v)m}{M} \right) \right] \quad (4.7)$$

it follows that:

$$\begin{aligned} F_{uv}^R &= F_{N-u, M-v}^R & F_{uv}^I &= -F_{N-u, M-v}^I \\ |F_{u,v}| &= |F_{N-u, M-v}| & \Phi_{u,v} &= -\Phi_{N-u, M-v} \end{aligned} \quad (4.8)$$

The first two relations should be combined in a complex form:

$$F_{uv} = F_{N-u, M-v}^* \quad (4.9)$$

where $z^* = a - ib$ is the conjugate of the complex number $z = a + ib$. This means that it is not necessary to compute all the coefficients F_{uv}^R , F_{uv}^I , but only half of them.

Let's consider the convolution in discrete bi-dimensional case between two matrices f_{ij} and h_{ij} , where h_{ij} is the matrix that contains the signal to be filtered while f_{ij} is the filter. The result of their convolution is the matrix g_{ij} :

$$g_{ij} = h_{ij} * f_{ij} \quad (4.10)$$

Switching to the frequency domain, for the convolution theorem applied to discrete case:

$$g_{ij} = h_{ij} * f_{ij} \Rightarrow H_{uv} \cdot F_{uv} \quad (4.11)$$

where G_{uv} and F_{uv} are the discrete Fourier Transform of the input matrix and filter respectively.

The discrete convolution theorem can be systematized as shown in Figure 4.6

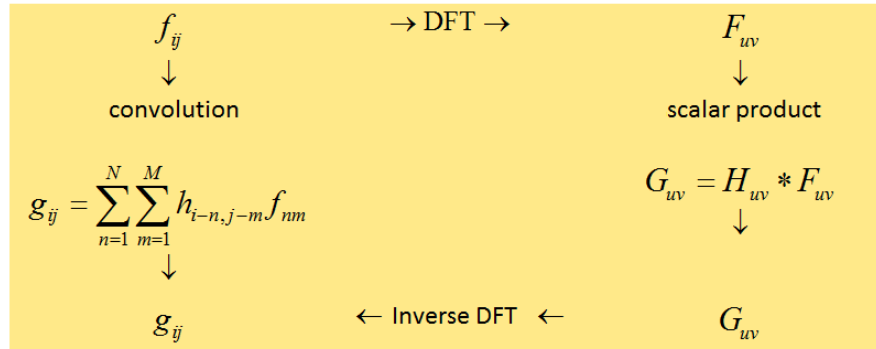


Figure 4.6: Fourier Transform: convolution and relations in the space and frequency domain.

From the computational points of view, a DFT is an onerous operation; the Fast Fourier Transform allows to exploit the recursive characteristics of the function (Brigham, 1988). For example in a bi-dimensional case with $n \times n$ dimensions, it allows the reduction of the number of operations from n^4 to $n^2 \log_2(n)$: if $n = 1000$ the number of operations decreases from 10^{12} to 10^7 .

The filtering in frequency of the differences HR-LR. The Butterworth filter seems to provide a good solution for the filtering problem. This filter indeed gives more weight to information of the central node of the window and decreases with continuity. In this case study matrices are big: in fact HD-1 and so also the matrix containing its differences with PST-A are composed by 116 millions cells. A methodology for the computation of the convolution between the corrections matrix and the filter is represented by the application of the discrete convolution theorem, it means trough the concatenated implementation of two FFTs, a scalar product between the two FFTs and finally an inverse FFT. Summarizing:

1. computation of the model of corrections,
2. construction of the Butterworth Filter,
3. computation of the FFTs of both corrections and filter,
4. product of the two FFTs,

5. Inverse FFT (IFFT) of the product for the reconstruction of the filtered corrections.

Calibration and recursive application of the filter. To study the behaviour of the Butterworth Filter first of all the filtering procedure has been applied on simulated models, in order to empirically calibrate both the filter parameters and its application modalities.

A simulated model has been created on a grid with row and column indexes (x and y directions) that go from 0 to 100 and with a cellsize equal to 1 ($N = M = 101$). Also a matrix containing simulated corrections already subsampled on the nodes of the previous grid has been constructed: this model occupies only the central part of the grid (cells from 40 to 60 contain valid values in both directions); the corrections are set all to a constant difference equal to 3 meters (Figure 4.7(a)). A discontinuity of 3 meters at the borders of the corrections is present. At the beginning a Butterworth filter with the following characteristics $D_0 = 2, n = 2, N = M = 5$ has been generated. The results of the application of the filter on the simulated corrections is reported in Figure 4.7(b): the discontinuity at the border remains too abrupt even after the filtering. Smoother results can be obtained increasing the filter dimension but this can cause a significant loss of information in the corrections (Figure 4.7(c)). Another solution to smooth the results is to apply again the filter to the corrections already filtered with the first iteration: in this case the discontinuity is smoothed but some information is missing (Figure 4.7(d)). In addition the filter should act preferably outside the corrections model, in order to smooth any discontinuities, but leave unchanged the corrections. Alternatively, the filter can be applied iteratively: at each iteration the original corrections different from zero replace the filtered corrections (Figure 4.7(e) and 4.7(f)). In this way the filter acts preferably in the area outside the corrections, smoothing the transition and preserving the corrections. The approach of filtering - substitution - filtering can be iterated any desired number of times, to properly smooth the discontinuities: the resultant effect is shown in Figure 4.8, where on the same graph the results of five consequently iterations are reported.

Note a final technical aspect. For the last iteration it has been chosen to leave the filtered corrections also inside the area covered by the model, rather than replace them again with the original values. In fact, some analyses on the slopes distribution of the real HELI-DEM case have shown that PST-A, even when subsampled, presents a roughness greater than HD-1. The choice of the use of filtered corrections at the last iteration avoids to produce a final DTM affected by morphometric inhomogeneities. The adopted procedure is schematized in the flow chart reported in Figure 4.9.

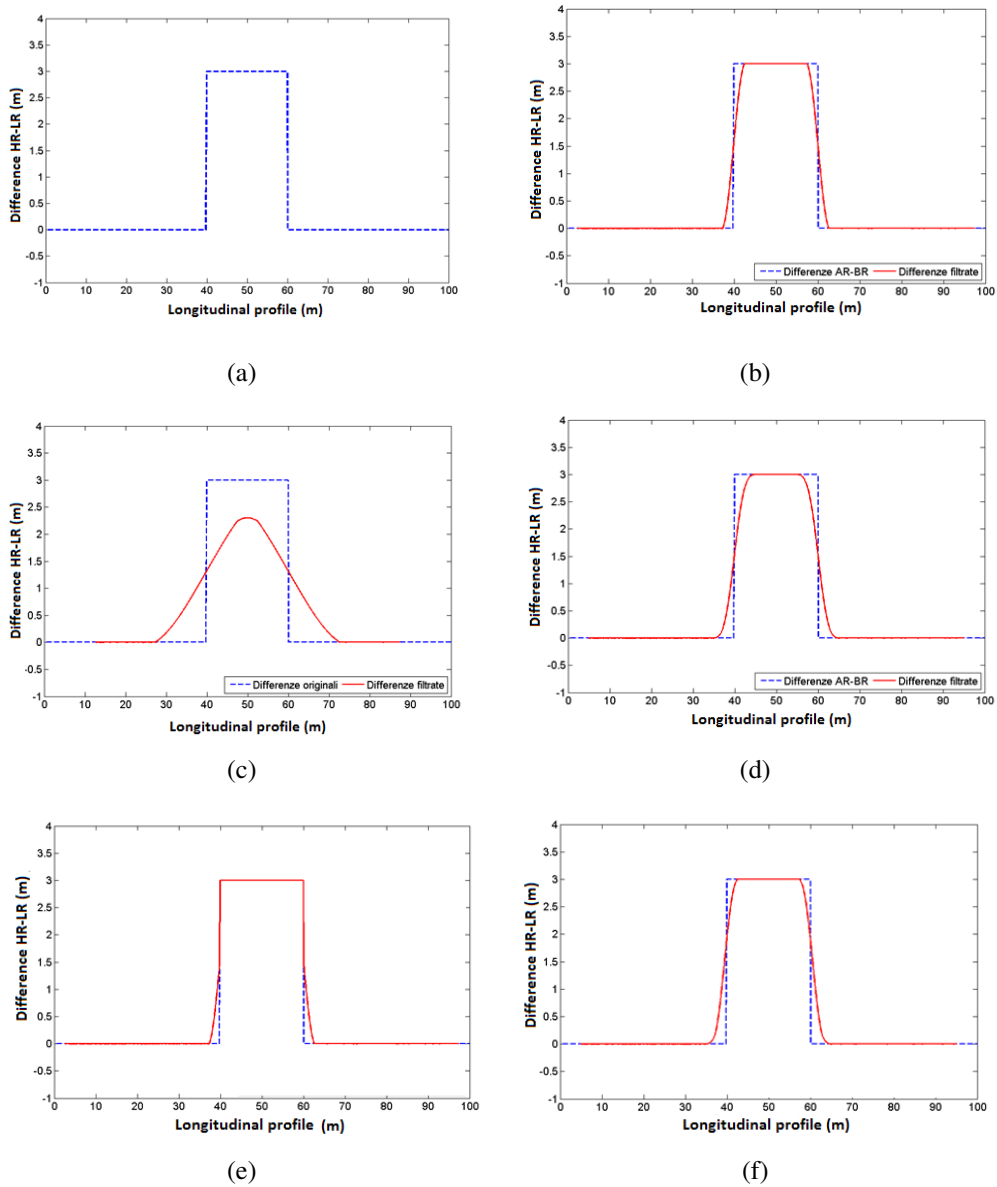


Figure 4.7: Application of Butterworth filter on simulated data. Simulated data (a). Application of Butterworth filter $D_0 = 2, n = 2, N = M = 5$ one time (b). Application of Butterworth filter $D_0 = 20, n = 2, N = M = 51$ one time (c). Application of Butterworth filter two times $D_0 = 2, n = 2, N = M = 5$ (d). Corrections filtered at the first iteration and consequent substitution of the original corrections (e) - the red line represents the input dataset for second iteration - and result of the second iteration (f).

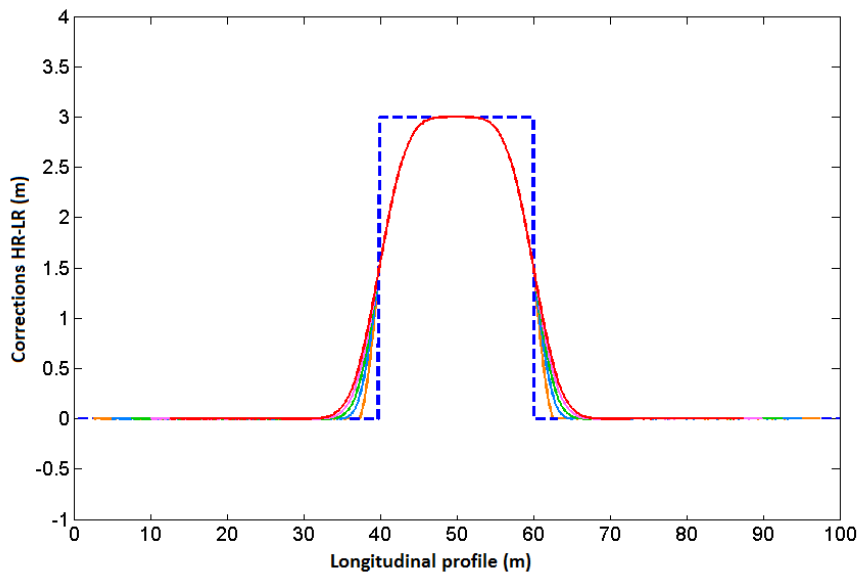


Figure 4.8: Filtered corrections after 5 iterations of filtering - substitution - filtering. Different colour lines represent the different iteration steps; at last iteration (red line) the substitution is not performed.

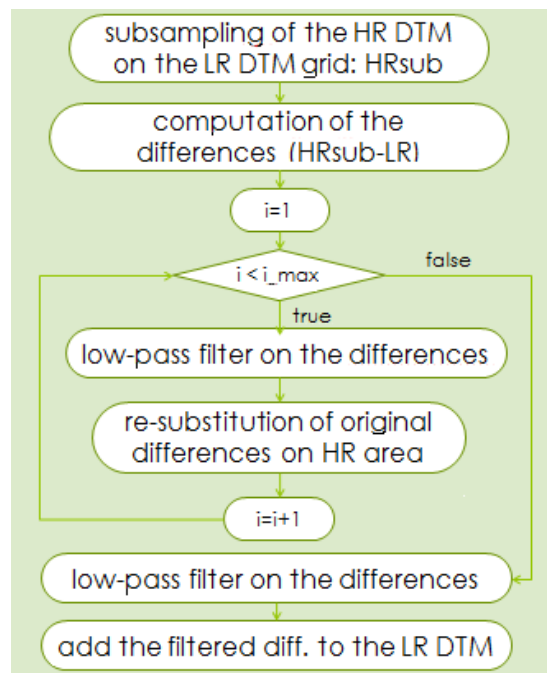


Figure 4.9: Flow chart of the corrections filtering procedure.

4.2.2 Application of the adopted procedure to HD-1 DTM

The procedure described in the previous paragraphs has been applied to produce the final HELI-DEM DTM. First of all the corrections model has been created, computing the differences (Figure 4.10 on the left) between the subsampled PST-A LiDAR DTM and the HD-1 DTM; a Butterworth filter with five iterations has been applied to the corrections. The filtered corrections have been then applied to HD-1: this corrected DTM will be called in the following HD-2. To visually analyse the benefits of using an iterative filter, firstly the results related to an area localized in the basin of Oglio River (Figure 4.10 on the right) have been analysed. In addition, from this area a cross section has been extracted to evaluate in detail the effect of the adopted procedure: in Figure 4.11 the original and the filtered corrections are represented. As can be seen, the final filtered corrections follow the trend of the original ones reducing high frequencies.

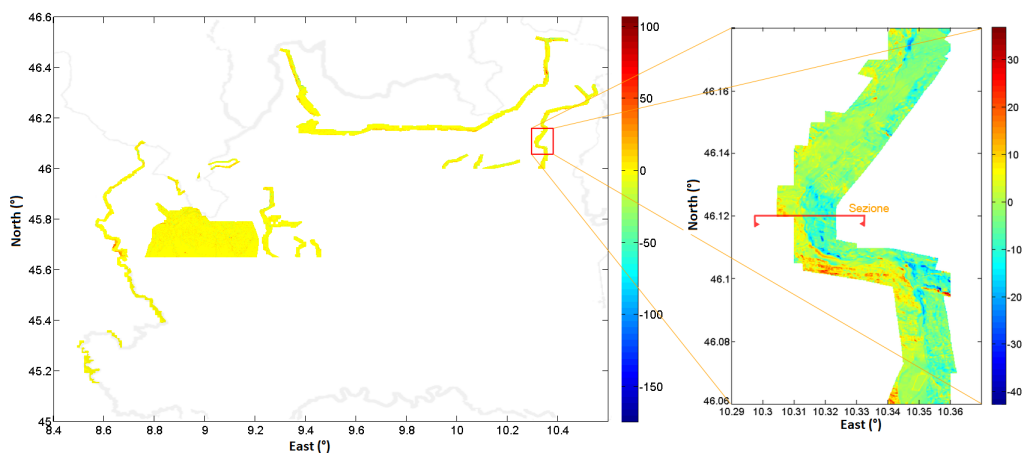


Figure 4.10: Differences between PST-A LiDAR DTM and HD-1 DTMs (on the left) and georeferencing of Oglio River section used as case study to test the behaviour of the adopted filtering procedure (on the right): differences values in meters.

In order to visualize the effect of the filter in a three dimensions, in Figure 4.12 the differences between PST-A and HD-1 DTMs inside Oglio River valley area are shown, before and after the application of the filter: particularly, the clear effect of the filtering at the border of the PST-A DTM is evident. For the same Valley, in Table 4.3 the statistics of the differences before and after the application of the correction are summarized: the bias is removed and the standard deviation is significantly reduced. The small residual differences are due to the fact that in the last iteration the filtered corrections are used instead of the original ones. Also the statistics of the differences for the global project area has been computed and are reported in Table 4.4. In this case the improvement given by the correction

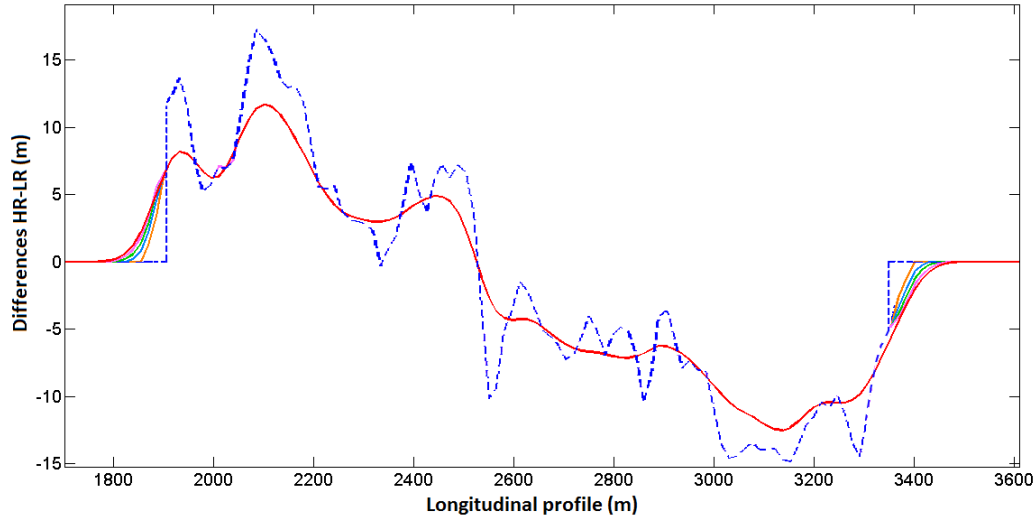


Figure 4.11: Profile of the differences between PST-A and HD-1 DTMs of Oglio River section: original corrections in blue, filtered corrections correspondent to the different iterations represented by the coloured lines.

	bias (m)	std (m)	max (m)	min (m)
PST-A - HD-1 (original)	-1.9	5.8	36.7	-42.7
PST-A - HD-2	0.0	1.1	23.1	-22.5

Table 4.3: Statistics of the differences between PST-A LiDAR DTM and HD-1 DTM (before the correction)/HD-2 DTM (corrected DTM): Oglio River area.

is even more evident: these results, that can be considered as internal validation, are satisfactory.

	bias (m)	std (m)	max (m)	min (m)
PST-A - HD-1 (original)	0.3	6.0	186.8	-174.6
PST-A - HD-2 (corrected)	0.0	0.4	108.4	-97.4

Table 4.4: Statistics of the differences between PST-A LiDAR DTM and HD-1 DTM (before the correction)/HD-2 DTM (corrected DTM): global HELI-DEM area.

4.2.2.1 Validation of the corrected DTM with RTK measures

The internal validation of the HD-2 DTM, i.e. its comparison with the PST-A DTM, gives very satisfactory results; for its external validation the RTK measures

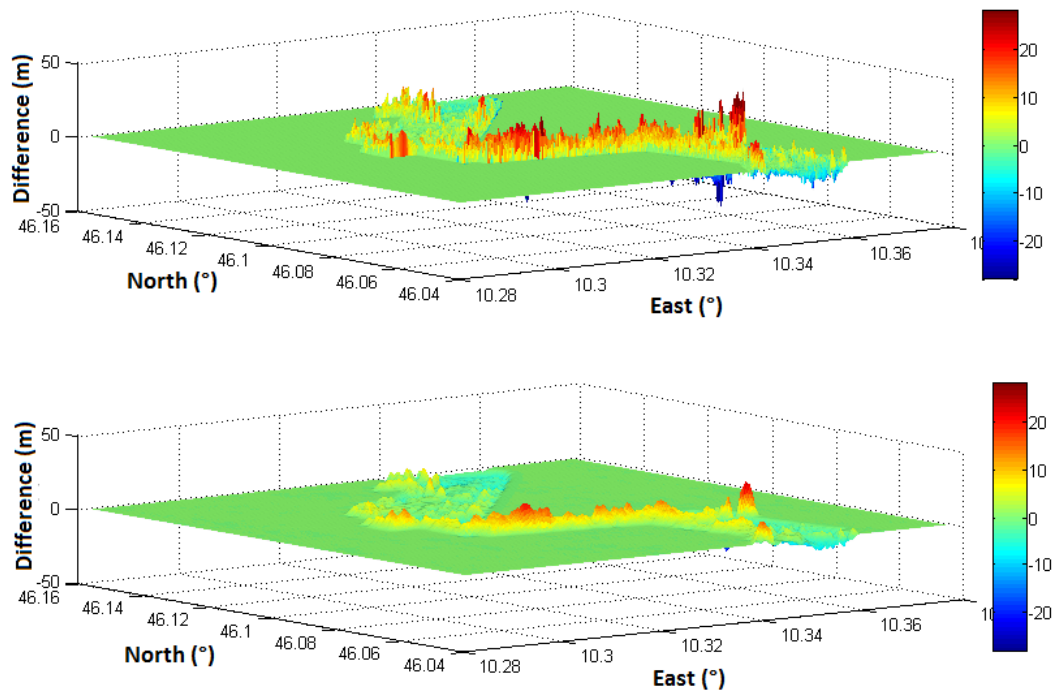


Figure 4.12: Differences between PST-A and HD-1 DTMs of the Oglio River Valley: original corrections above and filtered corrections below.

already collected in the Valtellina area (Adda River Valley) and described in Section 2.4.2 have been used. This analysis is useful to evaluate if the correction actually leads to an improvement of the final product. The elevations of the GPS points (943 points in total) of all the areas have been collected and merged into a unique dataset. Then HD-1, the subsampled PST-A and HD-2 have been interpolated through bicubic interpolation on the GPS points. In all the three cases the differences between the models and the GPS elevations have been computed.

	bias (m)	std (m)	max (m)	min (m)
HD-1 - RTK	3.4	5.5	24.2	0.0
PST-A - RTK	-0.3	1.0	7.2	0.0
HD-2 - RTK	-0.4	1.7	8.8	0.0

Table 4.5: Statistics of the modulus of the differences between HD-1, PST-A and HD-2 DTMs and RTK points (Valtellina area).

Table 4.5 summarizes the statistics for the three comparisons. The statistics of the comparison between PST-A LiDAR and RTK are significantly worse with respect to those reported in Tables 2.22 and 2.23 which were related always to the

comparison of the LiDAR DTM and RTK measures: in this case the LiDAR DTM is subsampled to $2 \cdot 10^{-4}$ degrees ($\simeq 20$ meters), while the original cellsize of the DTM is 10^{-5} degrees ($\simeq 1m$). In any case, they are, as expected, much better than those of HD-1. The statistics also demonstrate the reliability of the applied correction: the mean and standard deviation of the differences between HD-2 and RTK are better than those of HD-1 and are more similar to those of PST-A. The residual differences are due to the last application of the filter in which the original LiDAR data are not substituted.

4.3 Creation of the HELI-DEM geoserver to publish the input and final elevation data

The data collected for HELI-DEM project and the final products (the two DTMs HD-1 and HD-2) have to be made accessible to the community, using appropriate methods of publication of geographic data. The publication of geographic data is performed through the implementation of a geoserver (geoweb service), that is a web service oriented to the distribution of geographic data (Peng and Tsou, 2003). The realization of a geoserver allows to realize a decoupling between the data provider and the user: the server publicly displays to the client its functionalities, through the use of standard interfaces. These interfaces are independent (hence the decoupling) from the implementation. In the following the concept of geoservice and its standards are described and then also the choices made to generate the structure of the HELI-DEM geoserver.

To achieve a high level of accessibility to the data and thus to facilitate the fruition it is appropriate to move towards a distribution that occurs following standard procedures. In the context of the sharing and distribution of geographic referenced data, the Open Geospatial Consortium (OGC¹) is an important actor for which concerns the definition of standard procedures. OGC is an international consortium with more than 400 members, belonging to different skills: private societies (multinational as for example ESRI, Autodesk or Oracle, but also small societies, as for example OpenGEO which deals with the development of GeoServer or Camptocamp involved in the development of open source software such as OpenLayers), government agencies (NASA, USGS) and universities (Politecnico di Milano and La Sapienza Università di Roma in Italy). OGC aims to participate to the development of standard interfaces called OGC Web Service (OWS) which goal is to support interoperable solutions for the exchange of geographic data. In that way, using OGC standards, it is possible to provide data and services independently from the operating system, from the GIS software and

¹OGC - <http://www.opengeospatial.org/>

from the user configurations.

In Figure 4.13 the basic functioning scheme of a OWS service is shown: the client sends a standard request to the server; accordingly, the server accesses data, processes them, and sends the response to the client. Different types of requests exist, according to the OWS implemented service. In any case some basic elements are common: a GetCapabilities operation, to which the server answers with a list of processes or available data, a Describe request, to which the server answers with the description of a particular dataset or process, and finally a GetData or GetService, to which the server answers implementing a certain process or providing the required data. In this case the WCS, WFS and WMS standards have been taken into consideration, because they are directly implemented in the geoservice.

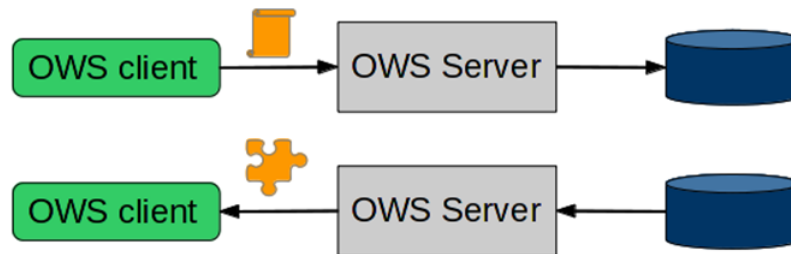


Figure 4.13: Basic functioning schema of a OWS service.

WCS (Web Coverage Service²) standard defines an interface to provide raster data. This standard provides the following three types of requests:

- GetCapabilities: request made by the client to the server in order to have the description of the server properties in terms of metadata relating to the service (service name, manager, contacts, etc.) and the list of the published data,
- DescribeCoverage: the name of a certain layer published by the server is specified and its proprieties (geographic extension, original reference frame, other reference frames in which the dataset is available, the supported output formats) are obtained,
- GetCoverage: this operation is required by the dataset; the client specifies how he wants to get the dataset, in accordance with the characteristics of the service offered by the server, indicating for example the resolution, the output format, the extension of the area of interest, the reference frame.

²<http://www.opengeospatial.org/standards/wcs>

WFS (Web Feature Service³) standard defines an interface to provide vectorial data. WFS provides the following standard requests (the first three are features of the basic version of WFS):

- **GetCapabilities:** to obtain a description of the server proprieties in terms of general data regarding the service,
- **DescribeFeatureType:** returns the description of the characteristics of a certain vectorial layer (feature) provided by the service,
- **GetFeature:** here the name of the feature which has to be obtained and some additional parameters are specified (reference frame, geographic extension, attributes list, etc.),
- **LockFeature:** provides a locking mechanism for a feature in order to ensure consistency during editing operations, preventing simultaneous requests for modification by multiple clients,
- **Transaction:** this request allows to create, modify and delete the elements of a feature published by a WFS server (a WFS server that supports transactions is called Transactional WFS).

New functionalities have been introduced with the new 2.2.0 version of the standard:

- **GetPropertyValue:** allows to query the WFS server by specifying the value of a property of the feature,
- **GetFeatureWithLock:** same operation of the **GetFeature**, but in this case the requested features are locked even if their modification operation has not yet been started (transaction),
- **CreateStoredQuery:** creates a query and saves it on the server making it available for future uses,
- **DropStoredQuery:** deletes a query saved on the server,
- **ListStoredQueries:** gives a list of the queries saved on the server,
- **DescribeStoredQueries:** gives a description of the queries saved on the server.

³<http://www.opengeospatial.org/standards/wfs>

In output, a WFS service can make available the data according to different formats, such as GML2, GML3, shape files, GeoJSON.

WMS (Web Map Service⁴) defines an interface to provide raster data as in case of WCS. In this case the output dataset is an image and the numeric matrix of the data is not given. The possible requests to the WMS are:

- GetCapabilities: to obtain the description of the server properties in terms of general information,
- GetMap: with this operation the client makes a request, specifying the raster layer he wants to obtain, the interest geographic extension, the reference frame, the resolution and the output format,
- GetFeatureInfo: this operation allows to query the specified raster: specifying the coordinates of the point of interest the value of the raster in that point can be obtained,
- GetLegendGraphic: this operation requires to the server the generation of an image which illustrates the graphic legend of the raster.

To implement the HELI-DEM geoserver, Geoserver⁵ program has been used. Geoserver is a multi-platform program, written in Java language, which allows to elaborate, visualize and share geographic geo-referenced data (Brovelli et al., 2011) at local level or in a distributed context using the standard published by the OGC. GeoServer is an Open Source project which relies on a large community of developers distributed around the world; it implements WMS (1.1.1 and 1.3 versions), WFS (1.0 and 1.1 versions), Transactional WFS (it allows to perform a vectorial editing on the published data), WCS (1.0 and 1.1 versions) and WPS (1.0 version). Regarding input data, Geoserver provides support for accessing spatial data from databases (PostgreSQL/PostGIS, ArcSDE, DB2 e Oracle) and through GDAL⁶ libraries allows to access to the main raster formats (TIFF, bigTIFF, geoTIFF, Arc/Info ASCII Grid, GRASS raster, PNG, GIF and many others). The output data can have different formats: JPEG, GIF, PNG, PDF, SVG, KML, GeorSS, shape file. Furthermore Geoserver allows to instantaneously re-project the data published on WMS and WFS services using the EPSG⁷ internal database which supports hundred of different reference frames. The Geoserver software has been selected and installed on a server which is physically located in

⁴<http://www.opengeospatial.org/standards/wms>

⁵<http://geoserver.org/>

⁶<http://www.gdal.org/>

⁷<http://www.epsg.org/>

the Geomatics Laboratory of Como Campus of Politecnico di Milano. The produced DTMs, HD-1 and HD-2, have been loaded and are available on the HELI-DEM geoserver. The access to the geoserver is free but not interactive. The users can access to these data and interact with them only through a cartographic geoportal expressly created by SUPSI, the Swiss partner in the HELI-DEM project. The geoportal offers to users some of the most commonly used features in terrain analysis: extraction of a portion of data, coordinates conversion, computation of contour lines for predefined elevations, profiles extraction, identification and morphometric characterization of basins. This part is not discussed here but is described in detail in (Cannata et al., 2013).

Chapter 5

Inverse approach to interpolate the final HD DTM

The HELI-DEM unified DTM has been created following the Direct method described in Section 4.1, where the three different medium and low resolution available DTMs have been firstly transformed to the reference frame of the final output grid, then they have been independently interpolated and finally averaged in the overlap areas. The Direct approach has proved several numerical problems that have been overcome by numerical regularizations. However, these problems can be completely bypassed by another approach that has been studied at the conclusion of the project.

In the following paragraphs the alternative method will be described; it will be tested using the HELI-DEM data and the output DTM will be cross-checked with the input data.

5.1 Description and implementation of the Inverse method

As already briefly explained in Section 3.3, the main difference between Direct and Inverse methods is the way in which the input DTMs are interpolated on the output grid. In particular in the former the input DTMs are transformed from their original reference frames to the reference frame of the output grid; then each transformed DTM is interpolated on the output grid and at the end the output DTMs are averaged in the overlap areas. HD-1 has been obtained following this procedure. The Inverse procedure is similar to the first one for the operations that are done: reference frame transformation, interpolation and merging through average. However, instead of the transformation of the input DTMs from their reference frames to the reference frame of the output grid, the opposite occurs:

the output horizontal coordinates of the nodes of the final grid, defined in the output reference frame, are back-transformed to the original reference frame of each input DTM. Each input DTM is therefore interpolated on the back-transformed horizontal coordinates of the output nodes. Since the input DTMs are gridded in their original reference frame, a bicubic interpolation is always possible: it is fully described in Section B.1.3.1. If at least one of the sixteen points has nodata value, nodata value is assigned to the interpolation output node. Therefore nodata is assigned to all the nodes that fall on the border of the input DTM. For the merging in the overlap areas, different methods can be implemented. At present, the simple average is computed. At this point for each input DTM a dataset containing the 3D coordinates (horizontal coordinates in the input reference frame and interpolated elevation) of all the output nodes is available. The dataset has then to be transformed again to the output reference frame; this can be done simply assigning each interpolated elevation to its node of the output grid; obviously this requires that the indexes of the positions of the nodes on the output grid have been previously saved. In this way for each node of the output grid located in the position (i, j) the following data are available: the horizontal coordinates and N interpolated elevations $[z_{ij,1} \dots z_{ij,N}]$, where N is the number of input DTMs to be merged. Considering that the values $z_{ij,1}, \dots, z_{ij,N}$ can assume a real value or a nodata value, the average is computed in this way:

$$\bar{z}_{ij} = \frac{z_{ij,1} + \dots + z_{ij,n}}{n}$$

where n is the number of valid elevations (real values). Two possibilities exist:

- if $n = 0$, nodata value is assigned to the output node,
- if $n \leq N$, the result is the simple average of the n real values.

The main advantage of using the Inverse approach with respect to the Direct one is that the interpolation on the output grid is performed from gridded data. For each output node, the sixteen nearest points are by definition well distributed in a square around it and no problems of ill-conditioning due to a bad distribution of the points exist. Therefore the estimation of the elevation through the system constructed with the sixteen points is well conditioned and it is not necessary to stabilize the system through the solutions described in the previous Chapter. Another advantage is that in this case it is not necessary to apply, at the end of the interpolation on the output grid, an erosion of the resultant elevation matrix. With this method, since the interpolation is performed only where sixteen input nodes are found, the interpolation is not possible on the border and outside the input data. In addition the research of the nearest points is much faster than in the Direct approach, because they are distributed on a regular grid and the search can be performed by simple indexing on rows and columns.

5.2 Application of the method to the HELI-DEM case study

The Inverse method has been implemented and tested on the HELI-DEM data. The idea is to produce a DTM with the same characteristics of HD-1 (Section 4.1): for simplification it will be called in the following HD-1b. The nodes of HD-1b coincide with those of HD-1. It has been decided to produce it by unifying the three low resolution DTMs of Lombardy, Piedmont and Switzerland. Differently from HD-1 where the Piedmont LiDAR DTM was used, in this case for Piedmont the choice has fallen on the regional DTM with a planimetric resolution of 50 meters. The first reason of this decision is the fact that the Piedmont regional DTM does not seem affected by significant biases or errors, while the LiDAR Piedmont DTM with 5 meters horizontal resolution has some problems as for example the overlapping but not consistent nodes. Moreover, for this thesis a first verification result is necessary: since the regional dataset is smaller than the LiDAR one, the computation time to process it should be reduced. The routines useful to perform the inverse approach have been implemented in MATLAB environment. The output grid has been converted from ETRF2000 to the three input reference frames, and each one of the three input DTMs has been interpolated on the grid nodes (Figures 5.1, 5.2, 5.3).

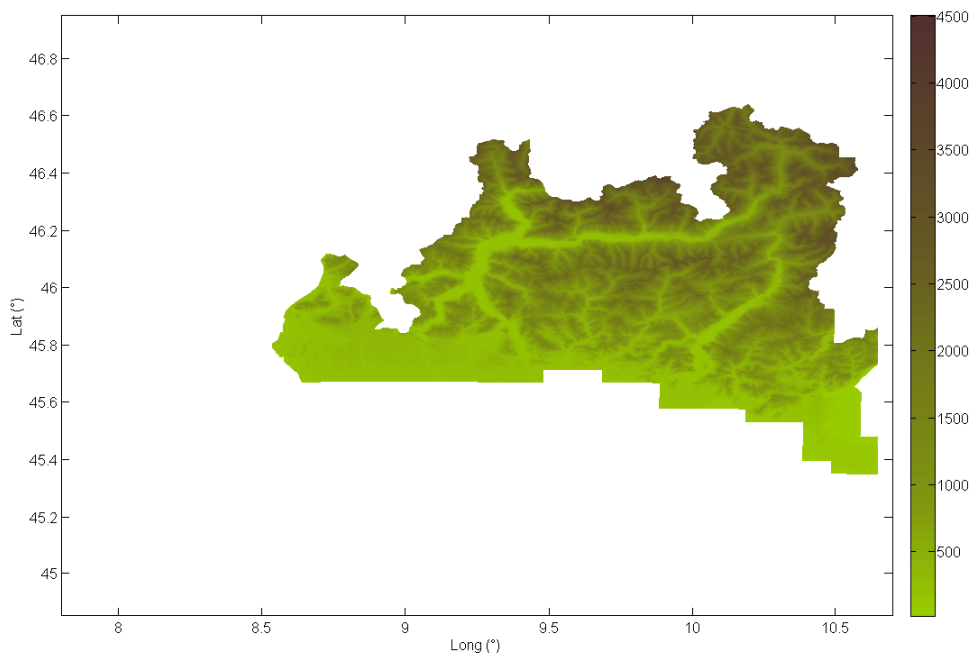


Figure 5.1: Result of the interpolation of the Lombardy DTM on the output HD-1b grid.

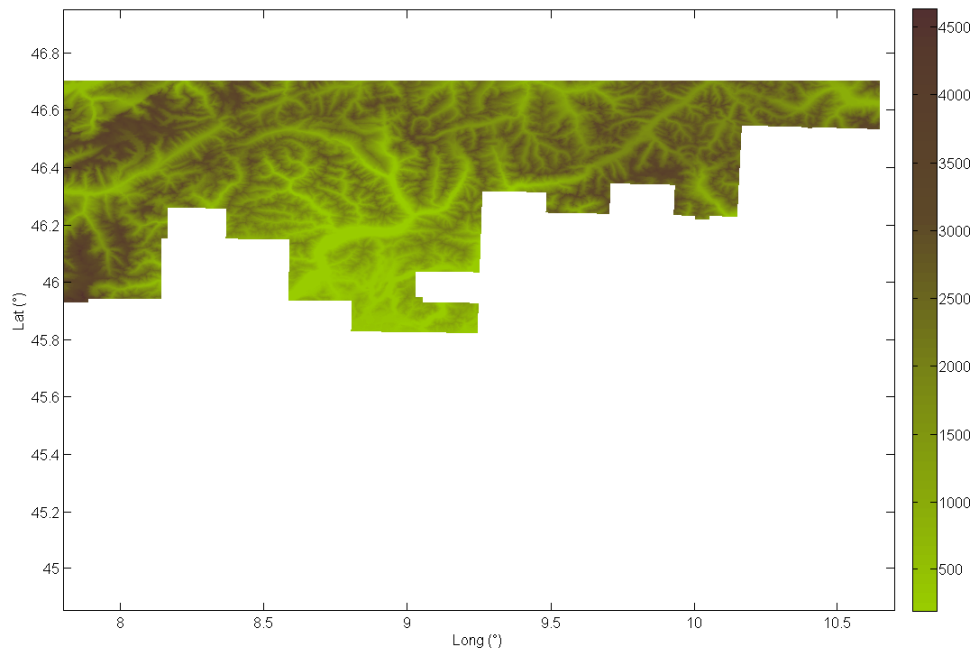


Figure 5.2: Result of the interpolation of the Swiss DTM on the output HD-1b grid.

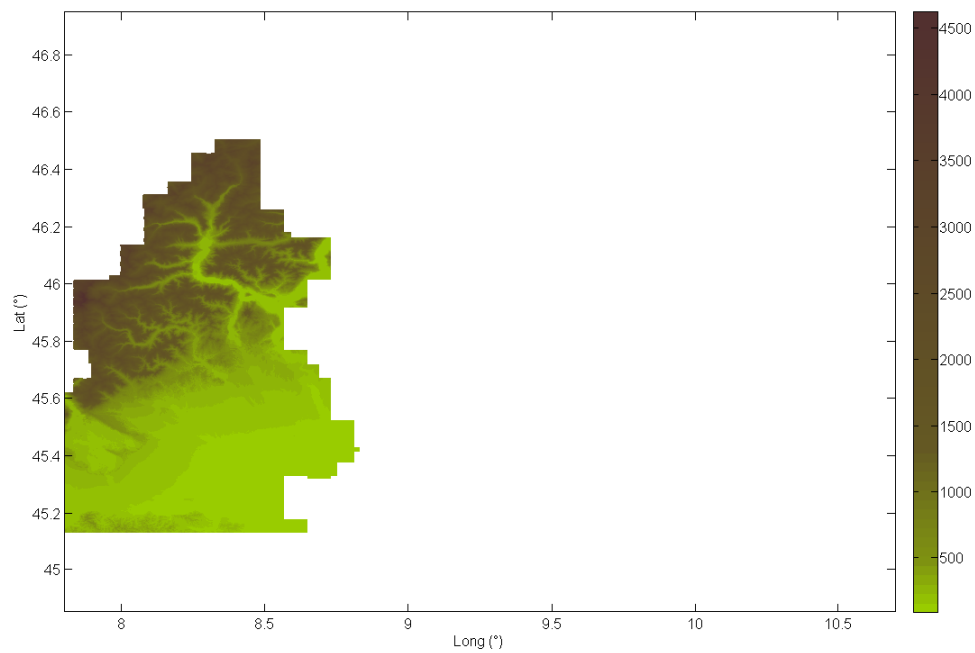


Figure 5.3: Result of the interpolation of the Piedmont DTM on the output HD-1b grid.

Some statistics have been computed on the three interpolated DTMs. In particular they have been compared considering the different couples of them. In Table 5.1 the differences between the two interpolated DTMs of Lombardy and Switzerland are summarized.

Statistics of elevation differences (m) Switzerland-Lombardy	
Number of useful nodes	67'850'049
Bias	-0.2
Std	18.6
Maximum	377.2
Minimum	-283.5

Table 5.1: Statistics of the differences obtained by individual interpolation of the Swiss and Lombardy DTMs on the HD-1b output grid.

Obviously the valid values are located only in the overlap areas. The differences are acceptable with respect to the nominal accuracies of the DTMs: the statistics are very similar to those obtained from the comparison between the two original Swiss and Lombardy DTMs, summarized in Table 2.8. The distribution of the differences is shown in Figure 5.4.

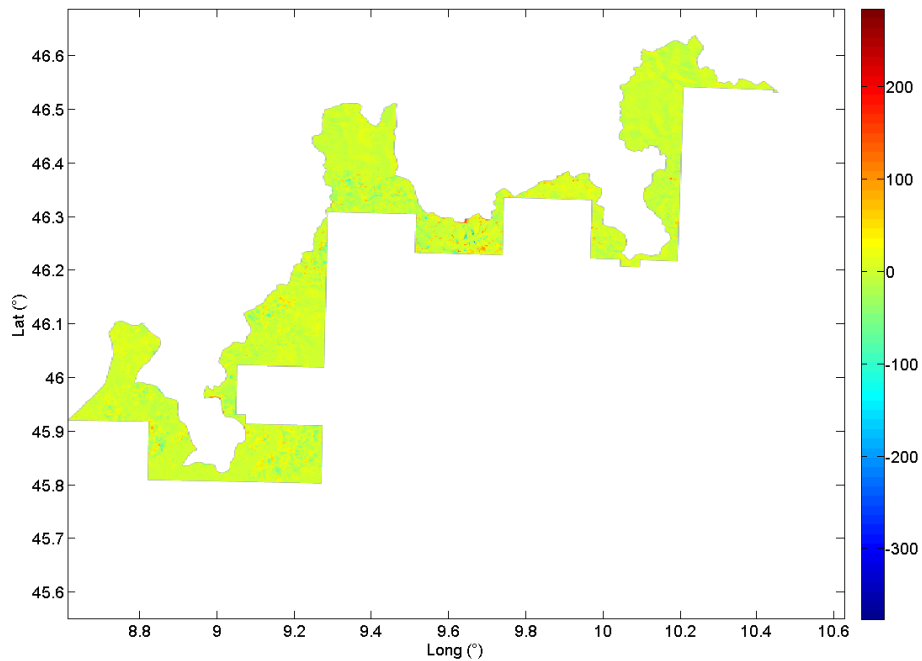


Figure 5.4: Differences obtained by individual interpolation of the Swiss and Lombardy DTMs on the HD-1b output grid.

The anomalous differences are located in the same anomalous areas relevant to the comparisons between the two original datasets. In the same way in Table 5.2 and Figure 5.5 the statistics and the distribution of the differences obtained by individual interpolation of the Lombardy and Piedmont DTMs on the HD-1b grid are reported.

Statistics of elevation differences (m) Lombardy-Piedmont	
Number of useful nodes	265'047
Bias	1.6
Std	5.1
Maximum	45.4
Minimum	-104.1

Table 5.2: Statistics of the differences obtained by individual interpolation of the Lombardy and Piedmont DTMs on the HD-1b output grid.

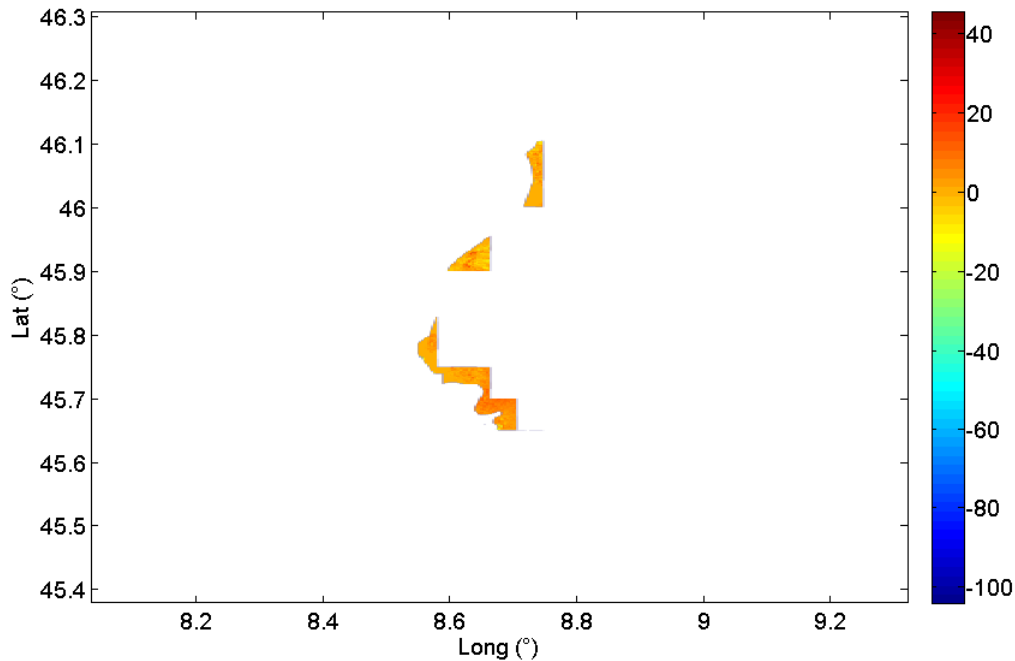


Figure 5.5: Differences obtained by individual interpolation of the Lombardy and Piedmont DTMs on the HD-1b output grid.

In Table 5.3 and Figure 5.6 the results for Swiss and Piedmont DTMs comparison are summarized.

Statistics of elevation differences (m) Switzerland-Piedmont	
Number of useful nodes	4'377'023
Bias	1.1
Std	20.1
Maximum	321.6
Minimum	-268.2

Table 5.3: Statistics of the differences obtained by individual interpolation of the Swiss and Piedmont DTMs on the HD-1b output grid.

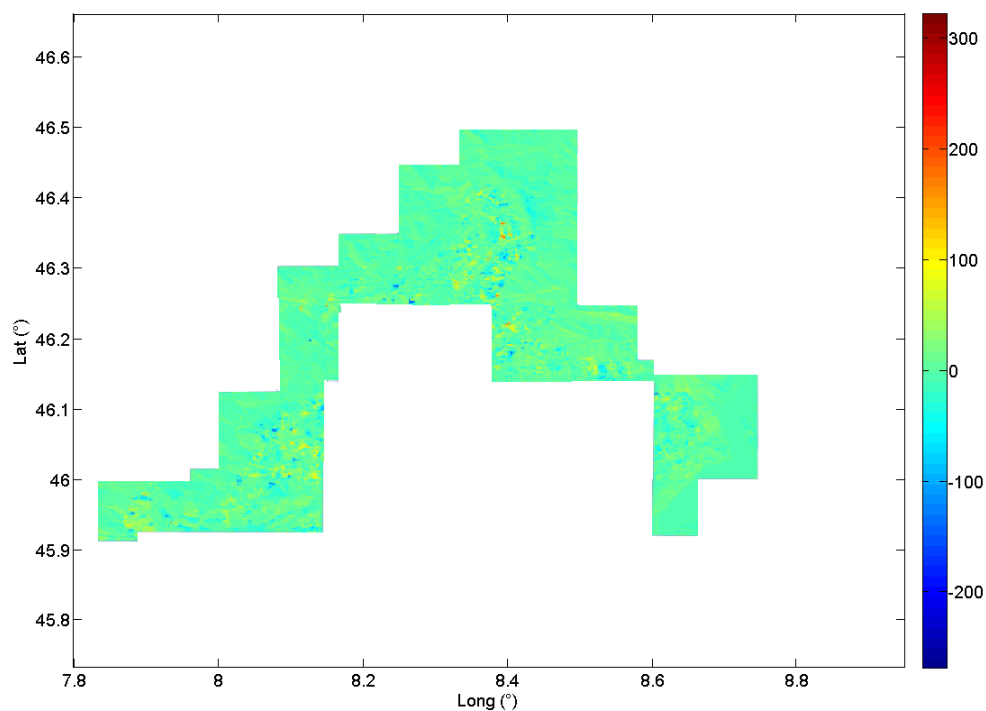


Figure 5.6: Differences obtained by individual interpolation of the Swiss and Piedmont DTMs on the HD-1b output grid.

For the two cross-checks between Piedmont and Lombardy DTMs and Switzerland and Piedmont DTMs, in both cases the statistics are similar to those obtained by the cross-validations of the original models: these comparisons have not been reported in this thesis but are reported in detail in (Biagi et al., 2013a). In general, from the three comparisons it seems that Piedmont DTM has a general bias in elevation of 1 meter with respect to the Lombardy and Swiss DTMs; but in both cases the number of useful points on which the statistics have been computed is small. Moreover this value is not significant if considering the nominal vertical

accuracies of the original DTMs. However in general the statistics are comparable with the nominal accuracies of the DTMs.

In order to verify the correctness of the interpolation method, each of the three interpolated DTMs has been back-interpolated on the nodes of the corresponding input DTM. This has been achieved following this procedure: for each input DTM, its nodes have been transformed from their original reference frame to ETRF2000, then their elevations has been estimated interpolating the corresponding final DTM through exact bicubic interpolation. The elevations thus obtained have been compared to the original ones. In Figure 5.7 the differences for the Lombardy DTM are shown and in Table 5.4 the statistics are summarized.

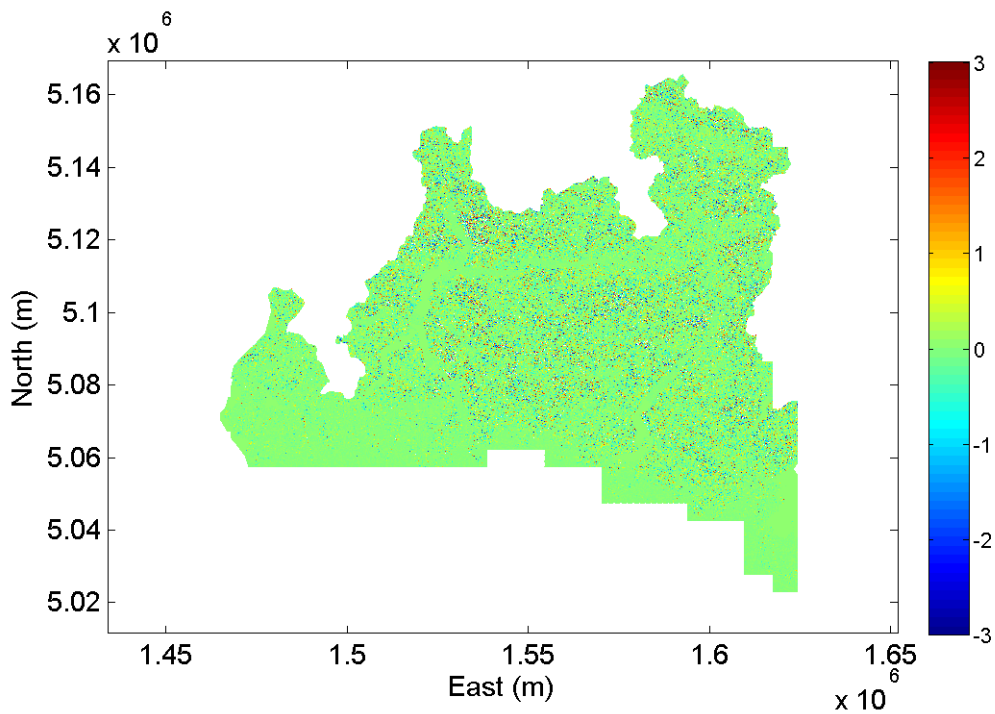


Figure 5.7: Differences between back-interpolated and original Lombardy DTMs (only the differences with an absolute value equal or lower than 3 meters are shown).

In the figure, to better visualize the distribution of the differences, only the differences whose absolute value is equal or lower than 3 meters have been plotted, because the 99.1% of the nodes belongs to this group. These differences are homogeneously distributed inside the region. Even if the maximum and minimum differences are high, statistics are good, with mean and standard deviation lower than a meter. In Table 5.5 the differences have been divided in eleven classes. Despite the presence of few nodes (6'828 with respect to the total of 30'028'763)

Cross-check results (m) for Lombardy	
Number of useful nodes	30'028'763
Bias	~ 0
Std	0.8
Maximum	222.7
Minimum	-141.2

Table 5.4: Statistics of the differences between back-interpolated and original Lombardy DTMs.

whose differences exceed 10 meters, the other 99.9% of the nodes has differences lower than 10 meters. In particular the differences whose absolute value exceeds 50 meters represent some computation anomalies; these differences regard however only 18 points and are all concentrated in one area. These differences are still under analysis.

Differences (m)	Percentage with respect to the total number of points
$\Delta H < -100$	$\sim 0\%$ (5 points)
$-100 \leq \Delta H < -50$	$\sim 0\%$ (4 points)
$-50 \leq \Delta H < -20$	$\sim 0\%$ (116 points)
$-20 \leq \Delta H < -10$	0.01%
$-10 \leq \Delta H < -3$	0.47%
$-3 \leq \Delta H < 3$	99.10%
$3 \leq \Delta H < 10$	0.45%
$10 \leq \Delta H < 20$	0.01%
$20 \leq \Delta H < 50$	$\sim 0\%$ (104 points)
$50 \leq \Delta H < 100$	$\sim 0\%$ (6 points)
$\Delta H \geq 100$	$\sim 0\%$ (3 points)

Table 5.5: Classes and percentages of elevation differences between back-interpolated and original Lombardy DTMs.

Back-interpolated and original Swiss DTMs do not present any anomalous value. This is probably due to the fact that the interpolation nodes are better disposed with respect to the original nodes than in the case of Lombardy. Figure 5.8 shows the distribution of the differences with an absolute value lower than 1 meter (98% of the nodes). From Tables 5.6 and 5.7 it can be seen that statistics are good, without the presence of high values of minimum and maximum, about the 100% of the differences are lower than 10 meters and the 99.9% lower than 3 meters.

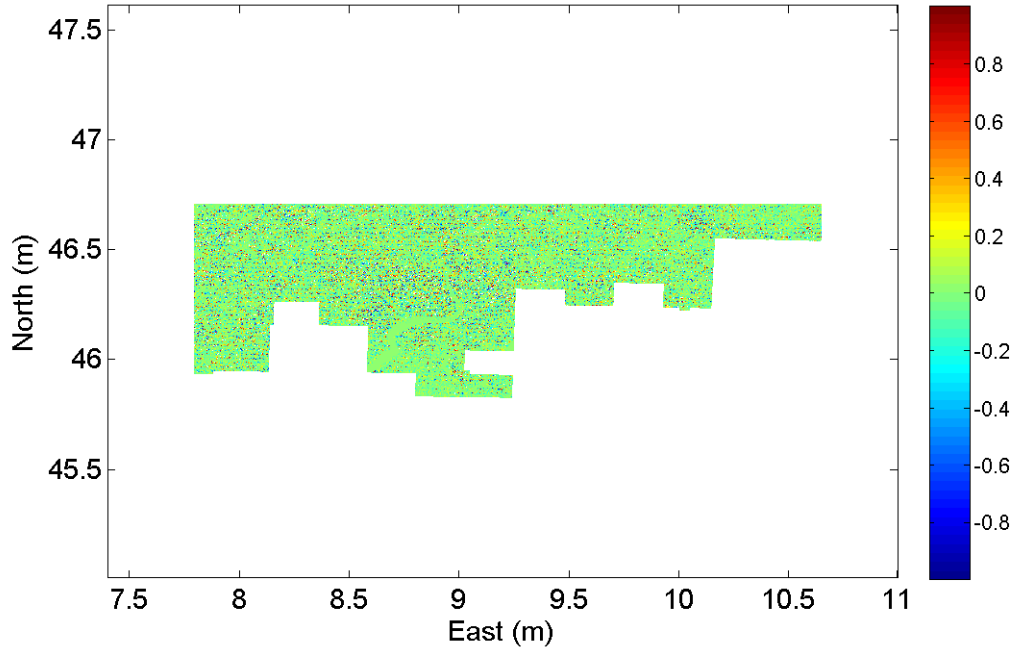


Figure 5.8: Differences between back-interpolated and original Swiss DTMs (only the differences with an absolute value equal or lower than 1 meter are shown).

Cross-check results (m) for Switzerland	
Number of useful nodes	11'909'270
Bias	~ 0
Std	0.3
Maximum	17.9
Minimum	-17.8

Table 5.6: Statistics of the differences between back-interpolated and original Swiss DTMs.

Also for Piedmont (Figure 5.9) the differences between the back-interpolated and original DTMs are satisfactory. All the nodes have differences (Table 5.8) smaller than 7 meters, with mean and standard deviations comparable with the vertical nominal accuracy of the Piedmont DTM. Also in this case the differences have been divided in eleven classes (Table 5.9) and, obviously, they are concentrated in the three central classes, with the most part of the data (99.99%) with an absolute difference lower than 3 meters. In all the three cases however the differences are acceptable if considering the nominal accuracies of the DTMs and the greatest differences are located in mountainous areas.

Differences (m)	Percentage with respect to the total number of points
$\Delta H < -100$	0%
$-100 \leq \Delta H < -50$	0%
$-50 \leq \Delta H < -20$	0%
$-20 \leq \Delta H < -10$	$\sim 0\%$ (31 points)
$-10 \leq \Delta H < -3$	0.04%
$-3 \leq \Delta H < 3$	99.90%
$3 \leq \Delta H < 10$	0.04%
$10 \leq \Delta H < 20$	$\sim 0\%$ (34 points)
$20 \leq \Delta H < 50$	0%
$50 \leq \Delta H < 100$	0%
$\Delta H \geq 100$	0%

Table 5.7: Classes and percentages of elevation differences between back-interpolated and original Swiss DTMs.

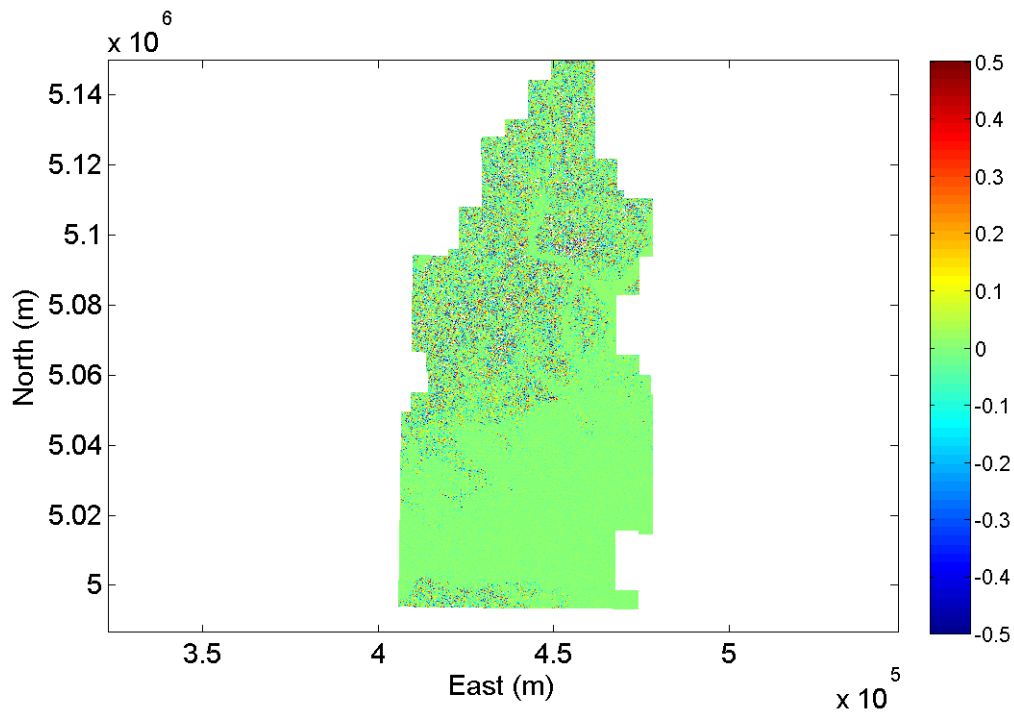


Figure 5.9: Differences between back-interpolated and original Piedmont DTMs (only the differences with an absolute value equal or lower than 0.5 meter are shown).

Cross-check results (m) for Piedmont	
Number of useful nodes	3'489'389
Bias	~ 0
Std	0.2
Maximum	6.7
Minimum	-6.8

Table 5.8: Statistics of the differences between back-interpolated and original Piedmont DTMs.

Differences (m)	Percentage with respect to the total number of points
$\Delta H < -100$	0%
$-100 \leq \Delta H < -50$	0%
$-50 \leq \Delta H < -20$	0%
$-20 \leq \Delta H < -10$	0%
$-10 \leq \Delta H < -3$	$\sim 0\%$ (3 points)
$-3 \leq \Delta H < 3$	99.99%
$3 \leq \Delta H < 10$	0.01%
$10 \leq \Delta H < 20$	0%
$20 \leq \Delta H < 50$	0%
$50 \leq \Delta H < 100$	0%
$\Delta H \geq 100$	0%

Table 5.9: Classes and percentages of elevation differences between back-interpolated and original Piedmont DTMs.

The unified final DTM has been constructed computing the average of the three DTMs in their overlapping areas. The resultant DTM (HD-1b) is shown in Figure 5.10: its statistics are summarized in Table 5.10.

Statistics of elevations (m)	
Number of grid nodes	116'000'000
Number of real valued grid nodes	88'477'603
Mean	1'301
Std	920
Maximum	4'616
Minimum	17

Table 5.10: Statistics of the elevations of HD-1b DTM.

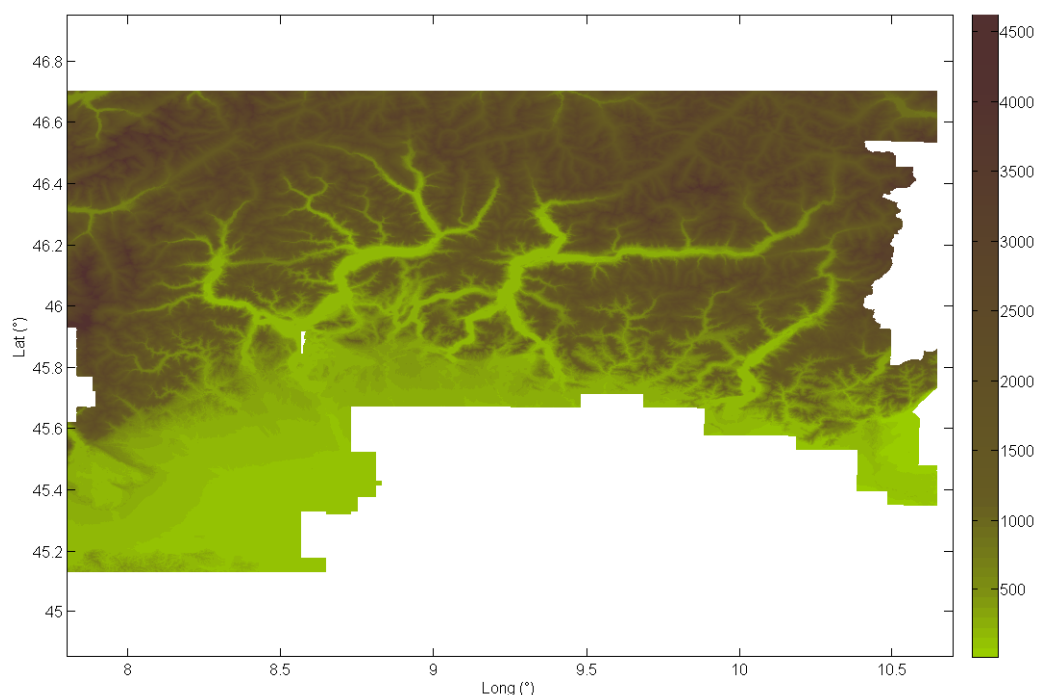


Figure 5.10: Unified HD-1b DTM resultant from the average of the three Lombardy, Piedmont and Swiss DTMs interpolated on the output grid.

At present the merging of the three interpolated DTMs has been performed through the simple average of the results in the overlap areas. However some analyses, that for time reasons can not be included in the thesis, useful to understand if at the borders between the different DTMs some inconsistencies have been introduced are being carried out.

The correction of points belonging to lakes has been performed following the same procedure described in Section 4.1.3 for the case of HD-1. As for the case of HD-1, also in this case a correction with PST-A has been applied to HD-1b; the final result will be called in the following HD-2b. The corrections are applied in the same way described in Section 4.2.2. As for HD-1 and HD-2 (Table 4.4), the comparisons between HD-1b/HD-2b and PST-A are satisfactory (Table 5.11). In fact the correction of HD-1b makes it much more similar to PST-A.

	bias (m)	std (m)	max (m)	min (m)
PST-A - HD-1b (original)	-0.35	4.6	97.1	-184.9
PST-A - HD-2b (corrected)	0.0	3.9	90.7	-132.1

Table 5.11: Statistics of the differences between PST-A LiDAR DTM and HD-1b (before the correction)/HD-2b (after the correction): global HELI-DEM area.

5.2.1 Validation of HD-1b and HD-2b DTM with RTK measures

HD-1 and HD-2 were externally validated through a comparison with the RTK points previously acquired for the external validation of PST-A in Valtellina Valley. This comparison is in detail described in Section 4.2.2.1. The same analysis has been performed for HD-1b and HD-2b. The two DTMs have been interpolated through bicubic interpolation on the RTK points and the differences have been computed; their statistics are summarized in Table 5.12. Also the statistics of the differences between PST-A and RTK measures are reported for a comparison: they are the same of Table 4.5.

	bias (m)	std (m)	max (m)	min (m)
HD-1 - RTK	3.4	5.5	24.2	0.0
HD-1b - RTK	1.9	3.8	12.1	0.0
PST-A - RTK	-0.3	1.0	7.2	0.0
HD-2b - RTK	-0.4	1.6	8.0	0.0

Table 5.12: Statistics of the modulus of the differences between HD-1b/PST-A/HD-2b DTMs and the 943 RTK points acquired in Valtellina area. In order to do an immediate comparison also the differences between HD-1 and RTK are reported.

Considering the vertical accuracies of the input DTMs used to construct HD-1b, the statistics are good both in case of HD-1b and HD-2b. As expected, the statistics demonstrate again the reliability of the applied correction: the mean and standard deviation of the differences between HD-2b and RTK are better than those of HD-1b and are more similar to those of PST-A.

Since the 943 points have been surveyed inside the twelve areas described in Section 2.4.2, a deeper analysis of the correction can be here done considering individually the zones. The most clamorous case in which the operation of the correction can be appreciated is the comparison of the three DTMs with the 64 RTK points surveyed in area VT02.

	bias (m)	std (m)	max (m)	min (m)
HD-1b - RTK (area VT02)	4.0	3.9	11.7	0.0
PST-A - RTK (area VT02)	0.1	0.1	0.2	0.0
HD-2b - RTK (area VT02)	0.2	0.7	1.3	0.0

Table 5.13: Statistics of the modulus of the differences between HD-1b, PST-A and HD-2b DTMs and RTK points (64 points in area VT02 in Valtellina Valley).

The statistics of this analysis are summarized in Table 5.13: as for the global set of points, also considering only the 64 points of this area, the values of mean and standard deviation of the corrected DTM are more similar to those of the PST-A than in case of HD-1b. In addition here HD-1b presents, in terms of bias and standard deviation, worse values with respect to the global comparison (where the bias is about 2 meters): in area VT02 HD-1b has a bias of about 4 meters compared to the RTK points.

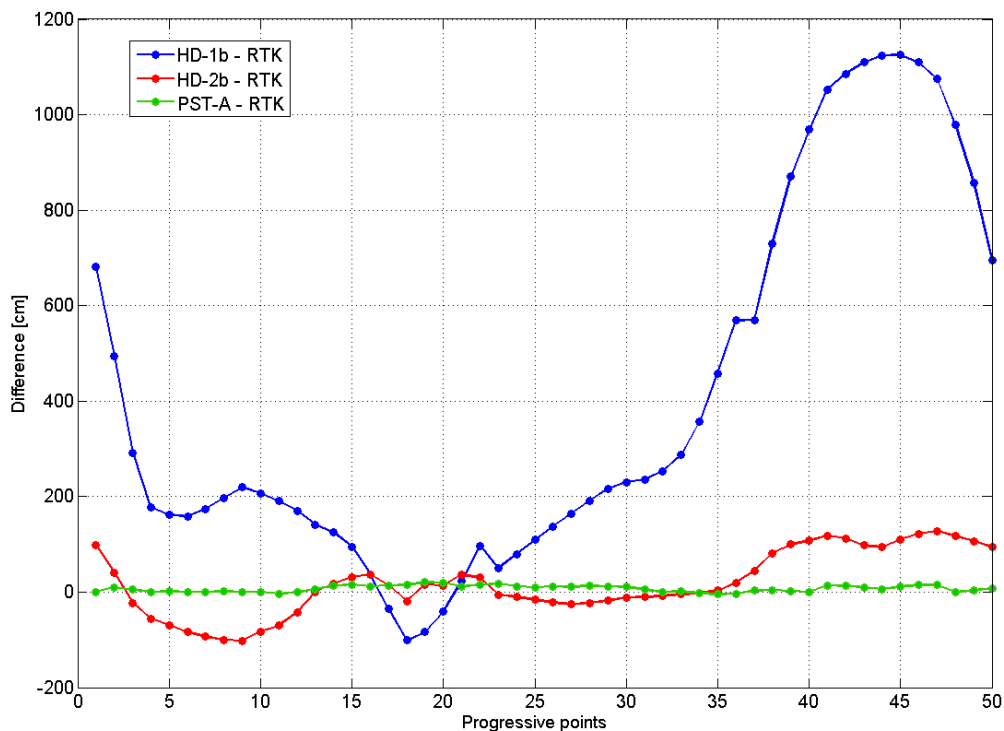


Figure 5.11: Progressive differences (cm) between HD-1b/HD-2b/PST-A DTM and RTK points in area VT02 in Valtellina Valley.

In order to verify the existence of such bias, in Figure 5.11 the differences between the three DTMs and the 64 points have been plotted on the same graphs, putting the points in increasing order of distance from the starting point. In the graph the bias of the unified DTM before the correction is clearly visible, with some points that present differences up to 11 meters. The differences between PST-A and RTK in this scale of representation are hardly recognizable because they are about zero. HD-2b follows the trend of the HD-1b case, but its differences are more similar to the high resolution case. This analysis confirms then the usefulness of the correction of HD-1b with the high resolution DTM.

Considering the global case, the statistics of the two DTMs obtained by the in-

verse merging approach (HD-1b and HD-2b) are better than those obtained by the direct approach (HD-1 and HD-2): this allows to affirm that the two approaches lead to satisfactory results and even better in the case of the second method.

Conclusions and Outlooks

In Italy and Switzerland, elevation data produced with different reference frames, technologies, accuracies and resolutions are available. The problem is that at the border between the two countries the different elevation models can be not consistent and can present some local biases. This can poses significant problems for specific tasks, like for example hydrogeological modelling. In these cases in fact a unique Digital Elevation Model would be very useful in order to analyse the scenario by a unified input dataset.

The HELI-DEM (HELvetia-Italy Digital Elevation Model) project, funded by the European Regional Development Fund (ERDF) within the Italy-Switzerland cooperation program, aimed at developing a unique DTM which would cover the alpine area between the two Italian Regions of Lombardy and Piedmont and the two Swiss Cantons of Ticino and Grisons. The project, with a duration of 36 months, started in September 2010. Its main goal was the creation of a unified Digital Terrain Model that covers the whole project area and is correctly georeferenced. This final product should be produced validating and integrating all the elevation data made available by the different project partners. The altimetric information have to be continuous and consistent at the nominal level of the input DTMs; therefore the resolution of the final DTM has to be at least equal to those of the original input DTMs and the vertical accuracy has to be in every area the best one obtainable from the input DTMs.

The two official regional DTMs of Lombardy and Piedmont and the national Swiss DTM were available. The Lombardy DTM, georeferenced in the Roma40 reference frame, Gauss Boaga cartographic coordinates, is characterized by a planimetric resolution of 20 meters and a vertical accuracy of about 10 m; the Piedmont Region DTM has a planimetric resolution of 50 meters, a vertical accuracy of 5 m and it is in ETRF89, cartographic coordinates. Also the Swiss DTM is in ETRF89 but in geographic coordinates, has a horizontal resolution of about 30 m and an accuracy of 2-3 m in height. Then two medium and high resolution DTMs were available, both acquired by LiDAR technique: the former covering the whole Piedmont Region with a planimetric resolution of 5 meters and a vertical accuracy of 0.5 m, the latter, named PST-A, covering the main river

basins of Piedmont and Lombardy and created by the Ministry of Environment inside the Piano Straordinario di Telerilevamento Ambientale (Extraordinary Plan of Environmental Remote Sensing), PST-A; this was the most accurate and resolute available DTM (respectively 10-50 cm of vertical accuracy and about 1 m of planimetric resolution). Both the two LiDAR DTMs are in the ETRF89 reference frame, the former in cartographic coordinates, the latter in geographic coordinates.

Basically these elevation data had to be merged to create a unique model. To do that several preliminary analyses have to be taken into account. First of all, since the data were in different reference frames, they had to be aligned to the same reference frame. Then, before their merging, the data had to be cross-validated in order to check their reciprocal consistency and the possible presence of biases; in addition they had to be externally validated in order to check their accuracy.

To cross validate the DTMs, two different analyses were carried out. The first was the cross-validation between cross-border DTMs with similar planimetric resolution, where they overlap, i.e. at the border between their domain. The second comparison, which could be considered as an external validation, was performed between low and high resolution DTMs in the areas where the latter ones was present. In this thesis firstly the cross-validation between the Lombardy and the Swiss DTMs is described in detail. Since the two DTMs had similar resolutions and accuracies, they were compared on some points located in random positions in their overlap area: the results were comparable with the nominal accuracies of the two input datasets; moreover they did not present global biases. However the differences presented an anomalous spatial distribution probably due to the restitutions rather than to the orography of the territory. Then the Lombardy Region DTM was externally validated with the PST-A: in this case the comparison was performed inside the areas where the latter was present, subsampling it on the nodes of the former and computing their differences. The differences were acceptable considering the whole set of points, but in some areas local biases seemed to be present. After the identification of the critical areas where the discrepancies exceeded acceptable values, in order to check the correctness of PST-A a comparison with some ad hoc surveyed RTK GNSS measures was performed; the RTK points were surveyed in twelve zones in the area of Valtellina Valley (Adda River Valley). The comparison with RTK points confirmed the correctness of PST-A.

All these operations represented some preliminary analyses to verify if the available data were useful for the creation of the final product of the project. The unified model had to be obtained through the merging of the available low/medium resolution DTMs. In particular the regional DTM was chosen for Lombardy area, the national Swiss DTM for Switzerland; for Piedmont the choice firstly fell on the LiDAR DTM with a planimetric resolution of 5 meters which covers the whole region. The output model, called HD-1, was obtained by harmonization, filtering

and interpolation of these three models. HD-1, georeferenced in ETRF2000 reference frame in geographic coordinates, had to be computed on a grid defined inside a geographic rectangle whose limits are 7.80° East and 10.70° East and 45.10° North and 46.70° North and with a spacing of $2 \cdot 10^{-4}$ sexagesimal degrees both in longitude and latitude: the output matrix is composed by 8'000 rows and 14'500 columns for a total of 116 millions nodes. Various analyses were performed in order to find the suitable interpolation and merging method. First of all in fact the regriding of gridded data on a new grid implies an interpolation. Since the stored elevations have been usually already filtered for the errors, attention has been focused on the so called interpolators, or better the predictors that pass through the observations and in particular on the already well known bilinear and bicubic polynomial surfaces. The comparison of the two models to interpolate originally gridded elevation data led to affirm that bicubic is better than bilinear, especially in mountainous area, as in case of HELI-DEM. A bicubic interpolator was therefore used to regrid the input DTMs. To merge the input DTMs to create the output HELI-DEM DTM, a Direct approach was used: the three DTMs were converted from their original reference frame to the reference frame of the output grid; then each DTM was independently interpolated on the nodes of the output grid; finally the results were averaged inside the overlapping areas. Where possible, an exact bicubic model was used to predict the elevation of the output nodes, in order to reproduce as much as possible the input data. In some cases it happened that, due to the bad configuration of the input points, the estimation was not possible; in all these cases two different solutions were used: the addition of new observations to the system and the removal of some interpolation surface parameters.

Since the direct approach proved several numerical problems that had been overcome by numerical regularizations, an Inverse approach has been studied at the conclusion of the project, in order to bypass these problems. The main difference between Direct and Inverse methods is the way in which the input DTMs are interpolated on the output grid. In the Inverse procedure the input grids are not transformed from their original reference frames to the one of the output grid, but the output horizontal coordinates of the nodes of the output grid are back-transformed from the output reference frame to the original reference frame of each input DTM. Each input DTM is therefore interpolated on the back-transformed horizontal coordinates of the output nodes. The advantage of this method is that a bicubic exact interpolation is always possible and well conditioned. This second product is called HD-1b.

In order to use also the information available in the PST-A high resolution DTM, this was used to correct HD-1 and HD-1b. The correction of each DTM was performed studying a suitable method that allowed to correct the low resolution data inside the areas where PST-A was present, without introducing biases at the

borders between the two. The correction was implemented performing a Fast Fourier Transform solution. In order to test the accuracy and the consistency of the two unified products and of the two corrected products, various analyses were performed: the external validation of the DTMs with RTK points allowed to affirm that the Inverse method provides better than the Direct method. Moreover, the implemented approach to correct the output low resolution DTM with high resolution data where they are available proves to be effective.

The output DTMs have been published on a geoservice, which is a multi-platform program, written in Java language and which allows to elaborate, visualize and share geographic geo-referenced data using the standard published by the OGC. In order to do that a Geoserver software has been selected and installed on a server which is physically located in the Geomatics Laboratory of Como Campus of Politecnico di Milano.

Appendix A

Reference systems and frames

The definition and realization of a Terrestrial Reference System is fundamental for spatial geodetic positioning.

A Terrestrial Reference System (TRS) is a spatial reference system that rotates with the Earth during its diurnal motion. It is defined by a set of conventions, algorithms and constants that determine the origin, the scale and the orientation of the system; its realization (TRF, Terrestrial Reference Frame) is performed through some constraints derived from physical and geometric observations from ground or space.

A catalogue of the Reference Frames is a geodetic distribution through the coordinates of fundamental points, such as the fundamental celestial bodies, the VLBI, SLR and GPS Permanent Stations for global networks or the coordinates of the zero order geodetic points for national networks.

A Reference Frame is characterized also by its *accuracy*, defined by the precision of the points that materialize it, and by the *deformation* in time, which represents the temporal variation of the positions of the points that materialize the reference frame (Caldera and Visconti, 2006).

Since the position of every point on the Earth changes in time due to the planet motions, periodic updates of the Reference System realization are needed to model the deformations.

A.1 ITRS and ITRF

ITRS (International Terrestrial Reference System) is a global reference system coherent at planetary scale. ITRS is defined with the following characteristics:

- origin in the center of mass of the Earth,
- Z axis that passes through the Terrestrial Conventional Pole,

- X axis defined by the intersection between the reference meridian (Conventional Greenwich) and the plane orthogonal to the Z axis (Conventional Equator),
- Y axis, so that it completes the counter-clockwise tern,
- lengths scale coherent to the time scale of the terrestrial geocentric dynamic (TCG),
- time evolution of the axes positions in order to assure a condition of non-rotation with respect to the tectonic plate.

In the estimation, the coordinates at an assigned zero epoch and the linear velocities of the ITRF stations are estimated.

The Terrestrial Conventional Pole (CTP) is defined as the mean of the positions of the pole during a certain time period. Different realizations of ITRS developed by the IERS (International Earth Rotation and Reference Systems Service) have occurred; they are called ITRF_{yy}, where the letter F highlights the fact that it is a specific realization of the ITRS, while the letters yy indicate the year of realization. The realizations are estimated by combining adjustments of the Permanent Stations networks of VLBI (Very Long Base Interferometry), SLR (Satellite Laser Ranging) and GPS. Each realization distributes the Cartesian geocentric coordinates $\underline{x}_0 = [x \ y \ z]$ of the Permanent Stations that have been used in the adjustment at a certain epoch t_0 and their velocities $\underline{\dot{x}}_0 = [\dot{x} \ \dot{y} \ \dot{z}]$, with hypothesis of linear displacement in time.

A coordinates estimation in a generic epoch t , different from the initial epoch t_0 , is:

$$\begin{aligned}\underline{x}(t) &= \underline{x}_0 + \underline{\dot{x}}(t - t_0) \\ \sigma^2(t) &= \sigma_0^2 + \dot{\sigma}^2(t - t_0)^2\end{aligned}$$

Some fundamental realizations are:

- ITRF89 (epoch $t_0 = 1994.0$), the first one,
- ITRF97 (epoch $t_0 = 1997.0$), the first that was based on long time series,
- ITRF2008 (epoch $t_0 = 1997.0$), the current one.

In particular ITRF2008 realization is estimated as:

- Z axis computed from observations of the VLBI Permanent Stations,
- geocenter position determined by observations of SLR satellite orbits,

- time derivatives of the axes position determined adding constraints of non-rotation with respect to the geodynamic model NNR-Nuvel-1A,
- lengths scale determined by observations of the VLBI and SLR Permanent Stations,
- combined adjustment of the VLBI, SRL and GPS networks.

Some Reference Systems defined at continental or national scale exist; in Italy for example the ETRF2000-RDN Reference Frame is relevant.

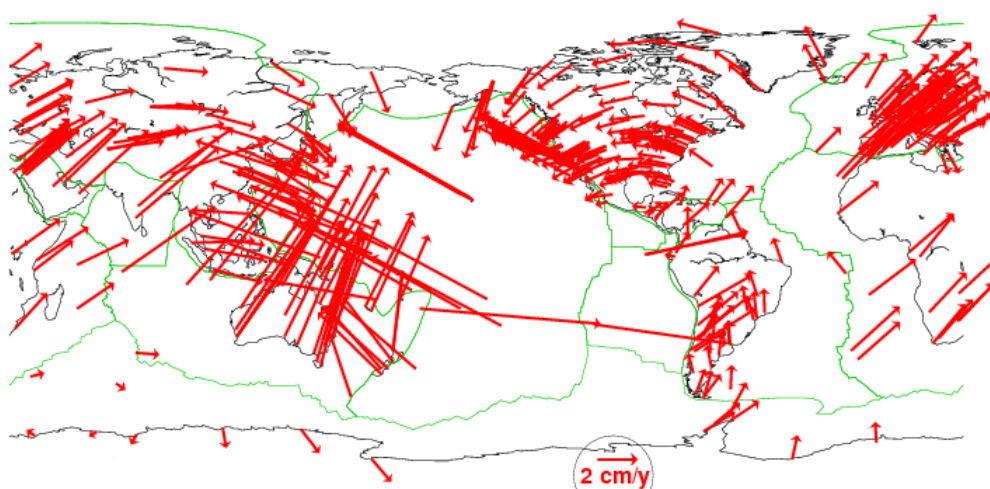


Figure A.1: ITRF2008 horizontal velocity field (Altamimi et al., 2001), in red the vectors representing the estimated velocities, in green the major plate boundaries.

A.2 ETRS89

To give a static description of the European territory for cartographic applications, the European Reference Frame IAG commission has started the ETRS89 Reference System through the use of the EPN (European Permanent Network) GPS Permanent Stations. ETRS89 is defined coincident to the ITRS at epoch 1989.0, but it follows consistently the geodynamic motion of the steady part of the European plate, which more or less coincides with the central zone of the continent.

Up to ITRF2000, one ETRF_y realization of ETRS89 corresponds to each ITRF_y realization and it is distributed through the coordinates and velocities of the European Stations. In the following, ETRF2000 remained even if ITRF has been updated. At present the transformation between each ITRF_y and ETRF2000

is provided; this transformation, is described by a similarity transformation that uses six parameters linearly dependent on time, combined with a linear propagation of the geodynamic velocities of the point to be transformed. At present epoch ($\simeq 2014.0$) in Italy the differences between ITRF_y and ETRF_y have currently a magnitude of 40-50 cm in planimetry.

A.3 ETRF89 - IGM95

Many nations have their own official ETRS89 realization. In Italy, the realization of ETRS89 has been firstly materialized by the IGM95 network of the Istituto Geografico Militare Italiano (IGMI). IGM95 is composed of about 2000 benchmarks, surveyed from the nineties by GPS surveys; they have been adjusted in ETRF89, and constitute a classic network of first order: the network is characterized by a vertex each 300 km² and a maximum distance between benchmarks of the order of 20 km. IGM95 is distributed by the IGM monographs.

The network has been determined using differential GPS techniques and constraining seven EPN points located in Italy to their ETRF89 coordinates, estimated at epoch 1989.0. The network has been also linked to the triangulation and leveling Italian networks.

Up to 2008 IGM95 had three problems (Biagi, 2009):

1. Italy does not homogeneously belong to the European Plate: since 1989.0 deformations of some centimeters have been occurred between the Northern and Southern regions of Italy,
2. instruments and elaboration methods used in the '90s were less accurate than those used today,
3. in 20 years, some local deformations may have occurred on the benchmark monumentations.

A.4 ETRF2000-RDN and ETRF2000-IGM95

In order to obviate the IGM95 obsolescence, in 2007 IGMI has began a new process to update the national network from a static to a permanent reference frame: this was done by the institution of an official national GNSS permanent network, adjusted in ITRF2005 and distributed in ETRF2000 ($t_0 = 2008.0$). In particular, the following operations were performed.

- Definition of a national permanent network of GNSS permanent stations, called Rete Dinamica Nazionale (Dynamic National Network, RDN),

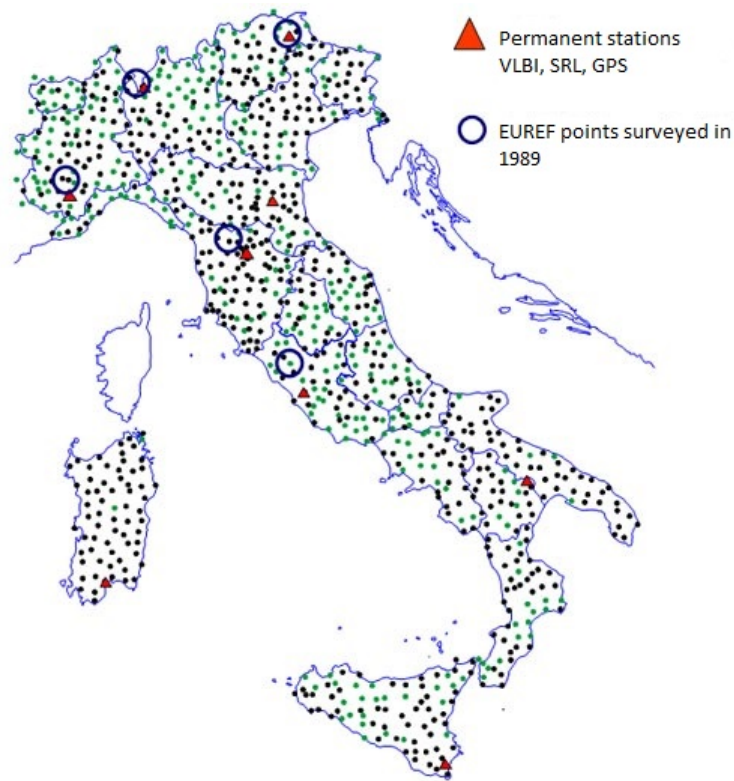


Figure A.2: IGM95 geodetic network.

- Adjustment of the network in ITRF2005 and in ETRF2000,
- Connection and adjustment in RDN of IGM95, in order to update its benchmarks coordinates.

In details, RDN is composed of 100 permanent stations, selected among the Italian existing stations by following the criteria of homogeneous distribution and quality. The network was processed for one month in the global ITRF2005 reference frame. These estimated coordinates were transformed to ETRF2000 at epoch 2008.0, by applying the official international transformation published by EPN. therefore, IGM95 baselines have been again adjusted in ETRF2000-RDN to newly estimate IGM95 benchmarks coordinates in ETRF2000. Note that the original IGM95 network has not been re-surveyed and re-adjusted: the old IGM95 set of baselines has been connected to RDN by surveying some baselines from 45 RDN permanent stations to at least three IGM95 nearest benchmarks each. After that, all the original surveyed IGM95 baselines have been adjusted again using the RDN ETRF2000 coordinates as constraint.

Therefore, ETRF2000-RDN is only a partial update of ETRF89-IGM95: although the reference frame is updated, ETRF2000-RDN partially still suffers of the technical problems described in the previous sections. In any case, for cartographic purposes, ETRF2000-RDN and ETRF2000-IGM95 are not the official Reference Frames for Italy.

A.5 ROMA40 - Gauss Boaga

Roma40 is the Italian historical Reference System, referred to the astronomic data and established in 1940.

The Roma40 Reference System is realized by terrestrial techniques. The reference ellipsoid is the International 1924 Hayford ellipsoid. It is locally oriented so that its normal direction coincides to the gravity vertical passing through the geodetic vertex of Roma Monte Mario measured in 1940.

Two different projections exist with respect to the meridians used as reference: West and East fuses. They are posed respectively at 9° and 15° with respect to the Greenwich meridian. Each projection covers a zone with an amplitude equal to 6° , separated by the meridian located at 12° . A cartographic projection defines the method to project on a Cartesian plane the coordinates of points located on the ellipsoid surface. The Roma40 Gauss-Boaga projection was proposed in 1940 by the IGMI. The Roma40 coordinates can be obtained “a posteriori” through transformation procedures and for this reason are not much accurate. This procedure is a mathematical transformation that computes the cartographic coordinates (x, y) on the plane from the geographic coordinates (ϕ, λ) .

The Roma40 Reference Frame was performed using the IGMI geodetic network of the first, second, third and fourth order. The coordinates are expressed in meters. To avoid the use of negative values for longitude, a coordinate equal to 1500000 m (instead of zero) is assigned to the central meridian of West fuse, called *false West*. In the same way a *false East* equal to 2520000 m is given to the East fuse. In this way the first value of the longitude coordinate indicates in which fuse the point is located (value 1 for the west fuse, value 2 for the East fuse). The accuracies of the coordinates are about 10 cm at the local scale and 1 m at the national scale.

Appendix B

Grid interpolation methods

In Digital Terrain Modelling, interpolation is used to obtain the elevation of a point that doesn't coincide with the stored nodes. Two implicit assumptions are usually adopted by the interpolation techniques:

- the terrain surface is continuous,
- there is a high spatial correlation.

Interpolation techniques can be classified according to different criteria. By the size of the used area, two different types of interpolators can be distinguished: *global* or *local* interpolators. In the first approach the surface is constructed by using the complete dataset of measured points that fall inside the interest area; from this surface the height of any other point within this area can be estimated from this surface. Global interpolators are more suitable for flat terrain or however for terrains with few abrupt changes in slope and height. Determining a single function which is mapped across the whole region, they have the disadvantage that a change in an input value affects the entire resultant surface. On the other hand local interpolators use only a window containing a sample of input points and not the whole dataset. Local interpolators are preferred for rough terrains and a change in an input value only affects the results within the considered window.

According to the exactness of the surface, the interpolation surface can be *interpolator* or *approximator*. An interpolator reproduce the observed values; in other words the result is a surface that passes through the observations. An approximator smooth the input data and the resultant surface doesn't pass exactly through the observed points. In case of best fitting the differences between observed and estimated values are minimized and the surface is the best possible fit. Approximators are used when there is some uncertainty about the given surface values, because in many data sets there are global trends, which vary slowly, overlain by local fluctuations, which vary rapidly and produce uncertainty (errors) in

the recorded values. The effect of smoothing will therefore be to reduce the effects of error on the resulting surface.

To construct a surface interpolation, a *deterministic function* or a *probabilistic model* can be used. In the deterministic interpolation the parametric model is a-priori decided: then the parameters are estimated. Stochastic methods incorporate the concept of randomness and the field model offers assessment of errors with predicted values. Splines and Inverse Distance Weighted are examples of deterministic methods, Kriging is a stochastic method.

Finally, interpolation can take place in either the *space domain* or in the *spectral domain*. Most interpolation techniques for terrain modelling are specifically designed for the space domain, but it is also possible to transform the data into a frequency domain and interpolate there.

In the following paragraphs the main interpolation methods used for the analyses described in this thesis are presented.

B.1 Exact interpolators of linear surfaces

The main problem of this thesis is the re-gridding of already filtered and gridded data, and not the creation of a digital model from original elevation data, that have to be cleaned by their errors. For this reason the choice of the interpolation method has fallen on a deterministic method and in particular on polynomial surfaces. In addition, since we want to keep the information contained in the DTM as unchanged as possible, where possible, an interpolator is preferable with respect to an approximator.

This section discusses some polynomial models to interpolate a linear surface that fits exactly to the input points.

B.1.1 Simple linear interpolation

A plane can be determined by three points; the mathematical function of a plane is:

$$z = a_{00} + a_{10}x + a_{01}y \quad (\text{B.1})$$

where a_{00} , a_{10} and a_{01} are the three coefficients and (x, y, z) is the set of coordinates of a point belonging to the surface. To compute these three coefficients, three input data with known coordinates, $P_1(x_1, y_1, z_1)$, $P_2(x_2, y_2, z_2)$ and $P_3(x_3, y_3, z_3)$, are required to build an isodetermined system as follows:

$$\begin{bmatrix} a_{00} \\ a_{10} \\ a_{01} \end{bmatrix} = \begin{bmatrix} 1 & x_1 & y_1 \\ 1 & x_2 & y_2 \\ 1 & x_3 & y_3 \end{bmatrix}^{-1} \begin{bmatrix} z_1 \\ z_2 \\ z_3 \end{bmatrix} \quad (\text{B.2})$$

Once the coefficients a_{00} , a_{10} and a_{01} are computed, the value z_P of any point P with a given set of planimetric coordinates (x_P, y_P) can be estimated by substituting them into B.1. If the input points are aligned, the system can not be solved and the elevation of the point P can not be estimated; in fact in this case the determinant of the \mathbf{A} matrix is null and the matrix cannot be inverted.

B.1.2 Bilinear interpolation

A bilinear interpolation can be performed for any four points that are not positioned along a line. The mathematical function is:

$$z = a_{00} + a_{10}x + a_{01}y + a_{11}xy \quad (\text{B.3})$$

where a_{00} , a_{10} , a_{01} and a_{11} are the set of coefficients. They can be determined by four equations that are formed by making use of the coordinates of four input points: $P_1(x_1, y_1, z_1)$, $P_2(x_2, y_2, z_2)$, $P_3(x_3, y_3, z_3)$ and $P_4(x_4, y_4, z_4)$. The system is the following:

$$\begin{bmatrix} a_{00} \\ a_{10} \\ a_{01} \\ a_{11} \end{bmatrix} = \begin{bmatrix} 1 & x_1 & y_1 & x_1y_1 \\ 1 & x_2 & y_2 & x_2y_2 \\ 1 & x_3 & y_3 & x_3y_3 \\ 1 & x_4 & y_4 & x_4y_4 \end{bmatrix}^{-1} \begin{bmatrix} z_1 \\ z_2 \\ z_3 \\ z_4 \end{bmatrix} \quad (\text{B.4})$$

As for the linear model, the height z_P of any point P with known coordinates (x_P, y_P) can be estimated once the coefficients a_{00} , a_{10} , a_{01} and a_{11} are computed, substituting its planimetric coordinates into equation B.3.

If the four known points are distributed on a regular square grid (Figure B.1 on the left), a simplified formula can be used to estimate directly the elevation of point i :

$$z_i = z_1 \left(1 - \frac{\Delta x}{d}\right) \left(1 - \frac{\Delta y}{d}\right) + z_2 \left(1 - \frac{\Delta y}{d}\right) \left(1 - \frac{\Delta x}{d}\right) + z_3 \left(\frac{\Delta x}{d}\right) \left(\frac{\Delta y}{d}\right) \quad (\text{B.5})$$

In this formula, points 1, 2, 3 and 4 are the four nodes of the square grid, and d is the length of the grid interval. This configuration is optimal. Some configurations produce on the contrary unsolvable systems: one example of bad configuration is shown in Figure B.1 on the right. It is simply demonstrable that this kind of configuration, which corresponds simply to the previous one, but rotated, produces an

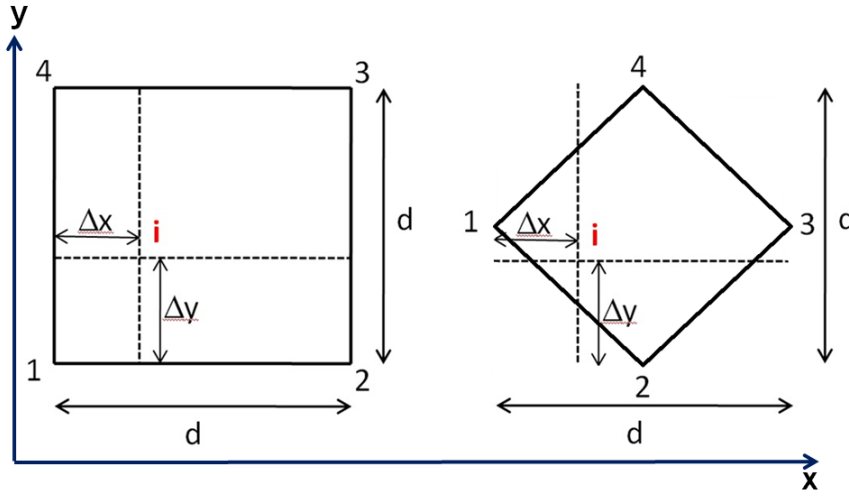


Figure B.1: Bilinear interpolation for square grids: optimal configuration on the left, bad configuration on the right.

unsolvable system. In fact assigning for example coordinates (0,0) to the baricenter of the rhombus and the following coordinates to the four nodes: 1 (-1,0), 2 (0,-

1), 3 (1,0), 4 (0,1). The design matrix, which becomes $\mathbf{A} = \begin{bmatrix} 1 & -1 & 0 & 0 \\ 1 & 0 & -1 & 0 \\ 1 & 1 & 0 & 0 \\ 1 & 0 & 1 & 0 \end{bmatrix}$,

is clearly singular.

B.1.3 Bicubic interpolation

A bicubic function can be used to interpolate a grid DEM. The mathematical function is as follows:

$$\begin{aligned}
 z = f(x, y) = \sum_{j=0}^3 \sum_{i=0}^3 a_{i,j} x^i y^j = & a_{00} + a_{10}x + a_{01}y + a_{20}x^2 + a_{11}xy + a_{02}y^2 + \\
 & + a_{30}x^3 + a_{21}x^2y + a_{12}xy^2 + \\
 & + a_{03}y^3 + a_{31}x^3y + a_{22}x^2y^2 + a_{13}xy^3 + \\
 & + a_{32}x^3y^2 + a_{23}x^2y^3 + a_{33}x^3y^3
 \end{aligned}
 \tag{B.6}$$

where $a_{00}, a_{10}, \dots, a_{33}$ are the sixteen coefficients to be determined, by the construction of sixteen equations. To solve the system sixteen points with known 3-D coordinates are needed. The system is the following:

$$\begin{bmatrix} a_{00} \\ a_{10} \\ a_{01} \\ \dots \\ a_{33} \end{bmatrix} = \begin{bmatrix} 1 & x_1 & y_1 & \dots & x_1^3 y_1^3 \\ 1 & x_2 & y_2 & \dots & x_2^3 y_2^3 \\ \dots & \dots & \dots & \dots & \dots \\ 1 & x_{16} & y_{16} & \dots & x_{16}^3 y_{16}^3 \end{bmatrix}^{-1} \begin{bmatrix} z_1 \\ z_2 \\ \dots \\ z_{16} \end{bmatrix} \quad (\text{B.7})$$

The height z_P of any point P with horizontal coordinates (x_P, y_P) can be estimated, once the coefficients are computed, substituting its planimetric coordinates into equation B.6. As for bilinear interpolation, also in this case a simplified formula exists.

B.1.3.1 Exact bicubic interpolation on a regular grid

If the observations are located on a regular grid, the interpolation on a point with know planimetric coordinates can be done using the sixteen nearest nodes (Biagi and Dermanis, 2002a).

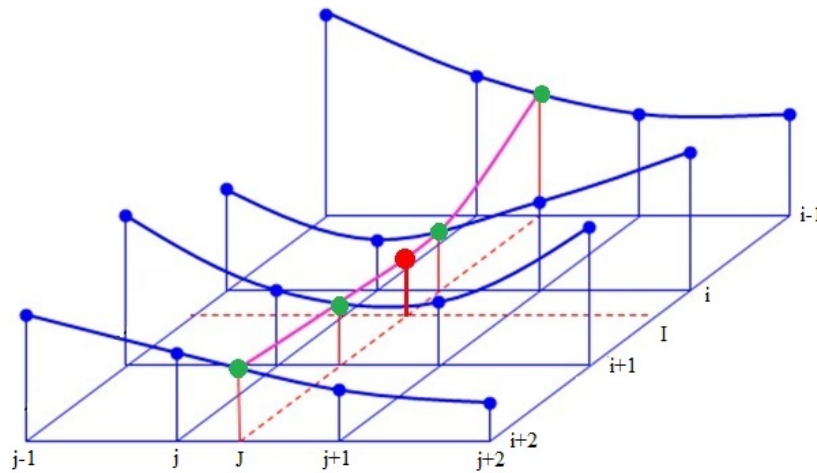


Figure B.2: Procedure of estimation of a point elevation through exact bicubic interpolation.

Considering the configuration of the interpolation point and of the observations shown in Figure B.2, to compute the value in the interpolation point (I, J) , four cubic interpolations can be performed along the first axis (for example j) and then a second interpolation can be done along the second axis (axis i). It has to be considered that a cubic interpolation allows to determine the third order polynomial, characterized by four unknown parameters, that passes through four

points in which the value of the polynomial is known. In the first step the four nodes of each of the four lines are used to compute the value of the point belonging to the same line and with J coordinate, following the schema:

$$\begin{array}{ccccccc}
 h_{i-1,j-1} & h_{i-1,j} & h_{i-1,j+1} & h_{i-1,j+2} & \rightarrow & h_{i-1,J} & \\
 h_{i,j-1} & h_{i,j} & h_{i,j+1} & h_{i,j+2} & \rightarrow & h_{i,J} & \\
 h_{i+1,j-1} & h_{i+1,j} & h_{i+1,j+1} & h_{i+1,j+2} & \rightarrow & h_{i+1,J} & \\
 h_{i+2,j-1} & h_{i+2,j} & h_{i+2,j+1} & h_{i+2,j+2} & \rightarrow & h_{i+2,J} &
 \end{array} \quad (\text{B.8})$$

Each interpolated value is given by the following expression:

$$\begin{aligned}
 h_{k,J} = & -\frac{1}{6}(J-j)(j+1-J)(j+2-J)h_{k,j-1} + \\
 & +\frac{1}{2}(J+1-j)(j+1-J)(j+2-J)h_{k,j} + \\
 & +\frac{1}{2}(J+1-j)(J-j)(j+2-J)h_{k,j+1} + \\
 & -\frac{1}{6}(J+1-j)(J-j)(j+1-J)h_{k,j+2}
 \end{aligned} \quad (\text{B.9})$$

with $k = i-1, i, i+1, i+2$.

At the second step the four values $h_{i-1,J}, h_{i,J}, h_{i+1,J}, h_{i+2,J}$ are used to perform the cubic interpolation along the i axis, in order to obtain:

$$\begin{aligned}
 h_{I,J} = & -\frac{1}{6}(I-i)(i+1-I)(i+2-I)h_{i-1,J} + \\
 & +\frac{1}{2}(I+1-i)(i+1-I)(i+2-I)h_{i,J} + \\
 & +\frac{1}{2}(I+1-i)(I-i)(i+2-I)h_{i+1,J} + \\
 & -\frac{1}{6}(I+1-i)(I-i)(i+1-I)h_{i+2,J}
 \end{aligned} \quad (\text{B.10})$$

The same result can be obtained if the interpolation process is inverted, thus at the first step four cubic interpolation are performed to compute $h_{I,j-1}, h_{I,j}, h_{I,j+1}, h_{I,j+2}$ and then the last interpolation is done along the j axis obtaining $h_{I,J}$.

B.2 Best interpolation of linear surfaces

This section discusses interpolation of bicubic when it is obtained from redundant observations by approximation approach.

B.2.1 Least Squares interpolation of a local surface

To describe a terrain model, an interpolation function that approximate the terrain can be used. In fact a surface passing through all the observations is not necessarily an approximation better than other kinds of surfaces: if the area is wide and there are many input observations available, it is necessary to use very high-order polynomials to achieve the exact interpolation of the surface. In this case, unstable oscillations can be caused by this type of function. Best interpolation (instead of exact interpolation) of curved surfaces is a method widely in use and the theory behind it is based on considering small variations on the terrain surface are so complex that they can be treated as a stochastic process.

There are many possibilities to best interpolate a surface, depending on the definition of “best”. In case of Least Squares approach, the term “best” means that the sum of the square errors is minimized. The mathematical expression is:

$$\sum_{i=1}^n e_i^2 = \min \quad (\text{B.11})$$

where e_i are the residuals of input data from the interpolation surface and n is the total number of input points. The Least Squares condition says that the surface that produces the least sum of square errors is the best.

The commonly used functions for curved surface interpolation are the second-order and third-order polynomials and bicubic functions. Depending on the function chosen, the number of parameters to be determined and, as a consequence, also the minimum number of needed observations, changes: if N is the number of parameters to be estimated, at least N observations are needed to solve the Least Squares system. In the following formulas a bicubic polynomial is used as observation equation; in this case the number of parameters is 16 and so at least 16 observations are necessary. The bicubic equation is given by B.6. With M ($M \geq N$, $N = 16$ in case of bicubic) input points M equations can be constructed. The system is the following:

$$\underline{z} = \underline{A}\underline{\xi} + \underline{\nu} = \begin{bmatrix} z_1 \\ z_2 \\ \dots \\ z_n \end{bmatrix} = \begin{bmatrix} 1 & x_1 & y_1 & \dots & x_1^3 y_1^3 \\ 1 & x_2 & y_2 & \dots & x_2^3 y_2^3 \\ \dots & \dots & \dots & \dots & \dots \\ 1 & x_n & y_n & \dots & x_n^3 y_n^3 \end{bmatrix} \begin{bmatrix} a_{00} \\ a_{10} \\ \dots \\ a_{33} \end{bmatrix} + \begin{bmatrix} \nu_1 \\ \nu_2 \\ \dots \\ \nu_n \end{bmatrix} \quad (\text{B.12})$$

where (x_i, y_i, z_i) are the 3-D coordinates of each observation. \underline{A} is a $[n \times 16]$ matrix and it is called “design matrix”; $\underline{\xi}$ is the vector with dimension $[n \times 1]$ containing the N unknown parameters that have to be estimated by Least squares. To vector \underline{z} of the observations is associated a covariance matrix C_{zz} :

$$\mathbf{C}_{zz} = \begin{bmatrix} \sigma_1^2 & \sigma_{12} & \cdots & \sigma_{1n} \\ \sigma_{21} & \sigma_2^2 & \cdots & \sigma_{2n} \\ \cdots & \cdots & \cdots & \cdots \\ \sigma_{n1} & \sigma_{n2} & \cdots & \sigma_n^2 \end{bmatrix} \quad (\text{B.13})$$

The diagonal of the matrix contains the variances of the observations; in other positions the covariances between couples of observations are present. The covariance observations matrix can be expressed also by:

$$\mathbf{C}_{zz} = \sigma_0^2 \mathbf{Q} \quad (\text{B.14})$$

where σ_0^2 is the a-priori variance or a common variance, matrix \mathbf{Q} is the cofactors matrix ($\mathbf{Q} = \mathbf{I}$ if the observations are independent and with equal precision).

The residuals can be written as follows:

$$\begin{bmatrix} \nu_1 \\ \nu_2 \\ \cdots \\ \nu_n \end{bmatrix} = \begin{bmatrix} 1 & x_1 & y_1 & \cdots & x_1^3 y_1^3 \\ 1 & x_2 & y_2 & \cdots & x_2^3 y_2^3 \\ \cdots & \cdots & \cdots & \cdots & \cdots \\ 1 & x_n & y_n & \cdots & x_n^3 y_n^3 \end{bmatrix} \begin{bmatrix} a_{00} \\ a_{10} \\ \cdots \\ a_{33} \end{bmatrix} - \begin{bmatrix} z_1 \\ z_2 \\ \cdots \\ z_n \end{bmatrix} \quad (\text{B.15})$$

and simplified as:

$$\underline{\nu} = \mathbf{A} \underline{\xi} - \underline{z} \quad (\text{B.16})$$

To estimate the unknown parameters, the vector $\underline{\hat{\xi}}$ is computed by the well known LS solution:

$$\underline{\hat{\xi}} = \begin{bmatrix} \hat{a}_{00} \\ \hat{a}_{10} \\ \cdots \\ \hat{a}_{33} \end{bmatrix} = \mathbf{N}^{-1} \mathbf{A}^T \mathbf{Q}^{-1} \underline{z} \quad (\text{B.17})$$

where $\mathbf{N} = \mathbf{A}^T \mathbf{Q}^{-1} \mathbf{A}$. If exactly 16 observations are used and are independent and with equal precision ($\mathbf{Q} = \mathbf{I}$), the parameters are estimated by the solution of the exact system:

$$\underline{\hat{\xi}} = \mathbf{A}^{-1} \underline{z} \quad (\text{B.18})$$

In this case, the bicubic surface acts as exact interpolator.

The height z_P of any point P with known coordinates (x_P, y_P) can be estimated, once the coefficients are computed, substituting its planimetric coordinates into equation B.6, or, similarly, by:

$$\hat{z}_P = \begin{bmatrix} 1 & x_P & y_P & \dots & x_P^3 y_P^3 \end{bmatrix} \begin{bmatrix} \hat{a}_{00} \\ \hat{a}_{10} \\ \hat{a}_{01} \\ \dots \\ \hat{a}_{33} \end{bmatrix} \quad (\text{B.19})$$

In case of a redundant system, the sigma a-posteriori can be estimated by:

$$\hat{\sigma}_0^2 = \frac{\hat{\underline{\underline{\varepsilon}}}^T Q^{-1} \hat{\underline{\underline{\varepsilon}}}}{n - N} \quad (\text{B.20})$$

where $\hat{\underline{\underline{\varepsilon}}} = \underline{\underline{z}} - \hat{\underline{\underline{z}}}$, n is the number of observations and N is the number of parameters (in case of bicubic model $N = 16$).

From the a-posteriori sigma the estimated parameters covariance matrix $C_{\hat{\underline{\underline{\varepsilon}}}\hat{\underline{\underline{\varepsilon}}}}$ and the estimated observations matrix $C_{\hat{\underline{\underline{z}}}\hat{\underline{\underline{z}}}}$ can be computed:

$$C_{\hat{\underline{\underline{\varepsilon}}}\hat{\underline{\underline{\varepsilon}}}} = \hat{\sigma}_0^2 \mathbf{N}^{-1} \quad (\text{B.21})$$

$$C_{\hat{\underline{\underline{z}}}\hat{\underline{\underline{z}}}} = \hat{\sigma}_0^2 \mathbf{A} \mathbf{N}^{-1} \mathbf{A}^T \quad (\text{B.22})$$

Coordinates normalization. In Figure B.3 an example of bad distribution of the input points around the interpolation node that produce an unstable exact bicubic system is shown. The example is taken from a real case discussed in this thesis: the output grid is the HELI-DEM unified DTM grid and the input points used for the interpolation are the nodes of the Lombardy regional DTM.

In bicubic interpolation some elements of \mathbf{A} matrix contains sums of the third order of the coordinates while other terms are of the very small; for example the first column filled with M ones. It can happen that when computing the inverse of the \mathbf{A} or \mathbf{N} matrix, some instability problems can occur. For this reason it can be useful to perform a normalization of the coordinates of the observations and the interpolation point in order to rescale the values in \mathbf{A} between 0 and 1. The coordinates of the interpolation point (x_P, y_P) are set to zero. Also the coordinates of the observations (x_i, y_i) have to be transformed:

$$x_{i,new} = \frac{(x_i - x_P)}{\Delta X} \quad y_{i,new} = \frac{(y_i - y_P)}{\Delta Y} \quad (\text{B.23})$$

where $\Delta X = \max|x_i - x_j|, \forall i, j$ and $\Delta Y = \max|y_i - y_j|, \forall i, j$.

As a consequence, since the coordinates of point P are (0,0) and all parameters, apart from the first one a_{00} depend on the planimetric coordinates of the observed

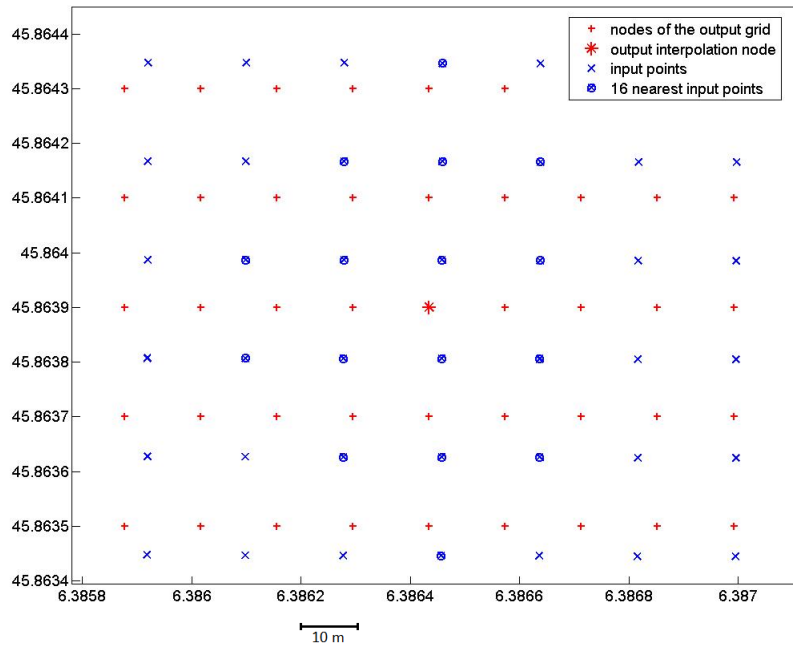


Figure B.3: Example of bad configuration of a bicubic exact system.

point, the coordinates normalization allows to simplify equation B.6 so that the elevation of the interpolation point can be estimated with the formula:

$$\hat{z}_P = \hat{z}(0, 0) = \hat{a}_{00} \quad (\text{B.24})$$

List of Figures

1.1	Eskimo stick carved to represent the coastline.	6
1.2	Example of terrain representation through contour lines.	6
1.3	Digital representations of the terrain.	7
1.4	Different types of models.	8
1.5	Example of subsidence model of Las Vegas area.	10
1.6	Difference between DSM and DTM.	11
1.7	Pattern of sampled data points.	13
1.8	Schema of cartographic digitalization methods.	17
1.9	Example of map digitalization.	18
1.10	GPS system: space segment, ground control system and user segment.	20
1.11	RTK GPS survey.	24
1.12	Absolute positioning: good and bad satellites configurations.	25
1.13	Example of stereopair.	27
1.14	Photographic coverage	28
1.15	Example of overlap photography.	29
1.16	LiDAR system.	31
1.17	Geometric distortions in SAR images	36
1.18	Comparison between LiDAR and InSAR.	37
1.19	Schematic representation of accuracy and precision of a model	40
1.20	Different DEM representation methods: GRID and TIN	44
1.21	Different DEM representation methods: GRID and TIN	45
1.22	SRTM configuration.	48
1.23	ASTER subsystems and their applications.	51
1.24	GMTED2010 global DSM.	52
2.1	Area of interest of HELI-DEM project.	59
2.2	Coverage of the local DTMs collected for the HELI-DEM project.	61
2.3	Overlapping areas of the DTMs collected for the HELI-DEM project.	62
2.4	GNSS permanent stations inside the HELI-DEM project area.	69

2.5	HELI-DEM network: reference frame core stations and HELI-DEM stations.	71
2.6	Corrections in longitude between the Roma40 and ETRF89 reference frames on the HELI-DEM area of interest.	72
2.7	Initial screen of the GK2CNV software.	73
2.8	Structure of the VERTO grids.	74
2.9	Area of the Lombardy DTM which presents some incorrect data. .	76
2.10	Slope of Lombardy DTM grid A3 which presents incorrect data. .	76
2.11	Border of Lombardy and Piedmont through Maggiore Lake and Ticino River.	77
2.12	Portion of Piedmont and Lombardy regional DTMs covering Maggiore Lake and Ticino River.	78
2.13	Overlapping area between Lombardy and Switzerland DTMs . . .	79
2.14	Overlapping area between Lombardy and Swiss DTMs and density of the randomly extracted points.	81
2.15	Histogram of the elevation differences between Lombardy and Swiss DTMs.	82
2.16	Normal test of the differences between Lombardy and Swiss DTMs.	84
2.17	Absolute values of the elevation differences between Lombardy and Swiss DTMs and borders of the Lombardy DTMs grids. . . .	85
2.18	Empirical covariance function of the differences between Lombardy and Swiss DTMs and exponential model.	86
2.19	Correlation between differences (Lombardy-Switzerland) in elevation and original elevations and slopes.	87
2.20	Histogram of the elevation differences between grid C2 of Lombardy DTM and grid e009n46 of Switzerland DTM.	88
2.21	Histogram of the elevation differences between grid D1 of Lombardy DTM and grid e010n46 of Switzerland DTM.	89
2.22	Area covered by the regional Lombardy DTM and the PST-A DTM.	91
2.23	Absolute values of the differences between Lombardy and PST-A LiDAR DTMs.	93
2.24	Subdivision of the Lombardy DTM in grids.	94
2.25	Differences of elevations between Lombardy DTM B1 grid and PST-A DTM, plotted in 3-D on Google Earth.	96
2.26	Histogram of the differences between Lombardy and PST-A DTMs on the Valley of San Giacomo.	96
2.27	Differences of elevations between Lombardy and PST-A DTMs on the Valley of San Giacomo.	97
2.28	Planimetric translations between the Lombardy LR and the PST-A LiDAR high resolution DTMs.	99
2.29	Landslide of Val Pola (Valtellina area, in Sondrio province). . . .	100

2.30	Example of IGM95 free monography of a geodetic point.	103
2.31	IGMI website with the map where the IGM95 monographies can be downloaded.	104
2.32	IGM95 points that fall inside the area of Lombardy LR DTM and inside the area of the PST-A DTM.	104
2.33	Levelling lines resurveyed by IGMI.	106
2.34	Selected areas for the external validation of the PST-A LiDAR DTM with GNSS RTK surveys.	107
2.35	GNSS RTK points and absolute height differences with respect to PST-A LiDAR DTM - area VT09.	110
2.36	Progressive differences between LiDAR DTM and RTK points in area VT07 and elevations of the points.	112
2.37	GNSS RTK points and absolute height differences with respect to PST-A DTM - area VT07.	113
2.38	GNSS RTK points and absolute height differences with respect to PST-A LiDAR DTM - area VT10.	113
3.1	Schema of the procedure of bilinear interpolation on the intersections between grid nodes and back-interpolation on the original nodes.	117
3.2	Grids A5 and E6 of the Lombardy low resolution regional DTM, covering lowland terrain.	121
3.3	Grids C5 and D5 of the Lombardy low resolution regional DTM, covering hilly terrain.	122
3.4	Grids B3 and C2 of the Lombardy low resolution regional DTM, covering mountainous terrain.	123
3.5	Elevations and aspect of the D46081032 PST-A grid.	127
3.6	Differences between the double-interpolated and original elevations and aspects of the D46081032 PST-A grid.	128
3.7	Example of bad configuration of an exact bicubic system on real data.	129
3.8	Example of TIN constructed with the Least Squares system observations.	133
3.9	Triangle of the TIN used to construct the pseudo-observation in the Finite Elements method.	133
3.10	Lombardy DTM data transformed from their original reference frame (Roma40) to those of the output HELI-DEM grid (ETRF2000).	137
3.11	Case study area of Triangolo Lariano in Lombardy.	138
3.12	Elevation differences of Lombardy and Swiss DTMs inside the case study area of Triangolo Lariano.	139

3.13	Condition number of the A matrix of the system obtained through bicubic interpolation of the Lombardy DTM and of the dataset obtained by the merging of the Lombardy and Swiss DTMs.	139
3.14	DTM and aspect obtained by application of DirectAndAverage and DirectOnMerged methods on the merging of Lombardy and swiss DTMs.	141
3.15	DTM and aspect resultant from the interpolation of the Lombardy DTM (with LS_{RO} regularization).	143
4.1	Unified HELI-DEM DTM (HD-1) obtained through the merging of Lombardy, Piedmont and Swiss low/medium resolution DTMs.	150
4.2	PST-A LiDAR DTM.	152
4.3	Example of discontinuity between PST-A and HD-1 DTMs: Oglio River valley.	153
4.4	Example of moving average 3x3 low pass filter matrix.	154
4.5	Example of low pass Butterworth filter.	155
4.6	Fourier Transform: convolution and relations in the space and frequency domain.	157
4.7	Application of Butterworth filter on simulated data.	159
4.8	Final results of application of Butterworth filter on simulated data.	160
4.9	Flow chart of the corrections filtering procedure.	160
4.10	Differences between PST-A LiDAR DTM and HD-1 DTMs and section of Oglio River.	161
4.11	Profile of the differences between PST-A and HD-1 DTMs of Oglio River section.	162
4.12	Differences between PST-A and HD-1 DTMs of the Oglio River Valley.	163
4.13	Basic functioning schema of a OWS service.	165
5.1	Result of the interpolation of the Lombardy DTM on the output HD-1b grid.	171
5.2	Result of the interpolation of the Piedmont DTM on the output HD-1b grid.	172
5.3	Result of the interpolation of the Swiss DTM on the output HD-1b grid.	172
5.4	Differences obtained by individual interpolation of the Swiss and Lombardy DTMs on the HD-1b output grid.	173
5.5	Differences obtained by individual interpolation of the Lombardy and Piedmont DTMs on the HD-1b output grid.	174
5.6	Differences obtained by individual interpolation of the Swiss and Piedmont DTMs on the HD-1b output grid.	175

5.7	Differences between back-interpolated and original Lombardy regional DTMs.	176
5.8	Differences between back-interpolated and original Swiss DTMs.	178
5.9	Differences between back-interpolated and original Piedmont regional DTMs.	179
5.10	Unified HD-1b DTM resultant from the average of the three Lombardy, Piedmont and Swiss DTMs interpolated on the output grid.	181
5.11	Progressive differences (cm) between HD-1b/HD-2b/PST-A DTM and RTK points in area VT02 in Valtellina Valley.	183
A.1	ITRF2008 horizontal velocity field.	191
A.2	IGM95 geodetic network.	193
B.1	Bilinear interpolation for square grids, optimal and worse cases.	198
B.2	Procedure of estimation of a point elevation through exact bicubic interpolation.	199
B.3	Example of bad configuration of a bicubic exact system.	204

List of Tables

1.1	Different GNSS positioning methods: achievable accuracies. . . .	25
1.2	Comparison of DEM acquisition methods	38
1.3	Accuracy indexes for the different levels of DEM according to the ISO/TC 211 standard.	42
1.4	Global DSMs: resolutions and accuracies.	46
1.5	SRTM X-SAR characteristics.	47
1.6	ASTER vs. SRTM.	50
2.1	Lombardy Region DTM.	64
2.2	Piedmont Region DTM.	65
2.3	Switzerland SwissTopo DTM.	65
2.4	High resolution (5 m) Piedmont Region DTM.	66
2.5	High resolution (1 m) Ministry of Environment PST-A LiDAR DTM.	67
2.6	Permanent network stations inserted inside the HELI-DEM transnational network.	70
2.7	Main characteristics of Lombardy and Switzerland regional DTMs.	79
2.8	Statistics of the elevation differences between Switzerland and Lombardy DTMs	82
2.9	Classes and percentages of elevation differences between Lombardy and Swiss DTMs.	83
2.10	Statistics of the elevation differences between grid C2 of Lombardy DTM and grid e009n46 of Switzerland DTM.	88
2.11	Statistics of the elevation differences between grid D1 of Lombardy DTM and grid e010n46 of Switzerland DTM.	89
2.12	Statistics of the elevation differences between all the overlapping grids couples of Lombardy and Swiss DTMs.	90
2.13	Main characteristics of Lombardy regional DTM and PST-A LiDAR DTM.	91
2.14	Statistics of the elevation differences between Lombardy DTM and PST-A DTM.	92

2.15	Classes and percentage of the absolute values of elevation differences between Lombardy and PST-A DTMs.	93
2.16	Statistics of the elevation differences between Lombardy and PST-A LiDAR DTMs, grouped by grids.	95
2.17	Statistics of the elevation differences between Lombardy and PST-A DTMs on the Valley of San Giacomo.	95
2.18	Classes and percentage of elevation differences between Lombardy and PST-A DTMs on the Valley of San Giacomo.	97
2.19	Translations and biases between the Lombardy DTM and the PST-A LiDAR DTM.	101
2.20	Statistics of the differences between the two DTMs (Lombardy and PST-A) and the IGM95 points.	105
2.21	Positions of the RTK survey areas: L: length of the path, h, ϕ, λ : approximate ITRF2008 position of the area.	107
2.22	Statistics of the elevation differences between interpolated PST-A DTM and GNSS-RTK (first survey campaign on June/July 2012).	109
2.23	Statistics of the elevation differences between interpolated PST-A DTM and GNSS-RTK (second survey campaign on October 2012).	110
3.1	Statistics of the elevations of six grids of the Lombardy regional DTM.	118
3.2	Statistics of differences in elevation between the original values and those obtained after two-times exact bilinear/bicubic interpolation on the six selected grids of the Lombardy regional DTM, grouped by terrain typologies.	119
3.3	Statistics of differences in slope between the original values and those obtained after two-times exact bilinear/bicubic interpolation on the six selected grids of the Lombardy regional DTM, grouped by terrain typologies.	120
3.4	Statistics of differences in aspect between the original values and those obtained after two-times exact bilinear/bicubic interpolation on the six selected grids of the Lombardy regional DTM, grouped by terrain typologies.	120
3.5	Statistics of the elevations of six grids of LiDAR PST-A high resolution DTM.	124
3.6	Statistics of differences in elevation between the original values and those obtained after two-times exact bilinear/bicubic interpolation on the six selected grids of the PST-A DTM, grouped by terrain typologies.	125

3.7	Statistics of differences in slope between the original values and those obtained after two-times exact bilinear/bicubic interpolation on the six selected grids of the PST-A DTM, grouped by terrain typologies.	126
3.8	Statistics of differences in aspect between the original values and those obtained after two-times exact bilinear/bicubic interpolation on the six selected grids of the PST-A DTM, grouped by terrain typologies.	126
3.9	Statistics of the input data of the case study area (Triangolo Lariano).	137
3.10	Number of nodes (with respect to the 915 that require a regularization) for which 1,2,3 points are added to the initial 16 observations in case of LS_{RO} solution or 1,2,3 parameters are removed from the 16 original parameters in case of SVD solution (Triangolo Lariano case study).	142
3.11	Statistics of the differences between the elevations obtained through Lombardy DTM interpolation on the output grid with SVD and with LS_{RO} regularization (Triangolo Lariano case study).	144
3.12	Statistics of various tests on the use of different regularization methods (Triangolo Lariano case study).	144
4.1	Statistics of the differences between the maximum and minimum elevations of the groups of coincident points belonging to Piedmont DTM.	148
4.2	Statistics of the results of the individual interpolation of the three low/medium resolution input DTMs on the output HD-1 grid. . . .	149
4.3	Statistics of the differences between PST-A LiDAR DTM and HD-1/HD-2 DTM: Oglio River area.	162
4.4	Statistics of the differences between PST-A LiDAR DTM and HD-1/HD-2 DTM: global HELI-DEM area.	162
4.5	Statistics of the differences between HD-1, PST-A and HD-2 DTMs and RTK points (Valtellina area).	163
5.1	Statistics of the differences obtained by individual interpolation of the Swiss and Lombardy DTMs on the HD-1b output grid. . . .	173
5.2	Statistics of the differences obtained by individual interpolation of the Lombardy and Piedmont DTMs on the HD-1b output grid. .	174
5.3	Statistics of the differences obtained by individual interpolation of the Swiss and Piedmont DTMs on the HD-1b output grid. . . .	175
5.4	Statistics of the differences between back-interpolated and original Lombardy DTMs.	177

5.5	Classes and percentages of elevation differences between back-interpolated and original Lombardy DTMs.	177
5.6	Statistics of the differences between back-interpolated and original Swiss DTMs.	178
5.7	Classes and percentages of elevation differences between back-interpolated and original Swiss DTMs.	179
5.8	Statistics of the differences between back-interpolated and original Piedmont DTMs.	180
5.9	Classes and percentages of elevation differences between back-interpolated and original Piedmont DTMs.	180
5.10	Statistics of the elevations of HD-1b DTM.	180
5.11	Statistics of the differences between PST-A LiDAR DTM and HD-1b/HD-2b DTM: global HELI-DEM area.	181
5.12	Statistics of the differences between HD-1b/PST-A/HD-2b DTMs and the 943 RTK points acquired in Valtellina area.	182
5.13	Statistics of the differences between HD-1b, PST-A and HD-2b DTMs and RTK points (64 points in area VT02 in Valtellina Valley).182	

Bibliography

- B. Acharya, J. Fagerman, and C. Wright. Accuracy assesment of dtm data: a cost effective approach for a large scale digital mapping project. *IAPRS*, 33, 2000.
- F. Ackermann. Airborne laser scanning: present status and future expectations. *ISPRS Journal of Photogrammetry and Remote Sensing*, 54(2):64–67, 1999.
- Z. Altamimi and C. Boucher. The itr89 and etrs89 relationship: New results from itr89. *Report on the symposium of the IAG Subcommission for Europe (EU-REF)*, 2001.
- Z. Altamimi, X. Collilieux, and L. Métivier. Itr89: an improved solution of the international terrestrial reference frame. *Journal of Geodesy*, 85:457–473, 2001.
- F. Amelung, D. Galloway, J. Bell, H. Zebker, and R. Lacznik. Sensing the ups and downs of las vegas: Insar reveals structural control of land subsidence and aquifer-system deformation. *Geology*, 27(6):483–486, 1999.
- ASPRS. *Manual of Photogrammetry*. ASPRS Publications, 1980.
- P. Axelsson. Processing of laser scanner data algorithms and applications. *ISPRS Journal of Photogrammetry and Remote Sensing*, 54:138–147, 1999.
- E. Baltsavias. Airborne laser scanning: basic relations and formulas. *ISPRS Journal of Photogrammetry and Remote Sensing*, 54(2):199, 1999.
- C. Barber and A. Shortridge. Light detection and ranging (lidar)-derived elevation data for surface hydrology applications. *Institute of water reseacrh, Michigan State University*, 2004.
- R. Barzaghi, A. Borghi, D. Carrion, and G. Sona. Refining the estimate of the italian quasi-geoid. *Springler Verlag*, 1987.

- P. Belotti, L. Biagi, M. A. Brovelli, A. Campi, S. Campus, M. Cannata, M. Credali, A. Manzino, F. Sansó, and G. B. Siletto. *Introduzione al progetto HELI-DEM (Helvetia Italy Digital Elevation Model). Chapter 1 of the book "Il progetto HELIDEM"*. Bollettino SIFET, special edition, 2013a.
- P. Belotti, L. Biagi, M. A. Brovelli, S. Campus, L. Carcano, M. Cannata, M. Cetti, M. Credali, P. Dabove, M. De Agostino, V. Guasco, A. M. Manzino, F. Sansó, G. B. Siletto, and C. Taglioretti. *Il progetto HELIDEM. Descrizione dei dati disponibili. Chapter 3 of the book "Il progetto HELIDEM"*. Bollettino SIFET, special edition, 2013b.
- L. Biagi. *I fondamentali del GPS*, volume 8. Geomatics Workbooks, 2009.
- L. Biagi and L. Carcano. Methodological problems merging local dtms: solutions and comparisons for a case study. *IAG Symposia Volumes, Hotine Marussi Symposium on Mathematical geodesy proceedings*, 2013.
- L. Biagi and A. Dermanis. *Telerilevamento. Informazione territoriale mediante immagini da satellite*. Casa editrice ambrosiana, 2002a.
- L. Biagi and A. Dermanis. *Telerilevamento. Informazione territoriale mediante immagini da satellite*. Casa Editrice Ambrosiana, 2002b.
- L. Biagi and F. Sansó. Il servizio di posizionamento in regione lombardia e la prima sperimentazione sui servizi di rete in tempo reale. *Bollettino SIFET*, 3, 2006.
- L. Biagi, M.A. Brovelli, A. Campi, M. Cannata, L. Carcano, M. Credali, M. De Agostino, A. Manzino, F. Sansó, and G. Siletto. Il progetto heli-dem (helvetia-italy digital elevation model): scopi e stato di attuazione. *Bollettino della Società Italiana di Fotogrammetria e Topografia*, 1:35–51, 2011.
- L. Biagi, L. Carcano, and M. De Agostino. Dtm cross validation and merging: problems and solutions for a case study within the heli-dem project. *Int. Arch. Photogramm. Remote Sens. Spatial Inf. Sci.*, XXXIX-B4:265–270, 2012.
- L. Biagi, M.A. Brovelli, L. Carcano, P. Dabove, M. De Agostino, A. Lucchese, A.M. Manzino, M. Negretti, C. Taglioretti, and M.G. Visconti. *Cross-validazione e validazione esterna dei DTM. Chapter 6 of the book "Il progetto HELIDEM"*. Bollettino SIFET, special edition, 2013a.
- L. Biagi, L. Carcano, P. Dabove, M. De Agostino, and A. M. Manzino. *Trasformazione di sistemi di riferimento dei dati. Chapter 3 of the book "Il progetto HELIDEM"*. Bollettino SIFET, special edition, 2013b.

- L. Biagi, P. Dabove, M. De Agostino, A. Manzano, C. Taglioretti, and M. G. Visconti. *Implementazione della rete GNSS di riferimento. Chapter 5 of the book "Il progetto HELIDEM"*. Bollettino SIFET, special edition, 2013c.
- E.O. Brigham. *The Fast Fourier Transform and its applications*. Prentice Hall, Englewood Cliffs, 1988.
- M. A. Brovelli, G. Giori, M. Mussin, and M. Negretti. Improving the monitor of the status of the environment through web geo-services: the example of large structures supervision. *TGIS*, 15:173–188, 2011.
- S. Caldera and M. G. Visconti. *Sistemi di riferimento per servizi di posizionamento GNSS: implementazione del caso lombardo*. Politecnico di Milano, Masters thesis, 2006.
- M. Cannata, M. Antonovic, and M. Molinari. *Il geoportale HELI-DEM. Chapter 12 of the book "Il progetto HELIDEM"*. Bollettino SIFET, special edition, 2013.
- A. Cina, A. M. Manzano, M. Piras, and M. Roggero. Rete test in piemonte, impianto e risultati. *Bollettino SIFET*, 2, 2004.
- M. De Agostino and A. M. Manzano. Validazione dei servizi della rete gnss della regione piemonte. *Bollettino SIFET*, 1:11–33, 2011.
- D. Donatelli, R. Maseroli, and M. Pierozzi. La trasformazione tra sistemi di riferimento utilizzati in italia. *Bollettino di Geodesia e Scienze Affini*, 4, 2002.
- T.P. Fang and L.A. Piegl. Delaunay triangulation using a uniform grid. *Computer Graphics and Applications, IEEE*, 13(3):36–47, 1993.
- A. Ferretti, A. Monti Guarnieri, C. Prati, and F. Rocca. Studi sul radar ad apertura sintetica (sar). *DEI - Politecnico di Milano*, 1998.
- L.C. Graham. Synthetic interferometer radar for topographic mapping. *Proceedings of the IEEE*, 62(2):763–768, 1974.
- D.A. Grejner Brzezinska, I. Kashani, and P. Wielgosz. On accuracy and reliability of instantaneous network rtk as a function of network geometry, station separation, and data processing strategy. *GPS Solutions*, 9(3):212–225, 2005.
- M. Hodgson, J. Jensen, G. Raber, J. Tullis, B. Davis, G. Thompson, and K. Schuckman. Adaptive filtering of aerial laser scanning data. *Photogrammetric engineering and remote sensing*, 71(7):817, 2005.

- W. Karel, N. Pfeifer, and C. Briese. Dtm quality assessment. *International Archives of Photogrammetry, Remote Sensing and Spatial Information Sciences*, 36(2):7–12, 2006.
- D. B. Kidner. Higher-order interpolation of regular grid digital elevation models. *International Journal of Remote Sensing*, 24:2981–2987, 2003.
- J. Kilian, N. Haala, and M. Englich. Capture and evaluation of airborne laser scanner data. *International Archives of Photogrammetry and Remote Sensing*, 31(3B), 1996.
- K. R. Koch. Parameter estimation and hypothesis testing in linear models. *Bollettino di Geodesia e Scienze Affini*, 3:145–159, 2007.
- W. Krabill, J. Collins, Swift R. Link, L., and M. Butler. Airborne laser topographic mapping results. *Photogrammetric Engineering and remote sensing*, 50:685–694, 1984.
- T. Kraub, H. Arefi, and P. Reinartz. Evaluation of selected methods for extracting digital terrain models from satellite born digital surface models in urban areas. *ISPRS Journal of Photogrammetry and Remote Sensing*, 2011.
- K. Kraus. *Photogrammetry: Geometry from images and laser scans*. Walter de Gruyter, 2007.
- K. Kraus and N. Pfeifer. Determination of terrain models in wooded areas with airborne laser scanner data. *ISPRS Journal of Photogrammetry and Remote Sensing*, 53(4):193–203, 2002.
- M. Lemmens. Airborne lidar sensors. *GIM International*, 21(2):24–27, 2007.
- J. Li and Z. Lihao. Distributed hydrologic model based on dem. *Hydroelectric Energy*, 4:002, 2004.
- Z. Li, Q. Zhu, and C. Gold. *Digital Terrain Modeling: Principles and Methodology*. CRC Press, 2005.
- X. Liu. *3-D Adjustment of a DTM/DSM without a priori homologous points*. Politecnico di Milano. Ph.D thesis, 2010.
- B. Makarovic. progressive sampling for dtms. *ITC Journal*, 28:111–130, 1973.
- B. Makarovic. From progressive sampling to composite sampling. *Geoprocessing*, 1:145–166, 1979.

- D.F. Maune, L.C. Huff, and G.C. Guenther. *Digital Elevation Model techniques and applications: the DEM user manual*. American Society for Photogrammetry and Remote Sensing, 2001.
- W. Meyer. *Concepts of mathematical modeling*. McGraw-Hill Book Company, 1985.
- ASTER GDEM Validation Team NASA. Aster global dem validation. *Summary Report*, 2009.
- U.S. Geological Survey NASA, U.S. Department of the Interior. Global multi-resolution terrain elevation data 2010 (gmted2010), summary report. 2011.
- J. Oksanen. *Digital Elevation Model error in terrain analysis*. Faculty of Science University of Helsinki. Ph.D thesis, 2006.
- Z.R. Peng and M.H. Tsou. *Internet GIS: Distributed Geographic Information Services for the Internet and Wireless Network*. John Wiley and Sons, 2003.
- N. Pfeifer and C. Briese. Laser scanning: Principles and applications. *3rd International Exhibition and Scientific Congress od Geodesy, Mapping, Geology, Geophysics, Cadaster GEO-SIBERIA*, 2007.
- B. Rabus, M. Eineder, A. Roth, and R. Bamler. The shuttle radar topography mission: a new class of digital elevation models acquired by spaceborne radar. *ISPRS Journal of Photogrammetry and Remote Sensing*, 57(4), 2003.
- W. G. Rees. The accuracy of digital elevation models interpolated to higher resolutions. *International Journal of Remote Sensing*, 21:7–20, 2000.
- T. Saaty and J. Alexander. *Thinking with models*. Pergamon Press, 1981.
- E. Shaw. *Hydrology in Practice*. CRC Press, 2005.
- I. Takos. Adjustment of observation equation without full rank. *Bollettino di Geodesia e Scienze affini*, 58:195–208, 1999.
- J.A. Thompson, J.C. Bell, and C.A. Butler. Digital elevation model resolution: effects on terrain attribute calculation and quantitative soil-landscape modeling. *Geoderma*, 100(1):67–89, 2001.
- D. Tovari and N. Pfeifer. Segmentation based robust interpolation - a new approach to laser data filtering. *International Archive of Photogrammetry, Remote Sensing and Spatial Information Sciences*, 36(3):79–84, 2005.

- G. Vosselman. Slope based filtering of laser altimetry data. *IAPRS*, 33(3B):935–942, 2000.
- R. Wack and A. Wimmer. Digital terrain models from airborne laser scanner data - a grid based approach. *IAPRS*, 34(3B):293–296, 2002.
- A. Wehr and U. Lohr. Airborne laser scanning: An introduction and overview. *ISPRS Journal of Photogrammetry and Remote Sensing*, 54(2–3):68–82, 1999.
- G. Whitmore and M. Thompson. *Manual of photogrammetry*. American Society for Photogrammetry, 1966.
- S. Wise. Assessing the quality for hydrological applications of digital elevation models derived from contours. *Hydrological processes*, 14(11-12):1909–1929, 2000.
- K. Zhang, S. Chen, D. Whitman, M. Shyu, I. Yan, and C. Zhang. A progressive morphological filter for removing non ground measurements from airborne lidar data. *IEEE Transaction on Geoscience and Remote Sensing*, 41(4):872–882, 2003.